Deepwater Thermoelectricity in Underwater Combo Power Grid System

Austin Asuquo

Department of Naval Architecture, Ocean, and Marine Engineering

University of Strathclyde

A thesis submitted for the degree of

Doctor of Philosophy

June 2024

Copyright

To God Almighty, the Creator of Heaven and Earth

To My Papa and Mama

To My Wife and Children

Acknowledgements

First, I acknowledge the grace of God Almighty for mercies and compassion in undertaking this Ph.D. at the University of Strathclyde, Glasgow, Scotland, in the United Kingdom. The University of Strathclyde is ‘The place of useful learning.’

I sincerely thank my Examination Committee, the External and Internal Examiners for their willingness to assess my work.

The Department of Naval Architecture, Ocean, and Marine Engineering is rated the number one (1st) in Europe and number three (3rd) worldwide for Marine/Ocean Engineering. I thank the staff of the Department for their assistance and support. I am grateful to my supervisors, Professor Julia Race, Dr. Byongug Jeong, and David Clelland, for their enormous support. I am equally thankful to Professor Dracos Vassalos, Professor Chengi Kuo, Professor Mehmet Atlar, Professor Erkan Oterkus, and Professor Selda Oterkus for their contributions.

I thank the International Society of Automation (ISA) for my Ph.D. Scholarship and to Glasgow Educational & Marshall Trust for Ph.D. Grant.

To my friends, colleagues, office/research centre mates, fellow Ph.D. researchers, and the Postgraduate community, I thank you for the good times, challenges, and achievements we have shared. May the souls of departed friends and colleagues rest in peace. Amen.

My appreciation and prayers to the memory of my father for all he did for me. My profound gratitude to my mother for her love and support. Thank you for standing by my side to my siblings, in-laws, and extended families.

Most importantly, I thank my beloved wife and children for their moral support and reassurance in seeing this work through. Finally, I thank my many friends, colleagues, and former bosses in the oil & gas industry across the globe (especially at Shell), with whom I have worked and shared experiences from 2000 to date. Sometimes, you need someone willing to take a chance on you. Late Dr. Joshua Udofia, former Deputy Managing Director, gave me the opportunity and foundation in Offshore Engineering. Andy Birch, former General Manager of Engineering & Development Major Projects, supported the transition to Deepwater. Joshua and Andy, I am grateful; thank you very much.

Abstract

Thermoelectrics convert heat energy to electrical energy through thermoelectric devices referred to as thermoelectric generators. Thermoelectric generators are solid-state elements without moving parts. They are noiseless, do not require any greenhouse gases, and can generate smaller (less than microwatts) and larger (greater than kilowatts) power levels based on the system design. Thermoelectric generators are reliable, durable, and can last very long. One of the several examples is the Voyager-01 spacecraft thermoelectric generator, launched by the US National Aeronautics and Space Administration (NASA) on September 5, 1977. The space probe has been operational for over four decades and has travelled above 23.429 billion km or 14.558 billion miles without maintenance.

More than half a century ago, thermoelectric generators were proven for subsea oil and gas applications. However, no deepwater or ultra-deepwater thermoelectric power system (DTEG) exists anywhere worldwide. This Ph.D. thesis presents an in-depth study on the extraction and conversion of heat from ultra-deepwater oil and gas reservoirs to electricity, depending on seabed conditions. Next, electrical energy becomes chemical energy for seafloor storage and utilisation. Furthermore, the converted electrical power was integrated into an underwater combo power grid system, thus paving the way for the first seabed-bound electrical power grid system for subsea equipment and beyond.

Publication

Published Work/Conference Proceeding related to this thesis:

Asuquo, A. Optimization of Thermoelectric Devices for Subsea Power, Control and Monitoring System. Subsea Expo 2018 (Global Underwater Hub). The World's Largest Annual Subsea Exhibition and Conference, 7 – 9 February 2018. *Speaker-Technology & Innovation Showcase Category*, Subsea Theatre, AECC, Aberdeen, United Kingdom.

https://www.subseaexpo.com/speakers/austin-asuquo/?d=2&rs=technology-showcase

Contents

List of Figures

List of Tables

Abbreviations

Abbreviation	Meaning
API	American Petroleum Institute
degC	Degree Celsius Temperature Measurement
DH	Drilling Hub (or Drilling Center)
DPP	Deepwater Power Plate
DPU	Deepwater Thermoelectric Power Unit
DTEG	Deepwater/Ultra-deepwater thermoelectric Power System
DTEM	Deepwater Thermoelectric Module
FLNG	Floating Liquefied Natural Gas
FLS	Flowline Sleds
FPSO	Floating Production Storage and Offloading
HPU	Hydraulic Power Unit
HSE	Health Safety and Environment
Info	Information
LNG	Liquefied Natural Gas
MBOPD	Thousand Barrels of Oil Per Day
MBWPD	Thousand Barrels of Water Per Day
MCM	Manifold Control Module
MMSCFD	Millions of Standard Cubic Feet Per Day
MSL	Mean Sea Level
PSI	Pounds Per Square Inch - Pressure
PSIA	Pounds Per Square Inch, Absolute – Pressure
PSIG	Pounds Per Square Inch Gauge - Pressure
ROV	Remotely Operated Underwater Vehicle
SCM	Subsea Control Module
SCSSV	Surface Controlled Subsurface Safety Valve
SEM	Subsea Electronic Module
TE	Thermoelectric Element or Device
TEM	Thermoelectric Module
Temp. Diff.	Temperature Difference, Subsea Temp. Diff (STD or SDT)
XTree	Christmas Tree

Symbols & Key Definitions

K	Thermal Conductance
τ	Thomson coefficient
α	Seebeck coefficient, Alpha
ΔT	Delta-T (Change in Temperature)
ω	Omega
θ	Theta
π	Peltier Coefficient
μ	Micro
η	Efficiency
Π	Pie
σ	Electrical Conductivity
ϕ	Thermal Efficiency Factor
L	Inductor
C	Capacitor
D	Diode
P	Power
V	Voltage
I	Current

Some Key Definitions

Shallow water – Subsea oil-gas well completion within the diver's reach or less than 200 meters of water depth

Deepwater – Subsea oil-gas well completion with water depths ranging from 200 to 1500 meters.

Ultra-deepwater – Subsea oil-gas completion in which the water depth exceeds 1500 meters.

DC and AC Power – DC or direct current power is electric current (from multiple sources) consistently flowing in a direction. AC Power, also known as alternating current power, is the flow of electric current with periodic changes in the flow direction.

Chapter 1

Introduction

1.1. Research Context

Deepwater or ultra-deepwater exploration and production involves large, complex, and multifaceted engineering practices. Developing oil and gas fields at ocean floors requires constantly identifying current or potential technical gaps within the operations and creating solution-based programs to resolve these deficiencies. Science, engineering, and management have established that continuous industrial-scale competency development schemes are essential to business growth.

However, there are conflicting views and opinions on the lack of research regarding how best to generate and transmit power to subsea equipment at the bottom of the sea in highly dynamic, remote, and hostile environments.

This research aims to identify and evaluate electricity generation and supply to equipment at seafloors for a changed oil and gas industry (subsea sector) in which subject knowledge has evolved.

This Chapter introduces the project by first discussing the background and context. Next are the research problems, the research aim, the objectives, and the research question. The significance and the limitations of the study are also discussed.

1.2. Study Background

The need for an alternative power supply to subsea equipment on the seafloor cannot be over-emphasized against the dependence on the platform (topside) power sources or power transmission from onshore (land-based) facilities. Moreover, seafloor-based power sources offer more benefits than the present method in which power transmission to the seabed is from power sources located at long tiebacks (20 km to more than 100 km) for deepwater or ultra-deepwater oil and gas fields.

Apart from reducing the cost of power generation and transmission, one of the main advantages of seafloor-based power sources is prompt response to critical power-demanding subsea equipment in an emergency. An example of the conventional subsea control and power system in which the failure of a platform-based power supply led to a major disaster is the Deepwater Horizon incident. Deepwater Horizon was an offshore drilling rig. The rig (with 126 people on board) was located about 81 kilometres off the coast of Louisiana. It was drilling an oil well at 1524 meters of water depth in an area known as the Macondo prospect within the US Gulf of Mexico.

Eleven (11) oil and gas workers died, and seventeen (17) others were severely injured on the 20th of April 2010 due to an explosion. The explosion resulted from an unplanned power failure of critical safety and control equipment, the BOP (blowout preventer) at the seabed (U. S. CBS, 2014). *Figure 1.1* is the picture of Deepwater Horizon hours before the incident. *Figure 1.2* illustrates the control and power system architecture for deepwater or ultra-deepwater oil-gas drilling (exploration) operations. *Figure 1.3* is Deepwater

Horizon during the incident, while *Figure 1.4* is one of the several aftermaths of the incident.

Figure 1.1 Deepwater Horizon-before the Incident (Deepwater-Horizon-56C17, 2010)

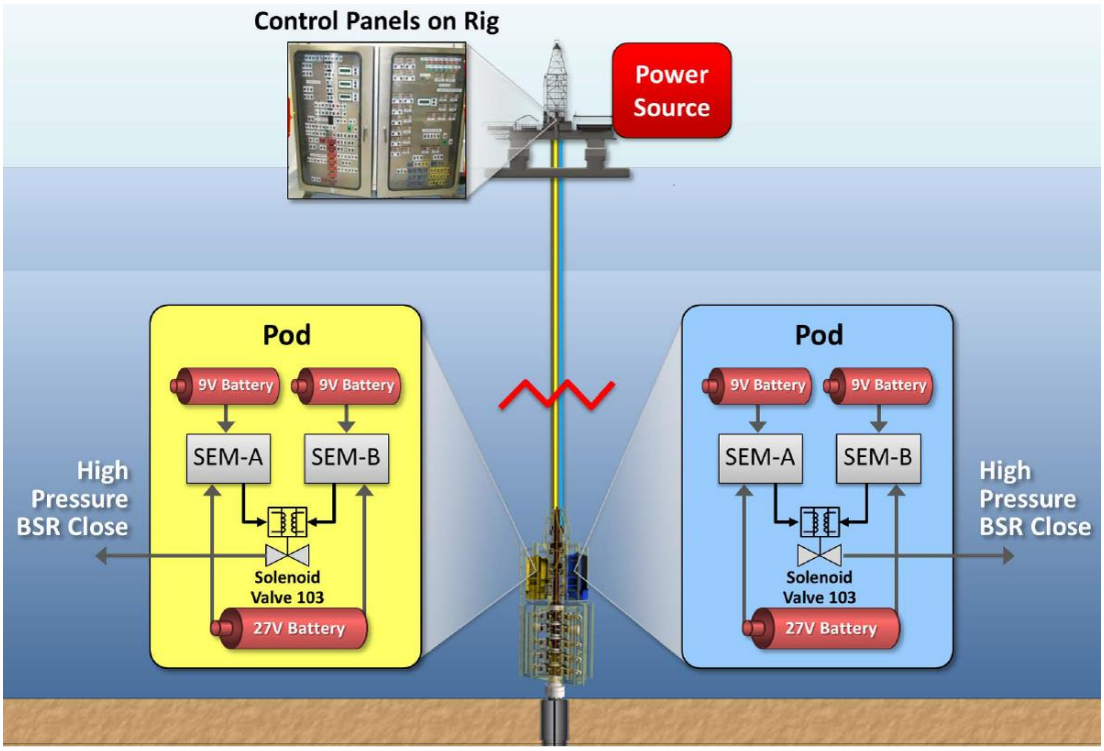

Figure 1.2 Subsea Control & Power System Architecture for Deepwater & Ultra-Deepwater Drilling Operations (MDL2179 PSC - Avansic, 2015)

Figure 1.3 Deepwater Horizon-Putting out the fire (National-Geographic, 2020)

Figure 1.4 After the Incident (National-Geographic, 2020)

Another example in which potential power loss at the topside of a production facility could lead to a catastrophe of enormous magnitude is presented in *Figure 1.5*. The illustration shows a hypothetical ultra-deepwater production field with a subsea oil and gas well #601, subsea Christmas tree (XTree), subsea manifold (601-PM-01), flowline/pipeline (601-PFL-01), sensors, other instrumentation, and control systems. Depending on the size of the production field, the FPSO (Floating Production Storage and Offloading facility)

might accommodate more than twice the number of workers on site compared to the drilling platform.

During production, hot oil and gas at high pressure and temperature continuously flow out of the subsea well through the subsea wellhead, XTree, manifold, flowline/pipeline, and 601-SSIV (subsea isolation valve) to the FPSO. An unplanned power failure from the topside to the seafloor equipment is a recipe for a disaster of significant magnitude. The absence of electricity on the seafloor will render critical safety and control equipment inoperable. As a result, the outcome of such a fatal failure can only be imagined. Further details on subsea systems and operations are available (Chakrabarti, 2005a)(Chakrabarti, 2005b).

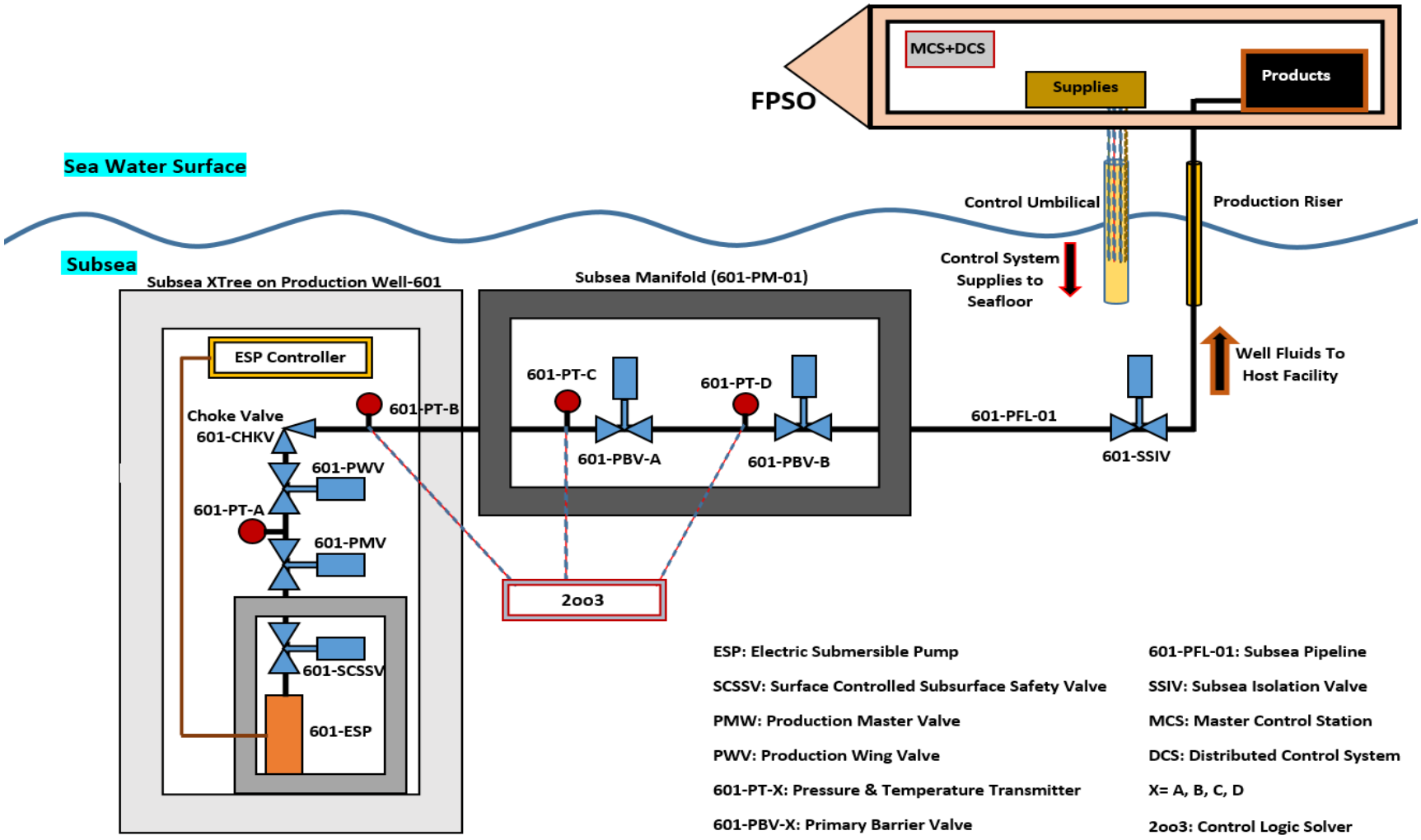

Figure 1.5 Ultra-Deepwater Production Control & Power System Architecture

1.3. Research Problem

Oil-gas exploration and production in deepwater or ultra-deepwater is quite challenging. Subsea controls and power system capabilities are the main drivers for the extraction and production of hydrocarbons from remote subsea wells. Although there are different types of subsea control and power system methodologies, the multiplexed electro-hydraulic control system is one of the famous traditional techniques. This technique places power sources on the platforms/topsides while essential operating equipment are several kilometres on the seafloor. Research has shown that unexpected power failure leading to blowouts can happen during drilling, well completion, workover, production, or wireline operations (Holand, 1996).

Studies have also shown that the subsea sector of the oil and gas industry typically generates and transmits power from platforms/topside or onshore to the seafloor (Thibaut and Leforgeais, 2012) (Bjerkreim *et al.*, 2009). This technique had gradually become the norm or the standard practice in the industry without any care for the dare consequences. Therefore, the need for seabed power generation and supply to subsea equipment is not generally shared in the industry. As a result, the existing research is inadequate for deepwater or ultra-deepwater oil and gas fields.

1.4. Research Aim, Objectives, & Research Question

Given the lack of research regarding seafloor power generation and supply to subsea equipment in deepwater or ultra-deepwater oil-gas fields, this study will aim to design an

ultra or deepwater thermoelectric power-generating system (DTEG) capable of harnessing geothermal heat from oil-gas reservoirs and converting it to electricity.

The project seeks to accomplish the following objectives to achieve the set aim:

1. Evaluation of subsea-based thermoelectric generators from previously published works within the subsea sector of the oil-gas industry and developed a more suitable concept to support deepwater and ultra-deepwater requirements.
2. Design and implement a test bench for testing and measuring power-generating capabilities of commercially available thermoelectric modules (TEMs).
3. Develop deepwater thermoelectric modules (DTEMs), deepwater thermoelectric power plates (DPPs), and deepwater power units (DPUs) that suit the deepwater and ultra-deepwater environment.
4. Create a control system strategy for energy harnessing and conversion to electric power, energy storage, supply, and utilisation on the seabed.
5. To design and operate an unconventional underwater power grid system. The power grid system will consist of a large deepwater thermoelectric power unit (DPU), other offshore-based renewables, and non-renewable power sources.

The research question for this project is thus:

How best can energy be generated at the seafloor to provide electrical power to critical subsea control equipment during deepwater or ultra-deepwater oil-gas exploration and production activities?

1.5. Scope of Research

This research combines experimental observations, mathematical models, and numerical simulations of deepwater thermoelectric power systems (DTEG). Secondly, developing subsea temperature difference models or templates as input to the deepwater thermoelectric power system was essential to this study. Thirdly, the research included implementing power conditioning algorithms and control system solutions capable of predicting DC and AC output voltage, current, and output power from DPPs, DPUs, underwater storage devices, and power supply to subsea equipment. Fourth, converting DC power (from the DPU) to AC power and delivery to an underwater electrical power grid system was crucial to this work. However, thermoelectric material development, characterization, and fabrication were not part of this research. Similarly, detailed AC power aspects of the deepwater power system are outside the scope of this work.

1.6. Research Significance

The significance of this research is in four categories: knowledge fulfilment, essential contributions of the DTEG power system, superiority of the DTEG power system over the conventional system, and vital requirements for continuous optimum power generation from the DTEG power system:

Knowledge Fulfilment

This study will contribute to the body of knowledge on a new approach to oil-gas exploration and production in deepwater or ultra-deepwater fields.

Secondly, this work will help address the current shortage of research in deepwater and ultra-deepwater, thereby providing real-world value to the oil and gas industry.

Thirdly, this work will encourage future collaboration efforts among academia and industrial stakeholders, leading to standardization, cost reduction, and technological advancements in thermoelectric power system solutions.

Fourthly, this research is poised to enhance the deployment of advanced technologies to create different types of thermoelectric power systems and opportunities for education and training. These opportunities will extend to underwater technologies, fostering expertise in the field.

Other Important Contributions of the DTEG Power System

The deepwater thermoelectric power system will reduce dependence on traditional power transmission from platforms/topsides-based power systems, thus eliminating the risk of unplanned power failures vis-à-vis blowout and explosion. Furthermore, this power system will mitigate power transmission losses often related to long-distance cable transmission from the surface to the seabed.

Secondly, the DTEG power system will provide a continuous, reliable, and uninterrupted power supply to critical safety and control systems on the seafloor. Therefore, there will be real-time systems monitoring, control, and data transmission from the seabed to the platforms/topsides, cloud, and land-based control centres. Thus, the real-time capability of the systems will enhance operational safety and efficiency.

Thirdly, the DTEG power system will achieve high energy density. It will allow the generation of substantial power in a compact form factor. It will reduce the reliance on extensive cabling. Additionally, this power system will minimize the cost of subsea operations and potential environmental impact.

DTEG Power System Superiority over Conventional System

This DTEG power system offers superiority over traditional power systems that transmit power from the surface to the seafloor. The DTEG system provides continuous and on-demand power directly to subsea equipment. Therefore, the DTEG system is a simplified power system with reduced complexity and a lower cable network.

In contrast, conventional power transmission involves complex cable networks running from platforms to seafloor-located equipment. Furthermore, heat dissipation and thermal management challenges in long cables will be eliminated by the DTEG power system.

Unlike the traditional power system, the DTEG power system will provide a direct electrical power supply to subsea equipment, ensuring power stability and power quality. The power system will reduce the risk of voltage fluctuations. This measure will provide

an overall safeguard for subsea equipment operating within specified voltage and frequency tolerances.

Lastly, compared to high-voltage cable transmission through traditional power systems, electromagnetic interference is minimal in DTEG power systems. This provision reduces the impact on sensitive subsea instrumentation, control, and communication systems.

Requirements for Continuous Operation of DTEG Power System

The underwater environment is challenging. Therefore, requirements must be addressed to achieve continuous and reliable operation of the DTEG power system in the oil and gas field. Some of the essential requirements include the following:

The deepwater thermoelectric power system components must seamlessly integrate into subsea infrastructure, such as subsea wellheads, hot fluid flow paths within subsea Christmas trees, BOPs, and subsea manifolds. Other subsea systems that will accommodate the DTEG power system components are subsea flowlines, pipelines, drilling risers, and production risers.

The DTEG power system and components design must be robust and durable to withstand high pressure and potential impacts on the seafloor. Therefore, DTEG power system components must be made of corrosion-resistant materials with the necessary protective coatings to ensure long-term structural integrity.

The DTEG power system's optimal performance is achieved through effective temperature management and prevention of systems overheating or overcooling at the

seabed. Hence, incorporating efficient heat transfer mechanisms and thermal insulation is crucial for long-term temperature management, leading to continuous operation.

The seafloor is prone to operating parameter fluctuations. Such parameters include temperature, seawater currents, and changes in sedimentation. Therefore, the DTEG power system and components should be designed to adapt to the seabed environment. The power system should also be integrated with adaptive control systems to optimise performance under changing seabed conditions. Additionally, the DTEG power system should have fault detection and early warning systems that provide real-time information on the system's performance on the seafloor.

1.7. Limitations of DTEG Power System

While the proposed DTEG power system in deepwater or ultra-deepwater oil and gas fields offers numerous benefits, it also has certain limitations that must be considered. Some of the shortcomings of this underwater power system are:

High performance of the DTEG power system is achievable in green-field oil and gas projects. However, retrofitting the power system on existing oil-gas infrastructure would be challenging due to compatibility issues. Therefore, careful feasibility study, modifications, and re-integration programs on brownfields are essential for improving the DTEG power system performance on such projects.

Secondly, uneven terrain, natural obstructions, and unsuitable infrastructures from previous oil-gas operations are some of the challenging features on the seafloor. These

factors can complicate the installation of the DTEG power system. Therefore, these factors should be reviewed, and system adaptability must be considered during the design phase.

Thirdly, ocean floors are typically characterised by sedimentation, fouling, and marine growth. These conditions may potentially affect the DTEG power system performance. Hence, incorporating regular maintenance and cleaning policies would go a long way to mitigate these effects and keep the power system at optimum performance.

1.8. Structural Outline

In ***Chapter 1*** (this Chapter), the context of the study has been introduced. The research aim, objectives and research question have been identified. The value of such research has been argued. Furthermore, the limitations of the study have been discussed.

In ***Chapter 2***, the existing literature on subsea thermoelectricity will be reviewed to identify key concepts and the necessary development approaches and strategies within the context of deepwater and ultra-deepwater oil-gas fields.

In ***Chapter 3***, suitable DTEMs (deepwater thermoelectric modules), DPPs (deepwater thermoelectric power plates), and DPUs (deepwater thermoelectric power units) for deepwater and ultra-deepwater oil-gas fields will be developed.

In ***Chapter 4***, control system algorithms and subsea temperature difference input will be created to act as power system interfaces. The outcome of the system arrangement will

result in electrical power characteristics, seafloor energy storage potentials, and electrical power supply to subsea equipment.

In ***Chapter 5***, an ultra-deepwater oil and gas field consisting of fifty-six (56) subsea wells tieback to an FPSO, a myriad of subsea equipment, a 6.4kW-DPU power unit, and a 6120 Ah capacity subsea battery bank will be developed.

In ***Chapter 6***, the 6.4kW-DPU power unit will be integrated into a unique underwater combo electrical power grid system consisting of renewable and non-renewable power sources.

In ***Chapter 7***, the oil-gas field design and development parameters in ***Chapter 5*** will be characteristically related to an ultra-deepwater oil and gas field in West Africa. The results of the experiments will also be validated.

Finally, ***Chapter 8*** will be the discussions and conclusions. This Chapter will highlight the research accomplishments, impediments, recommendations, plans for the future, and project conclusions.

Chapter 2

Literature Review

2.1. Introduction

Chapter 2 (Literature Review) explores the literature in three parts. This approach was necessary to understand thermoelectricity better. The first part examined the historical viewpoint of thermoelectrics. A discussion on contemporary issues of thermoelectric generators forms the second part of the chapter. The final section is a time-based (or timeline) review of thermoelectric power generation within the subsea sector of the oil and gas industry.

2.2. Thermoelectrics (TEM & TEG)

A thermoelectric generator (TEG) is a solid-state device that converts heat flow and temperature difference into a DC electrical power source. This work considers the TEG as an electrical power source with one or more thermoelectric modules (TEM). The composition of a thermoelectric module is several semiconductor devices that can generate voltage with the potential to drive current and produce electrical power.

Therefore, thermoelectrics can be described as the direct conversion of heat energy to electricity or vice versa. The transformation process is such that thermoelectric devices consisting of N-type and P-type legs semiconducting materials (also called thermo-elements, pellets, or dice) are electrically arranged in a series pattern on metallic strips called electrodes. These semiconductor legs are thermally parallel by electrical insulating mounted plates made from alumina or ceramic materials. These mounted ceramic plates, semiconductor legs or pellets, and metallic strips form a thermoelectric module (TEM). Apart from preventing electrical short-circuiting and acting as a dielectric cover, these mounted plates offer structural rigidity for the entire system.

There are two types of thermoelectric modules (TEMs). The first type is loosely called thermoelectric generator (TEG), while the second type is called thermoelectric cooler (TEC). The operating modes of both TEMs are different. The TEG uses temperature differences on the device's hot and cold sides to produce electrical power. Conversely, cold heat is transferred from the device's cold surface to the hot surface when an electrical voltage is applied to a TEC. The TEC is not the subject of this project; as such, there is no detailed discussion on thermoelectric coolers beyond this point.

As discussed above, a single thermoelectric module (TEM) is formed by joining a number of thermocouples, as shown in *Figure 2.3*. The thermocouples in *Figure 2.1* and *Figure 2.2* are contained in *Figure 2.3*. Therefore, the TEM uses the Seebeck effect to convert heat energy into voltage potential. The Seebeck effect occurs inside the thermocouples (or semiconductors) when charge carriers move as the temperature difference is applied on the thermocouple's hot-side and cold surfaces.

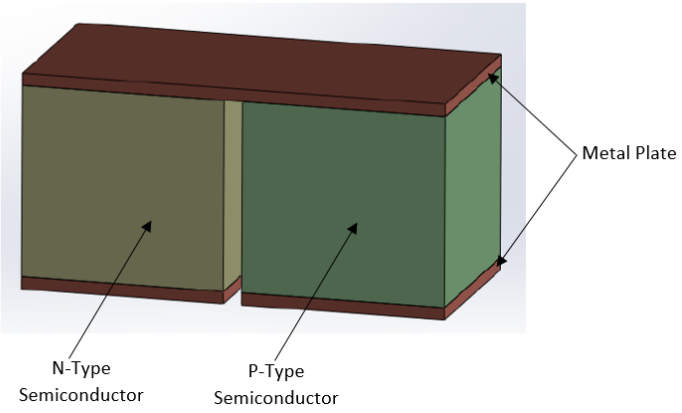

Figure 2.1 Thermoelectric Couple (without ceramic Plates)

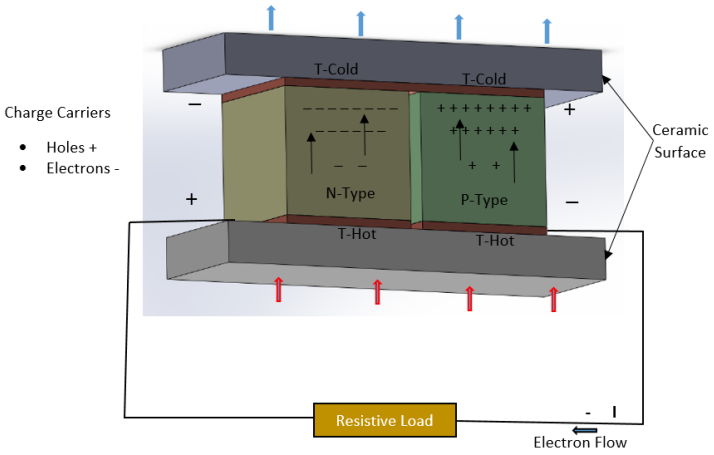

Figure 2.2 Thermoelectric Couple (with top & bottom plates)

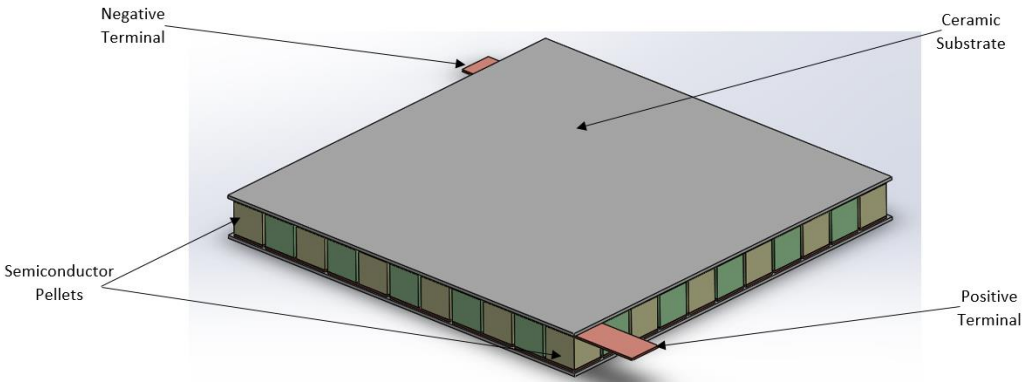

Figure 2.3 Schematic of Thermoelectric Module

In doped N-type semiconductors, electrons are the charge carriers, while charge carriers in a P-type doped semiconductor are called holes. Random movements of charge carriers within the system lead to diffusion and build-up of charge carriers. Charge build-up occurs at one end of the semiconductors by applying a temperature gradient. This charge build-up in the system eventually creates voltage potential (Marlow-Industries, 2016). The created voltage potential is proportional to the applied temperature difference across the thermocouple, as shown in *Figure 2.2*.

Therefore, from the illustrations, it can be inferred that the quantity of the generated electricity or the power system performance hinges on the temperature difference that reaches the thermoelectric legs enclosed within the ceramic plates, among other factors (García-Cañadas *et al.*, 2013)(Hatzikraniotis *et al.*, 2010).

From the above discussion, the TEM in *Figure 2.3* is a thermoelectric power-generating mechanism consisting of several thermocouples that can convert temperature difference to electrical voltage. A more considerable value of electrical voltage is produced when

several thermoelectric modules (TEMs) are connected in an appropriate configuration. In turn, the generated voltage drives electrical current, thus generating usable electrical power for subsea equipment. Hence, a thermoelectric generator (TEG) of any power rating consists of a thermoelectric module (TEM) or more than one thermoelectric module (TEMs).

To sum up, a thermoelectric generator (TEG) of a particular power rating consists of one or more thermoelectric modules (TEMs). The thermoelectric module (TEM) is made up of several thermocouples or semiconductor legs. Also, the TEM can be described as a device that can transform the fluid flow temperature difference between hot oil-gas wells and cold seawater environments into a functional DC (direct current) power source.

2.2.1. Brief History of Thermoelectrics

The conversion of heat into electricity and the transformation of electrical power back to heat energy is known as thermoelectricity. The conversion process from heat to electrical power involves fundamental physics such as the Seebeck, Peltier, and Thomson effects.

In his experiments in 1821, Thomas Johann Seebeck observed a continuous deflection of the needle of a compass magnet at the junction of two non-similar metals at different temperatures. He and his colleagues believed that the temperature difference caused magnetism. However, further findings revealed that induced electric current was responsible for the magnetic compass deflection according to Ampere's law. Nevertheless, the discovery was named the Seebeck effect in honour of Thomas Johann Seebeck. Based

on the Seebeck coefficient (α), *Equation (2.1)* defines the relationship between temperature difference (ΔT) and induced voltage (V).

$$V = \alpha \times (\Delta T) \tag{2.1}$$

The Peltier effect, named after Jean Charles Peltier, became prominent in 1834. Peltier discovered that once electric current (I) passes over a thermocouple of two non-similar conductors, a heating or cooling effect occurs at the conductor's junction relative to the current flow direction. Given that the Peltier coefficient is π, and (Q1) is the heat energy consumed or lost at the hot junction, while (Q2) is the heat energy supplied at the cold junction. Then *Equation (2.2)* and *Equation (2.3)* define the Peltier effect:

$$Q1 = 1 \times \pi \times (I) \tag{2.2}$$

$$Q2 = -1 \times \pi \times (I) \tag{2.3}$$

The Thomson effect (named after William Thomson in 1854) refers to the generation or absorption of heat energy when an electric current flows through a homogeneous conductor where a temperature gradient exists. If T represents temperature and (τ) denotes the Thomson coefficient. Then, the expression that defines the Thomson effect is as in *Equation (2.4),* in which (q) is the charge, $(\frac{\partial Q}{\partial x})$ correspond to the change in overall heat generated or absorbed, while per unit temperature gradient is denoted as $(\frac{\partial T}{\partial x})$.

$$q = \frac{\partial Q}{\partial x} = \tau \text{ x } I \text{ x } \frac{\partial T}{\partial x} \quad (2.4)$$

The exploitation of thermoelectric phenomena for power generation began around the end of the 19th and early 20th centuries. In 1911, Edmund Altenkirch examined the physical properties and the quality of materials that could convert heat to electricity and electricity generation back to heat. Research and development on improving thermoelectric semiconductor materials began from the theoretical and experimental works of Abram Ioffe in the Soviet Union in 1946 (G. S. Nolas, 2001). The reduction of thermal conductivity and other thermoelectric properties in advanced thermoelectric (TE) materials or nanomaterials led to a ground-breaking developmental effort in 1993 (Han, Li, and Dou, 2014)(Yang *et al.*, 2008). Despite that, the first functioning thermoelectric devices were in the 1950s and 1960s. Today, thermoelectric devices have progressively become important in various applications. The discovery in the 1990s positively steered the performance and efficiency of thermoelectric devices away from decades of stagnation. Further assessments on the progress in thermoelectricity, as well as broader progressions in thermoelectric materials, are available in (Ioffe A.F., 1957), (Rowe, D.M.; Bhandari, 1983), (Rowe, 1994), and (Chen *et al.*, 2012).

2.3. From The Old to Modern Generators

Using state-of-the-art thermoelectric generators to harvest waste heat energy has shown that thermoelectric generator materials, design, fabrication, and manufacturing processes

have taken a turn from what they used to be before the 1990s. The evidence is in low-power components such as wearable/implantable devices, sensor networks, and wireless appliances. On the other hand, high-power thermoelectric systems are in industrial electronic equipment, automobiles, and aerospace. The figure of merit and maximum power are among the underlying concepts in thermoelectrics irrespective of its power-generating potential, low or high-power system, as discussed below:

2.3.1. Maximum Power

Thermoelectric generators, or thermogenerators (TEGs), can convert heat to electricity, as explained in the sections above. The Seebeck effect forms the basis for the working of thermoelectric generators. Recent developments, design simplicity, and the absence of moving parts have made thermoelectric systems more advantageous. In addition, thermogenerators do not require extensive maintenance; hence, longevity is guaranteed in thermo-devices. Generally, they are environmentally friendly as they do not harbour harmful chemical substances.

The resulting power of TEG can be improved by connecting several thermopiles or semiconductors, as mentioned above. A thermopile, also known as a cell, consists of thermocouples. The basic configuration is that thermocouples are electrically linked in series (chain connection), while surface-mounted plates are thermally connected in parallel (Leonov *et al.*, 2007). The representation of a TEG on the application of

temperature difference (ΔT) on the hot surface or ($T_{Hotside}$), the cold surface or ($T_{Coldside}$), with an external resistive load (R_L) is depicted in *Figure 2.4*.

As illustrated in *Figure 2.4*, A and B are single or individual cells of different semiconducting materials. However, it is essential to note that each thermopile can generate electric voltage if a temperature difference (ΔT) is applied across the device's surfaces (hot & cold surfaces) with a load connected, as expressed in *Equation (2.5)* and *Equation (2.6)* (Yang *et al.*, 2013) (Pasquale, 2013).

$$\Delta T = T_{Hotside} - T_{Coldside} \quad (2.5)$$

$$V_{Out} = n \times \alpha \times A \times B \times \Delta T \quad (2.6)$$

From *Equation (2.6)*, the number of thermocouples is designated by (n), while the Seebeck coefficient of the materials of the thermocouple (A) and (B) is represented by $(n\ \alpha\ A\ B)$. Therefore, it can be inferred that the higher the number of thermocouples or semiconductors, the higher the output voltage. The voltage, in turn, drives electric current (I), thereby producing electric power. The device's maximum power is obtained if there is a match between the internal resistance of the device and the connected resistive load element (Yan and Chen, 2008)(Q. H. Zhang *et al.*, 2016). *Equation (2.7)* further expresses the Seebeck coefficient of the thermocouples:

$$\alpha \times A \times B = (\alpha A) - (\alpha B) \quad (2.7)$$

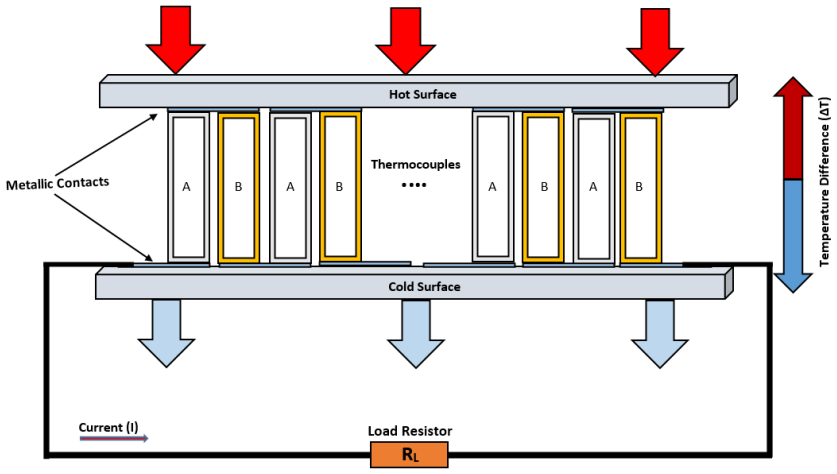

Figure 2.4 Electrical Current Flow through a TEG Device

2.3.2. Thermoelectric Figure of Merit (FOM)

The figure of merit (Z) of thermoelectric materials is a quality factor for determining materials' suitability for power generation. Several types of conductive and semiconducting materials are fabricated into thermoelectric devices. Therefore, choosing high-quality materials guarantees higher output voltage, higher electrical power, and lower internal electrical resistance (Han, Li and Dou, 2014). By extension, high-quality materials result in better electrical performance.

Example of new fabrication methods or the hosting substrate materials is silicon technology such as complementary metal oxide semiconductors integrated circuit (CMOS-IC) and complementary metal oxide semiconductors micro-electro-mechanical systems (CMOS-MEMS)(Yang *et al.*, 2013)(Kao *et al.*, 2010). Another fabrication

method is Alumina (Al2O3) and low-temperature co-fired ceramic (LTCC)-based technologies (Markowski and Dziedzic, 2008)(Markowski, 2016).

The third technique is polymers, polyimide, cellulose fibers, and fabric-based technology (Nguyen Huu, Nguyen Van and Takahito, 2018)(Park *et al.*, 2017)(Elmoughni *et al.*, 2019) for creating flexible thermoelectric devices or F-TEGs. *Figure 2.5* to *Figure 2.9* are illustrations of contemporary flexible and rigid thermoelectric generators.

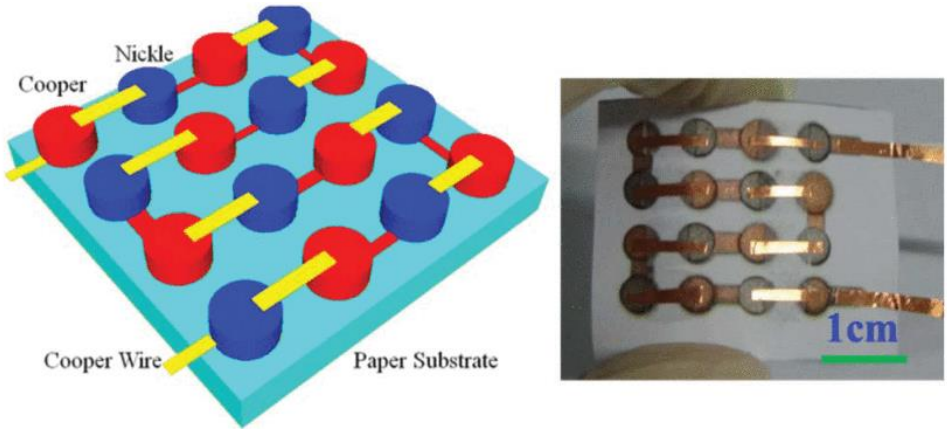

Figure 2.5 Flexible TEGs (Zhu, Xu and Jia, 2018)

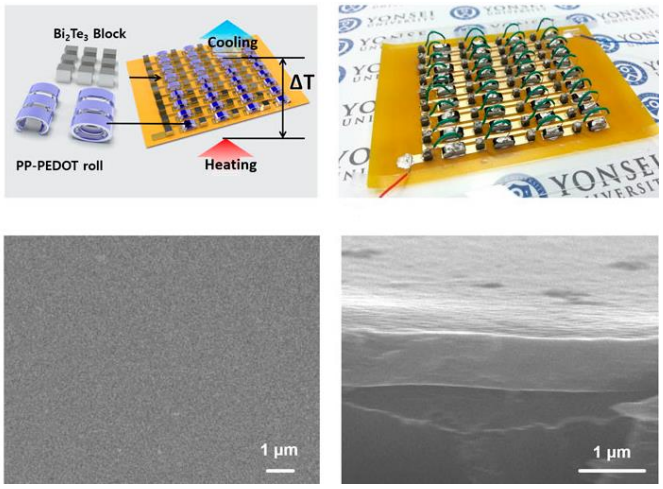

Figure 2.6 Flexible & Rigid TEGs (Park *et al.*, 2017)

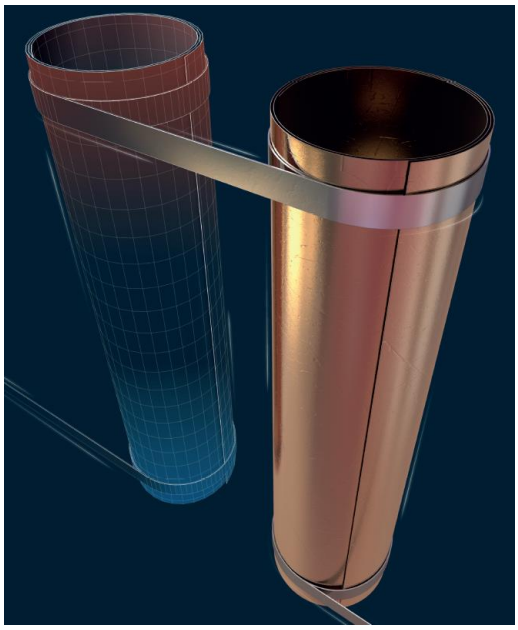

Figure 2.7 Thin Films-Lightweight Tubular TEG (Singh *et al.*, 2018)

Figure 2.8 Flexible TEG (Elmoughni et al., 2019)

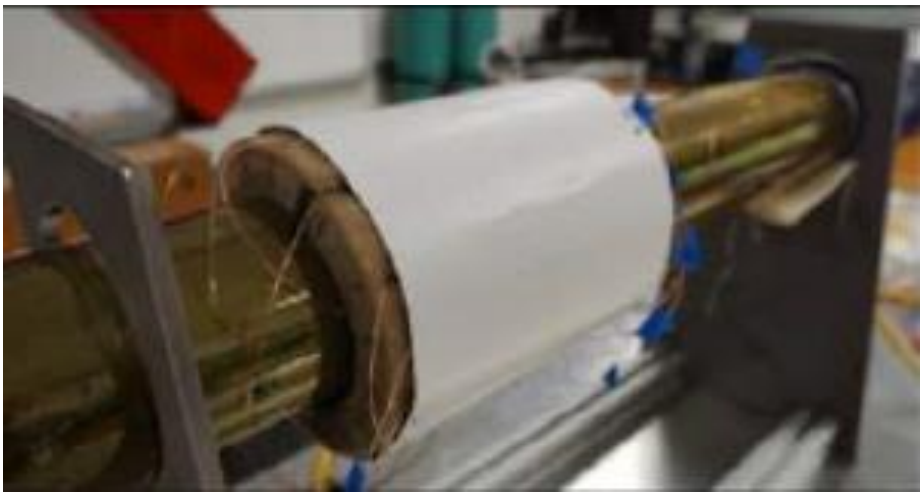

Figure 2.9 Flexible TEG (Iezzi *et al.*, 2017)

Unlike the earlier or old thermoelectric generators, the above illustrations of modern thermoelectric generators show that it is now possible to design, fabricate, and manufacture generators of different shapes and sizes, which might be formed into rigid or

flexible thermoelectric devices. Moreover, the new flexible thermoelectric generators (F-TEGs) can be fitted on structures exposed to temperature difference for energy harvesting in remote locations.

Additionally, nano-structuring techniques have been used to enhance the thermoelectric efficiency of flexible thermoelectric materials, thereby optimizing the performance of the flexible thermoelectric generators. Therefore, the F-TEGs can bend and adapt to various shapes while expanding application possibilities. Secondly, they are effective in environments with changing temperature profiles. Hence, flexible thermoelectric generators are adaptable in any environment and excel in applications with dynamic conditions. In contrast, the typical material composition of the rigid thermoelectric generators is Bismuth Tellurite (Bi2Te3) or Lead Telluride (PbTe), often referred to as bulk materials with limited flexibility. The lack of flexibility restricts their use to applications that do not require bending or conforming to curved or cylindrical surfaces like pipelines or flowlines. Nevertheless, rigid thermoelectric generators offer steady performance under consistent conditions.

From the discussions above, irrespective of the fabrication process, the thermoelectric figure of merit (FOM) or (Z) is the common denominator in any thermogenerator, as stated. The unit of FOM or (Z) is denoted by $({}^{1}/_{K})$. *Equation (2.8)* determines the value of (Z). However, it is noteworthy that the process of obtaining the value of (Z) is involved; it is not a simple or straight forward process.

$$Z = \frac{(\alpha^2)}{\rho \times k} = \frac{(\alpha^2 \times \sigma)}{k} \quad (2.8)$$

The units of the other parameters expressed in *Equation (2.8)* are as follows:

- Seebeck coefficient (α) = μV/K
- Electrical resistivity (ρ) = Ωcm
- Electrical Conductivity (σ) = 1/ρ = $(\Omega cm)^{-1}$
- Thermal or heat conductivity (k) = W/Mk

As mentioned, several compounds, conductive materials, and semiconductors can be used to fabricate thermo-devices. However, not every material is necessarily thermoelectric in characteristics. A good thermoelectric material has a high electrical output voltage (V_{Out}), lower internal resistance $(intR_{TEG})$, and potential for high-output electrical power (P_{Out}). Therefore, in addition to the quality factor, the value of (Z) determines how efficiently a thermoelectric material can transform heat energy into electricity.

The (Z) value of the thermogenerator is also temperature-dependent; as such, a higher value of (Z) for a thermoelectric material is needed in a particular temperature domain. Hence, the combination of (Z) and temperature (T) defines the term (ZT) as a dimensionless figure of merit (Kim *et al.*, 2015), (Snyder and Jones, 2017), and (Rowe, 1991).

Furthermore, *Equation (2.9)* defines the power factor of typical thermoelectric material. The energy conversion efficiency of materials is substantial if the (ZT) values are

considerably large. On the other hand, the Seebeck coefficient (α) and electrical conductivity (σ) of thermoelectric material must also be high. In contrast, the material thermal or heat conductivity (k) value must be low.

$$Power\ Factor = (\alpha^2 \text{ x } \sigma) \quad (2.9)$$

Developmental strategies for improving thermoelectric materials' (ZT) value have been challenging. Although, there is no set limit for the value of (ZT). For several decades, (ZT) value was approximately one (1) for materials such as bismuth telluride (Bi2Te3). Other thermoelectric materials with (ZT) value of one (1) are lead telluride (PbTe) and skutterudite (CoSb3) (Hébert, 2014) (Shu *et al.*, 2018).

Research and development efforts involving the synthesising of some thermoelectric materials, like copper selenide (Cu2−xSe) nanocrystals and PbTe0.7S0.3, have resulted in (ZT) values greater than two (2) (Olvera *et al.*, 2017)(Wu *et al.*, 2014).

Thermoelectric materials developed until the late 1960s are termed first-generation, with conversion efficiency and (ZT) values of approximately 5% but less than 10% and 1.0, respectively. (ZT) values from 1.3 to 1.7 for thermoelectric materials developed in the 1990s with thermoelectric conversion efficiencies ranging from 11% to 15% are considered second-generation thermoelectric materials. (ZT) value of 2.2 for a new category of materials has a thermoelectric device conversion efficiency of 15% to 20%. These new materials are third-generation thermoelectric materials (Zhao, Dravid and Kanatzidis, 2014).

2.3.2.1. Thermoelectric Materials

The previous section explored the figure of merit of thermoelectric materials. This subsection briefly discusses the composition of ten (10) thermoelectric materials. Their power generation ability and thermoelectric conversion efficiency are also brought to focus:

1. Bismuth Telluride (Bi2Te3)

Bismuth Telluride is a commercially established thermoelectric material for cooling and power generation. This material has a high thermoelectric performance at about 26.85 °C (near room temperature). It has a high Seebeck coefficient and low thermal conductivity. The conversion efficiency is around 5% to 8%. There are ongoing research activities to enhance the power generation efficiency of bismuth telluride via nanostructured Bi2Te3 films. Some of the limitations of Bi2Te3 are low efficiency at higher temperatures and being sensitive to impurities. Such sensitivity affects the electrical conductivity of the material.

2. Cobalt Antimonide (CoSb3)

Cobalt antimonide has a high melting point. Secondly, this thermoelectric material exhibits stability at high temperatures. Therefore, it is suitable for high-temperature applications. The Seebeck coefficient of CoSb3 is usually described as being moderate. Furthermore, cobalt antimonide has a high thermal strength in harsh environments. The

thermoelectric conversion efficiency ranges from 8% to 12%. However, the drawbacks of this material include being expensive and having an average efficiency value.

3. Silicon-Germanium Alloy (Si70Ge30)

Silicon-germanium alloy has good thermoelectric performance and is commonly applied in waste heat recovery, especially in the automotive sector. This thermoelectric material can withstand temperatures up to 726.85 °C. The efficiency value of Si70Ge30 is from 7% to 10%. However, some of the challenges of silicon-germanium alloy are high manufacturing costs and the need to be sensitive to temperature variations.

4. Bismuth Telluride Selenide (Bi2Te2.7Se0.3)

Bismuth telluride selenide is a thermoelectric material with enhanced stability at temperatures of about 126.85 °C. The efficiency value ranges from 6% to 9%. Compared to bismuth telluride, the thermoelectric efficiency of Bi2Te2.7Se0.3 is better. Bismuth telluride selenide has been integrated into flexible thermoelectric (F-TEG) devices for various applications. However, the disadvantage of this thermoelectric material is its sensitivity to composition changes.

5. Lanthanum Telluride (La3Te4)

Lanthanum telluride has good thermoelectric properties and can withstand temperatures slightly above 900 °C. The efficiency value of this material ranges from 8% to 11%. La3Te4 has enormous potential in the aerospace and automotive sectors. Doping strategies are used to enhance the electrical conductivity of lanthanum telluride. The main downside of this material is limited availability.

6. Ytterbium Manganese Antimonide (Yb14MnSb11)

The thermoelectric efficiency of Ytterbium Manganese Antimonide ranges from 12% to 15% at a temperature of 926.85. The improvement in efficiency is due to the complex crystal structure of the material. Yb14MnSb11 is suitable for power generation in remote locations. However, Ytterbium Manganese Antimonide is rare and not easy to come by. Therefore, this material is expensive.

7. Ytterbium Cobalt Antimonide (Yb-CoSb3)

The thermoelectric efficiency of Ytterbium cobalt antimonide is from 14% to 18%. Yb-CoSb3 is an excellent thermoelectric material, and its performance remains stable at temperatures up to 526 °C. The material is used for remote power generation in space stations. The challenges associated with Ytterbium cobalt antimonide are expensive and not readily available.

8. Silicon-Germanium Alloy (Si80Ge20)

Silicon-germanium alloy is compatible with semiconductors. It has moderate thermal conductivity and good thermoelectric conversion efficiency ranging from 7% to 10%. Si80Ge20 has a high potential for waste heat recovery in automotive exhaust systems and is used in flexible thermoelectric generators. High material cost and limited efficiency at severe temperatures are among the weaknesses of silicon-germanium alloy.

9. Bismuth Antimony Telluride (BiSbTe)

Bismuth antimony telluride is suitable for temperatures ranging up to 126.85 °C. This material thermoelectric conversion efficiency is from 7% to 10%. BiSbTe is used in localised energy harvesting, portable electronics, and power generation in medical devices. The challenges with bismuth antimony telluride include being expensive and sensitive to impurities.

10. Lead Telluride-Strontium Telluride Alloy (PbTe-SrTe)

This thermoelectric material has potential for use in temperatures slightly above 600 °C. The thermoelectric conversion efficiency of PbTe-SrTe is from 10% to 14%. Lead telluride-strontium telluride alloy is used in space missions and remote electric power systems. However, the presence of lead alloys in this material constitutes problems that have led to investigations for non-toxic alternatives and eco-friendly alloys.

Finally, *Table 2.1* summarizes the properties of the above ten (10) thermoelectric materials.

Table 2.1 Thermoelectric Material Properties

Thermoelectric Materials	Semiconductor Type	Temp. (°C)	ZT	Effy. (%)	References
Bi2Te3	P-Type Single Crystals	26.85	0.5	5 - 8	Jeon, HW. et al. (1991)(Jeon *et al.*, 1991)
CoSb3	N-Type Single Crystals	526.85	0.6	8 - 12	Caillat, T. et al. (1996)(Caillat, Borshchevsky and Fleurial, 1996)
Si70Ge30	N-Type Single Crystals	726.85	0.8	7 - 10	Dismukes, J. P. et al. (1964)(Dismukes *et al.*, 1964)
Bi2Te2.7Se0.3	N-Type Nanocomposites	126.85	1.0	6 - 9	Yan, X. et al. (2010)(Yan *et al.*, 2010)
La3Te4	N-Type Single Crystals	926.85	1.1	8 - 11	May, A.F. et al. (2010)(May, Fleurial and Snyder, 2010)
Yb14MnSb11	P-Type, Zintl Compound	926.85	1.1	12 -15	Brown, S.R. et al. (2006)(Brown *et al.*, 2006)
Yb-CoSb3	N-Type, Yb-filled Skutterudites	526.85	1.3	14 -18	Tang, X. et al. (2005)(Tang *et al.*, 2005)
Si80Ge20	N-Type Nanocomposites	926.85	1.3	7 - 10	Wang, X.W. et al. (2008)(Wang *et al.*, 2008)
BiSbTe	P-Type, Nanocomposites	126.85	1.4	7 - 10	Poudel, B. et al. (2008)(Poudel *et al.*, 2008)
PbTe-SrTe	P-Type Nanocomposites	626.85	2.2	10 -14	Biswas, K. et al. (2012)(Biswas *et al.*, 2012)

2.4. Applications of Thermoelectrics

Section 2.3 explores thermoelectrics from the old to the new generation. This section looks at the applications of thermoelectric generators. Thermoelectric generators are used across industries for low-power and high-power energy systems, as mentioned earlier. Thermoelectric power systems include body heat systems, waste heat, combustion, radioactive decay, and renewable sources. Generators with a small heat source for power output levels ranging from microwatt to milliwatt are called microgeneration thermoelectric generators. Examples of body heat thermoelectric systems (Amar, *et al.*, 2015)(Thielen *et al.*, 2017) are powered wristwatches (Leonov *et al.*, 2009), body heat-powered flashlights, body heat-powered medical sensors (Lay-Ekuakille *et al.*, 2009), internet of things (IoT), and wireless sensor networks (WSN) for environmental monitoring (Dilhac *et al.*, 2014)(Wang *et al.*, 2013).

Various high-power capacity thermoelectric systems are available in the literature. Some reported power systems in this category include a 100W power system described in (Ahiska and Dişlitaş, 2006). An electrical output power of 214W from a thermoelectric system is in (Kaibe *et al.*, 2012). More than 1 kW of electrical power is available (Crane, Jackson and Holloway, 2001). (Wilbrecht and Beitelschmidt, 2018) reported a 2.5 kW of electrical power. An achievement of 2.713 kW from a thermoelectric system is in (Aljaghtham and Celik, 2020). An average of 3.52 kW of total output power is reported (Casi *et al.*, 2021). The production of approximately 9 kW from thermoelectric generators is available (Kuroki *et al.*, 2015). Total electric power of 45.4 kW was obtained (Mohammadnia *et al.*, 2020). (Araiz *et al.*, 2020) provided a 45.838 kW thermoelectric

power system in their report. TEG generated 55.6 kW of electricity, as reported by (Yazawa, Shakouri and Hendricks, 2017). The thermoelectric system with a maximum of 172.3 kW was presented by (Elankovan *et al.*, 2019). An annual forecast of 136 MWh from thermoelectric power systems is obtained (Champier, 2017).

Heat is the usual by-product of energy conversion processes. Generally, heat is a by-product that is discharged into the environment during energy conversion. Some of the operations in which heat goes to the environment include automotive exhaust, steel foundries, wood stoves, gas flares, candles, hot water pipes, and solar photovoltaic panels. In addition, industrial electronic systems are sources of heat (Solbrekken *et al.*, 2004), (Zhou, *et al.*, 2008). These waste heat processes can be converted to electricity through thermoelectric generators.

The automobile industry is a significant player in waste heat recovery (Crane and Lagrandeur, 2010), (Orr *et al.*, 2016), and (Cao, Luan and Wang, 2018). Cases of thermoelectrics in the automobile industry include automotive exhaust thermoelectric generators (AETEG), electric vehicles, and hybrid-vehicle applications (Achparaki *et al.*, 2012). Additionally, biomass cooking stoves, camping stoves, grills, and space heating systems integrated with thermoelectric generators for combined heat and power are known as Combined Heat and Power systems (CHP) (Y. Zhang *et al.*, 2016)(Montecucco, Siviter and Knox, 2017).

In solar thermal energy systems, energy from the sun at high temperatures concentrates on the hot side of thermoelectric generators (Olsen *et al.*, 2014), (Kraemer, Poudel, H. Feng, *et al.*, 2011). A solar thermoelectric generator (STEG) converts thermal energy to

electricity. Heat sinks are on the cold side of the TEGs. The arrangement utilises ambient air to convert the sun's heat to electricity (Kraemer, Poudel, H. P. Feng, *et al.*, 2011)(Karthick *et al.*, 2019).

The deployment of thermoelectric generators in an extreme environment is not new. Spacecraft, mars rovers, lunar power stations, power generation in Antarctica, flashing light buoys, lighthouses, and nuclear pacemakers are examples of the severe locations in which different TEG power systems are available. In such circumstances, frequent repairs or maintenance are unnecessary due to reliability and the absence of mechanical moving parts. Thermoelectric systems via suitable radioactive materials in harsh environmental conditions, such as aerospace or space thermoelectric generators, are called radioisotope thermoelectric generators (Liu *et al.*, 2017)(Yuan *et al.*, 2018).

Radioisotope thermoelectric generators (RTG or RTEG) or spacecraft electrical power systems utilise thermoelectric components and heat from the natural radioactive decay to generate electricity. The blend of Plutonium-238, in the form of plutonium dioxide as the source of heat and thermoelectric elements, had been lightweight, compact, and reliable for radioisotope thermoelectric generators (Phil Davis, Bill Dunford, 2018). A prominent example, among others, is the Voyager-01. Voyager-01 is a radioisotope thermoelectric generator space probe launched by NASA (US National Aeronautics and Space Administration) in 1977. This spacecraft is still in operation, and it has covered more than 23.429 billion km or 14.558 billion miles from the Earth without maintenance downtime. Moreover, the craft's RTEG is expected to function until 2025 (Furlong *et al.*, 1999).

2.4.1. Subsea Thermoelectricity

The following subsections reviewed previous efforts that contributed to domesticating power systems on the seafloor. This survey evaluates ideas, opinions, projects, and other information from earlier papers. Furthermore, the subsection describes the usage of thermoelectric generators within the subsea sector of the oil and gas industry, highlighting what has been done in a timeline sequence. This section also identifies the limitations of the previous work. Thus taking the opportunity for a modernized deepwater or ultra-deepwater thermoelectric power system.

Based on the discussions from the beginning of this *Chapter* and the previous ***Chapter 1***, the remaining part of ***Chapter 2*** relates to the following:

- Subsea thermoelectric system methods
- Thermoelectric system output power
- Water depth of the subsea systems
- Region of the world/subsea system location

2.4.1.1. From the 1940s to the Year 1967

Underwater application of thermoelectric generators for autonomous subsea systems probably began more than half a century ago. Since the mid-20th century, the oil and gas industry has been grappling with providing independent power sources for seabed-located equipment. Johnson (Johnson, 1967: p. 2) proposed "a marriage between nuclear and offshore drilling industries for drilling of underwater wells." Johnson’s nuclear power

package consisted of two nuclear sources, a radioisotope thermoelectric generator (RTEG) and a reactor to supply power to the subsea blowout preventer (BOP) stack and Christmas tree (XTree).

Additionally, the nuclear reactor and RTEG were to provide heat and power. Uranium U235 produced heat from kinetic energy through its fission products, while an unstable isotope within the RTEG compartment produced heat from the kinetic energy of the radiation process. The RTEG was described as a micro-ampere and mega-curie nuclear battery. Strontium 90 and Cobalt 60 were considered suitable fuel sources for the RTEG system.

The report further explained that the amount of radioactive material at any point in time was proportional to the disintegration of the radioactive source. Based on the Atomic Energy Commission test data, Cobalt 60 could produce 1.7 W/g compounds, while Strontium 90 could produce 0.23 W/g compounds. Johnson explained that nuclear-powered drilling rigs could provide more than enough power for subsea operations.

The authors' sketches of the RTEG shown below are the thermoelectric power converters, isotope source, shielding, pressure vessel compartment, and control pod. However, information is unavailable to ascertain the RTEG implementation. However, the designed water depth and the planned location of the subsea systems are also unavailable. The illustrations in *Figure 2.10* and *Figure 2.11* indicate that the nuclear reactor was meant to provide electrical power for naval vessels. Uranium U235 was the intended fuel; 20 to 1000 megawatts was the estimated power range. He concluded by seeking the offshore

industry's willingness to provide a vision for an exciting future with the power system concept.

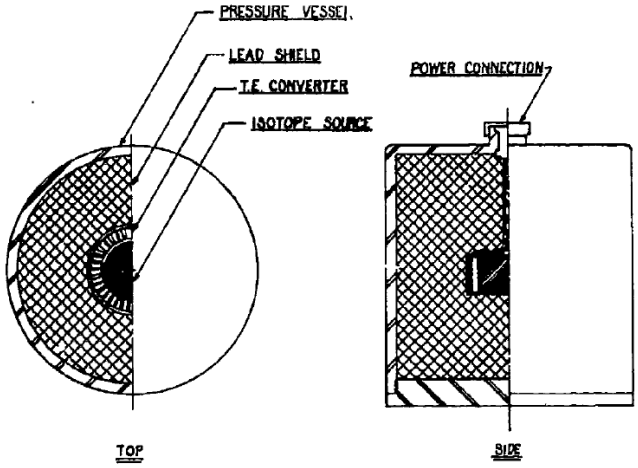

Figure 2.10 Radioisotope Thermoelectric Generator (RTEG) (Johnson, 1967)

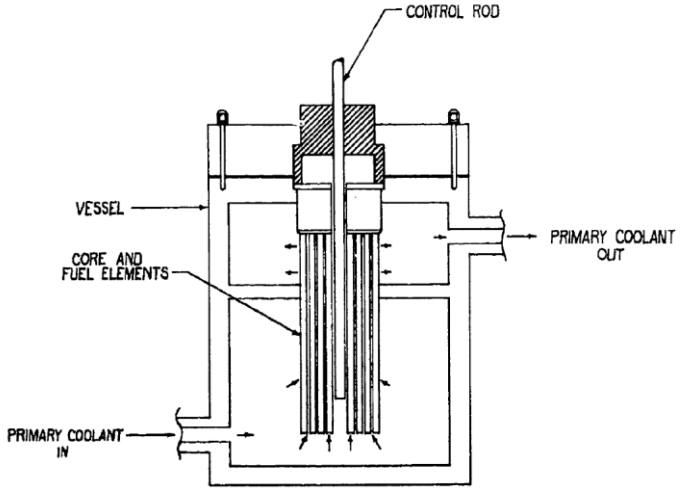

Figure 2.11 Nuclear Reactor for Subsea RTEG (Johnson, 1967)

Johnson's work was an excellent attempt to generate electricity on the seafloor for subsea equipment through nuclear and thermoelectric power systems referred to as radioisotope

thermoelectric generator (RTEG). RTEG is a power system that converts the heat or thermal energy generated by the radioactive decay of isotopes into electrical power via a thermoelectric process, as explained above in the report. Though the field implementation of Johnson's work cannot be ascertained, the advantages of the subsea RTEG would have included the ability to provide stable, predictable, and reliable power for extended periods (for decades). This type of power system has no moving parts. Hence, the risk of mechanical failure would have been minimal.

On the other hand, the disadvantage of this robust and reliable power system is the use of non-environmentally friendly radioactive materials. In the long run, this technology would have triggered severe safety concerns on the seafloor. Secondly, the manufacturing, transportation, and disposal of RTEG are risky processes. Hence, an accident in any of the processes would have led to environmental contamination. Thirdly, RTEG power output slowly decreases over time as the isotope gradually decays. Therefore, frequent replenishment would have been required for long-duration subsea operations. Fourthly, radioactive isotope production and handling are typically expensive operations. Thus, Johnson's RTEG would have needed a high initial cost.

While the radioisotope thermoelectric generator technology has some positive attributes, subsea RTEG contrasts with this study's research aim. This project focuses on designing and developing an ultra or deepwater thermoelectric power-generating system capable of harnessing geothermal heat from oil-gas reservoirs and converting it to electricity for subsea equipment on the seafloor.

2.4.1.2. From the Year 1969 to 1974

The first practical implementation of a subsea thermoelectric power system was probably in the Arabian Gulf, in the Middle East, at 22 meters of water depth. Reports are not available to ascertain if there were other thermoelectric power systems before the Arabian subsea project. Zakum subsea production scheme was intended to assess a range of seafloor production equipment operability (Lowd, *et al.*, 1969)(Goodfellow, *et al.*, 1974). Some equipment deployed for the pilot program included subsea wellheads, valves, actuators, flowlines, separators, instrumentation, and underwater power sources. (Goodfellow, *et al.*, 1974).

Power supply to subsea equipment was from a combination of six (6) power systems: underwater-based, non-underwater-based, on-site-based, and off-site (neighbouring non-subsea wellhead platform). The first power system was a subsea-based radioisotope thermoelectric generator (RTEG). The second power system was a standalone subsea thermoelectric generator (TEG), which uses the temperature difference between seawater and crude oil. The third system was an off-site and non-subsea oil expansion turbo generator. The fourth power source was a subsea-based gas expansion turbo generator. A vortex generator (a technique that utilises Ranke Hilsch-effect to obtain temperature difference in gas and lead tellurium thermoelectric modules (PbTe-TEMs)) was the fifth power source. Finally, the sixth power source was a 4.83-kilometre-long multicore submarine cable from a nearby wellhead platform carrying a DC power supply from an oil expansion turbo generator.

It was reported that the underwater pilot scheme was a success. The output power of the RTEG was given as 20W, the capacity of the off-site oil expansion turbo generator was 600W, and the provided capacity of the gas expansion turbo generator was 4kVA. However, the capabilities from the other three (3) power sources (standalone subsea TEG, the vortex generator, and multicore submarine cable DC power) were not provided.

Figure 2.12 is the Zakum subsea production unit showing the standalone thermoelectric power generator represented by the letter K. Instrumentation-control systems and other subsea equipment are denoted in the illustration.

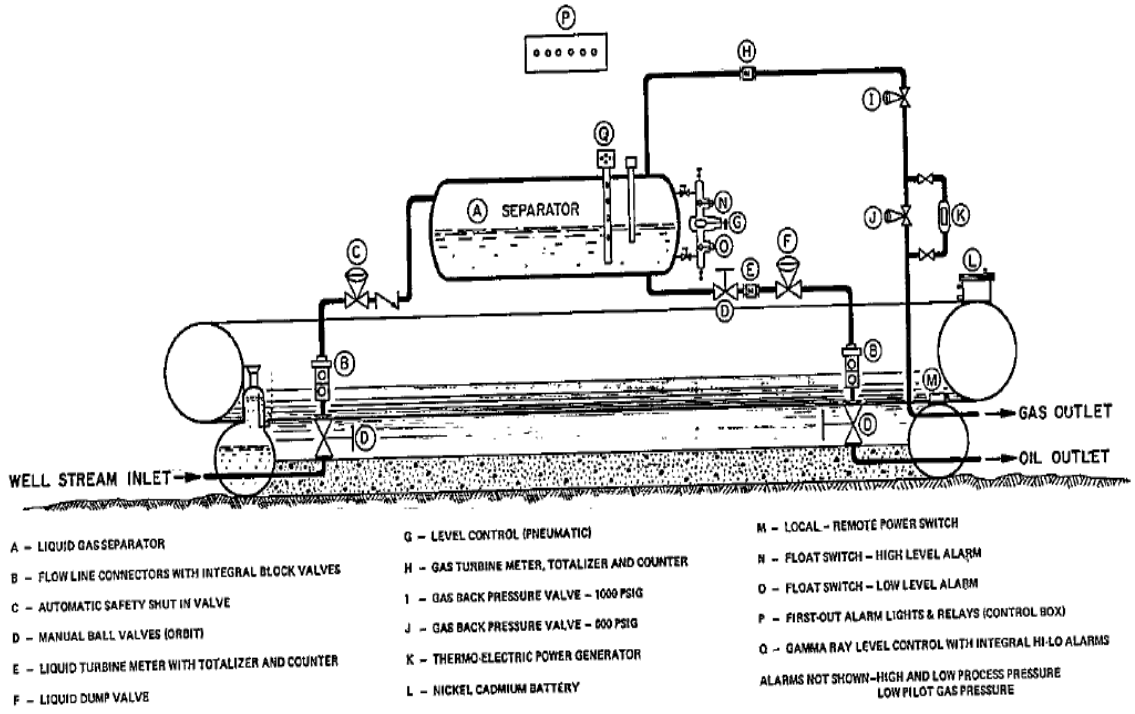

Figure 2.12 Zakum Subsea Production System (Lowd, et al., 1969)

The Zakum subsea pilot system successfully implemented six (6) different technologies. This project was one of the most important accomplishments of the subsea sector of the oil and gas industry in the Arabian Gulf in the late 1960s and early 1970s. Out of the six technologies, the subsea-based radioisotope thermoelectric generator (RTEG), subsea-based gas expansion turbo generator, and the standalone subsea thermoelectric generator (TEG) concern this research. The output power from the Zakum subsea RTEG was reported as 20W; as such, no further discussion on Zakum RTEG technology because the strength and weaknesses of the subsea-based radioisotope thermoelectric generator (RTEG) were discussed in **Subsection 2.4.1.1**.

Zakum subsea-based gas expansion turbo generator is the second power system of interest. This technology is often associated with gas turbine systems for electrical power generation. Generally, various fuels like natural gas, diesel, aviation fuels, and biofuels can be used to run expansion turbo generators. Therefore, the power output of such a power system is typically high due to the range and flexibility of the fuel sources. The Zakum subsea-based gas expansion turbo generator's output capacity was 4kVA.

Additional merits of this technology are:

- High thermal efficiency.
- Rapid start-up times.
- The capability to respond to power demand changes.

However, some of the demerits of the gas expansion turbo generator include lower efficiency at partial loads or where the power system is not functional at its maximum capacity. Secondly, it produces significant noise pollution and vibration during operation.

Therefore, the power system requires a high fuel consumption rate. Finally, a substantial initial capital cost is usually required for a subsea-based gas expansion turbo generator. A high initial cost is considered a significant drawback of this technology.

The Zakum standalone subsea thermoelectric generator (TEG) is the third technology of interest. This technology used the temperature difference between seawater and crude oil from the Arabian Gulf to generate electricity. Be that as it may, the power output capacity of the power system is not known. While this study supports subsea thermoelectricity, the Zakum subsea pilot project limitations include the need for more detailed information on the thermoelectric system methodology, including the properties and types of thermoelectric modules used in the project. The strength and applicability of the generated output power of Zakum TEG remain unknown.

Furthermore, the Zakum subsea thermoelectric generator scope was for shallow water; the safety of platform-based personnel, the environment, and assets was not the project's primary concern. Safety is the central theme of this work's proposed ultra-deepwater thermoelectric power system. A modern approach to ultra-deepwater energy harvesting and conversion to electricity will be outlined. The new approach sharply departs from the old thermoelectric power system technique. The output power from the underwater power system will be stored on the seafloor and directly supplied to critical subsea equipment. This new concept of energy generation at the seafloor will prevent unplanned power outages and emergencies.

2.4.1.3. From 1975 to the Year 1989

(Young, 1989) reported the only subsea-based related thermoelectric activity in the 1980s. The author described an autonomous subsea control system as an umbilical-less system or a system capable of thinking for itself. He explained that an oil and gas production system should be able to shut in or start up independently.

In the quest for an alternative power source to achieve these feats for such self-supporting subsea controls, the following power sources were considered:

1. Nuclear Power System
2. Recharge Battery System
3. Stirling Engines
4. Closed-Cycle Diesel Engines
5. Fuel Cells System

Nuclear power was the number one power source eliminated from his list, as chances of securing authorisation from the Department of Energy (DOE) were slim. After an intensive study, the remaining four options were also dropped. The common factor among the power sources was the requirement for frequent intervention after seafloor deployment.

In the discussion, the author was neither for nor against using subsea umbilicals but was left with two choices: a thermoelectric generator and an underwater water turbine driven by high-pressure, high-velocity flow from a water injection system.

The report described the subsea thermoelectric power system as a highly reliable option without moving parts with potential battery backup during system shutdown. However,

Young's argument favoured the underwater water turbine without clear-cut explanations of the moving parts of the water turbine system.

Additionally, satisfactory answers were not provided in the report to the questions on a production system without the need for water injection and provisions for chemical injection for a production system without an umbilical. Lastly, start-up issues were not adequately addressed when valves on the water injection Christmas trees were closed.

Records are not available to show if Young's underwater water turbine proceeded to implementation as the only underwater power system reported between 1975 and 1989. The underwater water turbine or marine hydro-kinetic turbine energy system converts ocean currents or tidal flows to electrical power. This technology's benefits are high energy density due to its capabilities for capturing significant ocean currents and tidal flows. Secondly, tidal currents can be predicted; thus, the technology allows efficient planning for subsea operations. Thirdly, underwater water turbines have a relatively low environmental impact.

On the other hand, the challenges of this technology include limited applicability because strong and consistent tidal or ocean currents are geographically location-specific. Secondly, underwater water turbines can disturb marine ecosystems, creating environmental concerns. Thirdly, having mechanical moving parts is a drawback. Also, it is an expensive technology. Finally, this research uses a thermoelectric generator to harness and convert waste heat from subsea oil-gas reservoirs into electricity.

2.4.1.4. From the Year 1989 to the 1990s

In the 1990s, von der Weid and his co-author's work was one of the subsea thermoelectric systems in Brazil that received attention (von der Weid, J. A.P. da Silva, *et al.*, 1993). The generator used the difference in temperature between crude oil and the surrounding seawater to generate electricity. The seawater temperature at the seafloor in the region is approximately ten (10°C) degrees Celsius, while the temperature of crude oil from subsea wells is typically above 60 °C.

The constructed generator had a heat source at the top of a stainless-steel block. Thermometers were used for temperature measurement between thermoelectric modules. Other components were resistor connections across the terminals of the thermoelectric modules and thermal insulation for maintaining heat flux between the experimental setup and the environment.

The authors achieved two prototype thermoelectric generator power systems rated 1-W and 10-W. However, it was not stated if the project proceeded to the offshore implementation phase. *Figure 2.13* shows the results from the 1-W subsea thermoelectric power system.

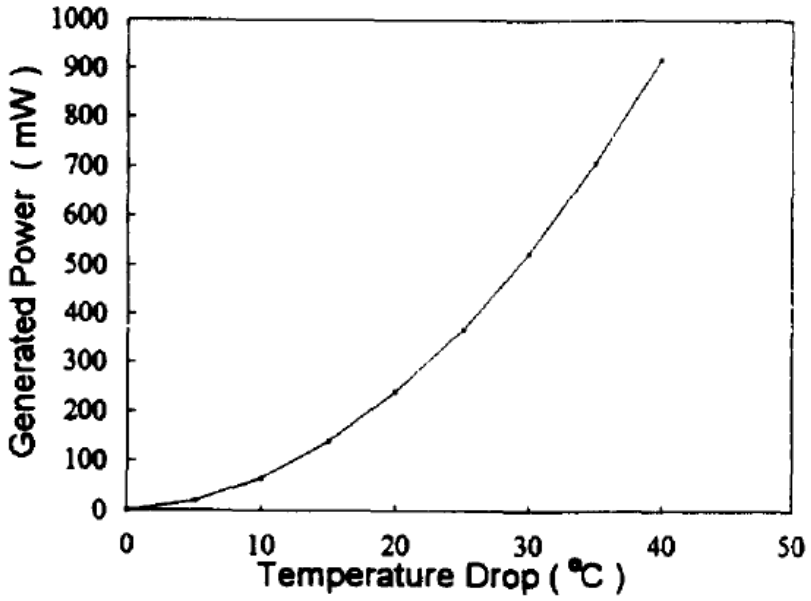

Figure 2.13 1-W *Subsea TEG* (von der Weid, J. A.P. da Silva, *et al.*, 1993)

Subsea thermoelectric power generation gained prominence in South America in the early 1990s. It was widely known that electric power could be generated on the Brazilian seafloor at a temperature difference of roughly 60 °C by 1993. The 1 W and 10 W TEGs were significant achievements, considering that the project was a collaboration between academia and the oil-gas industry. However, von der Weid and the co-author's work was manually intensive; low-standard thermometers and other devices were used for measurements and data acquisition. This research is geared toward deepwater or ultra-deepwater thermoelectric power generation; as such, modern computer-based data capture techniques, computer algorithms, and models will be used to predict the behaviour of the power system under varying seabed conditions.

Another thermoelectric power system that came to the limelight in 1993 was SPARCS, which stands for Subsea Powered Autonomous Remote-Control System (Theobald, 1993). SPARCS was planned to provide a low-cost power system solution to justify future subsea developments without needing electro-hydraulic control umbilicals. The systems had two power sources: a power supply from a turbine generator on a subsea water injection flowline and a subsea thermoelectric generator.

A hydraulic power system was also designed to operate the subsea wellhead system/downhole safety valves via a subsea unit. Signals from the underwater communication system for subsea Christmas tree valves, control, and sensor monitoring were via a seafloor-located acoustic telemetry system that used seawater as a transfer medium.

The predicted subsea production cost reduction for ten years was £72.5 million and £87 million per annum hydrocarbon reserves based on five single subsea wells at an offset of about 7.5 km. Saltire North Sea well number #15117-222 in the United Kingdom was nominated for the subsea demonstration activities for 18 months.

The estimated minimum electrical output power from the power sources was 100 W and three (3) phase AC power with a voltage rating ranging from 11 VAC to 20 VAC. *Figure 2.14* illustrates the proposed SPARCS system. However, further details on project execution were not given.

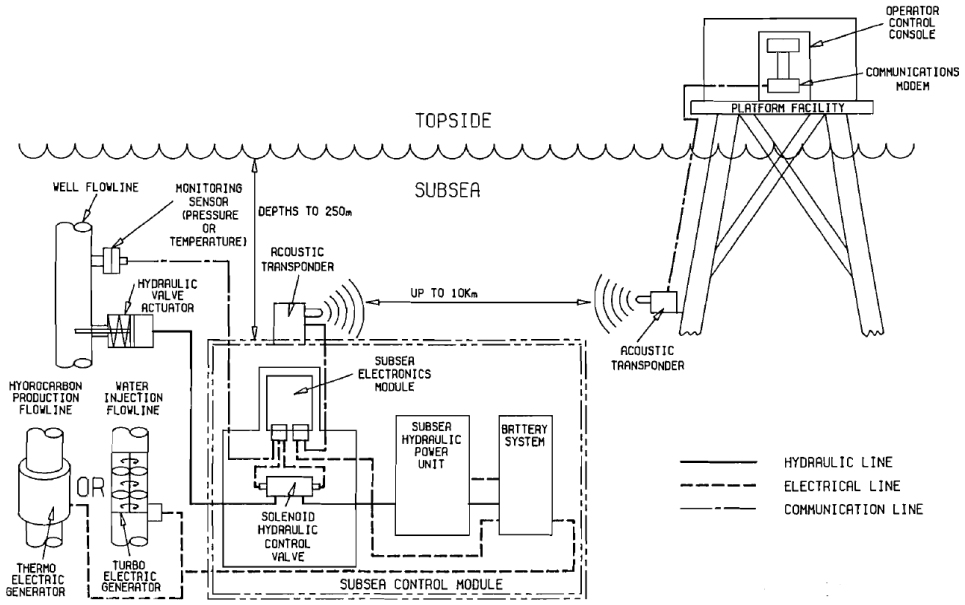

Figure 2.14 SPARCS System (Theobald, 1993)

(Theobald, 1994) reported that the field trial of the SPARCS project was due to start in 1995. The author explained that the design life of the SPARCS system was 20 years with periodic maintenance. The targeted system availability was expected to be 98%, with a possible downtime of only ten days. The prototype of the underwater thermoelectric generator at the pre-encapsulation stage is in *Figure 2.15*.

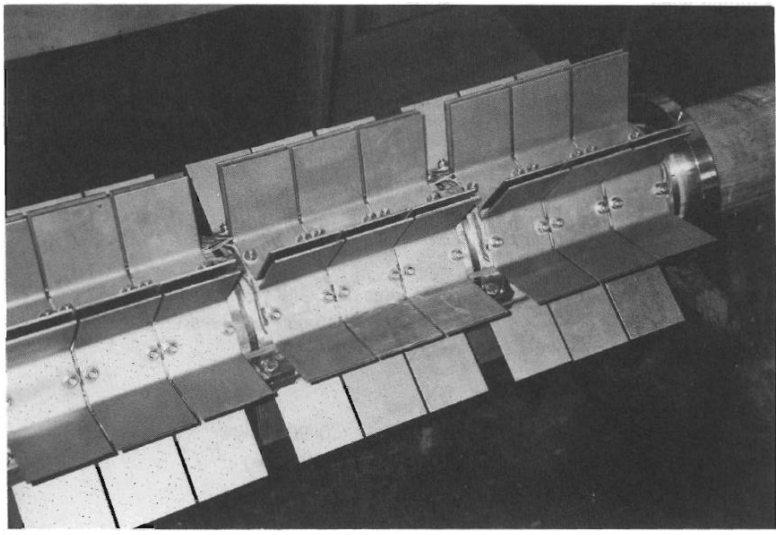

Figure 2.15 20 W TEG for SPARCS Project (Theobald, 1994)

SPARCS was a noteworthy attempt at mainstreaming subsea procedures on the seafloor, thereby reducing the cost of operations. The projections were for an output of 100 W from a subsea thermoelectric generator and 11 to 20 VAC three (3) phase AC power from a turbine generator. However, the idea of eliminating control umbilicals leaves more to be desired. Hence, the SPARCS approach was more like a one-size-fits-all solution.

The merits and demerits of the turbine and subsea thermoelectric generators were discussed above (**Subsections 2.4.1.2**. to **2.4.1.4**). The electric power generated from the proposed underwater power system will be converted to AC power and supplied to subsea equipment. Subsea system control, monitoring, and signal transfer will be wired (through control umbilicals). Furthermore, wireless (through non-wired communication channels) will be supported. The planned deepwater power system will support the latest 'seafloor-to-cloud-based' technology for redundant and reliable subsea operations.

A related publication (Loth, 1995) described the umbilical as the control system's most significant single-cost component in subsea projects for North Sea applications at about 150 m water depth and 15 km offset. The report stated that subsea system autonomy aimed to eliminate the umbilicals.

He stated further that electrical power requirement is one of the factors that could lower system cost and suggested using a thermoelectric device-powered control system in a closed-looped acoustical link as an attractive power and communication system. However, considering the low system charge rate, he pointed out that efficiency was of concern.

The second power system considered by the author was a system that utilises produced or injected fluids such as a gas expander unit. According to the author, the advantages of this type of power unit included a high charge rate. However, the problematic nature of subsea rotating equipment was of concern. Other challenges included the conditioning of produced fluids before use in the generator, and associated pressure drop across generator drivers were undoubtedly cause for concern.

The marginal field expert said an independent power-generating system of up to 120 W constantly from 8000 barrels of oil per day (BOPD) was possible through a closed-loop turbo alternator flowline generator integrated with a thermoelectric heat exchanger.

Figure 2.16 shows an umbilical-less system capable of transmitting electrical signals via pipe-wall and seawater to an offshore platform. While substantial cost savings are some benefits of the various alternative power options, the author concluded that a replacement for an electrohydraulic control system in subsea development does not exist.

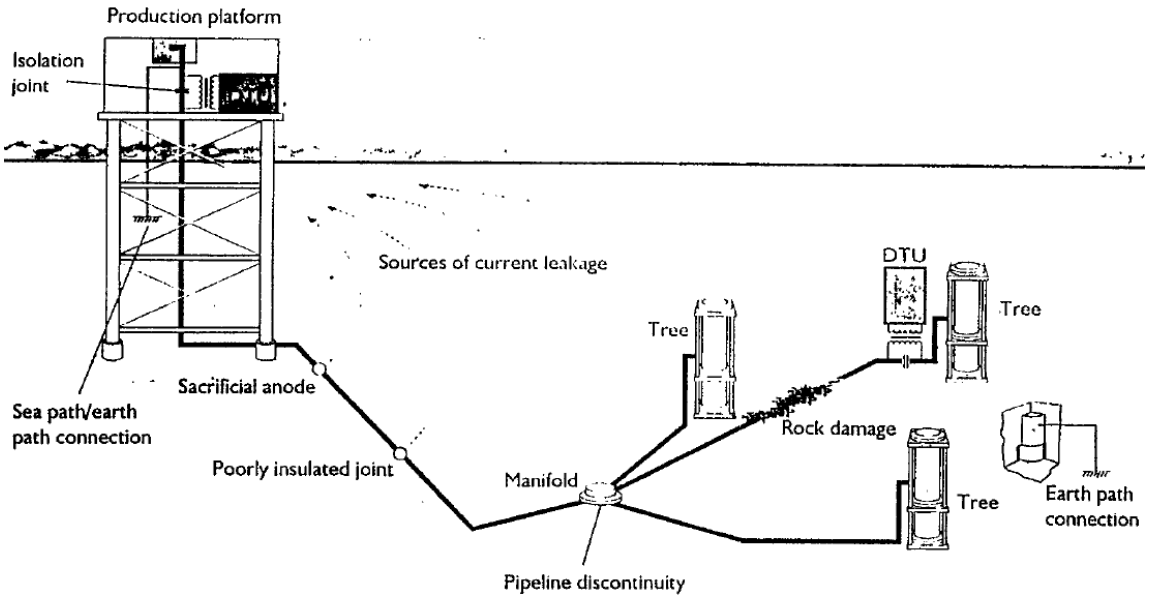

Figure 2.16 Umbilical-less System (Loth, 1995)

The positive support for electrohydraulic control systems using control umbilicals in subsea oil and gas field development in the North Sea was a breath of fresh air in 1995. Loth's overwhelming support for a turbo alternator flowline generator integrated with a thermoelectric heat exchanger was partly because of the low efficiency of the thermoelectric power system.

The highlights of turbo alternator power generation are as follows: this technology combines turbo alternator and thermoelectric devices to convert thermal energy into electrical power. The technique allows for dual energy conversion. That is, the capturing of mechanical energy (via alternator) and thermal energy (through thermoelectric devices). This double conversion approach enhances overall system efficiency.

The challenges of turbo alternator power generation include the requirement for sophisticated system engineering, resulting in a complex and cumbersome power system. The initial cost of such a system is high. Furthermore, the presence of mechanical moving parts is a drawback. Lastly, designing and maintaining any complex system often comes with several difficulties. As such, simplicity is suitable for remotely located power systems. This project supports simple and rouged technologies. The deployment of the electrohydraulic control system is also supported. In addition, this work is a pro-deepwater or ultra-deepwater thermoelectric power system poised to reduce the overbeating dependence on platform or topside-based power systems for oil-gas exploration and production.

Due to the need for an alternative power source, performance, cost, and reliability of subsea umbilicals and underwater batteries, (Auckland *et al.*, 1995) constructed a one-meter-long thermoelectric generator on 150 mm diameter pipework.

The laboratory-based setup consisted of thermoelectric modules machined and clamped on the pipework. Separately mounted hot and cold-water tanks were fitted with pump and piping fixtures for dispensing hot and cold water. The arrangements had thermocouples measuring temperatures in the hot water flow and the cold-water tank.

Figure 2.17 is a diagram of the power-generating system. The team reported that twenty watts (20 W) was derived from the power system. Further details on this project are not available.

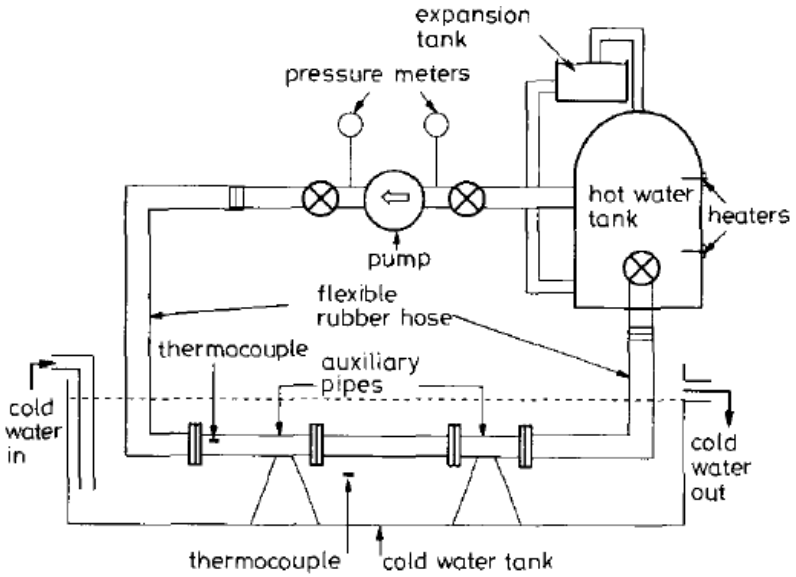

Figure 2.17 Thermoelectric Generator Test Rig (Auckland *et al.*, 1995)

Although this research championed deepwater thermoelectric power system, as evidenced in the above subsections, this project also supports the laboratory-based thermoelectric power system developed by (Auckland et al., 1995). The system generated 20W of electric power through thermoelectric modules on pipework, hot water, and cold-water fluid flow systems.

However, in Auckland's work, thermoelectric modules were machined and clamped on the pipework. The machining of thermoelectric modules, pipelines, or any flowline underscores the integrity and structural reliability of the thermoelectric modules and the pipework. Therefore, this project's deepwater thermoelectric power system will be designed and developed via a portable test bench (test rig) in which thermoelectric

modules and other power system devices are assembled and disassembled easily without the need for machining, cutting, uncoupling, or undermining the integrity of any of the parts of the power system.

In another development, (Dubourdieu *et al.,* 1997) reported prototype thermoelectric generators for a subsea production control system. In the submission, the North Sea seawater temperature was given as four degrees Celsius (4 °C), and the fluid-flowing mixture of oil, gas, and water temperature ranges from 90 °C to about 120 °C. At the same time, the seabed pressure rating was approximately 6527 psi.

Thermoelectric modules were machined on subsea flowlines in rows and columns connected in series and parallel configurations. Other components of the power system were the resistive load and battery system. The power device's electrical, thermal, and mechanical characteristics were tested at a wet dock in Cherbourg, France.

The underwater power system generated about 100 W at 70V after two (2) months of field testing. One of the thermoelectric generator characteristics curves against seawater at a subsea wellhead is in *Figure 2.18*.

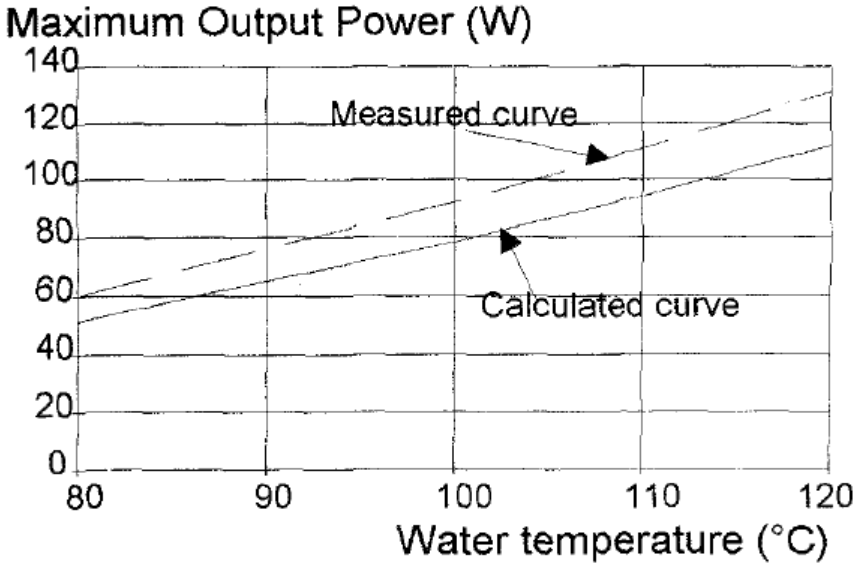

Figure 2.18 TEG Output Power vs Water Temperature (Dubourdieu *et al.*, 1997)

(Dubourdieu et al., 1997) work showcased some of the essential characteristics on and beneath the seafloor of the North Sea. Furthermore, achieving 100 W at 70 V after two (2) months of field testing at a wet dock in Cherbourg, France, proves that a thermoelectric power system can supply electricity to subsea equipment.

However, Dubourdieu's thermoelectric generator was made from machined-out thermoelectric modules on subsea flowlines. As previously mentioned, this research does not support the old method of altering or damaging the integrity and reliability of the power system components. Hence, this project will present a modern approach that is devoid of fiddling with power system components for energy harnessing and harvesting for deepwater oil-gas fields.

In their report, (Garbuglia *et al.,* 1997) concluded that over the years, various prototypes of autonomous underwater power generation techniques, including subsea batteries and thermoelectric generators, have been proven; however, industrial acceptance has not been gained. Furthermore, they said the oil and gas industry had shown less interest in autonomous control systems despite the enormous amount of work already presented.

Correspondingly, the lack of interest might have been attributed to the inability of these technologies to cover a broader spectrum of applications. In the report, the authors pointed out that the subsea sector of the industry was supposed to offer a form of leadership direction. Such a proposition should include a portfolio of different technologies to enable prospective operators and system developers to provide solutions on a complete system. Furthermore, the authors noted that an industry-driven autonomous control system could achieve low cost and risk reduction benefits.

(Garbuglia *et al.,* 1997) suggested that the field-based applicability of the technologies could boost operators' confidence. In addition, research initiatives on in-situ electric power, hydraulic power, and signal transmission could enable oil-gas system manufacturers and producers to face more challenging underwater scenarios.

Finally, against the backdrop of appointing a single supplier for all the technologies, the developers of the subsea control system stated that equitable opportunities should be provided to traditional and non-traditional suppliers to develop optimal products.

From the above, (Garbuglia *et al.,* 1997) report confirms that the subsea sector of the oil and gas industry can implement seafloor-based power systems that could eliminate the

dependence on platform-based power systems. Unfortunately, the industry lacks the zeal to give any of the several technologies the full backing they deserve. Such indictment introduced leadership weakness or a sense of inability. The effects of such leadership absence are still felt to this day. Therefore, this research fills the gap and brings back 'light at the end of the tunnel.' A deepwater thermoelectric power system will be designed and developed for deepwater and ultra-deepwater oil-gas fields. Secondly, this project will offer suggestions and recommendations that could be formulated into guidelines, regulations, and industry standards in subsea operations.

After a period of silence, it was reported that the SPARCS (Theobald, 1993) (Dubourdieu, *et al.,*1998) was suspended five years after project initiation. The project was replaced with APAC (Autonomous Power and Control System). Prototypes of the new APAC were built and independently tested to prove their feasibility.

A full-scale production system consisting of two (2) thermoelectric generators housed in a flowline spool was built and tested. Other components that made up APAC were lead-acid batteries, electro-hydraulic control systems, electronic elements, and hydro-acoustic communication systems. The 56 thermoelectric modules power system produced about 100 W at 70 V for 120 °C effluent temperature. The thermoelectric generator was the primary power source and was referred to as a reliable alternative to a platform-based power supply through umbilical.

Figure 2.19 and *Figure 2.20* depict the autonomous power and control system (APAC) as an umbilical-less subsea well control system, electrical-hydraulic-communication layout, and other underwater power system components. The final system development phase was a proposed subsea installation on a production well to prove long-term system performance and reliability. However, reports on field trials or other subsea thermoelectric projects are unavailable.

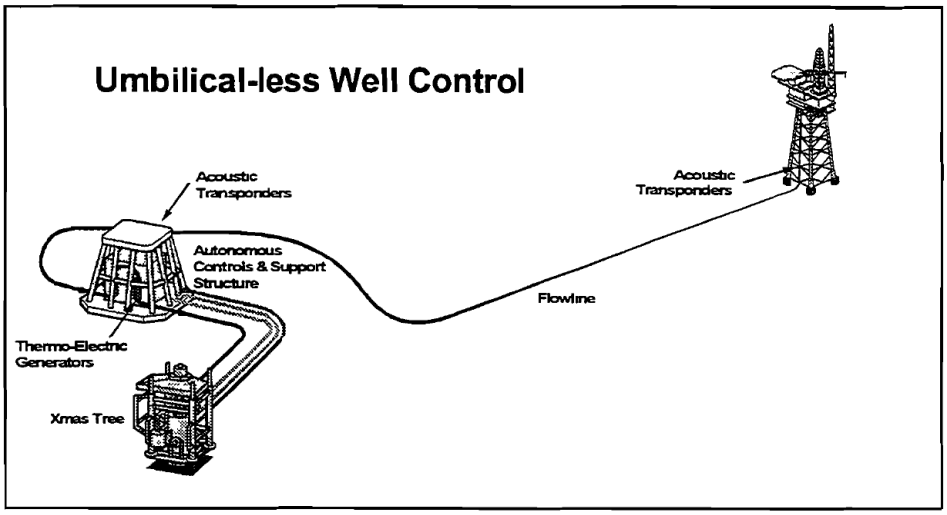

Figure 2.19 Layout of APAC for Subsea Producer (Dubourdieu *et al.*,1998)

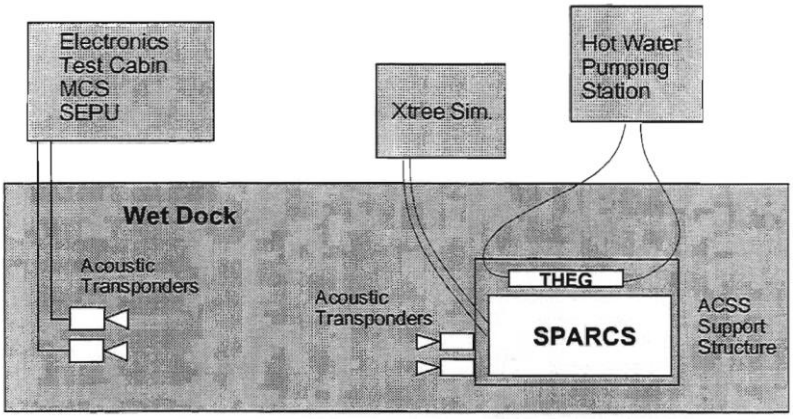

Figure 2.20 TEG and Components Performance Tests (Dubourdieu *et al.*, 1998)

The dissolution of SPARCS and the formation of APAC was not surprising due to the one-size-fits-all approach of the project. APAC thermoelectric power system generated approximately 100 W at 70 V from 56 thermoelectric modules on a flowline spool. The output power was considered a step in the right direction. However, the technique most frequently used in the 1990s involved machining thermoelectric modules on a flowline or pipeline. This research does not support this method because it directly affects the power system components vis-à-vis the output power. As discussed above, this deepwater thermoelectric power project will offer a more effective method of waste heat harvesting and conversion into electric power.

2.5. Subsea Thermoelectricity: Summary & Research Gaps

Studies have shown that waste heat from oil-gas reservoirs can be harnessed, converted into electric power, and supplied to subsea equipment on the seafloor. However, available

subsea project reports have not addressed the direct applicability of the technology to seabed-located subsea equipment. Additionally, the impacts of power failure from platforms or topsides-based power systems to subsea equipment, personnel safety, environmental issues, and loss of assets are not of concern in the papers under review. Such information is not available elsewhere. The bare minimum requirements for any subsea project are quality, functionality, operability, reliability, aesthetics, personnel safety, assets, and environmental protection. None of the above subsea thermoelectric projects encompasses the bare minimum.

Secondly, studies revealed that most subsea thermoelectric schemes are shallow water-prone systems, and obsolete methods of harnessing geothermal energy at the seabed were deployed. Furthermore, industry standards, regulations, codes, and guidelines on subsea thermoelectric power systems or other offshore renewables are yet to be created. In some cases, available information are too vague to help with design, manufacturing, installation, and operation. Indeed, these issues are pretty troubling.

Thirdly, the West African waters with various renewable energy potentials do not have a single thermoelectric power system or any offshore-based renewable power sources to support the numerous shallow-water, deepwater, and ultra-deepwater oil-gas operations. It is worrying that such a posture does not portray the oil and gas industry well. Thus, these factors influenced the design and development of a deepwater thermoelectric power system using the deepwater and ultra-deepwater characteristics in West Africa to overcome the challenges of underwater power generation and electricity supply to subsea equipment.

The next chapter ***(Chapter 3)*** introduces a new approach to creating a deepwater thermoelectric power system (DTEG) for harvesting and converting heat from deepwater or ultra-deepwater oil-gas reservoirs to electricity. Electrical energy will be stored as chemical energy and supplied as electrical power to seabed-located equipment. Furthermore, DC power will be transformed into AC power and delivered to an underwater electrical power grid system for possible supply to subsea equipment and back to shore when there is a surplus at the seabed. The new underwater power system will significantly reduce the dependence on the topside or platform-based electrical power transmission to the seafloor equipment during exploration and production. The new system will guide against unplanned power failure, thus preventing accidents and possible loss of life. The new power system will use flexible deepwater power plates on subsea infrastructures. To conclude, this underwater power system is not location-specific; the method can be deployed in any deepwater or ultra-deepwater oil-gas field across the globe.

Chapter 3

Deepwater Thermoelectric Power System

3.1. Introduction

Chapter 3 sets out the foundation for an underwater combo power system. This unconventional underwater combo power system combines offshore renewable energy and non-renewable energy potential in West Africa. This study examined the possibility of harvesting waste heat from deepwater or ultra-deepwater oil-gas reservoirs and converting it into electricity during oil-gas exploration and production. As such, the deepwater thermoelectric power system (DTEG) takes centre stage, as shown in the underwater combo power system architecture in *Figure 3.1.*

The underwater power system network has provisions for traditional platform-based power sources (power from a drilling rig and an FPSO), OTEC (Ocean thermal energy conversion), and other offshore-based renewable solutions. Furthermore, the illustration has power system components such as DC-DC converters, power conditioners, AC-DC rectifiers, DC-AC power inverters, and bidirectional converters. Other items are power-demanding components such as subsea AC equipment, subsea DC equipment (loads), subsea battery charging stations, and ROV/AUV charging stations.

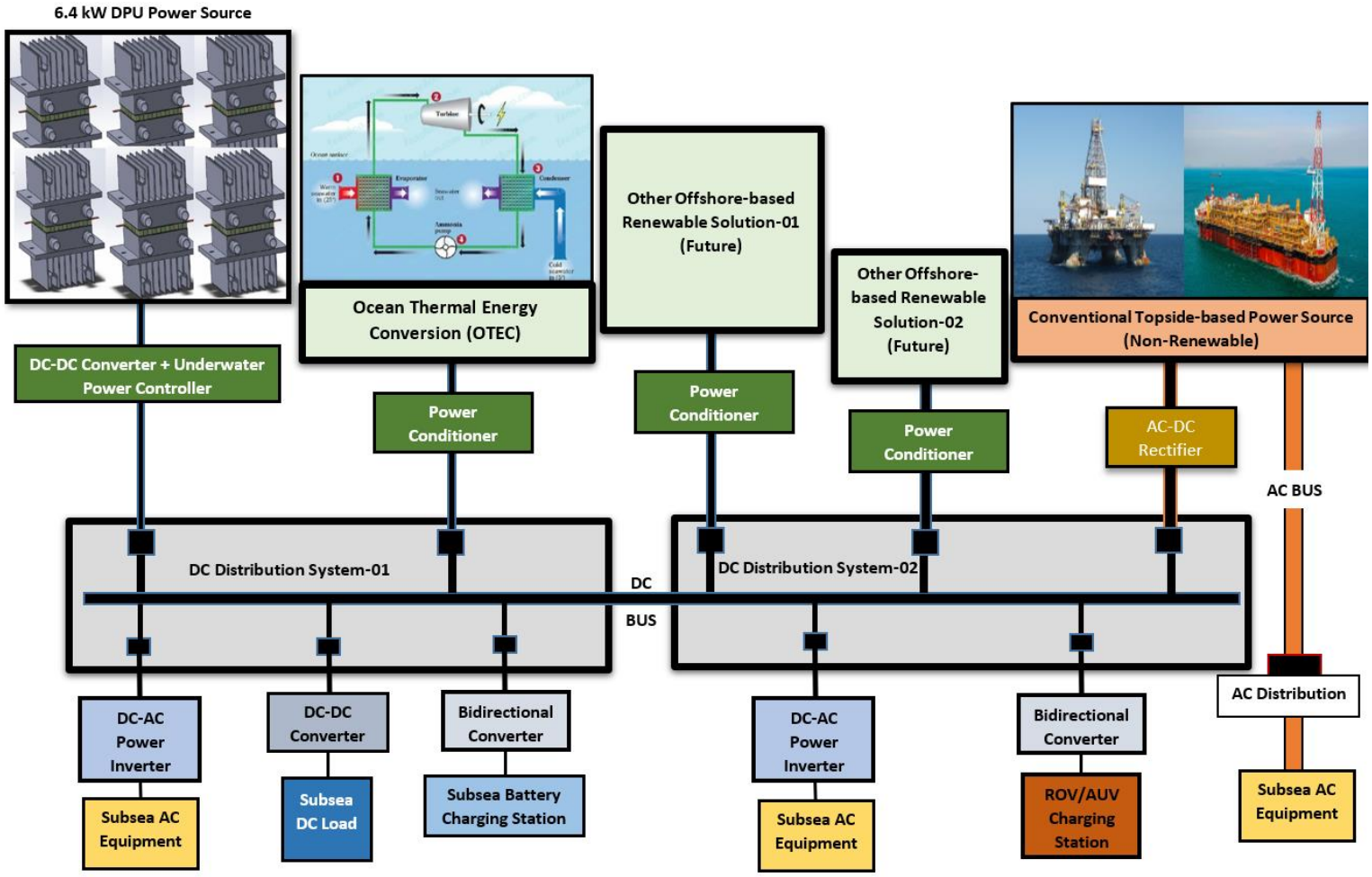

Figure 3.1 Underwater Combo Power System Architecture

The following section aims to develop deepwater thermoelectric modules (DTEMs), deepwater thermoelectric power plates (DPPs), and deepwater power units (DPUs) while attempting to answer the research question:

How best can energy be generated at the seafloor to provide electrical power to critical subsea control equipment during deepwater or ultra-deepwater oil-gas exploration and production activities?

3.2. Deepwater Thermoelectric Module

Based on ***Chapter 2*** (literature review), the most suitable TEM for deepwater thermoelectric power generation would be the nanotechnology-driven elements made from the 3rd generation thermoelectric materials in which the ZT values are upwards of 2.0. This thermoelectric materials category has a conversion efficiency of 15% to 20% (Kanatzidis *et al.*, 2014). Nano-tech TEM materials would make the conversion of waste heat to usable energy a seamless process during deepwater or ultra-deepwater oil-gas exploration and production.

Nanotechnology-based thermoelectric generators take advantage of the advancements in nanomaterials to boost energy conversion efficiency and performance. This class of materials uses nanostructured materials to increase thermoelectric properties, thus allowing better heat-to-electricity conversion. Nanostructured materials include nanoparticles, nanowires, and thin films. These material structures are manipulated at the nanoscale to achieve higher electrical conductivity while reducing thermal conductivity,

resulting in improved heat conversion into electricity efficiency. Nanotechnology-inspired materials are shown in *Figure 3.2*.

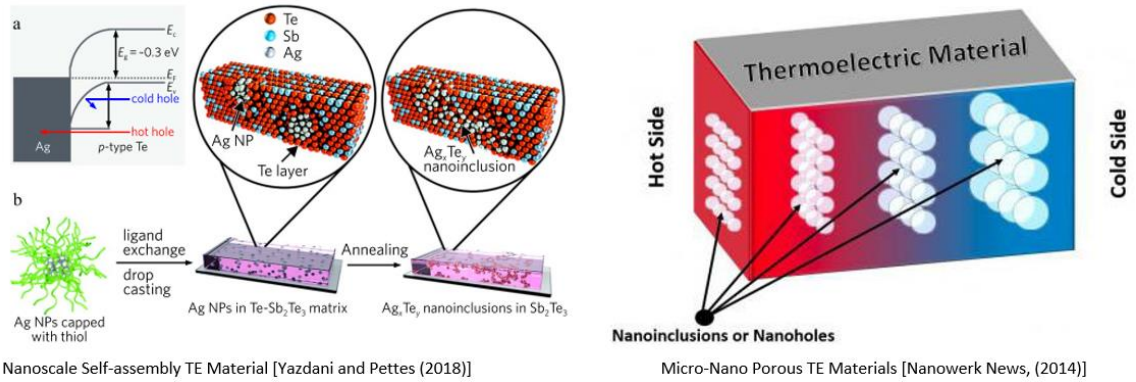

Figure 3.2 Nano-Tech inspired Materials (Yazdani&Pettes, 2018)(Nanowerk, 2014)

The advantages of nanotechnology-based thermoelectric generators are enhanced efficiency, improved performance, higher potential for waste heat recovery, flexibility, and custom or tailored material design. However, the disadvantages of this class of thermoelectric materials include challenges related to complex fabrication processes, scalability, and high-cost issues. Therefore, these issues must be addressed for the widespread commercial adoption of nanomaterials. Additionally, nanotechnology thermoelectric generators are primarily research-based or laboratory-scale power-generating systems. Transition to industrial-scale production methods for nanotechnology thermoelectric generators are yet to be established. For these reasons, flexible nanotechnology thermoelectric generators are not available in the marker. Hence, commercially available thermoelectric generator modules were used in this project.

3.3. Commercial Thermoelectric Modules

As stated above, the unavailability of flexible nanotechnology thermoelectric generators led to the use of commercially available thermoelectric devices and power system components. The global quest for green energy or sources from nature has increased the number of manufacturing houses for various renewable energy components and accessories. For example, thermoelectric modules and thermogenerator components were initially used for space projects and military applications from the 1940s to the 1960s. The main reason for this was their reliability in power generation and the need for little or no maintenance; as such, they were not widely available to the civilian populace (D. M. Rowe and Gao Min, 1998). However, the situation is different nowadays. Hence, in no particular order, some of the companies manufacturing thermoelectric modules (TEMs) and related components include:

- Melcor Corporation
- EURECA Messtechnik GmbH
- Z-Max Japan
- ADV-Engineering
- Thermion
- Kryotherm
- OSTERM
- Hi-Tech Technologies, Inc.
- Komatsu
- Hi-Z Technology, Inc.,
- P&N Technology (Xiamen) Co., Ltd.,
- TECTEG MFR.

- European Thermodynamics Limited

An assessment of thermoelectric modules for power generation from some of the above-listed manufacturers showed devices with power ratings ranging from 1 to 36 W from a single TEM at various operating temperature differences sold at diverse prices. For instance, a TEM rated at 36 W could be sold at USD 100.00 by Manufacturer-X. On the other hand, a TEM rated at the same 36 W from another manufacturer (Manufacturer-Y) could be sold for USD 60.00. Elsewhere, a 1-W TEM from Manufacturer-Z could cost USD 100.00. Hence, the market has no uniformity regarding thermoelectric module prices, sizes, shapes, and power ratings. Please note that trade names are not used in this work.

Another notable feature among the manufacturers was that the maximum power of each of the TEMs was obtained at different temperature differences. For example, the power level of a 1-W TEM could be obtained at a temperature difference of 200 °C for a specified resistive load value from Manufacturer-P. In contrast, Manufacturer-Q could derive a power level of 36 W TEM at 300 °C for a different resistive load value. Therefore, product operating characteristics vary among manufacturers. However, a common factor among commercial manufacturers was that the maximum power of a TEM at a specified resistive load was obtained when the temperature difference across the devices was upwards of 100 °C.

From the above discussion on commercially available thermoelectric modules, the subsea temperature difference for thermoelectric power generation is less than 200 °C. An example of deepwater oil and gas reservoirs in which the subsea well fluids temperature is slightly above 126 °C is the Cascade and Chinook fields in the US Gulf of Mexico

(GOM) (Haddad *et al.*, 2011)(Mattos *et al.*, 2013). Then, if the assumed maximum seabed temperature at the GOM is between 4 and 10 °C, the temperature difference would be approximately 116 °C. Therefore, a deepwater thermoelectric power system in the US Gulf of Mexico would be operating at about 122 °C to 116 °C.

Another example is the Gulf of Guinea. The oil-gas temperature from some deepwater and ultra-deepwater wells in Nigeria ranges from 40 to 116 °C while the seabed temperature is about 4 °C (Schoppa *et al.*, 2007)(Ekejiuba, 2021)(Li *et al.*, 2020). The temperature difference between oil-gas and the seabed in the North Sea is roughly 116 °C. In Brazil, the difference between the oil-gas reservoir fluid flow and seabed temperature is less than 80 °C (von der Weid, J. A.P. da Silva, *et al.*, 1993). Therefore, it was considered that the temperature difference for a deepwater thermoelectric power system is generally less than 200 °C. From these synopses, any of the above-listed manufacturers or duly qualified manufacturers knowledgeable in subsea systems can be called upon to manufacture suitable thermoelectric modules and devices for a deepwater thermoelectric power system.

Thermoelectric modules selected for this project were from Manufacturer-A and Manufacturer-B. (*Again, please note that trade names are not used in this work*). Device-TEM-00 was from Manufacturer-A. This research regarded Device-TEM-00 as a reference thermoelectric module (Ref-TEM). The reference TEM serves as a guide; thus, the information presented in *Table 3.1* was assumed to be typical for thermoelectric power-generating modules.

Three types of thermoelectric modules, namely Device-TEM-01, Device-TEM-02, and Device-TEM-03, were purchased from Manufacuturer-B. As shown in *Figure 3.3*, the TEMs were of different shapes, sizes, and prices. Low product cost, prompt delivery, and the author's proximity to Manufacturer-B were some of the reasons for the product choice. *Table 3.2* contains the operating specifications of the three thermoelectric modules from Manufacturer-B.

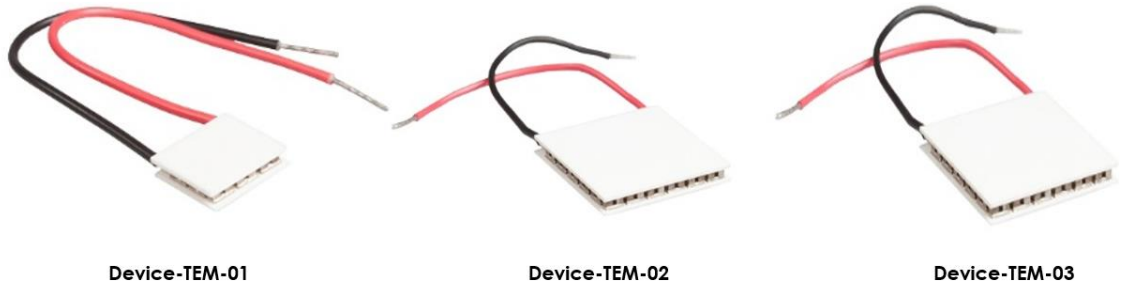

Figure 3.3 Thermoelectric Modules from Manufacturer-B

3.4. TEM Selection for Deepwater Power Output

After purchasing commercially available thermoelectric modules, the next step was a selection process based on the output power from the TEMs. As such, a test rig (or a test bench) was set up to pick a suitable TEM from the three (3) thermoelectric modules (Device-TEM-01, Device-TEM-02, and Device-TEM-03) from Manufacturer-B for potential deepwater application.

Table 3.1 Reference Thermoelectric Module (Manufacturer-A)

Thermoelectric Module (Ref-TEM)	**Device-TEM-00**
Parameters	**Value**
Hot-side Temperature (T-Hot)	250 °C
Cold-side Temperature (T-Cold)	50 °C
Matched Load Output Power (P-Max)	25.5 W
Matched Load Resistance (R-Load)	1.26 Ohms
Open Circuit Voltage (VOC)	11.3 V
Matched Load Output Current (Imp)	4.7 A
Matched Load Output Voltage (Vmp)	5.6 V
Heat Flow through Module	777 W
Hot-side Max. Temperature (T-Hot max)	350 °C
Cold-side Max. Temperature (T-Cold max)	50 °C
Heat Flux	17 W/cm2
Efficiency	4%
Maximum Compression	Not Provided
Mass	71 g
Length	0.0745 meters
Width	0.068 meters
Height	0.005 meters

The device's thermoelectric material was Bismuth Telluride (Bi2Te3). Device-TEM-01 had 31 thermocouples, while Device-TEM-02 and Device-TEM-03 had 127 thermocouples. As shown in *Table 3.2* or the datasheet, the maximum output power at different matched load resistances obtained from each device at the manufacturer's facility for a temperature difference of 220 °C is 2.50 W, 4.02 W, and 6.99 W, respectively.

Table 3.2 Thermoelectric Module Specification (Manufacturer-B)

Thermoelectric Modules (TEMs)	**Device-TEM-01**	**Device-TEM-02**	**Device-TEM-03**
Parameters	**Value**	**Value**	**Value**
Hot-side Temperature (T-Hot)	250 °C	250 °C	250 °C
Cold-side Temperature (T-Cold)	30 °C	30 °C	30 °C
Matched Load Output Power (P-Max)	2.50 W	4.02 W	6.99 W
Matched Load Resistance (R-Load)	0.36 Ohms	6.89 Ohms	3.65 Ohms
Open Circuit Voltage (VOC)	1.90 V	10.52 V	10.11 V
Matched Load Output Current (Imp)	2.63 A	0.76 A	1.38 A
Matched Load Output Voltage (Vmp)	0.95 V	5.26 V	5.05 V
Heat Flow through Module	Approx. 50W	Approx. 80.4W	Approx.139.8 W
Hot-side Max. Temperature (T-Hot max)	250°C	250 °C	250 °C
Cold-side Max. Temperature (T-Cold max)	175 °C	175 °C	175 °C
Heat Flux	Not Provided	Not Provided	Not Provided
Efficiency	Not Provided	Not Provided	Not Provided
Maximum Compression	1.0 MPa	1.2 MPa	1.2 Mpa
Mass	Not Provided	Not Provided	Not Provided
Length	0.02 meters	0.03 meters	0.04 meters
Width	0.02 meters	0.03 meters	0.04 meters
Height	0.003 meters	0.0037 meters	0.0041 meters

The essence of the device selection test was not about replicating the manufacturer's product results for each device; instead, it was about determining the device with the highest power output based on experimental conditions that represent a deepwater oil and gas setting. Thus, undertaking two practical tests was necessary:

1. TEM Suitability Selection Test
2. Thermoelectric Modules Configurations Test

From the above discussions in **Section 3.3**, the difference between subsea well fluids' and seafloor temperatures is generally less than 200 °C. Hence, a conservative maximum temperature difference in the two test categories was selected as 70 °C. A temperature difference of 70 °C was chosen for experiments to reflect real-life seafloor conditions to which thermoelectric modules will be exposed. In addition, 70 °C offers a global outlook to this project, acting as a based-temperature difference representing seabed temperature conditions in all geographical locations across the world. Thirdly, the 70 °C ensures the power system components are properly handled to avoid damage. Also, the selected temperature difference was easy to manage while serving as a guide against electrical hazards and other safety-related measures. Also, the matched load resistances used in these experiments were not precisely as specified by Manufacturer-B because the author did not have the exact components in his toolbox.

Nonetheless, in ***Chapters 4*** to ***7***, experiments will be conducted at temperature difference ranging from 0 °C to 150 °C, representing locations where oil-gas reservoir fluid flow temperature exceeds 100 °C. Lastly, The key components used in the test setup are in *Table 3.3*.

3.4.1. Hot and Cold Surfaces of TEMs

The first step before the TEM suitability selection test was identifying the hot and cold sides of the thermoelectric modules. The identification of the sides was made by attaching positive and negative wires (red wires for positive and black wires for negative) of the

thermoelectric modules to similar coloured cables (leads or probes) of digital Multimeter-DMM-X03.

Next, each thermoelectric module was placed on a tabletop (worktop). Then, a warm temperature (of the author’s palm/hand) was laid on the surface of the modules. A positive voltage reading on the multimeter indicated that the warm hand was touching the module's hot side, while a negative voltage reading meant the warm hand was on the module's cold side. This first step was crucial, as temperature specification differs for each side of the TEMs.

3.4.2. Ceramic Surfaces Clean-up

The next step was surface cleaning after identifying the hot and cold sides of the thermoelectric modules. Isopropanol (IPA), an alcohol (C3H8O) chemical compound, was used to clean the thermoelectric module's surface debris and grease. The clean-up of each module was to improve heat transfer between the TEM, interface material, and heat exchanger.

Table 3.3 Test Rig (Test-Bench) Components

Test Bench Key Components for Deepwater Thermoelectric Power System		
Item/Tag Name	**Functions/Services**	**Material/Remarks**
Thermoelectric Module-Device-TEM-01	Heat Conversion to Electrical Power	Bismuth Tellurite
Thermoelectric Module-Device-TEM-02	Heat Conversion to Electrical Power	Bismuth Tellurite
Thermoelectric Module-Device-TEM-03	Heat Conversion to Electrical Power	Bismuth Tellurite
Heat Exchanger	Heat Removing from Hotside to Cold side of Thermoelectric Module	Aluminium
Water Channel Block	Heat Removing from Hotside to Cold side of Thermoelectric Module	Aluminium
Hotside Block	Transfer of Heat from Hotplate-HPL-X01 to Hotside of Thermoelectric Module	Aluminium
Hotplate-HPL-X01	Supply of Heat/Vibration effect to Thermoelectric Modules	Represent Hot Oil & Gas from Reservoir
Water Hoses (Supply & Return)	Supply of Cold Water to TEMs Assemblies/Return of Warm Water to Water Tank	Represent Cold Sea Water
Aluminium Housed Clad Resistors	Support Heat conversion to Electrical Power	Match Resistive Loads
Flame proof Axial Metal Film Resistor	Support Heat conversion to Electrical Power	Match Resistive Loads
Carbon Film Resistors	Support Microcontroller operations/Heat to Electric Conversion	Carbon Film
Bypass and Blocking Diodes	Channeling of Electric Current in a direction	Solid state one way electrical valve
Laptop Computer-CPT-X02	Display of Temperature, Voltage and Current Data	Data Display Device
Voltage Data Recorder-HTK-01	DC Voltage Data Capture	Data Acquisition Unit
Current Data Recorder-HTK-02	DC Current Data Capture	Data Acquisition Unit
Microcontroller-Temperature Data Recorder-ADN-03	Temperature Data Capture for Hotside Block	Data Acquisition Units
Microcontroller-Temperature Data Recorder-ADN-04	Temperature Data Capture for Coldside Block	Data Acquisition Units
Microcontroller-Temperature Data Recorder-ADN-05	Temperature Data Capture for Cold Water Tank	Data Acquisition Units
Temperature Sensor-TPS-01	Temperature Sensor & Hotside Data Capture via ADN-03	Temperature Sensor
Temperature Sensor-TPS-02	Temperature Sensor & Coldside Data Capture via ADN-04	Temperature Sensor
Waterproof Temperature Sensor-TWS-01	Temperature Sensor for Cold Water Tank Data Capture via ADN-05	Temperature Sensor
Waterproof Temperature Sensor-TWS-02	Temperature Sensor for Cold Water Tank Data Capture via ADN-05	Temperature Sensor
Digital Multimeter-DMM-X03	Support/Comparing Captured & Measured Voltage and Current Data	Power Data Measurement Unit
Dual Channel Digital Thermometer-DDT-X04	Support/Comparing Captured & Measured Temperature Data	Temperature Data Measurement Unit
Stainless Steel Tray-SST-X05	Housing/Accomodating Thermoelectric Module Assemblies	Representing Subsea Structure
Water Pump-WP-01	Pumping of Cold Water to TEM Assemblies	Cold Water Supply
Water Pump-WP-02	Pumping of Cold Water to TEM Assemblies	Cold Water Supply
Water Pump-WP-03	Pumping of Cold Water to TEM Assemblies	Cold Water Supply

3.4.3. Interface Materials

After surface cleaning, the next step was to select and apply interface materials on thermoelectric modules. Different interface substances or heat transfer supporting materials can be used for surface mating between thermoelectric modules and heat exchangers. The function of the interface material or substances was to achieve optimum heat flow performance from the modules. However, among the different interface materials, some materials can be detrimental during power generation. Therefore, the advantages and disadvantages of some of the interface materials considered before choosing a suitable option are in *Table 3.4*.

A self-adhesive graphite sheet with a thermal conductivity of 10 W/m.K (watts per meter-Kelvin) was selected for this work. Thus, the test fixture had cut-out shapes of graphite sheets between each thermoelectric module and the heat exchanger.

3.4.4. TEM-Power System Assembly

As outlined in *Figure 3.4* and *Figure 3.5*, the aluminum-based heat exchanger consists of a hot block that transfers heat (high temperature) from the Hotplate-HPL-X01 through a thermoelectric module to a heat remover. A cut-out graphite sheet (the shape of the thermoelectric module under test) was sandwiched between the heat exchanger and the TEM. The heat absorber or heat remover consisted of a cold-water channel (cold-water inlet and warm-water outlet), an air-heat dissipater or heat sink, and a DC fan. The DC

fan was added to the system arrangement for completeness. It was not connected to any power source.

The hot block section of the heat exchanger, including the Hotplate-HPL-X01, represented warm heat emanating from drilling mud (drilling fluid) on the drilling platform. Usually, during deepwater or ultra-deepwater oil-gas drilling operations, the drilling mud is pumped through the drill pipes/riser compartments into a deepwater oil-gas well. Hot returning drilling mud and drill cuttings flow out from the subsea well through another part of the drill pipe/riser compartments to the mud pit on the drilling platform. Depending on the geographical location, the temperature of the returned drilling mud and cutting in the mud pit can be up to 150 °C (Chakrabarti, 2005a)(Chakrabarti, 2005b).

Similarly, during deepwater or ultra-deepwater oil-gas production, hot-produced fluids from reservoirs flow to the subsea wellhead at the seafloor. These hot fluids travel through subsea structures (or flow loops & paths on subsea XTrees and Manifolds, flowlines/pipelines, and production risers) on the seabed and beyond. This experiment's cold-water, cold-water-channel, and heat sink represent the surrounding cold seawater environment.

Apart from supplying even heating across its ceramic-coated stainless steel round top, the Hotplate-HPL-X01 can stir liquid at speeds ranging from 200 to 1500 rpm (revolutions per minute). The stirring feature of the hotplate (without a liquid container on the top) was advantageous in this experiment because it simultaneously provided constant vibrational and heating effects on any device placed on its round top. Comparatively, subsea structures at the seabed are usually under severe pressures, extreme temperatures,

vibration, and related harsh environmental effects. Hence, the Hotplate-HPL-X01 took care of vibrational, temperature effects, and even-heat distribution to the power-generating TEM under test.

The thermoelectric system assembly had sufficient clamping load, even clamping, and thermal isolation. Compression was applied to each TEM assembly via bolts thermally insulated by plastic bushes. The plastic bushes reduced parasitic thermal losses to the TEM under test. Belleville washers (not shown in *Figure 3.4*) and two (2) bolts were used to tighten the system assembly. The bolts permitted changes in compression as the system assembly stabilises. In addition, the washers allowed tolerance for thermal stresses when the system assembly was in operation. A careful bolt-tightening process led to even clamping and optimal thermal contact in the system. This action ensured an even load sequence and a steady turning rate for each of the two bolts holding the system assembly. However, it is essential to note that uneven clamping is capable of poor thermal contact, which can cause damage to the TEM under test. The system assembly had minimum parasitic thermal losses through thermal insulating foam material applied around each thermoelectric module.

Table 3.4 Thermoelectric Modules Interface Materials

Interface Materials	Advantages	Disadvantages
Thermal Grease	High thermal conductivity. Reduction of air gap on ceramic surfaces. Increases contact surface areas on ceramic surfaces	Operating conditions are less than 100 °C. Quick-dry out in long lifetime system application
Graphite Sheet	It does not have a quick-dry-out potential. Ideal for test purposes. It can be cut for any TEM shape. It can be easily removed after use.	Less than 2% thermal performance compared to thermal grease
Gap fillers	They are made from silicone material. Available in complex shapes and patterns It has greater tolerance when used at height. Capable of withstanding vibrational forces.	High thickness Lower thermal performance compared to graphite sheets and greases
Bonding Methods	It improved thermal contact. It offers permanent attachment to the module and heat exchanger.	Addition of thermal stresses on the module

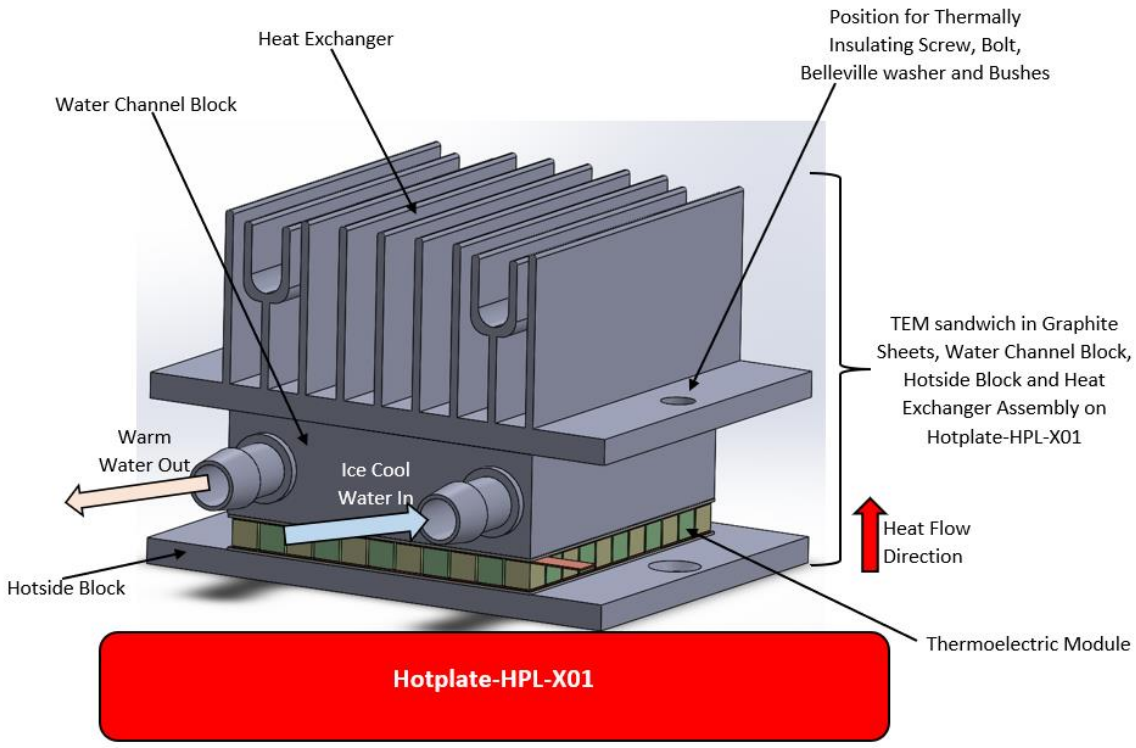

Figure 3.4 Oil-Gas Reservoir Representation (Hot Fluid Flow-to-Cold Seawater)

The next step was clamping the thermoelectric modules between the hot heat source and the cold heat exchangers. As shown in *Table 3.2*, the compression or clamping load required by Device-TEM-01 is 1.0 Mpa (Mega-Pascal). Device-TEM-02 required 1.2 Mpa, while Device-TEM-03 needed 1.2 Mpa. The tightening of bolts was to a particular torque for each module. The torque value to attain the expected clamping force (T_q) was calculated as follows:

$$T_q = \frac{C_{Tq} \text{ x } B_{size} \text{ x } P_C \text{ x } A_{TEM}}{N_{Screw}} \tag{3.1}$$

The terms in *Equation (3.1)* are defined as:

- C_{Tq} = Torque Coefficient
- B_{size} = Bolt Size
- P_C = Compression Pressure
- A_{TEM} = TEM Area
- N_{Screw} = Number of Screws

Values for torque coefficient (C_{Tq}), and nominal bolt size (B_{size}) for the two M5 steel bolts used in the experiment were 0.2 and 5.2mm, respectively.

The clamping force (T_{q1}, T_{q2}, and T_{q3}) for Device-TEM-01, Device-TEM-02, and Device-TEM-03 for each respective thermoelectric module were calculated as 0.208 N.m (Newton meter), 0.5616 N.m, and 0.9984 N.m. See **Appendix A (Derivative A.2)** for the details on the calculations.

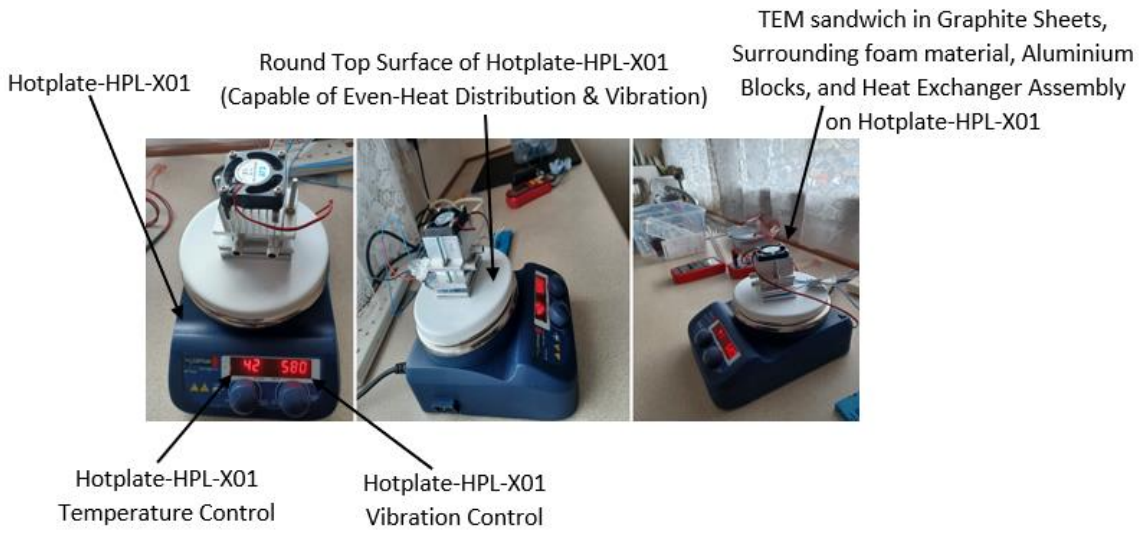

Figure 3.5 TEM-Power System Assembly on Hotplate-HPL-X01

3.4.5. Suitable TEM Selection Test

The test bench's design, development, and construction were in two categories, as mentioned in **Section 3.4**. The TEM selection test circuit diagram is in *Figure 3.6*. The system's setup is in *Figure 3.7* and *Figure 3.8*. Device-TEM-01 was the first module that was tested. The terminals of the TEM were connected to 0.5 Ohms load resistance (The specified resistor value of 0.36 Ohms was not available in the author's components/tool kit). The TEM in the power system assembly, as described in **Subsection 3.4.4**, was also linked to Voltage Data Recorder-HTK-01 for DC voltage data reporting. At the same time, a Current Data Recorder-HTK-02 reported DC current data.

Temperature Sensor-TPS-01 and Temperature Sensor-TPS-02 were configured on two (2) separate microcontroller boards as Temperature Data Recorder-ADN-03 and Temperature Data Recorder-ADN-04, respectively. Two (2) Waterproof Temperature Sensor-TWS-01 and Waterproof Temperature Sensor-TWS-02 were configured on a third microcontroller board as Temperature Data Recorder-ADN-05.

Temperature Data Recorder-ADN-03 captured temperature data via the hot block at the thermoelectric module's hot side. A thin metal blade (not shown in the assembly) was attached between the hot block and the TEM to facilitate the hot side temperature measurement. Temperature Data Recorder-ADN-04 measured the module's cold side temperature through the cold-water channel. Lastly, Temperature Data Recorder-ADN-05 recorded the cold-water tank temperature.

A dual-channel digital thermometer (Thermometer-DDT-X04) ensured minimal temperature deviation between the Hotplate-HPL-X01 and the module's hot side. The dual-channel digital thermometer (Thermometer-DDT-X04) was also used to check and compare the actual system temperature readings frequently and the temperature readings obtained via the microcontrollers. Similarly, the digital multimeter (Multimeter-DMM-X03) was used for continuous measurement of the precise voltage/current values and comparing the results with the data obtained via the Voltage Data Recorder-HTK-01 and Current Data Recorder-HTK-02, respectively. *Figure 3.6* is an illustration of the test system. *Figure 3.7* shows the test bench setup during the system's operation.

The Temperature Data Recorder-ADN-05, consisting of a microcontroller and two water-proof temperature sensors, served as a standalone data recorder, as shown in *Figure 3.6* and *Figure 3.8*. DC water pumps pumped ice-cold water at temperatures approximately 1 °C to 4 °C from a storage tank/container to the power system assembly through cold water hoses. The used water (or warm water) returned through the warm water outlet of the water channel to the water tank for re-circulation.

Figure 3.6, *Figure 3.7*, and *Figure 3.8* show cold water hoses to the inlet and warm water outlet from the TEM power system assembly placed on the hotplate (Hotplate-HPL-X01). In addition, medium-to-fairly large size ice blocks (from a refrigerator) were used to cool the returned water in the water tank, thus maintaining the cold-water temperature between approximately 1°C and 4 °C.

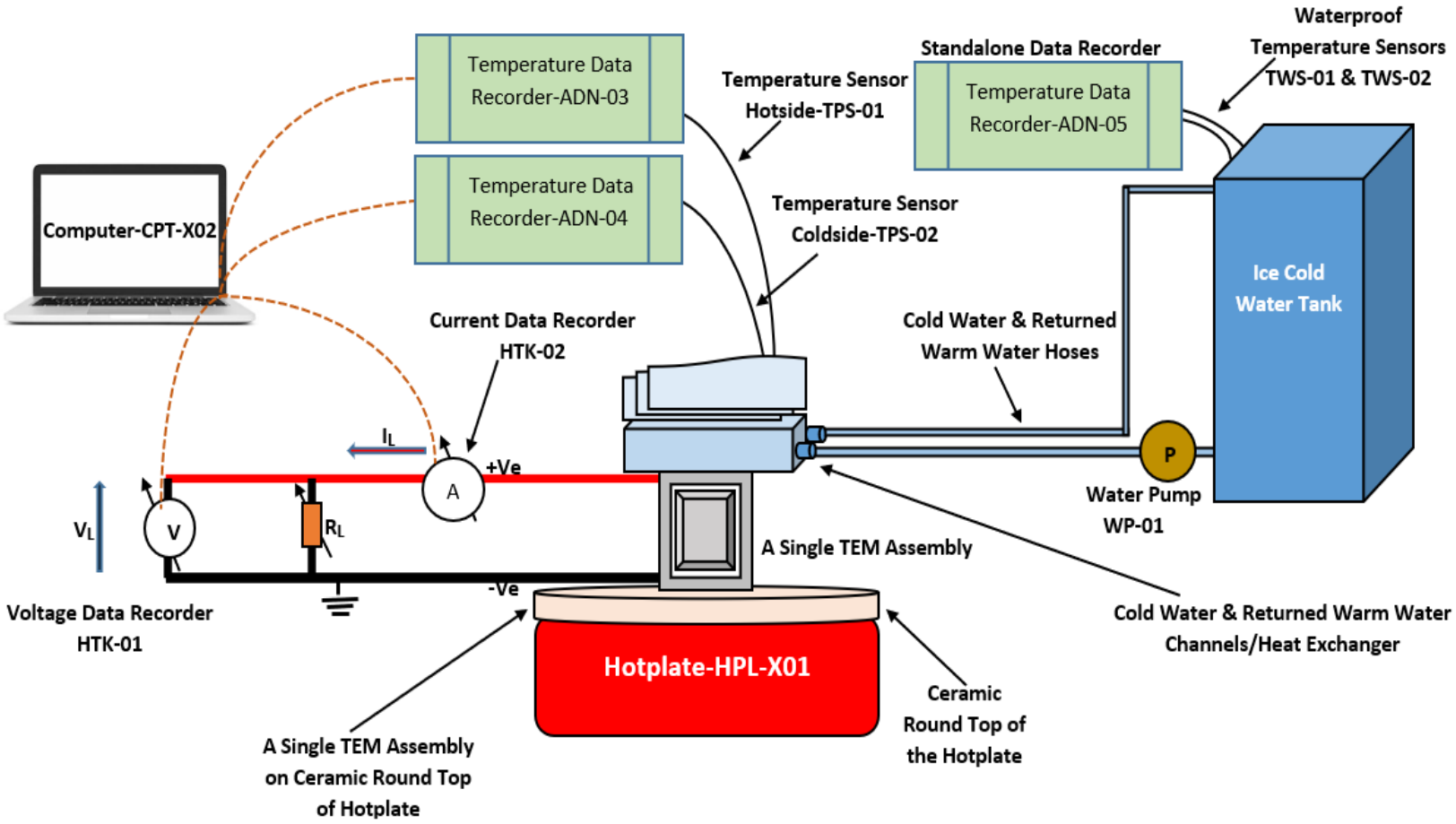

Figure 3.6 Test Bench Schematic-Single TEM Assembly

The stand-alone control system (the Temperature Data Recorder-ADN-05) had light-emitting diodes (or reporting LEDs) in its configuration. Transmitted alerts/blinking LED signals were checked from the cold-water tank. When the tank temperature was 4°C, the LED was Green. The yellow LED turned on when the tank temperature was lower than 4°C. The LED becomes Red when the cold-water tank temperature exceeds 4°C.

Cold water from the storage/recirculation tank was pumped at three flow rates. The low flow rate was 450 Litre/hour (0.45 m^3/h), the medium flow rate was 725 L/h (0.725 m^3/h), while the highest flowrate was 1000 L/h (1 m^3/h) for different experimental conditions.

As discussed above, the fifth data acquisition system was the standalone microcontroller-based temperature sensors, while the connections of the other four data capture systems were to Computer-CPT-X02. The two temperature measurement systems (Temperature Data Recorder-ADN-03 and Temperature Data Recorder-ADN-04), the DC voltage measurement info (Voltage Data Recorder-HTK-01), and electric current data (Current Data Recorder-HTK-02) were reported through their respective data interfaces and displayed at the Computer-CPT-X02. Additionally, breadboards, copper connecting wires, and crocodile clips were used to simplify the connection points at the TEM terminals, the system assembly, and parts of the system circuit.

The experiment began with the Device-TEM-01 power system assembly placed on the hotplate. Hot heat was supplied to the system assembly via the Hotplate-HPL-X01 while ice-cold water from the water tank was simultaneously pumped to the system assembly at

450 L/h (Litre/Hour). Next, the terminals of the Device-TEM-01 were connected to 0.5 Ohms load resistance. Finally, the other system components were connected, as shown in the illustration and demonstration setup.

The temperature difference to the system assembly was maintained at approximately 50 °C. Output voltage and current were recorded as ice-cold water continued to flow to the system assembly, consisting of the TEM under test on the hotplate, which was returned to the circulating tank.

The pump flow rate was changed from 450 L/h to 725 L/h (or medium flow rate), and the temperature difference to the system assembly was maintained at about 50 °C. The experiment was repeated for the new parameter setting. Again, the output voltage and current from the system assembly were recorded as ice-cold water continued to flow through the system assembly and warm water returned from the system assembly to the circulation tank.

For the third time, the pump flow rate was changed from 725 L/h to 1000 L/h (high flow rate), the temperature difference to the system assembly was roughly 50 °C, and the output voltage and current for the high flow rate condition were recorded during the experiment.

Finally, the average voltage and current values from the three flow rates (low, medium, and high conditions) were calculated. The calculated result for experimental case No. 1 at a temperature difference of 50 °C was 0.22V for voltage and 1.48A for current.

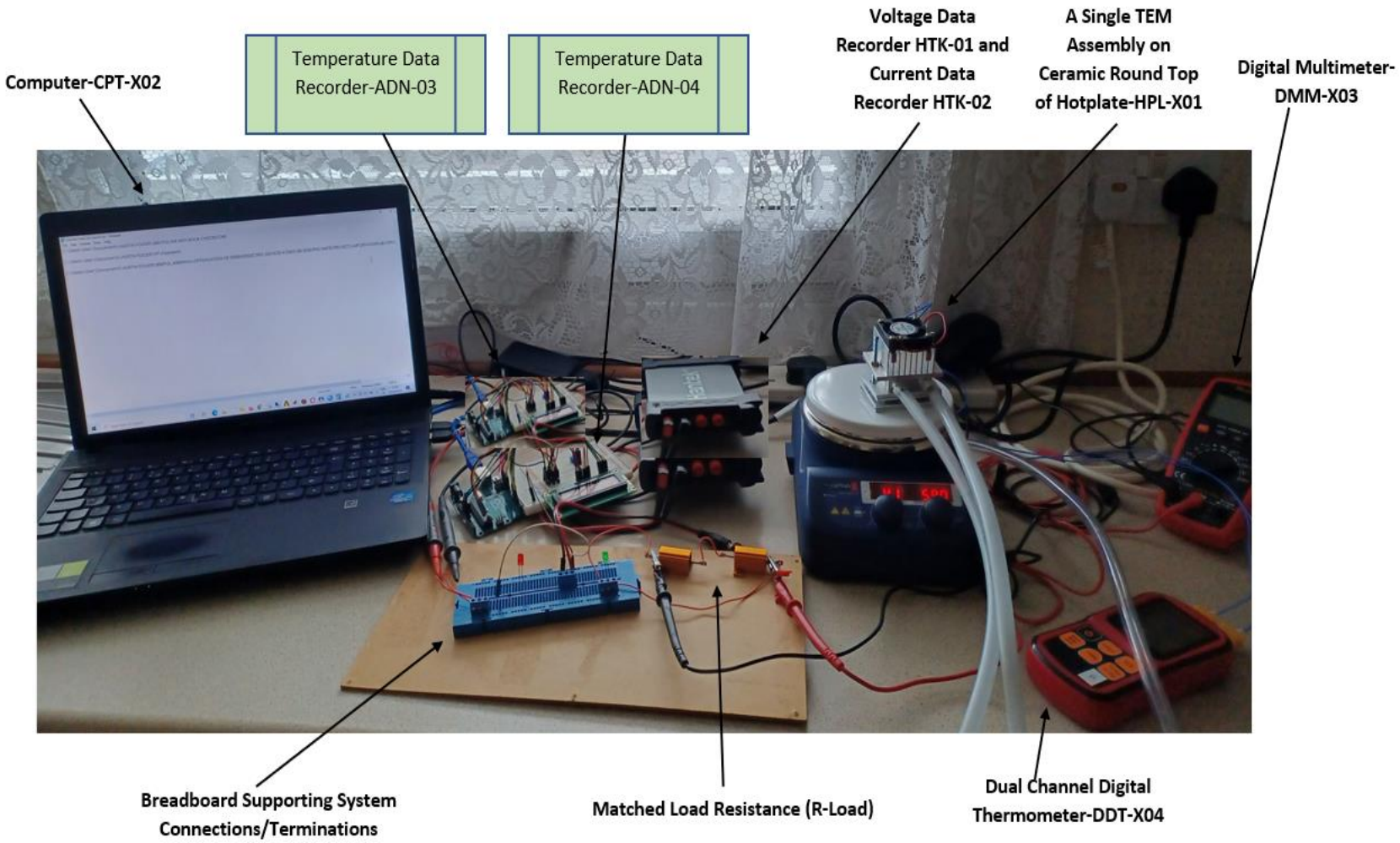

Figure 3.7 Test Bench Setup-Single TEM Assembly

Hence, the output power from Device-TEM-01 connected to 0.5 Ohms load resistance was 0.33W. The summary results from experimental case No.1 are available in *Table 3.5*, while the detailed results are available in **Appendix A (Table A.1)**.

The temperature difference setting was changed from 50 °C to 55°C during experimental case No. 2. At the three pump flow rates, 450 L/h, 725 L/h, and 1000 L/h, ice-cold water was separately conveyed to Device-TEM-01 connected to 0.5 Ohms load resistance. As discussed above, ice-cold water was pumped to the system assembly, consisting of the TEM under test and placed on the hotplate. Warm water from the system returned from the system assembly to the recirculation tank during low, medium, and high conditions. The average voltage and current from the three flow rates were calculated as 0.27V and 1.52A, respectively. Therefore, 0.41W was the recorded output power during experimental case No. 2, as summarized in *Table 3.5*. Detailed results of the experiment are available in **Appendix A (Table A.1).**

The temperature difference setting was changed from 55 °C to 60 °C during experimental case No.3. In experimental case No.4, the temperature difference was 65 °C. The temperature difference was 70 °C during case No.5. Ice-cold water was pumped to the system assembly for three pump flow rates (low, medium, and high) and returned to the circulation tank as Device-TEM-01 connected to 0.5 Ohms load resistance. The average

voltage, current, and output power in each scenario were calculated and recorded, as shown in *Table 3.5*. Experimental case No.5 concluded ***Group-A*** experiments with Device-TEM-01 under test. Detailed results for temperature differences ranging from 50 °C to 70 °C are available in **Appendix A (Table A.1)**.

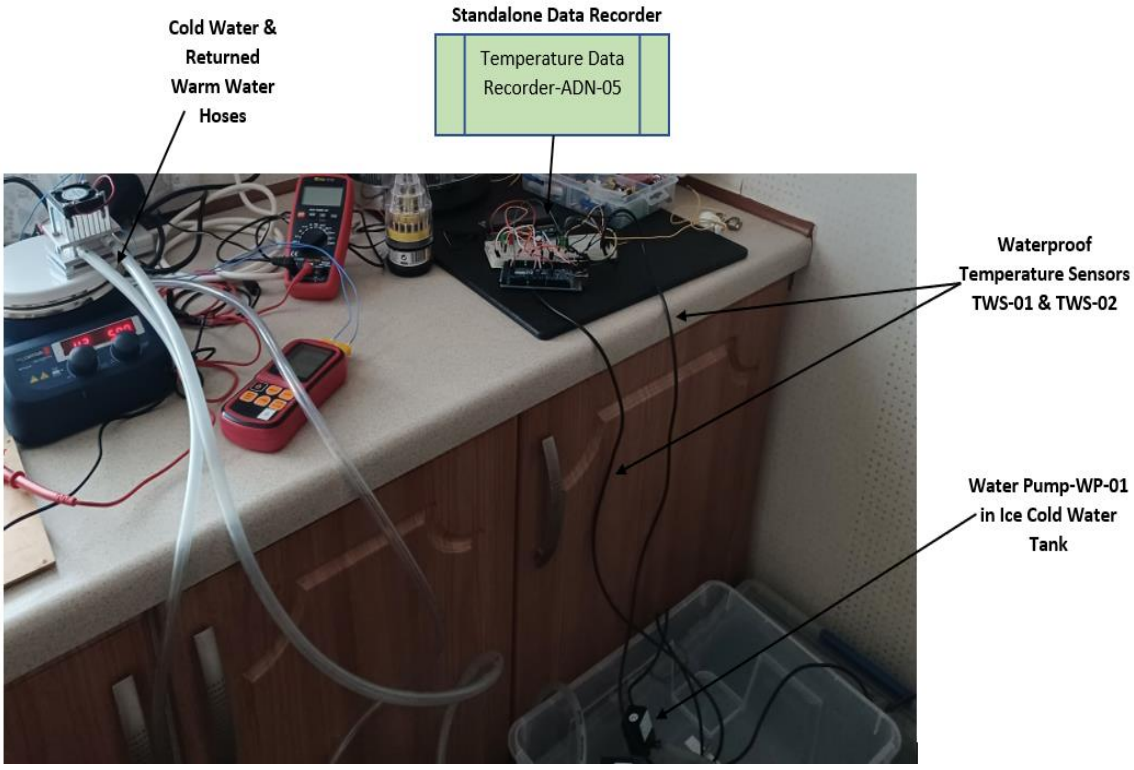

Figure 3.8 Standalone Temp. Monitoring System for 1-TEM Assembly

The system assembly containing Device-TEM-02 was set up in a manner similar to Device-TEM-01. However, the terminals of Device-TEM-02 were connected to a load resistance of 7 Ohms (specified 6.89 Ohms was not in the author's toolbox). Nonetheless,

the Device-TEM-02 on a load resistance of 7 Ohms and other system components constituted the ***Group-B*** experiment.

The temperature difference applied on the system assembly was 50 °C during experimental case No.1, and ice-cold water was pumped at 450 L/h, 725 L/h, and 1000 L/h to the power system. As explained above, the output voltage value and current value were recorded in each scenario. The calculated average voltage and current were 1.79V and 0.43A, respectively. Therefore, the output power was 0.77W during experimental case No.1. As was done previously, the experiments were repeated for cases No.2, No.3, No.4, and No.5 when temperature differences were 55 °C, 60 °C, 65 °C, and 70 °C for separate ice-cold water pumped at 450 L/h, 725 L/h, and 1000 L/h to the power system. The summarised results of the calculated average voltage, current, and output power obtained for the ***Group-B*** experiment in which Device-TEM-02 was connected to 7 Ohms load resistance are available in *Table 3.5*. More detailed experiment results are in **Appendix A (Table A.1)**.

The ***Group-C*** experiments were with Device-TEM-03 under test connected to 4 Ohms load resistance (The author did not have the specified 3.65 Ohms in his tool kit; hence, 4 Ohms was used). The five experimental cases, No.1, No.2, No.3, No.4, and No.5 procedures explained during ***Group-A*** and ***Group-B***, were repeated in ***Group-C*** for the five-temperature difference 50 °C, 60 °C, 65 °C, and 70 °C for low, medium, and high flow rate from the pump in the recirculation tank. The average voltage, current, and output

power obtained from Device-TEM-03 in each scenario were calculated as shown in *Table 3.5*. Detailed results of the ***Group-C*** experiment are in **Appendix A (Table A.1)**.

Table 3.5 Thermoelectric Modules - Summarised Test Results

Thermoelectric Module (TEM)	Device-TEM-01 on 0.5 Ohm Load			Device-TEM-02 on 7 Ohm Load			Device-TEM-03 on 4 Ohm Load		
Temp.Diff. (DegC)	Vol (V)	Current(A)	Power(W)	Vol (V)	Current(A)	Power(W)	Vol (V)	Current(A)	Power(W)
50	0.22	1.48	0.33	1.79	0.43	0.77	1.53	0.49	0.75
55	0.27	1.52	0.41	1.87	0.46	0.86	1.55	0.50	0.78
60	0.29	1.55	0.45	1.90	0.49	0.93	1.59	0.50	0.80
65	0.31	1.58	0.49	1.95	0.51	0.99	1.61	0.59	0.95
70	0.32	1.60	0.51	1.97	0.52	1.02	1.71	0.62	1.06

The summarized results are presented in *Table 3.5*, and the detailed results are available in **Appendix A (Table A.1)**. Both results show the electrical power outputs obtained at three (3) different resistive load values from each of the three (3) TEMs at temperature difference values between 50 and 70 °C.

From the table of results, the output power values when temperature difference at 70 °C and other experimental conditions were 0.51 W, 1.02 W, and 1.06 W from Device-TEM-01, Device-02, and Device-TEM-03, respectively. Device-TEM-03 had the highest output power under the same experimental conditions as represented in the (green-colour) bar graph in *Figure 3.9*. The experiment was repeated to ascertain the output power from the

thermoelectric module. The results obtained during the second or repeated test are denoted as Device-TEM-03 on 4 Ohms Load_Test2 in **Appendix A (Table A.1)**.

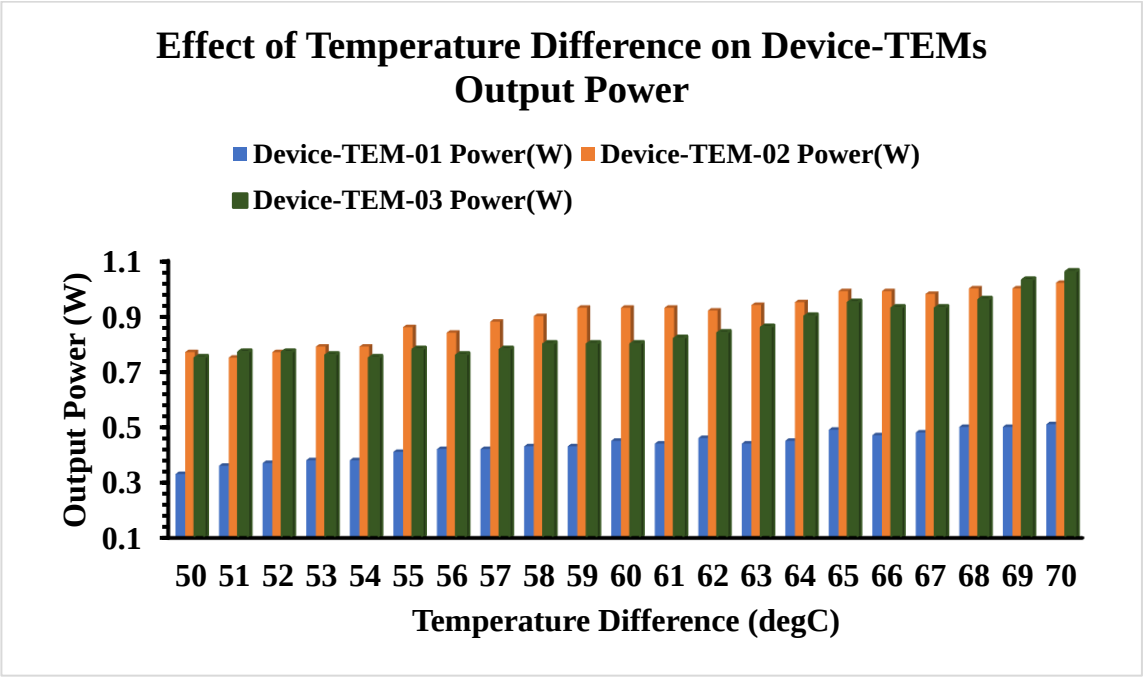

Figure 3.9 Output Power vs Temperature Difference on TEMs

From the results in **Appendix A (Table A.1)**, the mean, standard deviation, and standard error of the output power from Device-TEM-01_Power (W), Device-TEM-02_Power (W), Device-TEM-03_Test1 Power (W), and Device-TEM-03_Test2 Power (W) were determined as contained in *Table 3.6*. *Figure 3.10* shows the measured output power error bars from the four thermoelectric modules (TEMs) test categories. The confidence interval at 95% for the output power from the Device-TEM-03_Test1 is presented in *Table 3.7* alongside the upper and lower confidence intervals at 95%.

Table 3.6 Mean, Standard Deviation, & Error TEM Output Power

Attributes	Device-TEM-01_Power (W)	Device-TEM-02_Power (W)	Device-TEM-03_Test1 Power (W)	Device-TEM-03_Test2 Power (W)
Mean	0.4339	0.9000	0.8495	0.8515
Standard Deviation	0.0511	0.0812	0.0922	0.0993
Standard Error	0.0080	0.0127	0.0146	0.0155

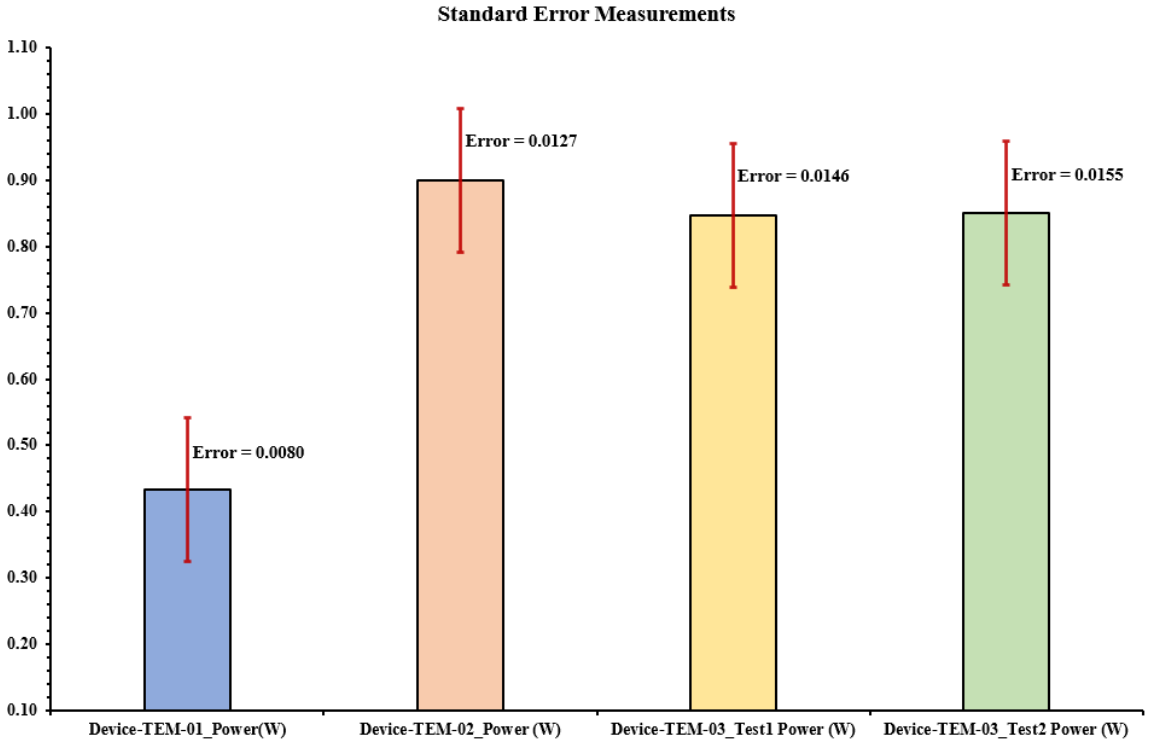

Figure 3.10 Error Bars of TEM Output Power Measurements

Table 3.7 Output Power Confidence Intervals for Device-TEM-03

Device-TEM-03_Test1	
Mean	0.8495
Standard Error	0.014579358
Median	0.81
Mode	0.76
Standard Deviation	0.092207959
Sample Variance	0.008502308
Kurtosis	-0.264783429
Skewness	0.907558999
Range	0.32
Minimum	0.75
Maximum	1.07
Sum	33.98
Count	40
Confidence Level(95.0%)	0.029489536
Upper CI (95.0%)	0.878989536
Lower CI (95.0%)	0.820010464

Further analysis was carried out, and *Table 3.8* shows Pearson's correlation for temperature differences against the output power from Device-TEM-03_Test1. *Figure 3.11* is the scatter plot that corroborates the output power from the thermoelectric device when the temperature difference is applied to it.

Table 3.8 Pearson's Correlations, Temp. Diff. & TEM Output Power

Pearson's Correlations

	n	Pearson's r	p
Temp. Diff. (degC) - Device-TEM-03_Power (W)	41	0.922	< .001

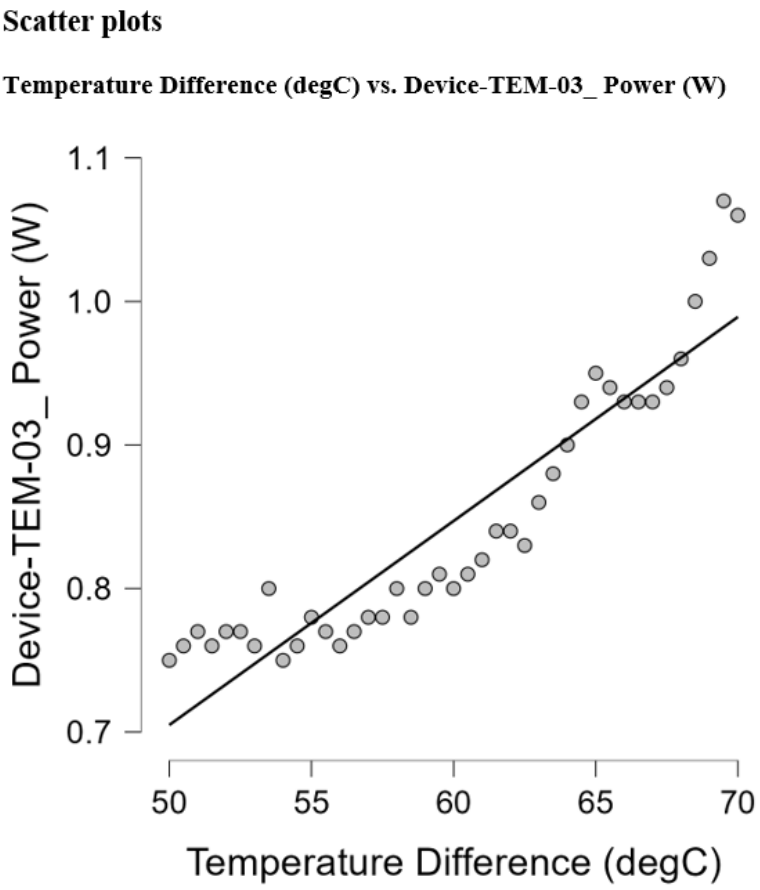

Figure 3.11 Scatter Plots, Temp. Diff. against TEM Output Power

A significant positive correlation between temperature difference and output power from the thermoelectric module was found, $r(39) = 0.922$, $p < 0.001$. As shown by Pearson's correlation and the scatter plots above, the p-value from the results of the experiments is less than 0.05. Therefore, there is a statistical relationship between temperature difference and output power. Hence, it can be concluded that the experiments are repeatable, and the outcomes are valid.

Secondly, the absence of nanotechnology-based flexible thermoelectric modules in the market led to using commercially available TEMs via the test bench developed for this research. The findings from the experiments reveal that as the temperature difference increases, the output power from the TEMs also increases. Additionally, the generated power of a thermoelectric module depends on the temperature applied on the hot side and the temperature of the module's cold surface. Existing information from past studies shows a correlation between temperature difference and output power from thermoelectric devices.

Thirdly, the test bench results indicated that temperature difference from 50 °C to 70 °C influences the output power of Device-TEM-03 from 0.75W to 1.06W. However, for the exact temperature difference and other experimental conditions, the output power from Device-TEM-01 was less than Device-TEM-02 and Device-TEM-03. It may have been because it had 31 thermocouples and the smallest surface area of the three thermoelectric modules. Device-TEM-02 and Device-TEM-03 had 127 thermocouples and larger surface areas. Be that as it may, under the same experimental conditions, the output power of Device-TEM-03 was larger than Device-TEM-02. As such, Device-TEM-03 was selected as the potential deepwater thermoelectric module (DTEM).

From the above discussion, the selected potential deepwater thermoelectric module (Device-TEM-03) is not the ideal DTEM. It is neither nanotechnology-based nor a flexible thermoelectric module as intended. Nanotechnology-based flexible thermoelectric modules are not commercially available. Future research can further address these anomalies.

Fourthly, the water depth of most deepwater or ultra-deepwater oil and gas fields ranges from 1500 meters to 3000 meters and beyond. The pressure rating at the seabed on such sites typically exceeds 5000 psi. The seafloor is naturally rough, unpredictable, and constantly characterized by movements and vibration. The temperature difference between reservoir fluid flow and seawater at the ocean floor ranges from about 60 °C to nearly 150 °C depending on the geographical location or continent of the world. As discussed above, a cautious temperature difference of 70 °C was selected as the maximum used during the experiments.

Nevertheless, the selected deepwater thermoelectric module (Device-TEM-03) or DTEM was assumed to be a flexible thermoelectric module (Flex-DTEM) with a maximum operating temperature difference of 150 °C and a pressure rating of 6000 psi. Furthermore, it is essential to note that the experimental conditions of the test bench are no way nearer to what is obtainable in any deepwater oil and gas field. These are fundamental limitations also shared by other research. Future studies should consider conducting additional experiments or field trials at wet duck or oil and gas field tests.

3.4.6. TEMs Configurations and Operation

As mentioned in **Section 3.4**, the second thermoelectric module selection procedure is the TEM configurations test. A single thermoelectric module (Device-TEM-03 or Flex-DTEM) cannot generate sufficient electric power for the desired power system. Furthermore, a thermoelectric power system for deepwater system usage would require

more than one (1) module to raise the voltage and current for a more usable power level. Thus, another purchase was made for five (5) additional Device-TEM-03 modules from Manufacturer-B to increase the test system's power level. Hence, six (6) TEMs were used to determine the power system behaviour under additional experimental conditions. As stated in the previous section, it was assumed that the six (6) TEMs (Device-TEM-03) were flexible deepwater thermoelectric modules (Flex-DTEM).

Cut-out graphite sheets were sandwiched between the five (5) new TEMs and assembled following the same procedures described in **Subsections 3.4.1** to **3.4.4**. Thus, the individual power system assemblies were labelled Mod-A, Mod-B, Mod-C, Mod-D, Mod-E, and Mod-F. The TEM assemblies were separately tested for open circuit voltage (VOC) by not connecting the resistive load to the modules' terminals. The VOC test was the first step in the second round of deepwater power system experiments.

Each system assembly was placed on the Hotplate-HPL-X01, and the terminals were connected to the digital Multimeter-DMM-X03. A water hose fitted with a pump at 1000 L/h from the ice-cold water tank was attached to the water channel inlet. At the outlet of the water channel block was the returned water hose. A temperature difference of 70°C was set on each assembly. The dual-channel digital thermometer-DDT-X04 ensured that the maximum temperature difference was maintained. Each system assembly's open circuit voltage at these experimental conditions was recorded.

The average open-circuit voltage (VOC) from each thermoelectric module (Mod-A, Mod-B, Mod-D, Mod-E, and Mod-F) under the test at a temperature difference of 70°C was

calculated as 2.95V. Thus, the VOC test confirmed the potential electrical capability of each thermoelectric module (TEM).

The 6 TEMs assemblies (Mod-A, Mod-B, Mod-C, Mod-D, Mod-E, and Mod-F) were housed in a Stainless-Steel Tray (SST) and placed on the Hotplate-HPL-X01, as shown in *Figure 3.12*. Support structures were placed inside the tray to add weight to the SST and its content. These support structures prevented the tray from falling off the hotplate as the system vibrated on the hotplate.

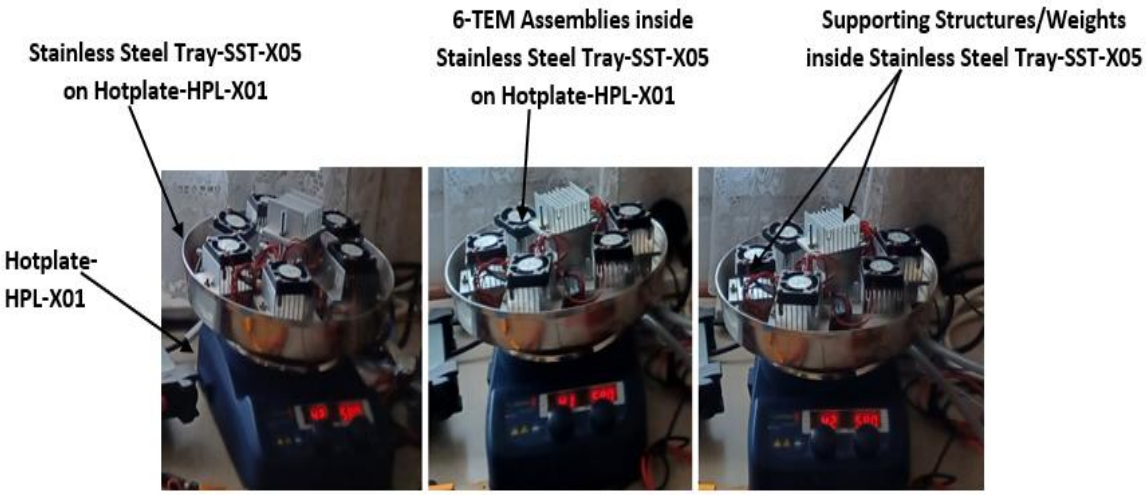

Figure 3.12 6-TEM Assemblies in SST on Hotplate-HPL-X01

The design, development, and construction of the second test bench for the TEMs configuration and operation are shown in *Figure 3.13*, *Figure 3.14*, and *Figure 3.15*. The overall system setup described in *Figure 3.13* is shown in *Figure 3.14* and *Figure 3.15*.

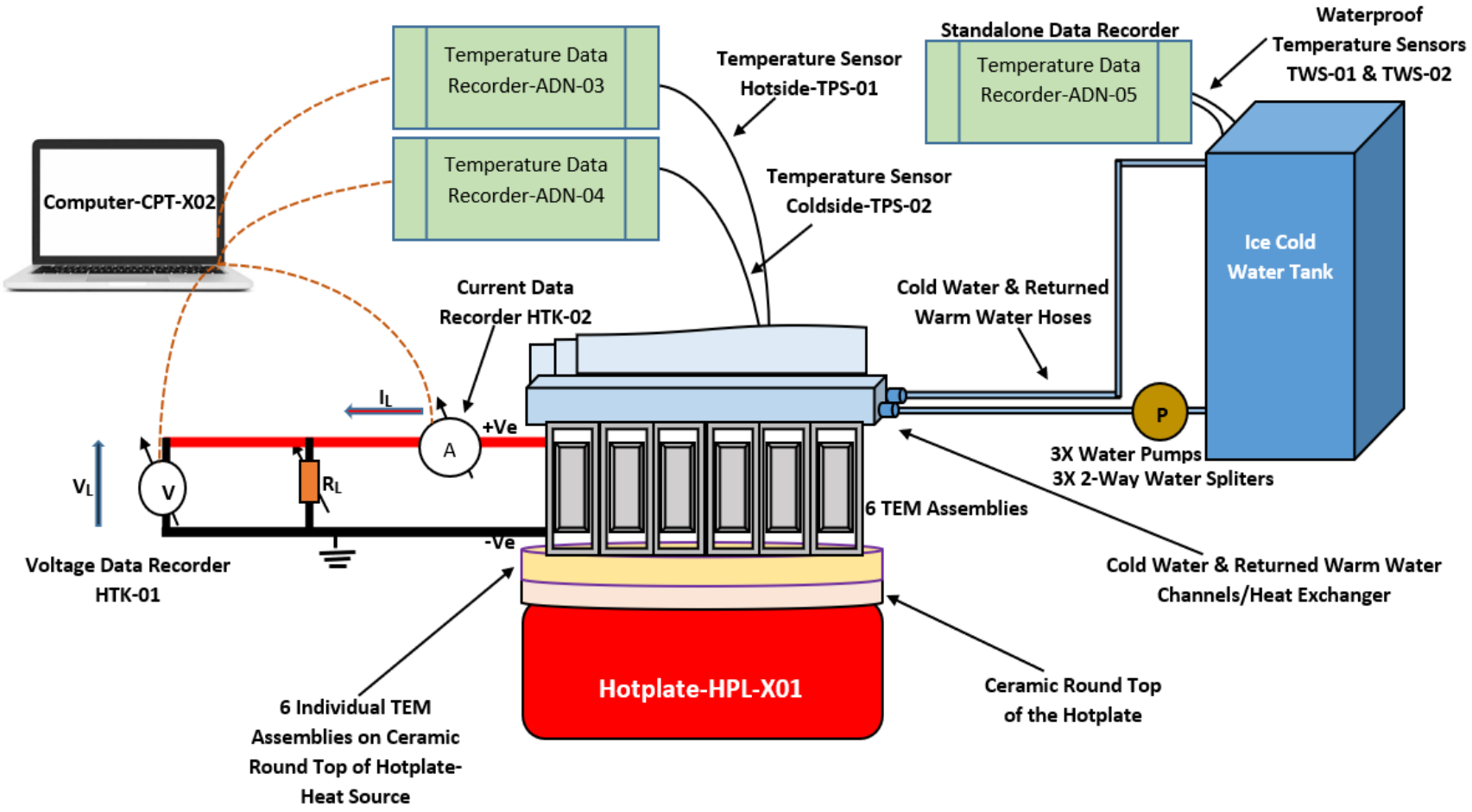

Figure 3.13 Test Bench Schematic-Six TEMs Assemblies

3.4.6.1. Series Connections of 6 Device-TEM-03 Modules

Inside the SST, Mod-A was connected to Mod-B. Next, Mod-B was connected to Mod-C, Mod-C to Mod-D, Mod-E, and Mod-F in a chain-like pattern known as a series connection, as shown in *Figure 3.16*.

Temperature Data Recorder-ADN-03, Temperature Data Recorder-ADN-04, and Temperature Data Recorder-ADN-05 were connected as temperature sensors/data recorders. The terminals of the system assemblies were connected to 4 Ohms load resistance (the specified resistor value of 3.65 Ohms was unavailable in the author's toolbox). The TEMs assemblies, as described in **Section 3.4.5**, were linked to the Computer-CPT-X02 via Voltage Data Recorder-HTK-01 for DC voltage data reporting. Also, the terminals of the system assemblies through the Current Data Recorder-HTK-02 were connected to the computer to report electric current data.

Through Temperature Data Recorder-ADN-03, temperature data from the hot side of a system assembly were acquired inside the SST. Also, via the Temperature Data Recorder-ADN-04, the cold side temperature data was obtained through the cold-water channel of a system assembly inside the SST. Acquired temperature information from the hot and cold sides was displayed on Computer-CPT-X02.

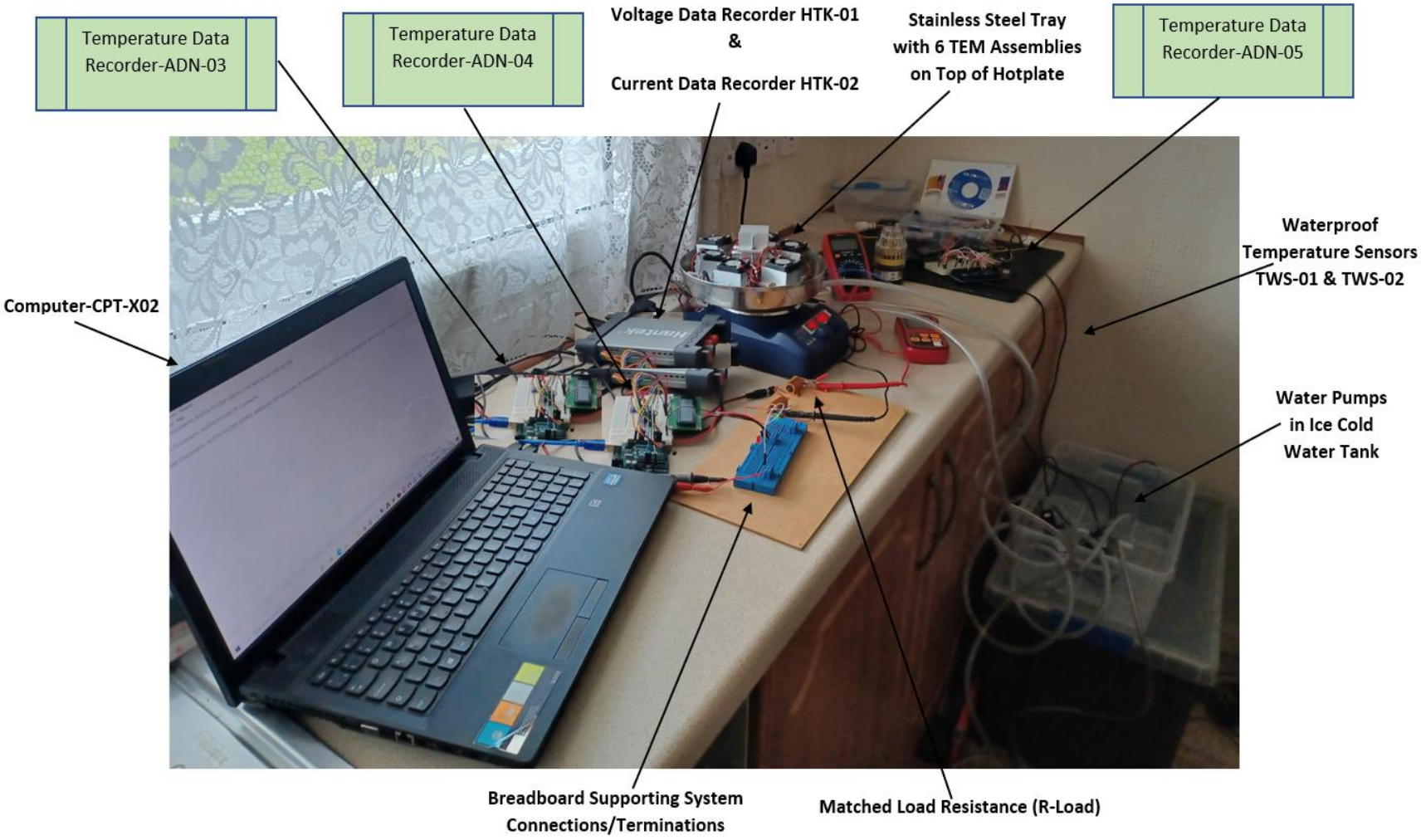

Figure 3.14 Test Bench Setup 6-TEMs Assemblies

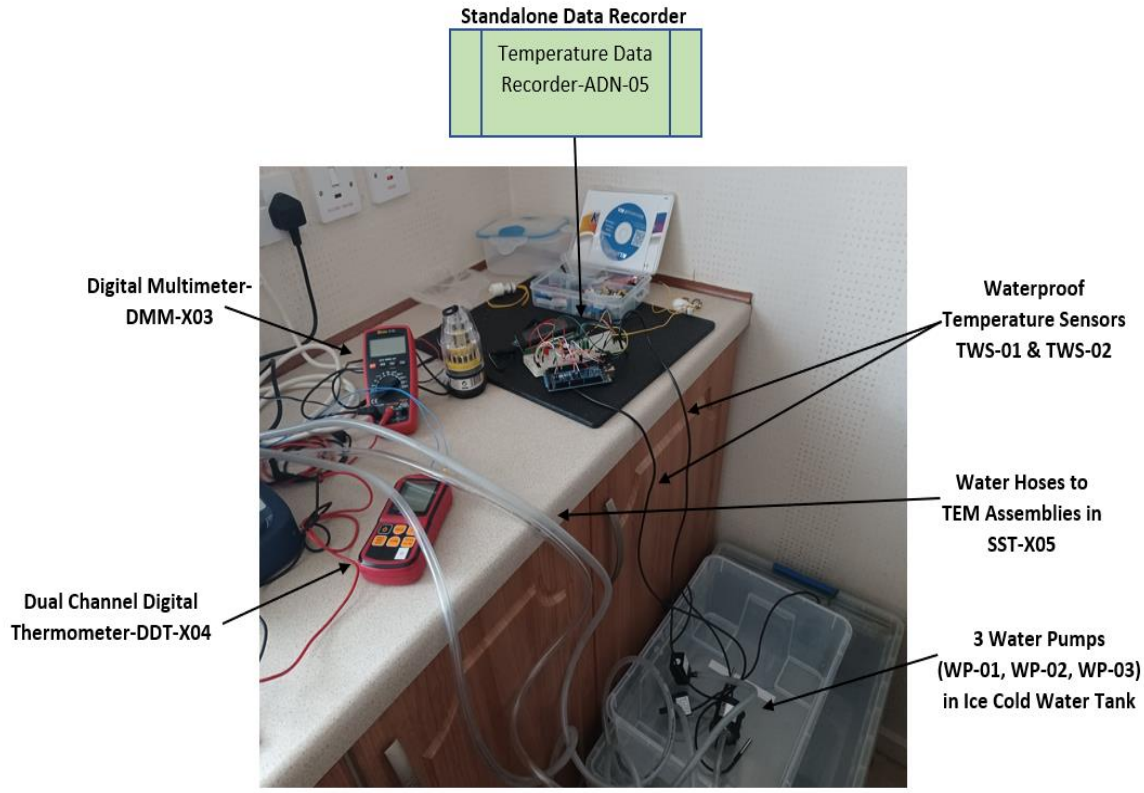

Figure 3.15 Standalone Temp. Monitoring System for 6-TEM Assemblies

The fifth system was the Temperature Data Recorder-ADN-05, which recorded the cold-water tank temperature. As was done previously, the system configuration was standalone; the system information was not reported on Computer-CPT-X02. Instead, transmitted alerts/blinking LED signals were observed from the cold-water tank. When the tank temperature was 4 °C, the LED was Green. The Yellow LED was turned on when the tank temperature was lower than 4 °C. The LED becomes Red when the cold-water tank temperature exceeds 4 °C.

The six system assemblies inside the SST were individually connected to water hoses fitted with three water pumps and splitter arrangements. The flow rate of the pumps was set at 1000 L/h (high flow rate), and ice-cold water from the tank was pumped to the cold-water inlet channel. The warm or used water was returned to the tank through a different water hose at each system assembly's water-channel outlets. The next step was to maintain the temperature difference between the system assemblies inside the SST and the Hotplate-HPL-X01 at 70°C.

Copper connecting wires, breadboards, and crocodile clips were used to simplify the various connection points in the power system. In addition, the dual channel digital thermometer (Thermometer-DDT-X04) ensured minimal temperature deviation between the Hotplate-HPL-X01 and the module's hot side at regular intervals.

Also, the dual channel digital thermometer (Thermometer-DDT-X04) was used to regularly check and compare the system temperature readings and those obtained via the microcontrollers. Likewise, the digital multimeter (Multimeter-DMM-X03) was used to continually measure and compare voltage/current data of the Voltage Data Recorder-HTK-01 and Current Data Recorder-HTK-02.

Computer-CPT-X02 displayed the voltage and current data via the Voltage Data Recorder-HTK-01 and Current Data Recorder-HTK-02. Also shown on Computer-CPT-X02 were temperature readings from Temperature Data Recorder-ADN-03 and Temperature Data Recorder-ADN-04. Hence, the voltage and electric current values were recorded and calculated accordingly, as was done in the previous section.

The experiment was repeated for the second and third time at 70 °C temperature difference and cold-water flow rate of 1000 L/h. Again, the voltage and electric current values of the second and third experiments were recorded. Finally, the average power was calculated from the three recorded voltage and electric current values. Thus, the output power of the six series-connected system assemblies, Mod-A, Mod-B, Mod-C, Mod-D, Mod-E, and Mod-F, was 6.08 W. The three (3) sets of experiments concluded the Series-Connected System-Test No. 01. These results are available in *Table 7.8*.

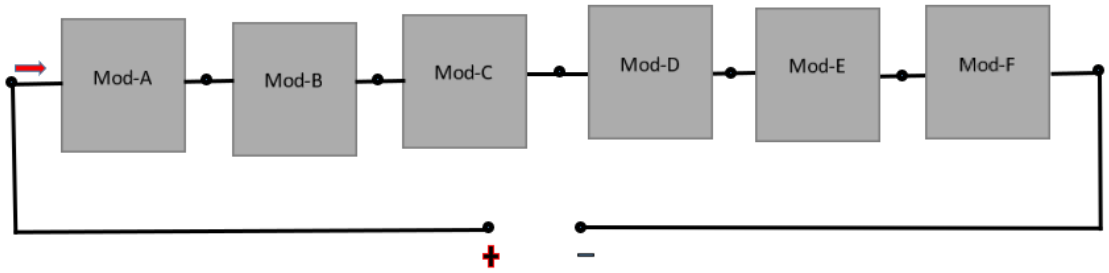

Figure 3.16 Series Connected TEMs Assemblies in SST

Series-Connected System-Test-02

The series connected thermoelectric modules or system assembly configuration during Test No.2 is shown in *Figure 3.17*. The illustration shows that Mod-A, Mod-B, Mod-C, Mod-D, Mod-E, and Mod-F were connected in a chain-like sequence. Next, a piece of wooden material (about 2 cm x 2 cm x 0.5 cm) was placed inside the SST before mounting the Mod-F assembly on top of the wooden piece. As a result, Mod-F was partially in contact with the stainless-steel tray. The wooden piece created a weak link in the series chain, thereby introducing mismatch losses in the system.

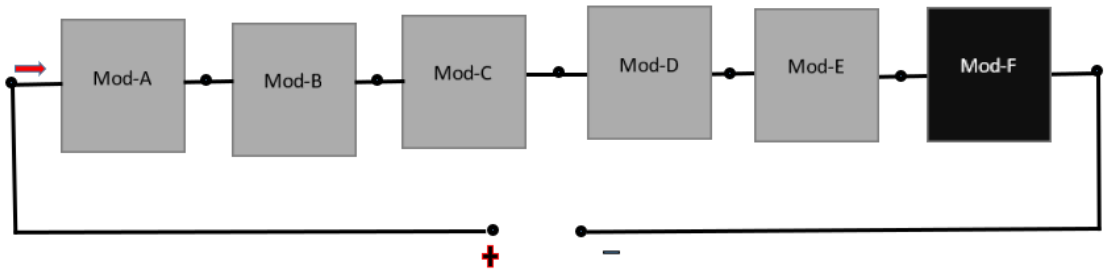

Figure 3.17 Series TEMs in Mismatch Loss Condition

The same Series-Connected System Test No. 01 component connection procedures were repeated in Test No.2. The Voltage Data Recorder-HTK-01 and Current Data Recorder-HTK-02 were connected via the terminals of the thermoelectric device assemblies in the stainless-steel tray. The hot-side and cold-side temperature sensors were connected to the corresponding hot-side and cold-side of different TEM assemblies. Computer-CPT-X02 displayed the voltage and current data. Also, on the Computer-CPT-X02 display were hot and cold sides temperature data. The standalone Temperature Data Recorder-ADN-05 ensured the cold-water temperature in the tank was maintained. At a flow rate value of 1000 L/h, a temperature difference of 70 °C between the Hotplate-HPL-X01 and ice-cold water to system assemblies, and a load resistance of 4 Ohms. As was previously done, the experiment was repeated three (3) times. The output DC power during each case was 0.00 W. See *Table 7.8* for the results of the experiment.

Series-Connected System-Test-03

The system assemblies were connected during the third series-connected system experiment, as illustrated in *Figure 3.18.* The wooden-mounted Mod-F assembly and the non-wooden material-mounted Mod-A, Mod-B, Mod-C, Mod-D, and Mod-E were in a chain-like connection as previously. However, two bypass diodes, (BPD-01) and (BPD-02), were introduced into the circuit. BPD-01 was connected (in parallel) to Mod-A, Mod-B, and Mod-C, while BPD-02 was connected to Mod-D, Mod-E, and Mod-F, as in *Figure 3.18.*

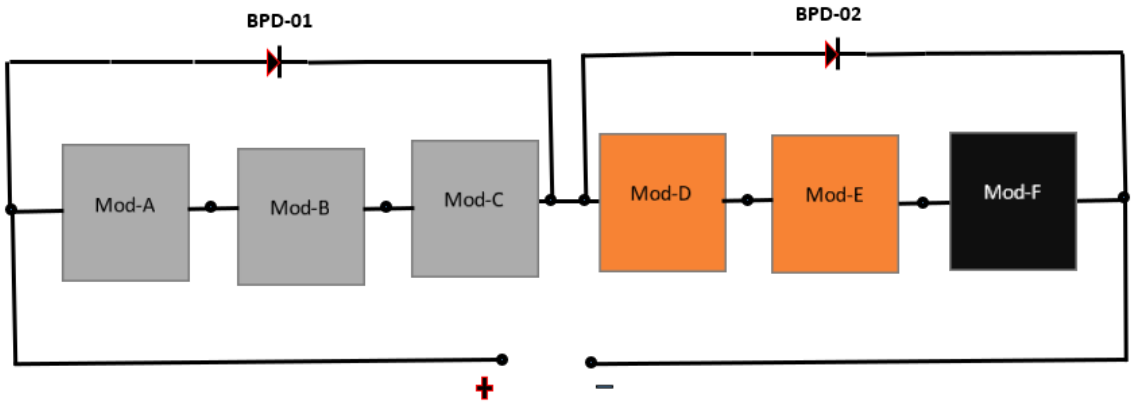

Figure 3.18 Bypass Diodes in Series-Connected TEMs

The DC voltage recorder and current recorder were connected via the terminals of the thermoelectric device assemblies in the stainless-steel tray. The hot-side and cold-side temperature sensors were connected to the corresponding hot-side and cold-side of different TEM assemblies. The standalone Temperature Data Recorder-ADN-05 ensured the cold-water tank temperature was monitored.

At a flow rate value of 1000 L/h, a temperature difference of 70 °C, and a load resistance of 4 Ohms. As was previously done, the experiment was carried out three (3) times. It was observed that the bypass diodes eliminated the effects of the mismatch losses and the supposedly failed Mod-F in the power system. Thus, the BPD-02 offered an easy electric current flow path around the non-performing Mod-F. However, the non-performing Mod-F in the assembly prevented Mod-D and Mod-E from actively contributing to system power output. As a result, the average power for the series-connected cases for Mod-A, Mod-B, Mod-C, Mod-D, Mod-E, and Mod-F was calculated as 3.08 W.

Further info on the results for Series-Connected System-Test-01, Series-Connected System-Test-02, and Series-Connected System-Test-03 are available in *Table 7.8*.

3.4.6.2. Parallel Connections of 6 Device-TEM-03 Modules

The second round of experiments with the six Device-TEM-03 was the parallel configurations of the thermoelectric modules. In this sub-section, the six (6) TEMs power system assemblies (Mod-A, Mod-B, Mod-C, Mod-D, Mod-E, and Mod-F) were connected in three parallel strings to determine the output power.

Figure 3.19 illustrates the 6 TEM assemblies and connections within the stainless-steel tray (SST). This arrangement is the Parallel-Connected System-Test No.04. The DC voltage recorder (Voltage Data Recorder-HTK-01) and current recorder (Current Data Recorder-HTK-02) were connected via the terminals of the thermoelectric device assemblies in the stainless-steel tray.

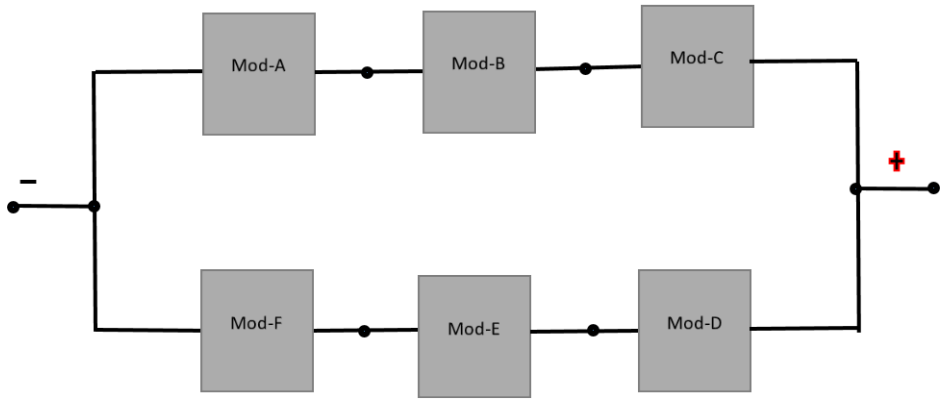

Figure 3.19 Parallel Connected TEMs Assemblies in SST

The hot-side and cold-side temperature sensors were connected to the corresponding hot-side and cold-side of different TEM assemblies via Temperature Data Recorder-ADN-03 and Temperature Data Recorder-ADN-04, respectively. Computer-CPT-X02 displayed the voltage and current data. Also, on the Computer-CPT-X02 display were hot and cold sides temperature data. The standalone Temperature Data Recorder-ADN-05 ensured the cold-water temperature in the tank was monitored and maintained.

Cold water at a flow rate of 1000 L/h was pumped to each assembly at 4 °C. As a result, the cold water and heat from the Hotplate-HPL-X01 retained a temperature difference at 70 °C for the system assemblies. In addition, a load resistance of 4 Ohms was connected to the module's terminals, as was previously done in **Subsection 3.4.6.1**. Similarly, the dual channel digital thermometer (Thermometer-DDT-X04) ensured minimal temperature deviation between the Hotplate-HPL-X01 and the module's hot side at regular intervals. Also, the Thermometer-DDT-X04 was repeatedly used to check and compare the actual

system temperature readings and the temperature readings obtained via the microcontrollers. Likewise, the digital multimeter (Multimeter-DMM-X03) was used to continually measure the precise voltage/current measurement and compare the results with the data obtained via the Voltage Data Recorder-HTK-01 and Current Data Recorder-HTK-02, respectively.

The experiment was carried out three (3) times for parallel-connected Mod-A, Mod-B, Mod-C, Mod-D, Mod-E, and Mod-F. Voltage and current readings were recorded on each occasion. Finally, the average power of the parallel connected TEMs was calculated. Hence, Parallel-Connected System-Test No.04 was 6.25 W, as shown in *Table 7.9*

Parallel-Connected System-Test-05

The second parallel-connected system experiment, or Parallel-Connected System-Test-No.05, is illustrated in *Figure 3.20*. The same wooden piece in **Subsection 3.5.6.1** created a failure effect in the parallel-connected assemblies. The wooden piece was placed inside the SST before mounting the Mod-F assembly on top of the wooden material. The Parallel connected module configuration of Mod-A, Mod-B, Mod-C, Mod-D, Mod-E, and Mod-F on the piece of wood is in *Figure 3.20*. As mentioned, the wooden material created a weak link and mismatch losses in the parallel arrangement.

As was done previously, the voltage recorder, electric current recorder, hot side, and cold side data acquisition system were connected at their respective points. In addition, the

standalone Temperature Data Recorder-ADN-05 ensured the cold-water temperature in the circulation tank was monitored and maintained.

Again, at a flow rate of 1000 L/h, cold water was pumped to each assembly at 4 °C. The cold water and heat from the Hotplate-HPL-X01 maintained a temperature difference of 70 °C. A load resistance of 4 Ohms was connected to the module's terminals.

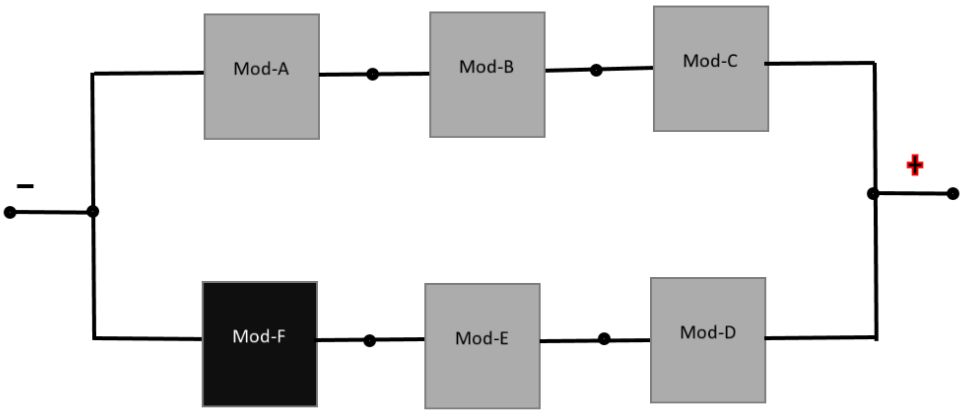

Figure 3.20 Parallel Connected TEMs in Mismatch Loss Condition

As previously, Thermometer-DDT-X04 and Multimeter-DMM-X03 were used to cross-check the results regularly. The experiment was carried out three (3) times. On each occasion, voltage and current readings were recorded. Lastly, the average output power of the parallel-connected Mod-A, Mod-B, Mod-C, Mod-D, Mod-E, and Mod-F was calculated as 1.51 W. See *Table 7.9* for details.

Parallel-Connected System-Test-06

The third parallel-connected system experiment, or Parallel-Connected System-Test-No.06 system configuration, is shown in *Figure 3.21*. The system consists of the wooden-mounted Mod-F and non-wooden material-mounted assemblies: Mod-A, Mod-B, Mod-C, Mod-D, and Mod-E. In this case, six (6) bypass diodes (BPD-01, BPD-02, BPD-03, BPD-04, BPD-05, and BPD-06) and two blocking diodes (BLKD-01 and BLKD-02) were introduced in the circuit. As shown below, bypass diodes (BPD-01), (BPD-02), and (BPD-03) were connected in parallel across Mod-A, Mod-B, and Mod-C, while bypass diodes (BPD-04), (BPD-05), and (BPD-06) were connected in parallel across Mod-D, Mod-E, and Mod-F. The blocking diode connections (BLKD-01) and (BLKD-02) are illustrated in *Figure 3.21*.

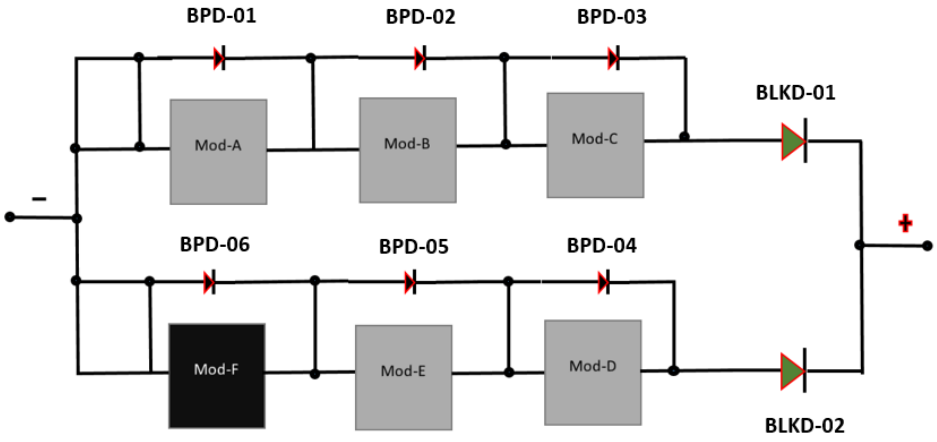

Figure 3.21 Bypass Diodes & Blocking Diode in Parallel Connected TEMs

The standalone Temperature Data Recorder-ADN-05 ensured the cold-water tank was monitored and maintained. The voltage and current recorders were connected via the

terminals of the thermoelectric device assemblies in the stainless-steel tray. The hot-side and cold-side temperature sensors were connected at their corresponding hot-side and cold-side of TEMs assemblies.

At a flow rate of 1000 L/h, cold water was pumped to each assembly at 4 °C. A load resistance of 4 Ohms was connected to the module's terminals. The cold water and heat from the Hotplate-HPL-X01 maintained a temperature difference of 70 °C.

As previously discussed, the bypass diodes eliminated mismatch losses and TEM failure in the system. In addition, it was observed that BPD-06 provided an easy electric current flow path around the non-performing Mod-F. As a result, the first current flow direction was via (BPD-01) to (BPD-02). From (BPD-02) to (BPD-03) and from (BPD-03) to BLKD-01. The second current flow direction was through (BPD-06) to (BPD-05). From (BPD-05) to (BPD-04) and from (BPD-04) to BLKD-02.

It was also noticed that a backward flow (backflow) of electric current to the thermoelectric module assemblies was prevented by the blocking diodes (BLKD-01 and BLKD-02). Following the previous approach, the experiment was carried out three (3) times. On each occasion, voltage and current readings were recorded. The average output power of the parallel-connected Mod-A, Mod-B, Mod-C, Mod-D, Mod-E, and Mod-F, calculated in this case, was 5.11 W.

Refer to *Table 7.9* for further details on the results for Parallel-Connected System-Test-04, Parallel-Connected System-Test-05, and Parallel-Connected System-Test-06.

3.4.6.3. Thermoelectric Power System Test Results

The practical conversion of thermal energy to electricity via thermoelectric modules has been demonstrated. Device-TEM-03 was chosen from the other modules (Device-TEM-01 and Device-TEM-02) because of its highest power-generating capability compared to the others. Furthermore, Device-TEM-03 modules were configured separately in series and parallel networks for power level boosting since a single module can only generate a small amount of power.

However, it was detected from the six experimental cases in **Subsection 3.4.6.1** and **Subsection 3.4.6.2** (Series-Connected System-Test and Parallel-Connected System-Test) that there were variations in the output power based on the system assembly's configuration.

Changes in the output power during mismatch conditions or faulty thermoelectric modules in the system were also observed. For instance, the output power was 0.00 W in the series-connected modules when a wooden piece was placed before mounting the Mod-F assembly and the other assemblies inside SST. On the other hand, the power output from the parallel configuration was 1.51 W when the same wooden piece was placed before mounting Mod-F and the other system assemblies inside the SST.

The circuit output power in both series and parallel situations was improved by introducing bypass diodes. The diodes (BPD-01 and BPD-02) eliminated mismatch losses and potential power losses in the presumed faulty device by redirecting current flow away from the defective or non-performing TEM assembly, thus increasing power output from

0.00 W to 3.08 W in the series-connected modules. Similarly, the bypass diodes in the parallel-connected modules pushed the output power from 1.51 W to 5.11 W. In addition, the blocking diodes (BLKD-01 and BLKD-02) prevented power backflow to SST assemblies in the parallel connected devices, thus preventing significant fault conditions in the power circuit.

Both scenarios indicated that connecting thermoelectric modules in a single configuration (series connection alone or parallel connection alone) is not a complete solution-proven approach, especially for a seafloor application. That means separately connected series thermoelectric modules and separately connected parallel thermoelectric modules are prone to faults when a failure occurs in any module assemblies. Furthermore, the severity of such power problems is more significant in series configurations than in parallel arrangements.

Hence, the best practice for deepwater or ultra-deepwater thermoelectric power systems would be a complete combined series-parallel configuration approach. The combined series-parallel configuration with bypass and blocking diodes in **Subsections 3.4.6.1** and **3.4.6.2** above can be described as a partial combined series-parallel configuration method. The complete combined series-parallel configuration scheme for deepwater or ultra-deepwater thermoelectric power systems will have bypass, blocking diodes, integration of subsea electronic monitoring, fault detection, control, real-time reporting systems, and other subsea electronic systems described in **Section 1.6**. Additional electronic systems required for a holistic underwater power system are presented in ***Chapters 4***, ***5***, ***6***, and ***7***.

A combined series-parallel configuration without bypass and blocking diodes is examined below in **Section 3.4.7**, **Section 3.4.8**, and **Section 3.4.9**. Further discussions and the summation of test results for the six (6) Device-TEM-03 in **Subsections 3.4.6.1** and **3.4.6.2** are available in **Section 7.4.1**.

3.4.7. Error Analysis of Combined Series-Parallel System

The parallel configuration discussed above is called the partial combined series-parallel arrangement when electronic components like the bypass and blocking are integrated into the power system network. *Figure 3.22* is a potential combined series-parallel thermoelectric assemblies without electronic devices consisting of string-01 and string-02.

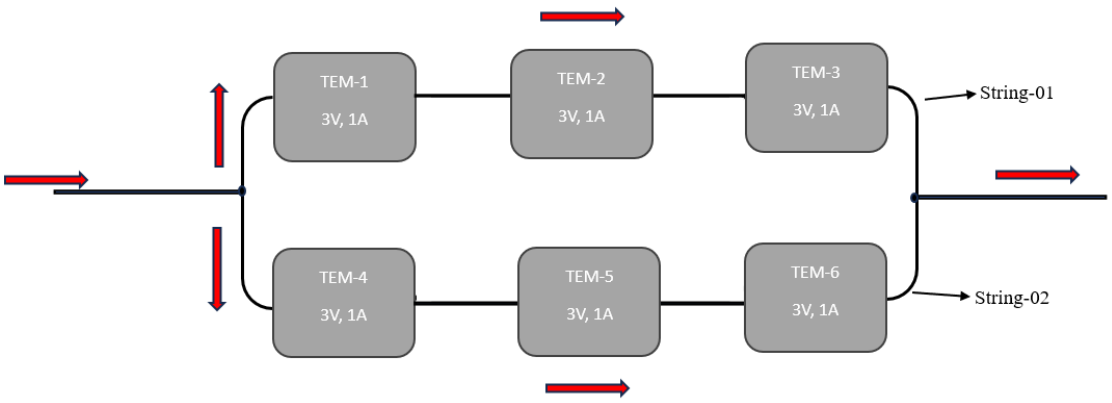

Figure 3.22 Combined Series-Parallel Network (without Electronic Device)

As the illustration shows, string-01 and string-02 are two series networks of six thermoelectric assemblies. Electrical power flow in the system (as indicated in the red arrows) is from left to right. The six thermoelectric modules were assumed to be from the same manufacturing batch. Hence, each thermoelectric module's (TEM) voltage and current ratings are 3V and 1A, respectively. Series string-01 is made of TEM-1, TEM-02, and TEM-03 while series string-02 consist of TEM-04, TEM-05, and TEM-06.

Error Analysis

Table B.1 and **Table B.2** in **Appendix B** were used to perform the error analysis for the six thermoelectric module assemblies. The study involves setting up calculations to simulate the impact of variations in voltage and current on the overall system's parameters to understand the possible power system behaviour on the seafloor.

Parameters

As stated above, the assumed voltage of each TEM is 3V. At the same time, the current is 1A as defined on the TE-Module, voltage, and current columns in **Table B.1** and **Table B.2** in **Appendix B**. Calculated voltage and current for string-01 and string-02 are also on the tables. The error analysis was carried out in two stages (Stage A and Stage B).

STAGE-A

Series Configuration within String-01 and String-02

On simulating the power system, the total voltage across string-01 and String-02 in a series connection was the sum of the individual TEM voltage:

String-01 Total Voltage = TEM1_(3V) + TEM2_(3V) + TEM3_(3V) = 9V

String-02 Total Voltage = TEM4_(3V) + TEM5_(3V) + TEM6_(3V) = 9V

Simultaneously, the current passing through each module is the same as the total current of the string in a series configuration:

String-01 Total Current = 1A

String-02 Total Current = 1A.

Parallel Configuration of String-01 and String-02

The voltage across each string (string-01 and string-02) is the same in a parallel connection:

Total Voltage of String-01 and String-02 = Voltage of a single string = 9V

The total current in a parallel connection is the sum of the currents from each string:

Total Current = Current from String-01_(1A) + Current from String-02_(1A) = 2A

The outcomes of the simulations are demonstrated in **Table B.1** in **Appendix B** and the bar chart in *Figure 3.23*.

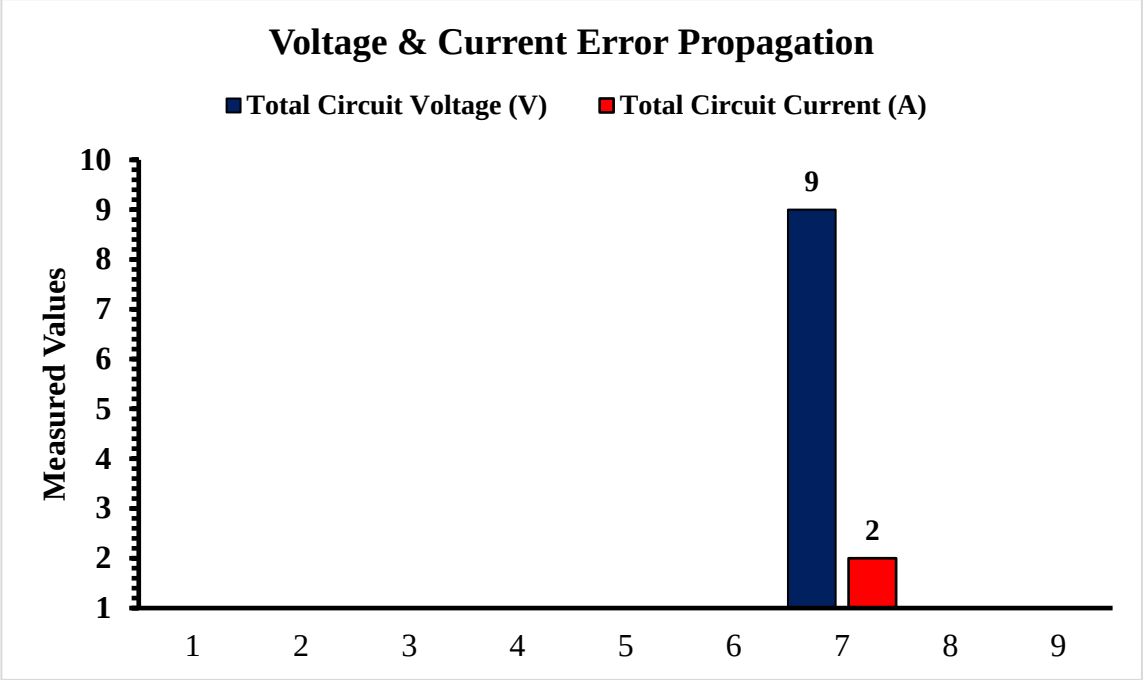

Figure 3.23 STAGE-A Output Voltage & Current

STAGE-B

In Stage B, unpredictable sea conditions led to the thermoelectric power system not operating at its full potential. Hence, it was assumed that an output voltage of 2.5V from TEM-3 while TEM-1 and TEM-2 generated 3V each and a current of 1A from the TEMs. Also, the output voltage from TEM-4, TEM-5, and TEM-6 was 3V each, while the output current of 0.5A was obtained from the TEM assemblies, **see Table B.2**.

Series Configuration within String-01 and String-02

On simulating the power system, the total voltage across string-01 and String-02 in a series connection was the sum of the individual TEM voltage:

String-01 Total Voltage = TEM1_(3V) + TEM2_(3V) + TEM3_(2.5V) = 8.5V

String-02 Total Voltage = TEM4_(3V) + TEM5_(3V) + TEM6_(3V) = 9V

Simultaneously, the current passing through each module is the same as the total current of the string in a series configuration:

String-01 Total Current = 1A

String-02 Total Current = 0.5A

Parallel Configuration of String-01 and String-02

The voltage across each string (string-01 and string-02) is not the same in a parallel connection:

Total Voltage of String-01= 8.5 and

Total Voltage of String-02 = 9V

The total current in a parallel connection is the sum of the currents from each string:

Total Current = Current from String-01_(1A) + Current from String-02_(0.5A) = 1.5A

The outcomes of the simulations are demonstrated in **Table B.2** in **Appendix B** and the bar chart in *Figure 3.24*.

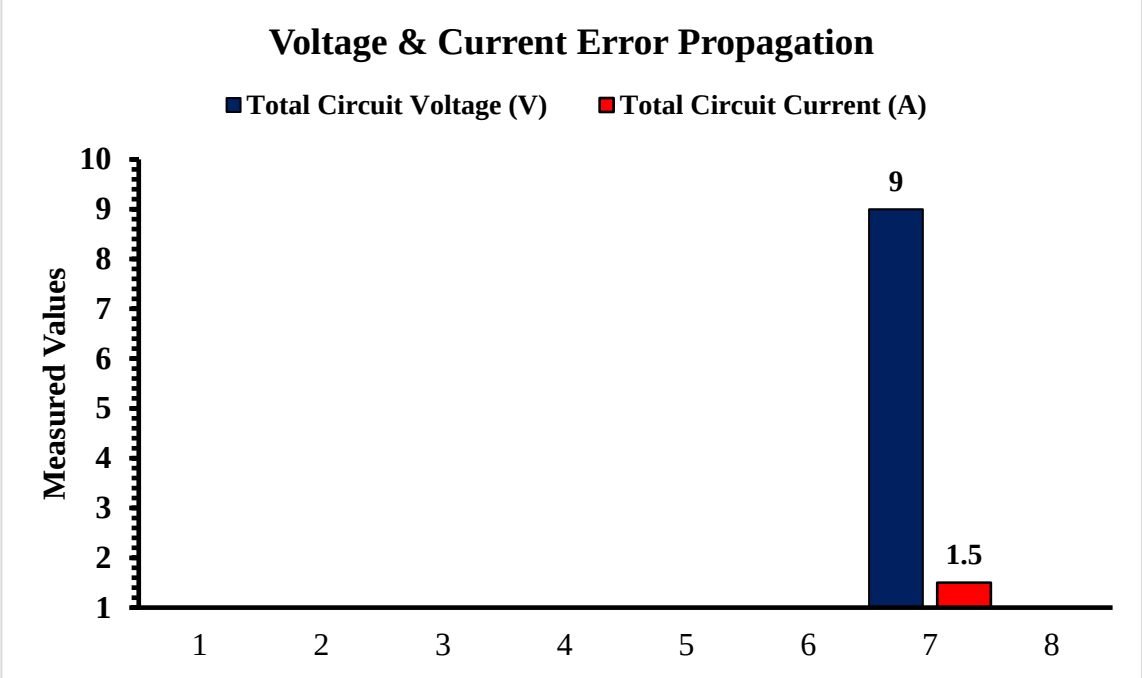

Figure 3.24 STAGE-B Output Voltage & Current

Error Propagation

The results obtained from Stage-A and Stage-B simulations are summarised in the voltage and current error analysis below:

Voltage Error Analysis

Voltage Error in a Single String: An error in the voltage of an individual TEM assembly within a string directly impacts the total voltage of the affected string.

Voltage Error involving Strings: If a string within the network has a different total voltage due to TEM assemble output variations, it affects the overall power system total voltage.

Current Error Analysis

Current Error in a String: Errors in individual TEM assembly currents within a string will likely cause uneven power distribution among TEM assemblies. However, the errors will not disturb the total current of the affected string.

Current Error involving Strings: Variations in the total current generated by each string could cause uneven electrical power output between the two strings.

Sensitivity Analysis

Identifying the most essential factors in a power system network is critical. Errors in thermoelectric module voltages within a string could extensively affect the output voltage of that string. Consequently, the overall total system voltage could be altered. Secondly, unequal current outputs between strings can lead to unbalanced power generation.

Error Mitigation Strategies

Ensuring uniformity in thermoelectric module specifications is essential to minimize system voltages and current variations. Secondly, it is equally crucial to implement monitoring and control systems to detect and balance outputs between the strings.

In conclusion, this analysis demonstrated the potential impact of errors in individual thermoelectric module assemblies on the overall output voltage and current of combined series-parallel power system. Therefore, the selected flexible deepwater thermoelectric module (Device-TEM-03) above was assumed to be from the same manufacturing batch. Individual Device-TEM-03 has the same voltage and current rating. In addition to using bypass diodes and blocking diodes, the seafloor power system network was assumed to integrate with subsea electronic systems to detect and balance outputs between the strings in the network.

3.4.8. Marinisation of Device-TEM-03 Modules

During subsea drilling campaigns in ultra-deepwater oil and gas fields, temperature readings of used or returned drilling mud with drill cuttings through drilling-riser annulus to shale shaker and mud-pit on drilling platforms from some subsea wells can be up to 150 °C. As previously discussed, the temperature of oil, gas, and water mixture at the seafloor is typically around 60 °C in Brazil and some locations in South America. The temperatures in subsea production systems resulting from heat transfer (conduction, convection, and radiation) from reservoir fluids are usually high but generally less than 200 °C (Bai and Bai, 2019). Furthermore, the seafloor is typically hostile, high-risk, and generally uncertain. The temperature at the bottom of the sea in some geographical locations is about 4 °C (Chakrabarti, 2005a). Depending on the site, the pressure rating at the seabed might be up to 6000 psi or more (Dubourdieu *et al.*, 1997). The downhole

pressure for most deepwater oil and gas wells exceeds 19,000 psi (Sanders *et al.*, 2012). To overcome these challenges, the Flex-DTEM was assumed to be marinised.

Several critical steps are involved in marinizing a deepwater thermoelectric module (Flex-DTEM). Marinisation is carried out to ensure the functionality and durability of the Flex-DTEM under high-pressure and ultra-deepwater conditions. Some of the critical steps reviewed in this research are grouped into system specifications, requirements, operating conditions, and assumptions, as stated below:

System Specifications, Requirements, Operating Conditions, & Assumptions

Flex-DTEM: It was assumed that the selected deepwater thermoelectric module or Device-TEM-03 was high-quality and could withstand ultra-deepwater conditions. Therefore, the Device-TEM-03 materials, insulation, and performance can overcome extreme environments.

Subsea Casing and Enclosure: It was assumed that waterproof casings with high-pressure resistance were designed to house and protect the Device-TEM-03. The Flex-DTEM with associated electronics was also protected from water ingress and high-pressure conditions.

Heat Source and Heat Sink: Hot fluid flowing from oil and gas reservoirs is the heat source, while the surrounding cold seawater is the heat sink. Hence, it was assumed that a consistent temperature gradient between the hot and cold sides of the Flex-DTEM was always maintained.

Materials Selection: All components exposed to seawater, including casings, connectors, stainless steel, specialised alloys, and wiring, were assumed to use corrosion-resistant materials.

Subsea Sealing: Preventing water infiltration into sensitive areas, subsea-based sealing capable of implementing high-quality seals, gaskets, O-rings, and epoxy was assumed in this project.

Pressure Resistance: The pressure at about 3000 meters of water depth is typically high; as such, all the components of the deepwater power system were assumed to be rated more than 6000 psi to withstand the high pressure encountered at such water depth. Furthermore, it was assumed that rigorous pressure testing in simulated conditions was conducted to validate systems' integrity at depths of more than 3000 meters.

Subsea Temperature difference Stability: Temperatures between the hot-flowing fluids and cold seawater guarantee efficient energy conversion. Hence, 150 °C was the hot side temperature while 4 °C was the cold side temperature. The temperatures were assumed to be stable and controllable.

Flexibility & Subsea Power Output Optimization: Flexibility & Subsea Power Output Optimization: The impact of different bending and flexing conditions was part of the considered assumption. The Flex-DTEMs are mounted on subsea flow structures; hence, investigating power output and efficiency aimed at optimizing the power system performance while maintaining flexibility was necessary.

Durability & Reliability: It was assumed that the Flex-DTEM and all power system components were designed for long-term operation without degradation in performance.

Electrical Installation: It was assumed that all electrical components were adequately insulated to prevent short circuits caused by water ingress.

Testing and Validation: Comprehensive testing in controlled environments was assumed to ensure the Flex-DTEG functionality and performance under simulated ultra-deepwater conditions. Hence, the Flex-DTEM datasheet is shown in *Table 3.9.*

Table 3.9 Flexible DTEM Datasheet

Deepwater Thermoelectric Module (Flex-DTEM) Data Sheet	
Parameter	**Values**
Operating Pressure Rating	More than 6 000 PSI
Temperature Rating	Minus (-) 10 °C to Plus (+)190 °C
Heat Flow Through Module	139.8 W
Matched Load Resistance (RL)	4 Ohms
Maximum Operating Voltage (Vmp)	5.06 V
Maximum Operating Current (Imp)	1.32 A
Open Circuit Voltage (VOC)	10.09 V
Maximum Operating Power (Pmp)	6.99 W
Hot-side Operating Temperature (T-Hot)	150 °C
Cold-side Operating Temperature (T-Cold)	0 °C
Hot-side Max. Temperature (T-Hot max)	190 °C
Cold-side Max. Temperature (T-Cold max)	10 °C

3.4.9. Deepwater Power Plates (DPPs)

The power demand from subsea equipment during exploration or production activities is usually high. Therefore, a higher power system requires more than six (6) Flex-DTEMs.

Based on the results obtained from the different system configurations for the six Device-TEM-03 modules in **Subsections 3.4.6.1**, **3.4.6.2**, the outcomes of **Subsections 3.4.7**, **3.4.8**, with all assumptions taken into consideration, several Flex-DTEMs were connected in a series-parallel pattern to form a deepwater power plate (DPP) or Flex-DPP. Furthermore, the desired Flex-DPP layout having bypass diodes, blocking diodes, and subsea electronic systems arrangement was selected to avoid system failure and losses, thus guaranteeing maximum output power from the power system.

Mathematical Equations (Ferrotec, 2001)(S&PF MODUL., 2007) were used for the Flex-DPP formation of higher power levels. The Flex-DPP formation consists of parallel (p), and series (s) connected Flex-DTEMs. When temperature difference due to hot fluid flow from the oil-gas reservoir and cold surrounding seawater is applied on the surfaces of a single Flex-DTEM, a potential difference or open circuit voltage (V_{OC}) can be obtained. Electric current flows through the circuit when a load is connected to the terminals of the Flex-DTEM. The formula for calculating the current is expressed in *Equation (3.2)*.

$$Current\ (I) \quad = \quad \left(\frac{V_{OC}}{R_{in} + R_{Load}}\right) \tag{3.2}$$

Where:

V_{OC} is Open Circuit Voltage.

R_{in} is the Internal Resistance of the DTEM.

R_{Load} is Load Resistance.

With the load placed on the Flex-DTEM, the power at the load is calculated using *Equation (3.3)*:

$$P_{Load} = \frac{V_{OC}^2}{(R_{in} + R_{Load})^2} \text{ x } R_{Load} \quad (3.3)$$

If the resistance of the optimal load is equal to the internal resistance of the Flex-DTEM (that is $R_{opt} = R_{in}$), then maximum power is obtained. At the maximum power point, the optimum current, voltage, and maximum power can be calculated using *Equations (3.4), (3.5),* and *(3.6),* respectively.

$$I_{opt} = \left(\frac{V_{OC}}{2 \text{ x } R_{in}}\right) = \frac{I_{SC}}{2} \quad (3.4)$$

$$V_{opt} = \left(\frac{V_{OC}}{2}\right) \quad (3.5)$$

$$P_{Max} = \frac{V_{OC}^2}{(4 \text{ x } R_{in})} = \left(\frac{V_{OC} \text{ x } I_{SC}}{4}\right) \quad (3.6)$$

Where I_{SC} is short circuit current.

As stated above, a Flex-DPP is formed when several Flex-DTEMs are connected in parallel (p) and series (s) for different higher output levels. The open circuit voltage and the internal resistance of a Flex-DPP can be determined using *Equation (3.7)* and *Equation (3.8).*

$$V_{OC}^{DPP} = V_{OC} \quad \text{x} \quad p \tag{3.7}$$

$$R_{Opt}^{DPP} = R_{in} \quad \text{x} \quad \left(\frac{p}{s}\right) \tag{3.8}$$

At optimum load conditions, *Equation (3.9)*, *Equation (3.10)*, and *Equation (3.11)* can determine the optimum current, optimum voltage, and maximum power of the Flex-DPP, respectively.

$$I_{Opt}^{DPP} = \left(\frac{V_{OC} \quad \text{x} \quad s}{2 \quad \text{x} \quad R_{in}}\right) = \left(\frac{I_{SC} \quad \text{x} \quad s}{2}\right) \tag{3.9}$$

$$V_{Opt}^{DPP} = \left(\frac{V_{OC} \quad \text{x} \quad p}{2}\right) \tag{3.10}$$

$$P_{Max}^{DPP} = (P_{Max} \quad \text{x} \quad p \quad \text{x} \quad \text{s}) \tag{3.11}$$

The expressions in *Equation (3.2)* to *Equation (3.11)* were used to develop a power tool in MATLAB/Simulink. The power tool can compute the power parameters of a deepwater thermoelectric power plate (Flex-DPP). By inputting a required number of parallel and series Flex-DTEMs at the input side, the power tool uses the input information to determine five critical parameters of the desired Flex-DPP. The computed power parameters are maximum power (P_{Max}^{DPP}), optimum voltage (V_{Opt}^{DPP}), open circuit voltage

(V_{OC}^{DPP}), optimum current (I_{Opt}^{DPP}), and short circuit current (I_{SC}^{DPP}) of the desired Flex-DPP. *Figure 3.25* and *Figure 3.26* are screenshots of 251.6 W (or 250 watts) and 349.5 W (or 350 watts) Flex-DPP configurations computed by the thermoelectric power tool.

As shown in the illustration, the 251.6 W or 250 W power plate consisted of six (6) Flex-DTEMs connected in series and six (6) Flex-DTEMs connected in parallel. The computed maximum output power of the intended Flex-DPP was 250 W, the optimum voltage was 30.33 V; the open-circuit voltage was 60.66 V, the optimum operating current was 8.31A while the short circuit current of 2.77A as shown in *Figure 3.25*.

When five (5) Flex-DTEMs were inputted in the series input box and ten (10) Flex-DTEMs in the parallel channel, the computed output of the power tool was a Flex-DPP configuration in which the maximum output power of 349.5W (approximately 350 W), optimum operating voltage of 25.27V, an open circuit voltage of 50.55V, optimum current of 13.85A, and a short circuit current of 2.77A as shown in *Figure 3.26*. The 250 W deepwater power plate (250W-DPP) formation was selected for this deepwater power system.

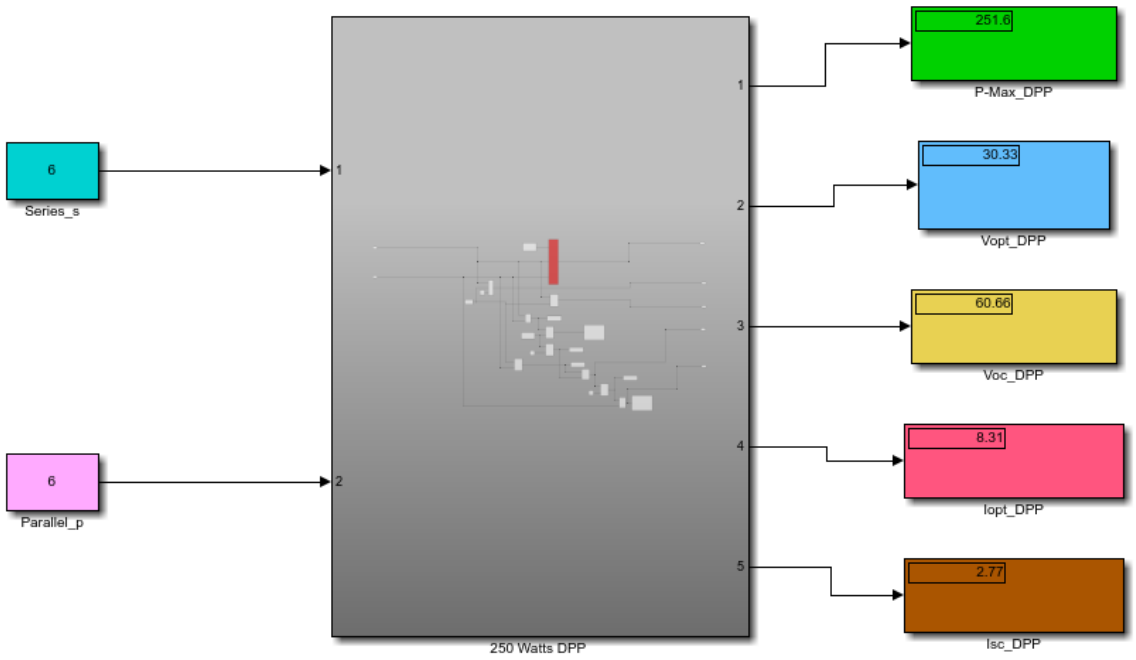

Figure 3.25 Electrical Power Computing Tool (250W-DPP)

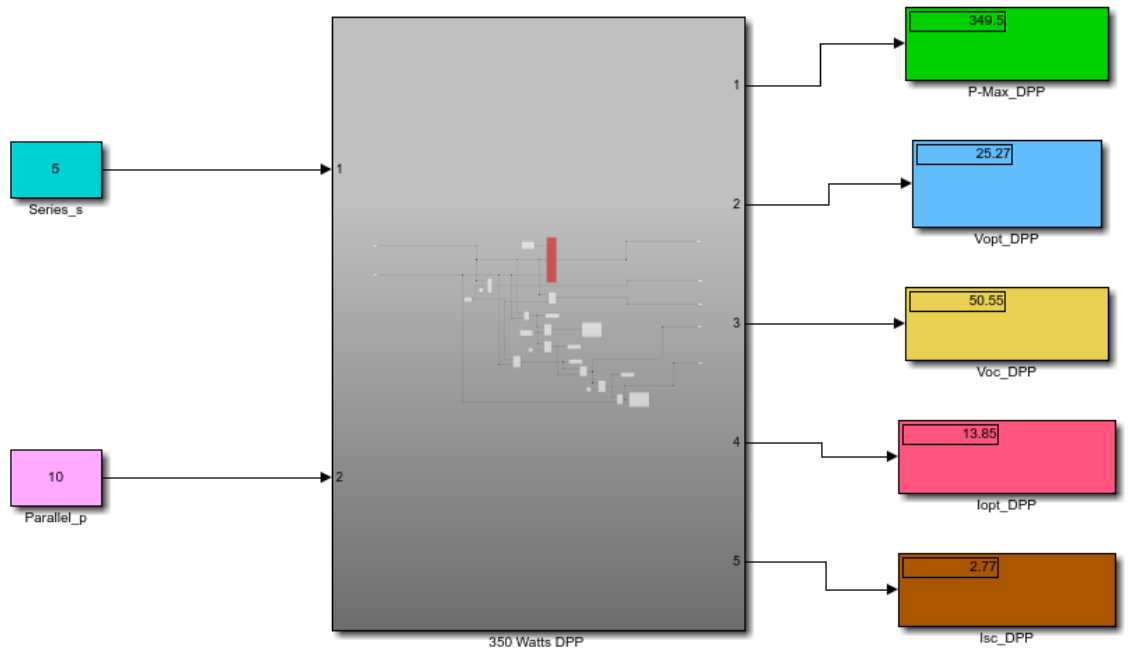

Figure 3.26 Electrical Power Computing Tool (350W-DPP)

3.4.9.1. Dual Redundant DPP Configuration

Consideration was given to subsea systems reliability regarding dual redundant power system configuration. Under such review, the Flex-250W-DPP would have 72 Flex-DTEMs instead of 36 Flex-DTEMs in a *System-A* and *System-B* formation. *System-A* of the dual redundant framework would have 36 Flex-DTEMs, while *System-B* would have the other 36 Flex-DTEMs. *System-A* and *System-B* would then be arranged and connected in parallel for 250 W output power.

The power system makeup in such an arrangement would improve the availability at a system level without affecting the individual *System-A* or *System-B* reliability. Secondly, the DPP would be less likely to fail or lose power generation on any single fault condition. Thirdly, a faulty system would not have to be replaced immediately; hence, power generation could continue until it is appropriate for replacement. Finally, the dual redundant approach would be expensive but more effective than a single system formation.

Nevertheless, the composition of the selected Flex-250W-DPP for this work was the 36 Flex-DTEMs, as shown in *Figure 3.27*. The Flex-250W-DPP system configuration had six (6) bypass diodes (black), two (2) blocking diodes (green), and subsea electronic systems. Information on the components and assumptions for the flexible 250-W deepwater power plate are stated in *Table 3.10*.

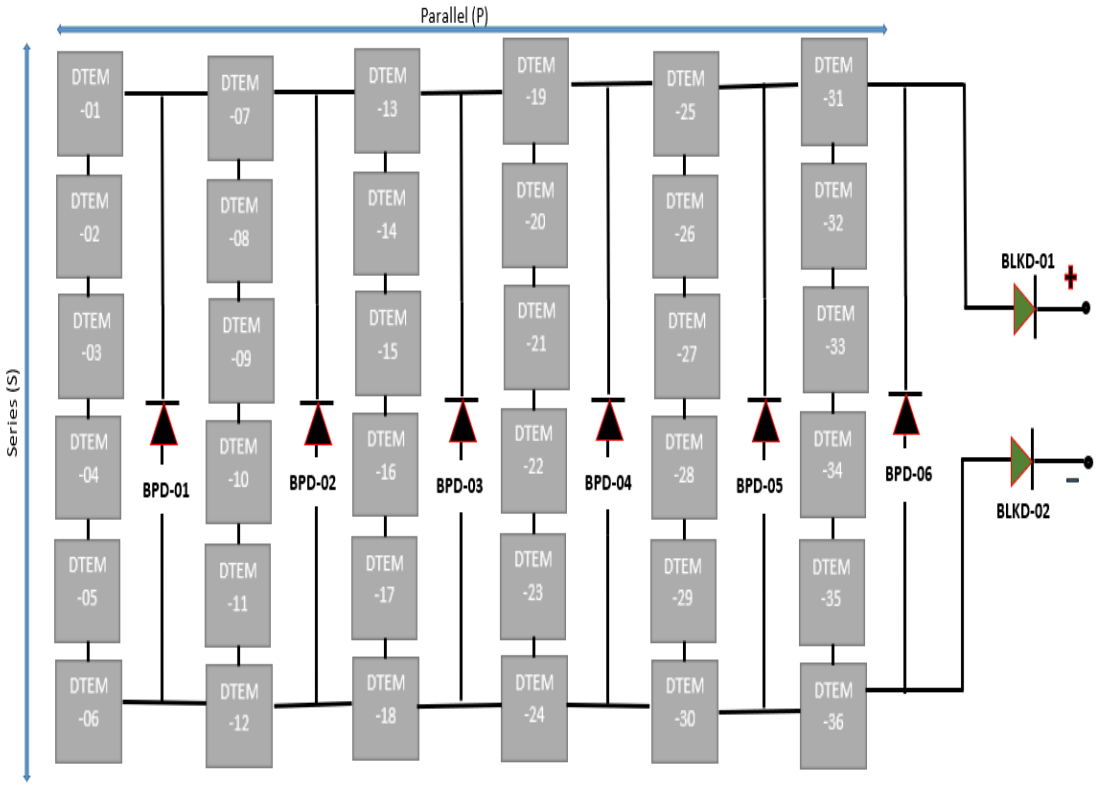

Figure 3.27 250W-DPP System Configuration

3.4.9.2. Standalone 250W-DPP Power Source

The 250W-DPP developed in **Section 3.4.8** is a DC power-generating system that needs to function as an independent power source. Therefore, for the Flex-250W-DPP model to operate independently or as a standalone power source, the Soltech-215 mould in MATLAB/Simulink specialised power systems libraries was reprogrammed to suit the functionality of a thermoelectric power generator by modifying the temperature and irradiation parameters of the system script. Thus, *Figure 3.28* represents a standalone or self-contained 250W-DPP power generating unit with subsea temperature difference (SDT) input ranging from 0 °C to 150 °C and output DC power of 250W.

The Flex-250W-DPP is assumed to be a single deepwater power plate consisting of 36 Flex-DTEMs connected in series-parallel configuration, bypass diodes, blocking diodes, and subsea electronic systems, as previously discussed. The Flex-250W-DPP as a single unit is mounted on a subsea structure for waste heat harvesting, harnessing, and conversion to electricity. Details on the operation of this deepwater power system are in ***Chapter 4***.

Table 3.10 250W-DPP Datasheet

250 W Deepwater Power Plate (250W-DPP) Data Sheet	
Parameter	**Values**
Operating Pressure Rating	6 000 PSI
Temperature Rating	Minus (-) 10 °C to Plus (+)190 °C
Total Number of DTEMs	36
Number of DTEMs in Parallel (p)	6
Number of DTEMs in Series (s)	6
Protection Bypass Diodes	6
Protection Blocking Diodes	2
Maximum Operating Voltage (VDPP)	30.33 V
Maximum Operating Current (IDPP)	8.31 A
Open Circuit Voltage	60.66 V
Maximum Operating Power (PDPP)	251.6 W
Hot-side Operating Temperature (T-Hot)	150 °C
Cold-side Operating Temperature (T-Cold)	0 °C
Hot-side Max. Temperature (T-Hot max)	190 °C
Cold-side Max. Temperature (T-Cold max)	10 °C

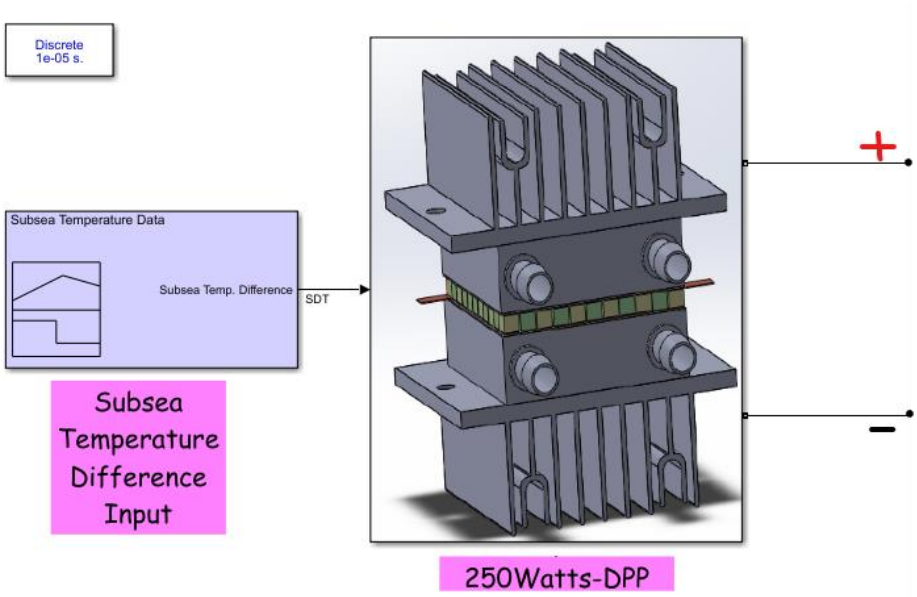

Figure 3.28 Standalone 250W-DPP Power Generating System

3.4.10. Deepwater Power Unit (DPU)

The electrical power requirement for a deepwater or ultra-deepwater power plant exceeds 250 W. Therefore, the single Flex-250W-DPP will not be sufficient to provide electricity for an oil and gas field. Many electrical power-demanding subsea equipment are usually installed on the seafloor and inside the subsea oil-gas wells in most ultra-deepwater fields. As such, connecting several Flex-250W-DPP systems in parallel and series arrangements leads to forming deepwater power units (DPUs) of various higher power ratings.

The power rating of a DPU can be determined if the power parameters of the Flex-250W-DPP that make up the DPU are known. At the maximum power point, the maximum power (P_{Max}^{DPP}) of a Flex-250W-DPP can be calculated using *Equation (3.12)*.

$$P_{Max}^{DPP} = (V_{Max}^{DPP} \text{ x } I_{Max}^{DPP}) \quad (3.12)$$

Where (V_{Max}^{DPP}) and (I_{Max}^{DPP}) are the voltage and current of the Flex-250-DPP at maximum power point. Furthermore, by substituting the values of the desired voltage (V_{Max}^{DPU}) and current (I_{Max}^{DPU}) at the maximum power point of the DPU into *Equation* (3.13*)* and *Equation (3.14),* the number of series string (Ns) and parallel string (Np) connected Flex-250-DPP within the DPU framework can be determined.

$$N_S = \left(\frac{V_{Max}^{DPU}}{V_{Max}^{DPP}}\right) \quad (3.13)$$

$$N_P = \left(\frac{I_{Max}^{DPU}}{I_{Max}^{DPP}}\right) \quad (3.14)$$

Finally, the maximum power of a DPU at the maximum power point is calculated using *Equation* (3.15*)*.

$$P_{Max}^{DPU} = (N_S \text{ x } N_P \text{ x } P_{Max}^{DPP}) \quad (3.15)$$

Equations (3.12) to *Equation* (3.15*)* were used for calculating deepwater thermoelectric power units (DPUs) ranging from 1279 W to 10440 W, as presented in *Table 3.11*.

The 6395 W DPU consists of ($N_P = 5, N_S = 6$) Flex-250W-DPP, maximum power point voltage (V_{Max}^{DPP}) value of 174V, and maximum power point current (I_{Max}^{DPP}) of 36.75A was

selected for this project. The calculations are available in **Appendix C**. The design of an ultra-deepwater oil and gas field with a subsea equipment power requirement of 6.4-kW-DPU is in Chapter 5. The operation of the 6.4-kW-DPU power system is explained in ***Chapters 6*** and ***7***.

Table 3.11 Range of DPUs & Output Power Properties

Deepwater Power Units (DPUs)	Parallel (P)-Series (S) Configuration	Max. Power Point Voltage (V_max)	Max. Power Point Current (I_max)
1279 W	P2, S3	87.00	14.70
2558 W	P3, S4	116.00	22.05
3410 W	P4, S4	116.00	29.40
4263 W	P4, S5	145.00	29.40
5329 W	P5, S5	145.00	36.75
6395 W	P5, S6	174.00	36.75
7673 W	P6, S6	174.00	44.10
8952 W	P6, S7	203.00	44.10
10440 W	P7, S7	203.00	51.45

3.5. Chapter Summary

A test rig (test bench) was designed, developed, and constructed in this Chapter. Commercial thermoelectric modules Device-TEM-01, Device-TEM-02, and Device-TEM-03 were tested for deepwater oil and gas operation. The Device-TEM-03 was the selected deepwater thermoelectric module. It was assumed that Device-TEM-03 were flexible deepwater thermoelectric modules (Flex-DTEM). Further experiments were carried out on six (6) potential deepwater thermoelectric modules.

An electrical power parameters computing tool was developed. The power tool computed and established electrical specifications for Flex-250W-DPP and Flex-350W-DPP deepwater power plates (DPPs). The Flex-250W-DPP formation was picked for this project. Nine (9) different compositions of deepwater power units (DPU) ranging from 1279 W to 10440 W were formed. The 250 W deepwater power plate (Flex-250W-DPP) for energy harvesting developed in this Chapter is operational in ***Chapter 4***.

Chapter 4

Waste Heat to Electricity, Energy Storage & Utilisation

4.1. Introduction

Power electronics components were designed into electrical power system interfaces. The power system interfaces were implemented to assist in managing waste heat harnessing, harvesting, and power generation from ultra-deepwater oil-gas reservoirs. Energy storage and utilisation in this Chapter were performed through these electronic interfaces and the flexible deepwater power plate (Flex-250W-DPP) developed in ***Chapter 3***.

4.2. Deepwater Thermoelectrics Input/Output Parameters

Complexities characterise the deepwater and ultra-deepwater environment. Therefore, developing deepwater thermoelectric power sources and their electronic systems to monitor and control such power systems at 3000-meter water depth involves a multifaceted approach. Fundamental thermoelectric equations like the Seebeck effect, electrical conductivity, and thermal conductivity have been discussed and utilized in

Chapters 2 and ***3***. Heat transfer processes such as conduction, convection, and radiation to capture heat flow within subsea systems and interactions with surrounding seawater were mentioned in ***Chapter 3***. Power system models, equations, electronic systems, and algorithms are developed for computing energy conversion efficiency based on temperature gradient and electrical load in this Chapter, ***Chapters 6*** and ***7***.

The main input parameter to the power system is subsea temperature differential ranging from 0 °C to 150 °C across the flexible deepwater thermoelectric modules (Flex-DTEMs). As discussed in ***Chapter 3***, Flex-DTEMs are contained in the 250 W flexible deepwater power plates (250W-Flex-DPPs). The deepwater thermoelectric power unit (6.4kW-DPU) comprises several 250W-Flex-DPPs. Other input variables include electrical load specifications such as voltage, current, power, and the impact of these parameters on the power system.

The output parameter of the deepwater power system is the generated electrical power based on subsea temperature gradient and electrical load. The other outputs of the underwater power system were based on factors such as the energy conversion efficiency, energy storage, and utilization potentials of the thermoelectric system.

In the following sections, it is essential to note that the DC output power from the deepwater power system will initially be supplied to DC-powered subsea equipment and subsea batteries. In the second instance, the deepwater power system and subsea battery will jointly provide the DC power to subsea equipment in this Chapter. However, in ***Chapters 6*** and ***7***, the DC output power from the deepwater power system will be

transformed into AC power and delivered to an energy storage facility called the underwater electrical power grid system.

Additional input and output criteria considered for the remaining parts of this work include the appropriate use of the Seebeck coefficient, electrical conductivity, thermal conductivity of thermoelectric materials, uniform temperature, and heat distribution across the DTEMs to ensure optimal power system operation and overheating prevention.

It was assumed that the deepwater thermoelectric power system and its relevant electronics operated in steady-state conditions, and transient effects or changes at the seafloor over time had no impact on the overall system. Furthermore, the behaviour of thermoelectric materials was assumed to be stable and consistent despite the subsea environment's high pressure and corrosive nature. Lastly, guaranteed data transmission, control signals, redundant or fail-safe systems, continuous monitoring, and control were other assumptions made on this underwater power system.

4.3. Conversion of Oil-Gas Reservoirs Heat to Electricity

The flexible deepwater thermoelectric module (Flex-DTEM or DTEM), the deepwater power plate (Flex-DPP), and deepwater power units (DPUs) developed in ***Chapter 3*** are characterised by a single operating point at any given time. Generally, the output power from DTEMs, DPPs, DPUs, or any thermoelectric device varies based on the properties of input parameters to the power-generating device. These output power characteristics were discussed in ***Chapter 3***.

As discussed above, the primary input parameter for this deepwater power system is the subsea temperature difference (STD). The variability of the output electric power from a thermoelectric device implies that a specialised power interface is needed to stem the varying output power conditions. Such a power interface enables the DTEM, DPP, or DPU to function optimally at their respective operating points. The following subsections focus on operating the Flex-250W-DPP at maximum energy harvesting potential and conversion to electrical power.

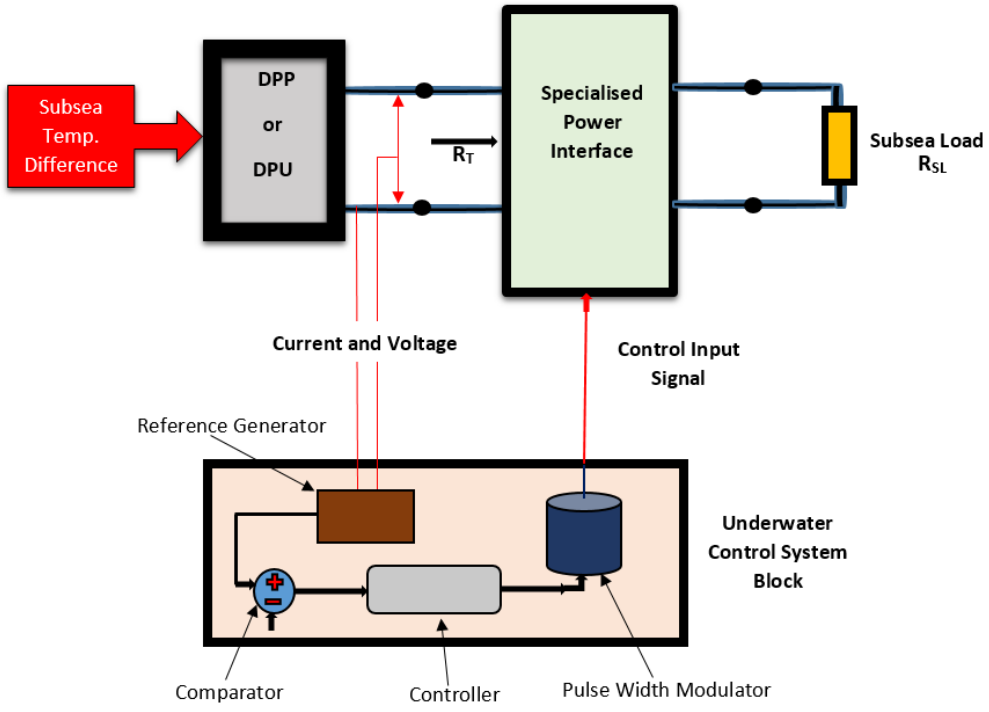

Figure 4.1 Underwater Power System Control Topology

Hence, the Flex-DPPs and the DPUs developed in the previous Chapter are assumed to have dual functions as energy harvesting devices and power sources mounted on subsea

structures (hot fluids flow loops, flowlines, pipelines, risers, etc.) in a deepwater or ultra-deepwater oil-gas field.

Figure 4.1 is this project's control system topology for an underwater power point tracking system. The layout is a power system that contains a specialised power interface with an input impedance or terminal impedance (R_T) from the deepwater power plate (DPP) or deepwater power unit (DPU). A varying subsea load or equipment (R_{SL}) that requires DC voltage is connected at the outlet of the power interface. An underwater control system block links to the specialised power interface and the output side of the DPP or DPU. The input to the DPP or DPU is a subsea temperature difference (STD).

The considered power interface for this application was a subsea DC-DC power converter, as stated in **Section 3.1**. Typically, the control system input for a DC-DC power converter is the duty cycle (d). There are two categories of DC-DC power converters; the first group is the isolated converter, while the second group is the non-isolated power converters. A transformer removes the DC component in an isolated converter circuit's inlet and outlet sides. In contrast, the non-isolated DC-DC converters do not have a transformer within the circuitry. Instead, the DC path between the input and output sides is retained in this power converter class (Lee, Jeong and Han, 2011).

Examples of isolated converters include fly-back, forward, and push-pull converters. Others are half-bridge and full-bridge converters. On the other hand, the three primary non-isolated converters are boost converters (also known as step-up converters). The second is the buck converter (or the step-down converter), while the third is the buck-boost converter (with both step-up and step-down features) (Wu, 2006)(Choi, 2013). Any

of the non-isolated converters can be used for control of input impedance or terminal impedance (R_T) of the Flex-DPP or DPU.

As illustrated in *Figure 4.1*, the voltage signals across DPP or DPU are sensed and measured. Similarly, the current signals flowing through DPP or DPU are also sensed and measured. A reference generator unit within the underwater control system block appropriately processes the terminal voltage signals (v) and current signals (i) of the power source (DPP), as illustrated in the diagram. The output signal of the reference generator is a reference signal. The reference signal is compared (by a comparator) with the actual system feedback signal (variable power from the power source) such that R_T remains constant irrespective of varying subsea loads (R_{SL}) and subsea temperature difference input. Therefore, the power system's terminal impedance (R_T) becomes regulated.

The comparator unit continuously compares the reference and feedback signals; the output error signal from the comparator is passed through a control mechanism (a controller), ensuring that the error signal is always zero. The controller's output passes to a pulse width modulating (PWM) unit to generate the necessary pulse width signals. Pulse width signals activate the duty cycle control input of the non-isolated DC-DC converter (or the specialised power interface).

4.4. Subsea DC-DC Converter

The selected non-isolated converter in this application was the subsea DC-DC boost converter (step-up converter). *Figure 4.2* illustrates the boost converter interfaced with the flexible deepwater power plate (DPP) and subsea load or equipment (R_{SL}) with subsea temperature difference input onto the DPP.

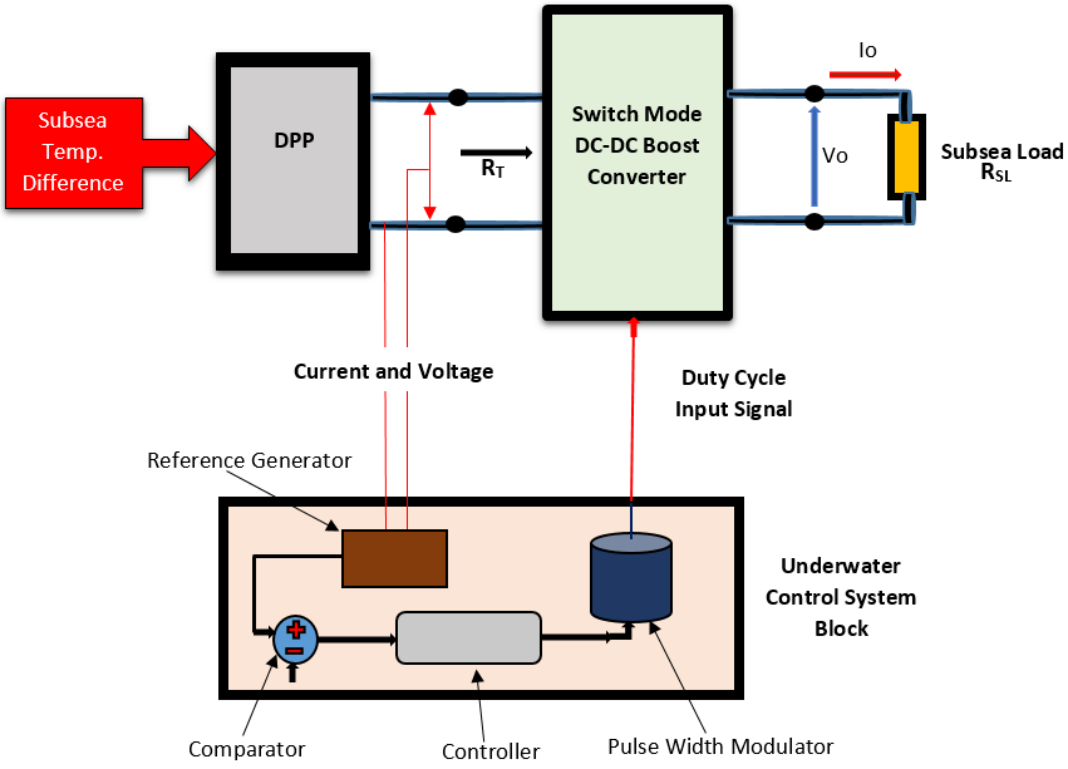

Figure 4.2 Subsea DC-DC Boost Converter as Power Interface

The subsea DC-DC converter or switch-mode DC-DC boost converter in *Figure 4.2* has ON and OFF capabilities enabled by a power semiconductor switch called IGBT (insulated-gate bipolar transistor), as shown in *Figure 4.3*. The power switch or IGBT is

represented by (Q) in the circuit diagram. Other components of the boost converter include an inductor (L) at the power inlet side, a diode (D), and a capacitor (C) at the power outlet side of the circuit.

The terminal voltage across the DPP is denoted by (V_T) while the current flowing through the DPP terminals is (I_T). The current passing through the inductor (L) is the same as (I_T); therefore, the value of the current (I_L) is the same as (I_T). The output voltage of the circuit is (V_O).

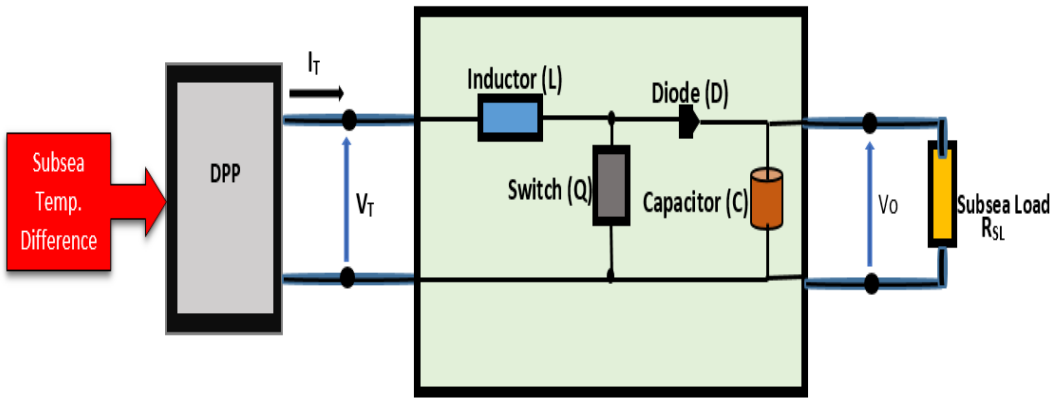

Figure 4.3 Power Switch (Q) in Subsea Boost Converter

The power switch (Q) can be ON or OFF at a given time. The circuit switching time (or period) for the power semiconductor switch Q is denoted by (T_S). (Note: if the switching frequency of the switch is (Q), then the reciprocal of the switching frequency ($1/Q$) becomes (T_S)). When the power switch (Q) turned to the ON position (dT_S) represents the ON time of the switch. When the switch (Q) turns to the OFF position, the OFF time becomes [$(1-d)T_s$].

4.4.1. ON-Time of Power Switch

During the ON time of the switch (Q), the electric current (I_T) from the Flex-DPP flows via the inductor (L) and the power switch (Q). The diode turns OFF during the ON time of the switch Q, while the capacitor (C) continuously discharges (flow out of current from the capacitor) to the subsea load (R_{SL}). The current flow directions at the input and output parts are as indicated in the circuit diagram in *Figure 4.4*. The voltage across the inductor during switch ON time is (V_L). Therefore, the voltage (V_T) is constant during the ON time while the current (I_L) *increases* linearly.

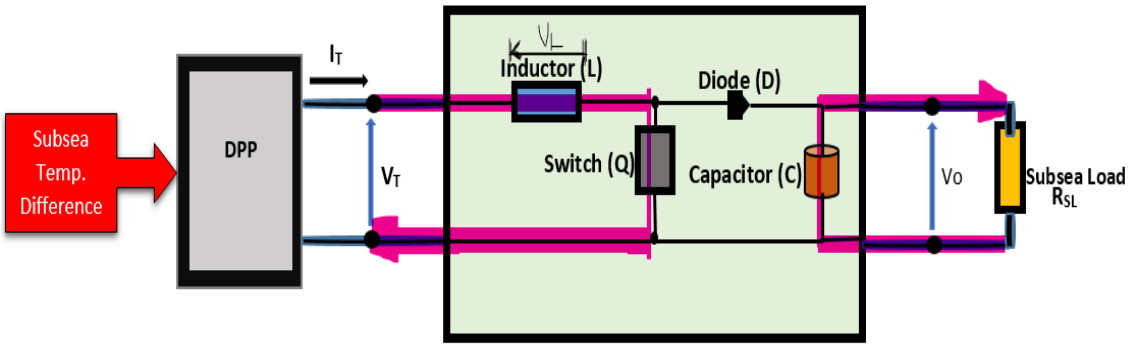

Figure 4.4 Power Switch (Q) ON-Time

4.4.2. OFF-Time of Power Switch

During the power switch (Q) OFF time, the inductor current (I_L) or stored magnetic charges in the inductor flow through the diode (D). The inductor current charges the output capacitor (C) and flows through the subsea load (R_{SL}). The current flow paths are indicated on the circuit diagram in *Figure 4.5*.

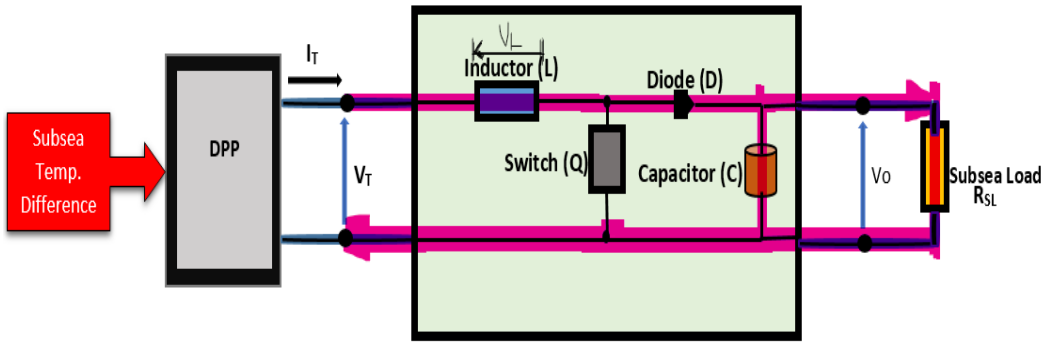

Figure 4.5 Power Switch (Q) OFF-Time

The inductor voltage during the power switch OFF time is $(V_T - V_O)$. The current flow through the inductor *decreases* because the inductance current discharges to the capacitor and subsea load. Therefore, the *average inductor current* value is equivalent to the *terminal current* (I_T) value during power switch (Q) OFF time.

4.4.3. Subsea Boost Converter Input/Output Relation

The input voltage (inlet) and output voltage (outlet) relationship of the subsea boost converter, the Flex-DPP with subsea temperature difference input, and the subsea load (R_{SL}) can be linked mathematical to the terminal voltage (V_T) of the DPP and the output voltage (V_O) of the subsea power converter.

Consider that the *average voltage* flowing through the *inductor is zero* in the steady state during the ON and OFF times of the power switch. Therefore, the *volt-seconds balance* across the *inductor* is thus:

$$\{ \ (V_T \quad \text{x} \quad dT_S) \ \} \ + \ \{ \ (\ V_T \ - \ V_O) \quad \text{x} \quad (1-d)T_s \ \} \ = \ 0 \qquad (4.1)$$

Simplifying and rearranging *Equation (4.1)* is:

$$V_O \ = \ \left\{ V_T \quad \text{x} \quad \left(\frac{1}{1 \ - \ d} \right) \right\} \qquad (4.2)$$

The deepwater power circuitry's input and output *electric current relationship* utilises the *current flow* through the *capacitor*. This relationship is also called *amps-seconds balance*. The *average current flow* through the *capacitor is zero* during the power switch ON and OFF times. That means charge build-up or losses are not allowed in the capacitor at a steady state. Given that the current flow through the capacitor is (I_O), the balanced charge and discharge current through the capacitor becomes:

$$\{(-I_O)dT_S\} \quad + \quad \{(I_T - \ I_O) \quad \text{x} \quad (\ 1 \ - \ d)T_S\} \ = \ 0 \qquad (4.3)$$

Simplifying and rearranging *Equation (4.3)* results in the expression in *Equation (4.4)*:

$$I_O \ = \ \{I_T \quad \text{x} \quad (1 \ - \ d)\} \qquad (4.4)$$

Dividing *Equation (4.2)* by *Equation (4.4)* provides the relationship linking the inputs and outputs of the DPP with its subsea temperature difference, subsea DC-DC boost converter, and subsea load.

$$R_{SL} = \left(\frac{V_O}{I_O}\right) = \left\{\left(\frac{V_T}{I_T}\right) \quad \text{x} \quad \left(\frac{1}{(1-d)^2}\right)\right\} = \frac{R_T}{(1-d)^2} \qquad (4.5)$$

4.5. Underwater Control System Block

Several techniques are available for tracking the optimum operating power of thermoelectric generators. The difference in these methods depends on system complexity, reliability (or effectiveness), and cost. Some of the techniques in the literature (Engineer *et al.*, 2015)(Ni *et al.*, 2011) include:

- Incremental conductance
- Fractional short circuit current
- Fractional open circuit voltage
- Fuzzy logic
- Neural networks
- Perturb and Observe/Hill-Climbing
- Etc.

A single control system block can also be attained if two or more of these methods are combined. However, remotely located subsea equipment does not require system complexity. Furthermore, deepwater or ultra-deepwater system failure could be catastrophic; hence, reliability and simplicity were essential for this underwater power system requirements. The Perturb and Observe (P&O), also called the Hill-Climbing control technique, was selected for this deepwater application.

4.5.1. Hill-Climbing Method

The Hill-Climbing approach adopted for this power system utilizes the duty cycle of the subsea DC-DC boost converter or switch-mode boost converter described in **Section 4.3**. The output voltage and current signals of the DPP or DPU are continuously sensed and measured. Optimum power is tracked when there is a change in power (dP), voltage (dV), and change in the duty cycle.

Furthermore, the power value at present (or the immediate power) and the previous power value (the past or old power) are compared at every sampling period to determine the appropriate duty cycle. If the incremental or stepwise power (dP) is greater than zero, the duty cycle increases, thus making the value greater than zero.

However, if the stepwise power (dP) is less than zero, the duty cycle reduces, thereby making the value of the duty cycle less than zero. Therefore, optimum or maximum power is tracked in the system when the change in power (dP), including the change in the voltage (dV), is equal to zero, as expressed in *Equation (4.6)*.

$$\frac{dP}{dV} = 0 \tag{4.6}$$

Depending on the value of the extracted power through the Flex-DPP power generator, the change in duty ratio is multiplied by a dynamic constant as expressed in *Equation (4.7)*:

$$\frac{dP}{dV} = \frac{d(V \times I)}{dV} = I + V\frac{dI}{dV} = 0 \tag{4.7}$$

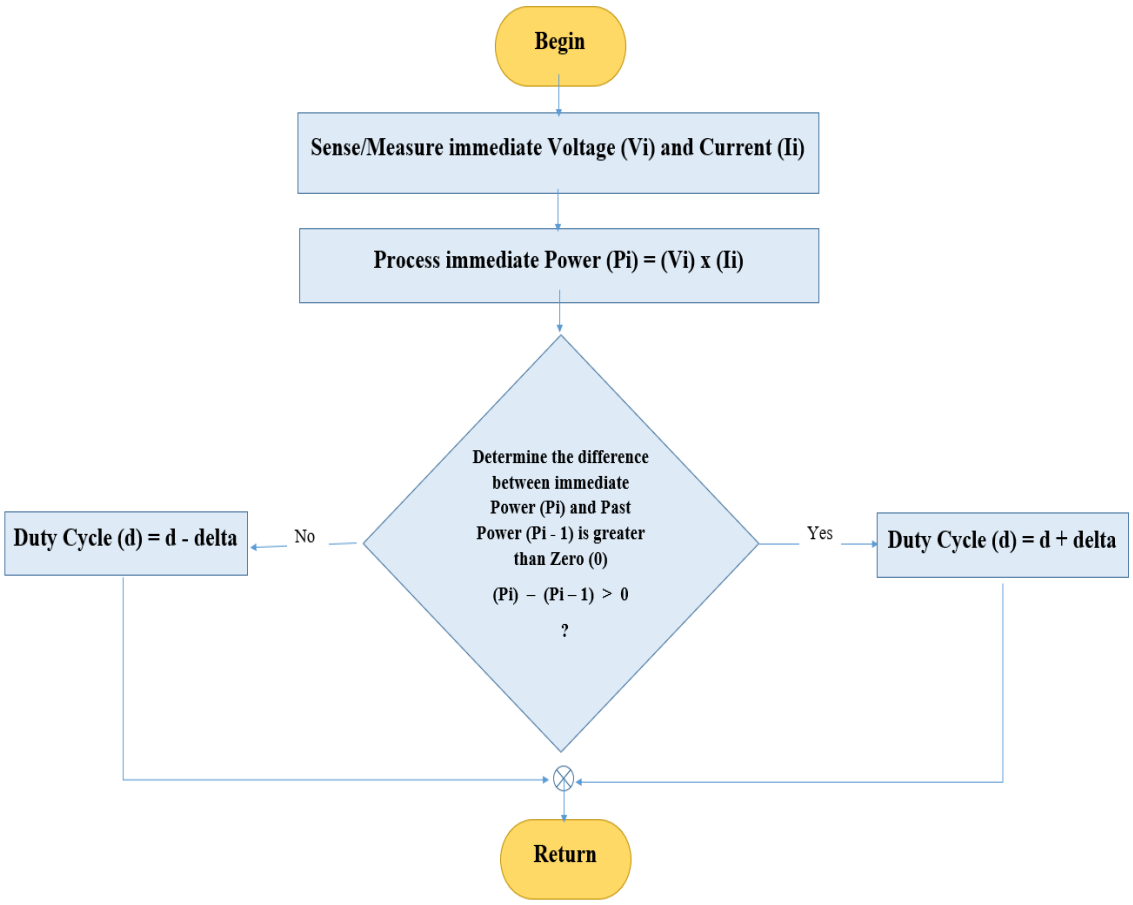

Figure 4.6 Hill-Climbing Flow Chart

Figure 4.6 is the Hill-Climbing system flow chart for the deepwater thermoelectric power system. The Hill-Climbing control system algorithm was developed in MATLAB for the underwater control system block discussed in *Figure 4.1*. **Appendix D (Algorithm D.3)** shows a copy of the MATLAB script. From this point on, this control system block is called the underwater power controller. Further information on DC-DC boost converters or switch mode converters, the Hill-Climbing/P&O algorithm can be found in

(Indragandhi, Subramaniyaswamy and Logesh, 2017)(Hasaneen and Mohammed, 2008)(Esram and Chapman, 2007)(Kamala Devi *et al.*, 2017).

4.6. DPP, Boost Converter & Power Tracking

The flexible 250 W deepwater power plate (250W-DPP) developed in ***Chapter 3***, the subsea DC-DC boost converter, and the underwater power controller algorithm were realized in MATLAB/Simulink for optimum power point tracking of the thermoelectric power source. *Figure 4.7* is the power system model showing the subsea power converter or switch-mode DC-DC boost converter (components within the dark red boarders) interfaced between 250W-DPP with subsea temperature difference and subsea load (R_L) or subsea equipment. The underwater power controller (Orange colour block on the bottom left-hand side).

The power computing unit, the efficiency computation unit, and oscilloscopes are the other essential components constituting the deepwater thermoelectric power system (DTEG), as shown in the power system model. As mentioned earlier, the output of the underwater power controller is the duty cycle, represented by a Magenta-coloured block on the power model.

The duty cycle becomes an input to the PWM block (Gray/Green colour block on the left). As previously explained, the output PMW signals represented by a Gold-coloured Goto block activate the IGBT's ON or OFF power switch on the subsea DC-DC boost converter.

Also shown in the model are the main components for the subsea DC-DC boost converter: the inductor (L), the power switch (IGBT), the power diode (D), and the output capacitor (C), as described in **Section 4.3** and **Section 4.4**. Furthermore, the subsea boost converter was assumed to work in continuous conduction mode (CCM). Therefore, electric current or energy transfer from the inductor during switching cycles does not become zero (Howimanporn *et al.*, 2003).

Other assumptions for this implementation were that the maximum subsea load or equipment resistance capability would be up to 50 kilo-Ohms. A switching frequency (f_s) of 100 kHz and a minimum duty cycle (d_{min}) of 0.1 was taken for the functionality of the power system. Thus, the minimum operating inductance was calculated using the equation below. Details on the calculation are available in **Appendix D (Derivation D.1)**.

$$L_{min} = \frac{R_{Lmax} \times d_{min} (1 - d_{min})^2}{2 \times f_s} \tag{4.8}$$

The calculated minimum inductance was 20.25 mH or 0.02025 H. However, the value of the operating inductance used for this power system model was 2e-3 H (or 0.002 H) and 0.1 Ohms internal resistance (also known as equivalent series resistance (ESR)).

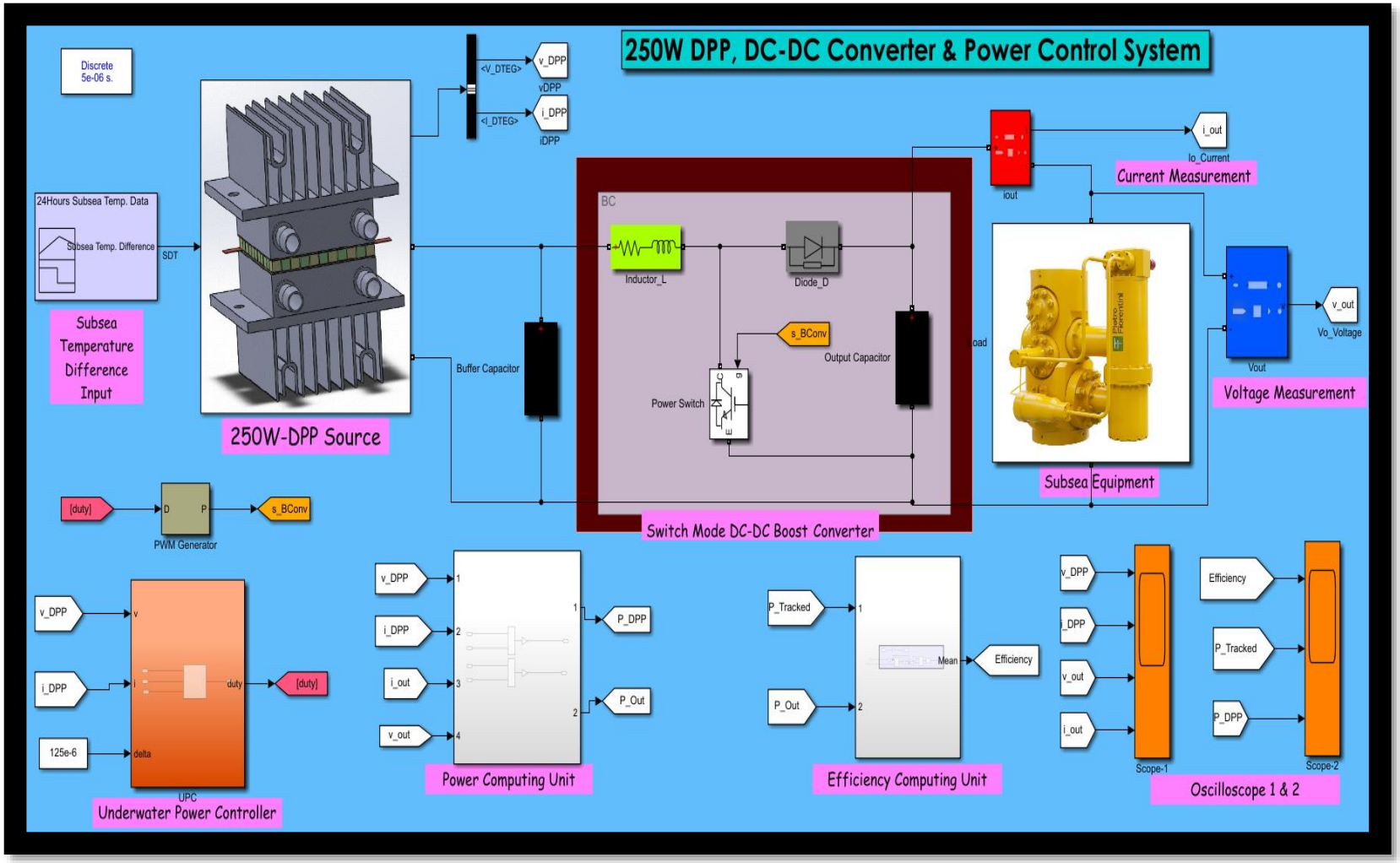

Figure 4.7 250W-DPP, DC-DC Converter & Subsea Equipment

The circuit's minimum capacitance (C_{min}) was estimated on the assumption that ripple voltage ($V_r = 2V$) was equally divided between ESR and the capacitance. In addition, a maximum output voltage (V_O) of 370V was assumed. Other assumptions made in calculating the minimum system capacitance were the maximum duty cycle (d_{max}) value of 0.9 and minimum load resistance (R_{Lmin}) value of 10 ohms. The calculated minimum capacitance was performed using *Equation(4.9)*. The calculation is in **Appendix D (Derivation D.2)**.

$$C_{min} = \frac{d_{max} \text{ x } V_O}{f_s \text{ x } R_{Lmin} \text{ x } V_r} \tag{4.9}$$

The calculated minimum capacitance was 170 μF. A capacitance value of 100 μF and 1e-4 Ohm resistance was used for the buffer capacitor (at the output of the Flex-250W-DPP) and the output capacitor (at the power outlet side of the step-up converter). The primary responsibility of the buffer or terminal capacitor (the capacitor across the Flex-250W-DPP) was suppressing surge voltages, thus preventing any damage to the power system.

The values for the IGBT or power switch internal resistance during the on-time (ROn) and snubber resistance (RS) for the power circuit were 1e-3 Ohms and 1e5 Ohms, respectively.

The power diode (D) parameters setting was 0.001 Ohms for internal resistance (R_{On}), and forward voltage (V_F) value was 0.8 V. Other data for the diode were the snubber resistance (R_S) of 500 Ohms, as well as the snubber capacitance (C_S) of 250e-9 F.

4.6.1. 250W-DPP & Power System Operation

As shown in *Figure 4.7*, the Flex-250W-DPP output voltage and current were sensed, measured, and calculated when the subsea temperature difference was applied across the deepwater thermoelectric power generator or DPP. Subsea temperature difference data from 0 °C to 150 °C was supplied from the subsea temperature difference input channel to the Flex-250W-DPP (see *Table 3.10* for additional info).

The DPP voltage signals ($vDPP$) and current signals ($iDPP$) were sensed and measured through a bus selector (black and white rectangular bar at the output of DPP). At the same time, power computation was done via the Grey-coloured rectangular block named the output power-computing unit shown in the power system model.

Sensed DPP voltage ($vDPP$) and current ($iDPP$) signals were passed on to the underwater power controller block. The underwater power controller operating philosophy was based on the Hill-Climbing control algorithm described in **Subsection 4.5.1**.

The control algorithm determines the power value via the measured voltage and current signals. Theoretically, the calculated power signal passes through filters and toggles switches within the control mechanism. The immediate or present power value was compared with past or old power values, and the outcome was duty cycle values, as explained above. The underwater power controller block output was an appropriate duty cycle at a delta sample interval (step change) valve 125e-6.

The duty cycle passes through a PWM (pulse width modulator) generator. Within the PWM generator, triangular carriers swing from the negative (-1) limit to a positive (+1)

limit. The output of the PWM generator was a PWM signal sent to the gate terminal of the power switch (IGBT) on the subsea DC-DC boost converter, as discussed in **Sections 4.3** and **4.4**. 5kHz was the switching frequency at a sample time of 5e-6 seconds.

4.6.1.1. DPP & Power System Experiment

At this stage, the deepwater thermoelectric power system (DTEG) experiment was based on the power system model in *Figure 4.7*, as described in **Section 4.6.1**. Various subsea temperature difference inputs (from 0 °C to 150 °C) and subsea equipment of three different load resistance values (20 Ohms, 50 Ohms, and 100 Ohm) were connected to the power system to investigate the system behaviour at varying experimental conditions.

Output power from the energy harvester or the Flex-250W-DPP power source was obtained by sensing, measuring, and calculating the DPP voltage and current values. Likewise, computing the output power of the subsea power converter or the switch mode DC-DC boost converter through the power converter's voltage and electric current measurement units was evaluated accordingly.

As discussed in ***Chapter 3***, the Flex-250W-DPP represented a flexible deepwater thermoelectric power plate containing 36 DTEMs, 6 protection bypass diodes, 2 protection blocking diodes, and subsea electronic systems. Another assumption was that the Flex-250W-DPP as a single unit was installed/mounted as part of a subsea structure or flowline in an ultra-deepwater oil and gas field. Hot oil and gas from subsea reservoirs

flowed through subsea structures at temperatures up to 150 °C. The cold side temperature range on the Flex-250W-DPP was from 0 °C to 10 °C as denoted on the device datasheet.

The subsea temperature difference input, the subsea power converter, and the underwater power controller's functionality determined the performance of the Flex-250W-DPP and the power output of the thermoelectric energy harvester. The capabilities of this Flex-250W-DPP are valid for any DPP or DPU. Further details on the Flex-250W-DPP and DPUs are in **Subsection 3.4.9** and **Subsection 3.4.10**, respectively.

Load Resistance-20 Ohms Connection @ 20 °C: Test-01

The experiment began by connecting a 20-ohm load resistance subsea equipment, as represented on the DTEG power system model in *Figure 4.7*. The other system parameters were discussed above. Next, the subsea temperature difference input was 20 °C, and the power system was simulated.

At the end of the simulation, the measured output voltage and current at the terminals of the Flex-250W-DPP (referred to as P_DPP on the power system model) were 15.93V and 0.98A, respectively. Hence, the power drawn from subsea oil and gas reservoirs through the Flex-250W-DPP was 15.62W.

Secondly, electrical power obtained from the Flex-250W-DPP through the terminals of the subsea DC-DC converter (or P_Out on the power system model) was 15.72W. Thirdly, the tracked power from the Flex-250W-DPP via the combined action of the subsea DC-

DC converter and the underwater power controller (represented as P_Tracked on the power system model) was 33.33W.

Therefore, when the subsea temperature difference at the seabed was 20 °C, waste heat was extracted and harnessed from the subsea oil and gas reservoirs through the DTEG system and delivered 33.33W of electrical power and delivered to the connected subsea equipment, which had a load resistance of 20 ohms. The summary results on the 20 Ohms load resistance on the subsea equipment connection @ 20 °C: Test-01 are available in *Table 7.10*. Detailed results of this experiment are in **Appendix D (Table D.4)**.

Load Resistance-20 Ohms Connection @ 50 °C: Test-02

In Test-02 or Load Resistance-20 Ohms on subsea equipment Connection @ 50 °C, the subsea temperature difference input was changed from 20 °C to 50 °C while the load resistance value remained at 20 Ohms. Again, the experiment was repeated; the DTEG power system was simulated. The output voltage and current from the Flex-250W-DPP derived via oil and gas structures were measured accordingly. The extracted power at the Flex-250W-DPP or P_DPP during this time was 83.51W.

The output voltage and current flow measured at the terminals of the subsea DC-DC boost converter were 41.47V and 2.07A, respectively. Therefore, P_Out, or 85.97W, was obtained at the terminals of the DC-DC power converter. At the same time, 83.33W or P_Tracked was tracked and delivered to the subsea equipment through the joint efforts of the subsea DC-DC converter and the underwater power controller. *Table 7.10* provides

the summary results of this experiment; additional details are available in **Appendix D (Table D.4)**.

Load Resistance-20 Ohms Connection @ 70 °C: Test-03

In Test-03, the subsea temperature difference input was changed from 50 °C to 70 °C. The load resistance value remained at 20 Ohms, and the experiment was repeated thrice. The power from the Flex-250W-DPP or P_DPP was 118.20W, while the measured power through the subsea power converter or P_Out was 115.85W. The tracked or P_Tracked power supplied to subsea equipment through combined operations of the subsea boost converter and the underwater controller block was 116.70W. These results are in *Table 7.10* and **Appendix D (Table D.4)**.

Load Resistance-20 Ohms @ 90 °C, 110 °C, 130 °C & 150 °C: Test-04 to Test-07

The experiment continued for the fourth, fifth, sixth, and seventh time for subsea temperature difference (STD) inputs of 90 °C, 110 °C, 130 °C, and 150 °C, respectively, for a load resistance value of 20 Ohms as explained in *Test-01* to *Test-03*. *Table 7.10* shows the summary results obtained in these experiments, while detailed results are in **Appendix D (Table D.4)**. *Figure 4.8* and *Figure 4.9* shows the plots when subsea equipment had a load resistance of 20 Ohms on the deepwater thermoelectric power system.

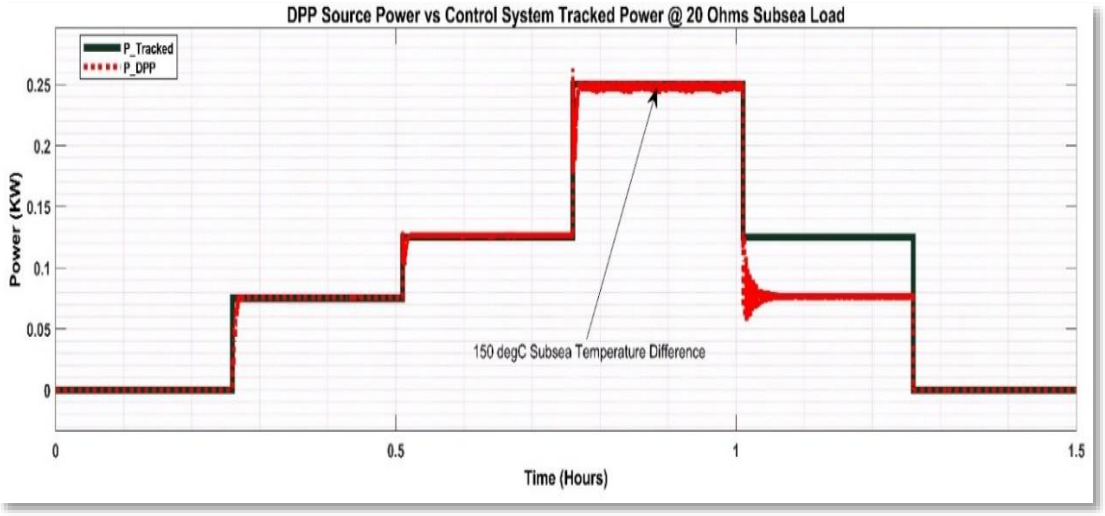

Figure 4.8 20-Ohms Load Resist. on Subsea Equipment & DTEG Power System

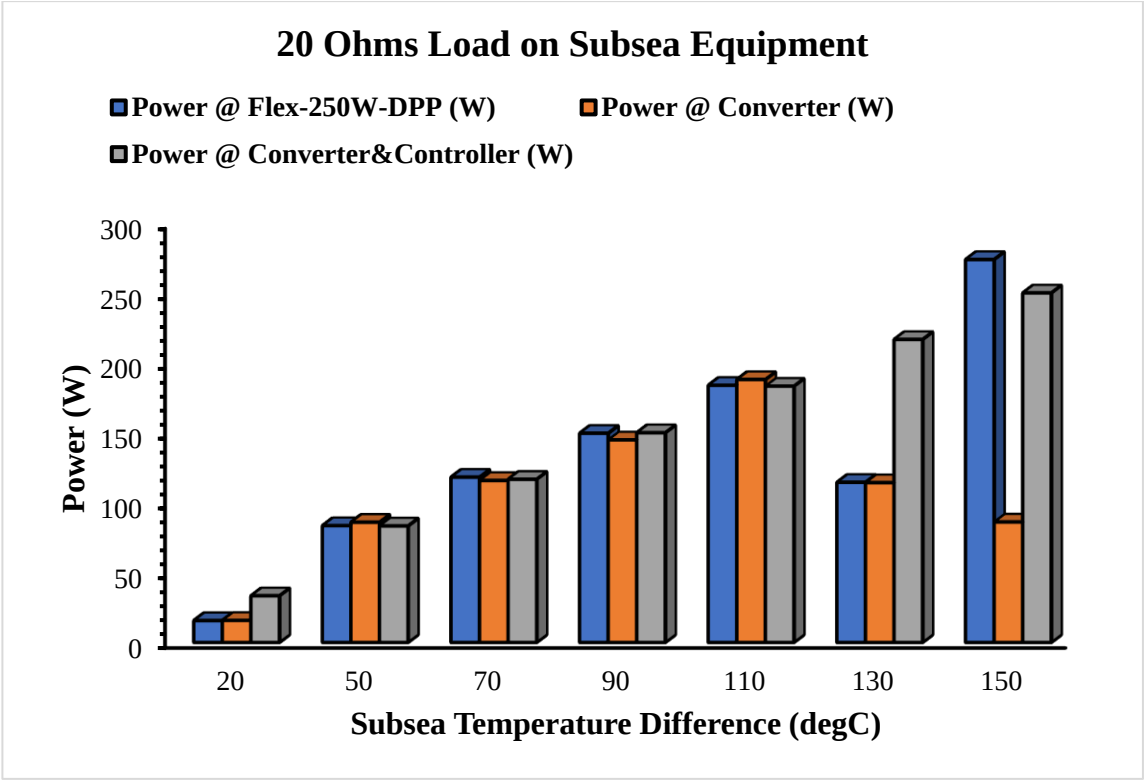

Figure 4.9 DC-Power to Subsea Equipment on 20-Ohms Load

Load Resistance-50 Ohms Connection @ 20 °C: Test-08

In the second experimental case, the load resistance value of the subsea equipment was changed from 20 Ohms to 50 Ohms. In Test-08, the temperature difference input was 20 °C. As discussed above, the DTEG power system parameters were in place, and the system was simulated. The power obtained from the terminals of the Flex-250W-DPP or P_DPP was 32.72W. The measured output voltage value of 40.33V and output current of 0.81A was received at the terminals of the subsea DC-DC boost converter or P_Out of 32.53W. In contrast, the tracked power (P_Tracked) that was delivered to subsea equipment via the DC-DC converter and the underwater power controller was 33.33W. See *Table 7.11* for the summary results; further details are available in **Appendix D (Table D.5)**.

Load Resist.-50 Ohms @ 50 °C, 70 °C, 90 °C, 110 °C, 130 °C &150 °C: Test-09 to 14

The 50 Ohms load resistance on subsea equipment experiment was repeated for the second and third times when subsea temperature difference inputs were 50 °C and 70 °C. Subsea temperature difference for the fourth and the fifth experiments was 90 °C and 110 °C, while 130 °C and 150 °C were the input subsea temperature difference during the sixth and the seventh experiments. The results of all seven (7) experiments at the various conditions are available in *Table 7.11* and **Appendix D (Table D.5)**. The plots for the 50 Ohms load resistance on subsea equipment connected to the DTEG power system are shown in *Figure 4.10* and *Figure 4.11*.

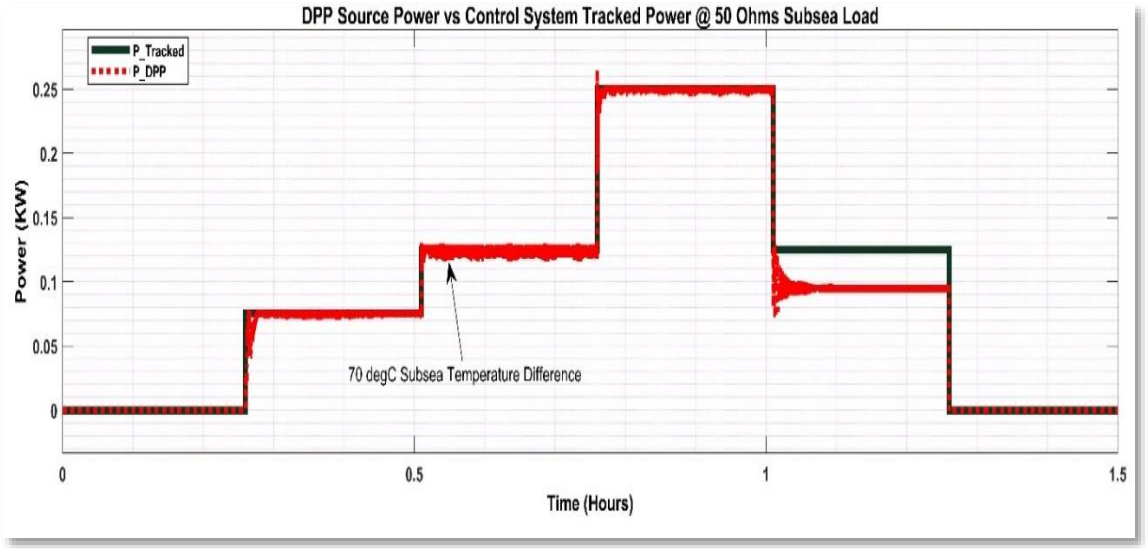

Figure 4.10 50-Ohms Load Resist. on Subsea Equipment & DTEG Power System

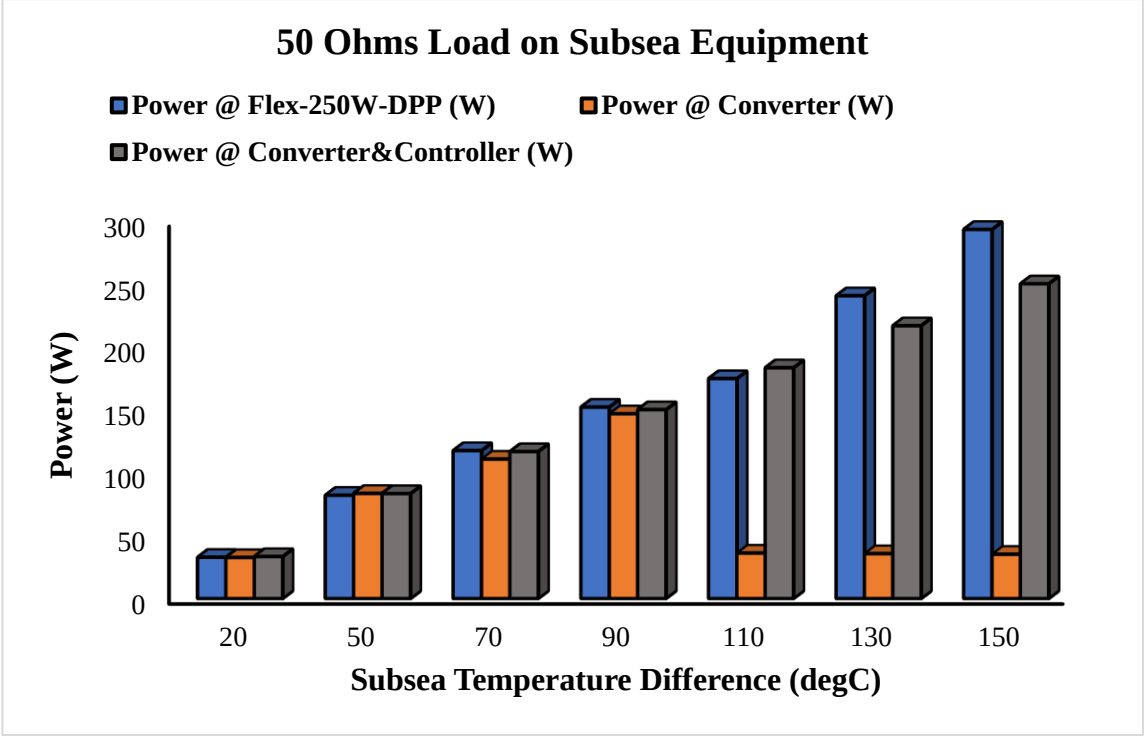

Figure 4.11 DC-Power to Subsea Equipment on 50-Ohms Load

Load Resistance-100 Ohms Connection @ 20 °C: Test-15

The third category of the experimental case was with subsea equipment having a load resistance of 100 Ohms. All other parameters of the DTEG power system were in place, as discussed above. The subsea temperature difference input at the start of the experiment was 20 °C, and the power system was simulated. The power derived from subsea oil-gas reservoirs and seawater through the Flex-250W-DPP terminals was 32.82W. The power value measured at the subsea boost converter or P_Out was 30.48W. The power conveyed to subsea equipment jointly by the subsea DC-DC boost converter and the underwater power controller block or P_Tracked was 33.33W.

Load Resist.-100 Ohms @50 °C, 70 °C, 90 °C, 110 °C, 130 °C, &150 °C: Test-16 to 21

The experiment was repeated for the second time when the subsea temperature difference input was 50 °C. In the 3rd experiment, the subsea temperature difference was 70 °C before changing the input temperature difference to 90 °C in the fourth experiment. Subsea temperature difference settings for the 5th and 6th experiments were 110 °C and 130 °C, respectively. Finally, the subsea temperature difference input in the seventh experiment was 150 °C. The load resistance value on the subsea equipment was 100 Ohms in all seven experiments. Details on the results obtained during this case are available in *Table 7.12* and **Appendix D (Table D.6)**. The plots for the 100 Ohms load resistance on the deepwater thermoelectric power system are shown in *Figure 4.12* and *Figure 4.13*.

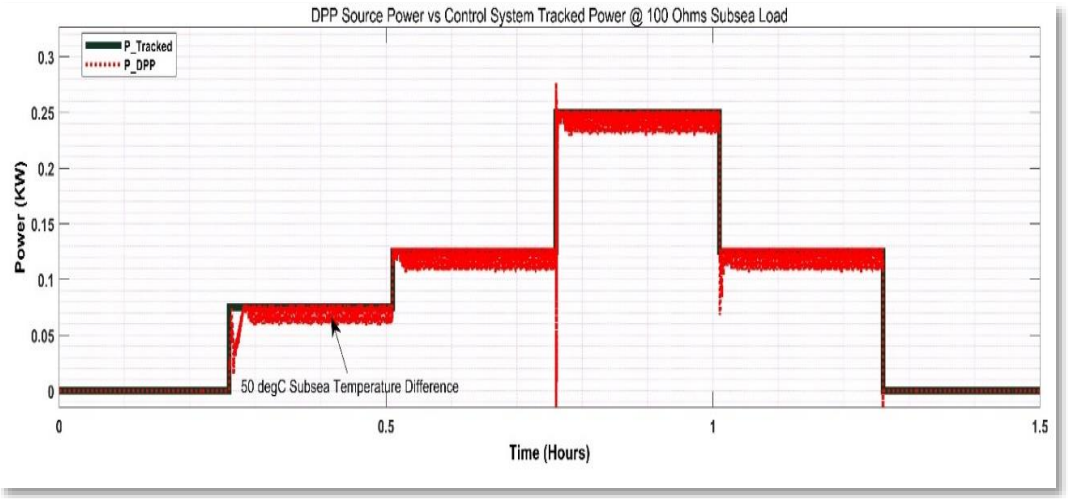

Figure 4.12 100-Ohms Load Resist. on Subsea Equipment & DTEG Power System

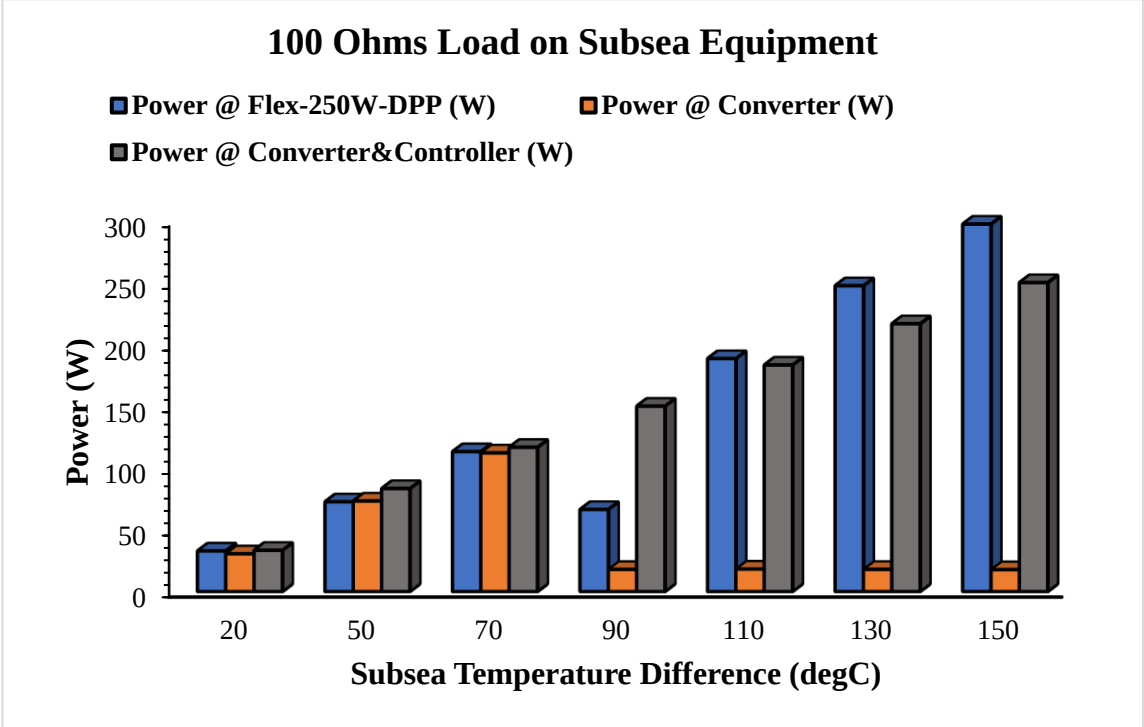

Figure 4.13 DC-Power to Subsea Equipment on 100-Ohms Load

4.6.1.2. Outcome of Load Resistances on DTEG Power System

The output of the three experiments with 20-ohm, 50-ohm, and 100-ohm load resistances on subsea equipment indicated that the Flex-250W-DPP mounted on a subsea structure can harness waste heat from oil-gas reservoirs and surrounding seawater. The harnessed heat was converted to electricity and supplied to DC-powered subsea equipment on 20-ohm, 50-ohm, and 100-ohm load resistances. The bar charts above show the variation in the amount of power measured at the terminals of the power source, the DC-DC converter, and the power supplied to subsea equipment via the joint action of the DC-DC converter and underwater controller.

Figure 4.14 shows that irrespective of the disparity in load resistances and fluctuating subsea temperature difference, the underwater controller's algorithm delivered the required power to the subsea equipment through the DC-DC converter.

The average power and standard deviation for the 20-ohm, 50-ohm, and 100-ohm load resistances on subsea equipment are 147.62W and 76.03W, respectively. *Table 4.1* presents the calculated power parameters. Error bars for the 20-Ohms load on subsea equipment (represented as No.1), 50-Ohms load on subsea equipment (designated as No.2), and 100-Ohms load on subsea equipment (described as No.3) are shown in *Figure 4.15*.

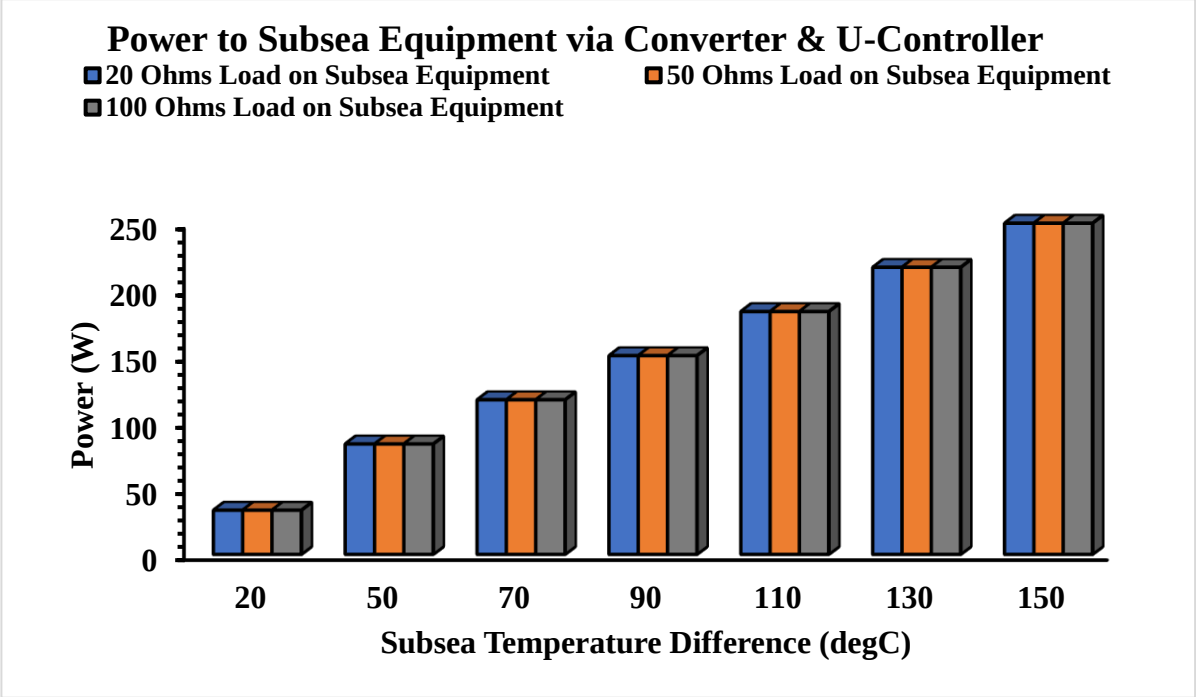

Figure 4.14 Power to Subsea Equipment via Converter & U-Controller

Table 4.1 Calculated Power & Load Parameters

Attributes	**20-Ohms Load on Subsea Equipment**	**50-Ohms Load on Subsea Equipment**	**100-Ohms Load on Subsea Equipment**
Average	147.6228571	147.6228571	147.6228571
Standard Deviation	76.03057734	76.03057734	76.03057734

Further analysis was carried out, and *Table 4.2* shows Pearson's correlation for subsea temperature differences against the output power supplied to subsea equipment on varying load conditions. *Figure 4.16* shows the scatter plots that corroborate the output power from the deepwater thermoelectric power system when the subsea temperature difference is applied. The DC-DC converter, the combined performance of the DC-DC converter,

and the underwater controller eventually delivered the output power to DC-powered subsea equipment.

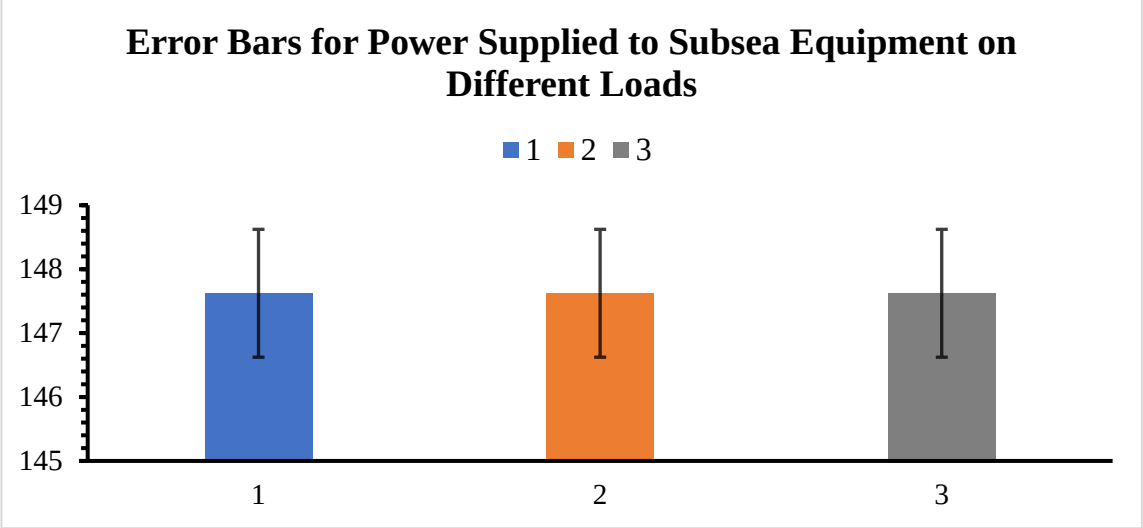

Figure 4.15 Error Bars-Power to Subsea Equipment

Table 4.2 Pearson's Correlations-Power to Subsea Equipment

Pearson's Correlations

	n	Pearson's r	p
Subsea Temp. Diff. (°C) - Power to Subsea Equipment (W)	60	1.000	< .001

A significant positive correlation was found between subsea temperature difference and the power supplied to subsea equipment from the Flex-250W-DPP, $r(58) = 1.0$, $p < 0.001$. As shown by Pearson's correlation and the scatter plots above, the p-value from the results of the experiments is less than 0.05. Therefore, a statistical relationship exists between subsea temperature difference and output power to subsea equipment. Hence, it can be concluded that the experiments are repeatable, and the outcomes are valid.

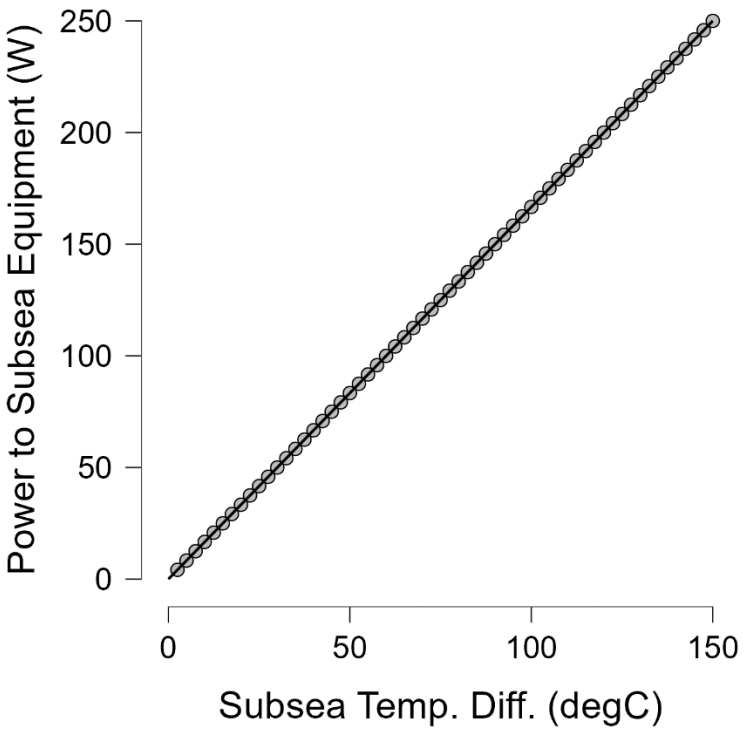

Figure 4.16 Scatter Plots-Subsea Temp. Diff. vs Power to Subsea Equipment

The test results indicated that subsea temperature difference from 0 ℃ to 150 ℃ influences the output power of Flex-250W-DPP, the DC-DC converter, the underwater power controller, and the power supplied to subsea equipment. Hence, the predictive capabilities of deepwater thermoelectric power systems and power electronic systems are enhanced for real-world ultra-deepwater applications.

4.6.1.3. The Efficiency of the Power System

Parasitic resistances were present in the power system while operating the Flex-250W-DPP with subsea temperature difference input, the underwater power controller, and the subsea DC-DC boost converter. These assumptions lead to power losses in the DTEG Power system (Kazimierczuk, M. K. and Ayachit, 2015). Such parasitic resistances include IGBT on-resistance, diode forward resistance (R_F), and diode threshold voltage (V_F). Other impediments in the power system circuit were the equivalent series resistance of the inductor and the capacitors. The current flowing through the inductor was also thought to have no ripples. Hence, the inference that the current flowing through the inductor was the same as the input current from the Flex-250W-DPP.

The IGBT conduction losses in the power system circuit are referred to as (P_{IGBT}) power loss. It was also assumed that the duty cycle increases at the load resistance current led to a rapid increase in conduction losses. Therefore, the transistor's output capacitance switching loss (P_{SW}) was considered linear.

Similarly, it was assumed that the diode conduction losses, or diode power losses (P_D), were due to the rapid increase in the diode forward resistance with an increasing duty cycle in the load resistance current on the subsea equipment.

The inductor losses (P_L) increase with an increased duty cycle at the load resistance current on subsea equipment. Likewise, power losses at the output capacitor were expected. The output capacitor power loss was denoted by (P_{CO}). Therefore, the total power loss (P_{TL}) of the underwater controller in conjunction with the subsea boost converter during the

operation of 250W-DPP with subsea temperature difference inputs was as expressed in *Equation (4.10)*:

$$P_{TL} = P_{IGBT} + P_{SW} + P_D + P_L + P_{CO} \quad (4.10)$$

Hence, the system efficiency (η) was calculated as follows:

$$\eta = \frac{Power\ Output\ (Po)}{Power\ Output\ (Po) + P_{TL}} \quad (4.11)$$

$$\eta = \frac{(Po)}{(Po) + P_{TL}} = \frac{1}{1 + \frac{P_{TL}}{P_O}} \quad (4.12)$$

The above parameters for efficiency were factored into the power system model. The power system was connected to a 20 Ohms load resistance and simulated for subsea temperature difference input from 0 °C to 150 °C. *Figure 4.17* shows the efficiency of the underwater power controller and the subsea DC-DC power converter. The computed efficiency via the efficiency computing unit was above 97%. Further details on the system efficiency (the operation of the underwater controller and the DC-DC converter) are available in **Appendix D (Table D.7)**.

The mean, standard deviation, and standard error for the system efficiency were calculated as shown in *Table 4.3*. The data below in *Table 4.4* presents the efficiency and the respective time stamp of the system efficiency. The system efficiency contains 231 datasets based on a 21-hour time frame. At the first-time stamp, or the first 21 hours, the

recorded system efficiency was 0.024725238%, while 0.028927305% was the recorded system efficiency at 231 hours, or the last time stamp. **Appendix D (Table D.7)** shows detailed time and system efficiency.

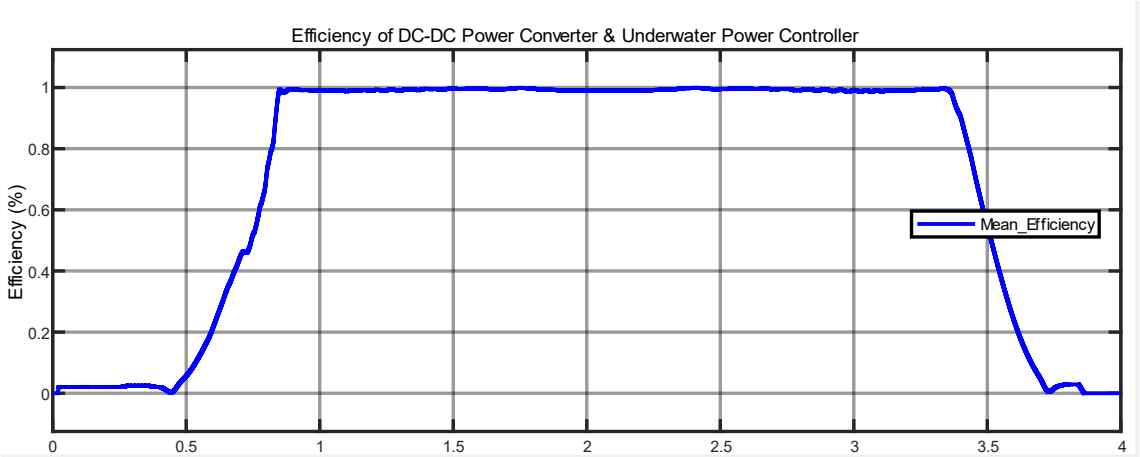

Figure 4.17 Systems Efficiency of Power Controller & DC-DC Converter

Table 4.3 Calculated System Efficiency Information

System Efficiency Data	
Mean:	**0.7327**
Standard Deviation:	**0.3971**
Standard Error:	**0.0261**

The system efficiency data and time stamps were plotted in the pie chart in *Figure 4.18*. The pie chart shows data on system efficiency proportions in percentages (for the various time stamps).

Table 4.4 Time Stamps & System Efficiency

Time (Hours)	System_Efficiency_(%)
T21	0.024725238
T42	0.399424875
T63	0.990591928
T84	0.992205369
T105	0.996609669
T126	0.990482590
T147	0.994261233
T168	0.992256556
T189	0.991160465
T210	0.655559912
T231	0.028927305

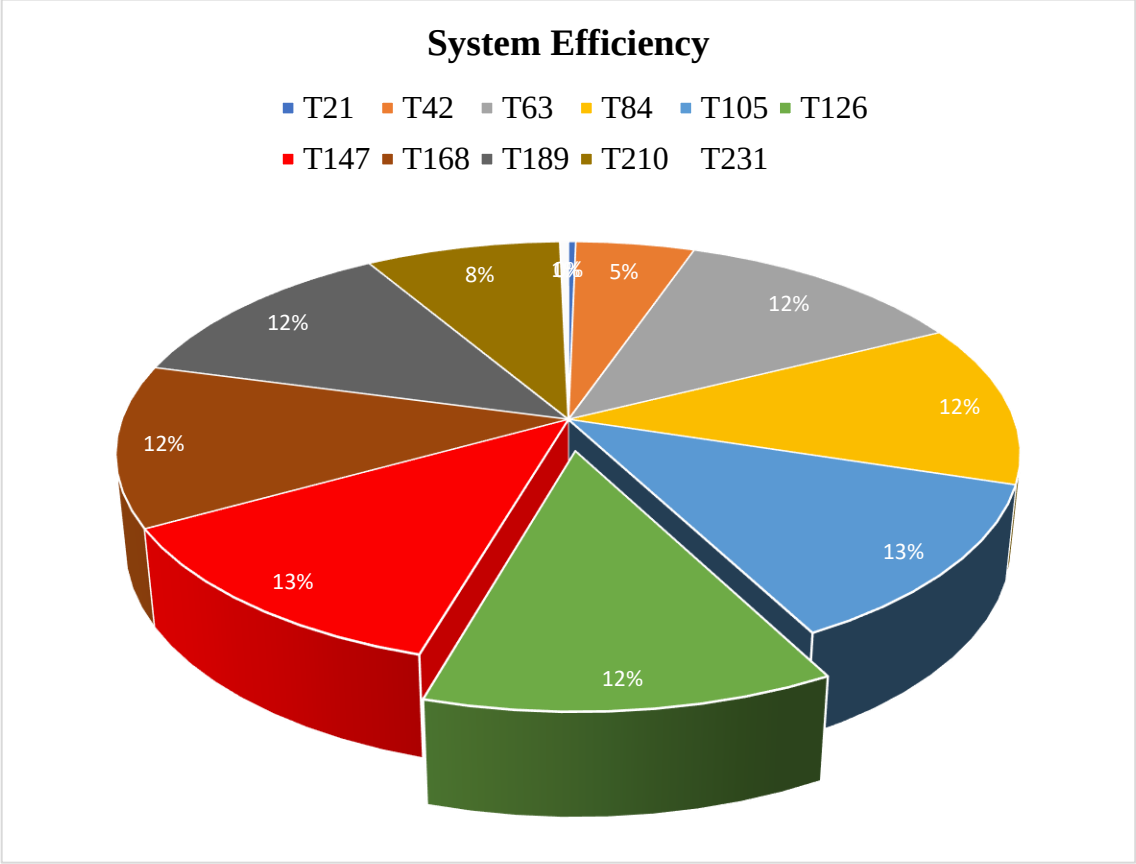

Figure 4.18 Systems Efficiency Proportions

In other words, the chart shows the proportion of system efficiency at the recorded time stamps in percentages. The results demonstrated that 12 percent attained more system efficiency as the subsea DC-DC power converter and underwater power controller operated under the influence of subsea temperature difference from 0 °C to 150 °C.

The overall system efficiency (Schaltz, E. and Man, 2017) of the deepwater thermoelectric power system (DTEG) comprising the Flex-250W-DPP, the subsea temperature input, the underwater power controller, and the subsea DC-DC power converter was also computed.

The power system was simulated for subsea temperature difference from 0 °C to 150 °C. *Figure 4.19* shows the plots of the overall system efficiency of the deepwater thermoelectric power system. The overall power system efficiency computed below was slightly above 94%.

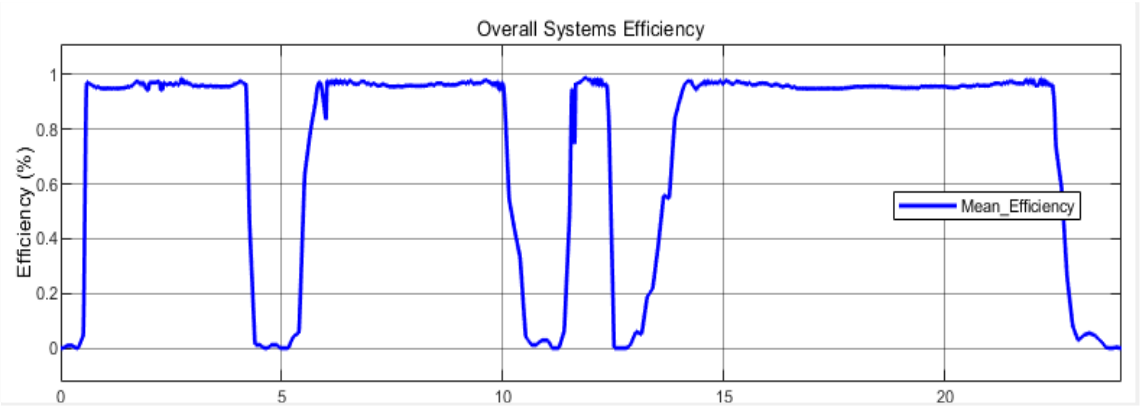

Figure 4.19 Overall Efficiency of the Deepwater Power System

Again, the mean, standard deviation, and standard error for the overall systems efficiency were calculated, as shown in *Table 4.5*. The data in *Table 4.6* are the overall systems efficiency and the respective time stamp.

Table 4.5 Calculated Overall Systems Efficiency Information

Overall Systems Efficiency Data	
Mean:	**0.7653**
Standard Deviation:	**0.3660**
Standard Error:	**0.0241**

Table 4.6 Time Stamps & Overall Systems Efficiency

Time (Hours)	**Overall Systems_Efficiency_(%)**
T21	0.960305448
T42	0.969229735
T63	0.969837527
T84	0.958992136
T105	0.406992200
T126	0.835390557
T147	0.965152538
T168	0.953695985
T189	0.957076254
T210	0.961850493
T231	0.003234558

As mentioned previously, the overall systems efficiency has 231 datasets based on a 21-hour time frame. At the first time stamp, the logged overall systems efficiency was 0.960305448%, while 0.003234558% was the recorded efficiency at 231 hours. Refer to **Appendix D (Table D.7)** for the detailed time stamp and overall systems efficiency.

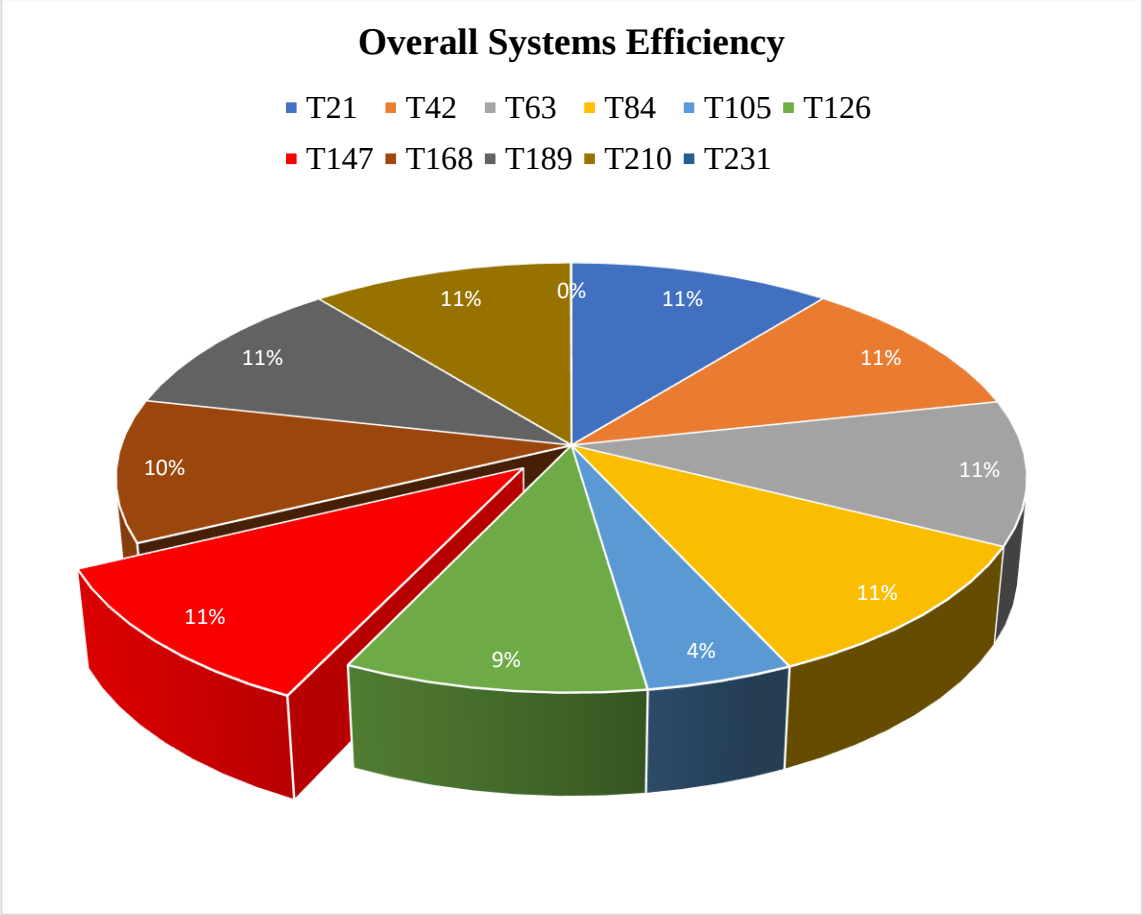

Figure 4.20 Overall Systems Efficiency Proportions

The overall systems efficiency data and time stamps were plotted, as shown in *Figure 4.20*. The overall systems efficiency proportions in percentages for the various timestamps demonstrated that 11 percent achieved more of the overall systems efficiency as the deepwater thermoelectric power system (DTEG) comprising the Flex-250W-DPP, the underwater power controller, the subsea DC-DC power converter, and the subsea equipment operated under the influence of subsea temperature difference from 0 °C to 150 °C.

4.7. Deepwater Energy Storage & Utilisation

Most renewable energy sources are inherently intermittent (Hardisty, 2008), (Bunn and Muñoz, 2016); however, the energy fluctuation rate varies from one power source to another. Among sustainable offshore renewable sources, OTEC (ocean thermal energy conversion) and geothermal energy sources suffer negligible intermittent effects. Thus, OTEC and geothermal energy sources have a considerable advantage over other energy sources. The deepwater thermoelectric power generation system (DTEG) is within the geothermal category; as such, this power system is favourably placed for low power generation interruptions. Additionally, there is a need for a suitable energy storage system to guide against unforeseen circumstances on the seafloor.

The two possible deepwater or ultra-deepwater energy storage techniques are compressed air storage (Cavallo, 2007) and battery technology (Heuberger *et al.*, 2017). The compressed air storage system involves energy storage in underground caverns or airbags tied to the seabed. Battery technology converts electrical energy to chemical storage via a suitable or stationary subsea battery.

The option chosen for this research was the subsea battery. The leading battery technologies within the renewable energy arena are lead (Pb) acid-based, lithium (Li) based, sodium (Na) based, and Nickel (Ni) based. Depending on the application, all batteries have individual advantages and disadvantages. The general characteristics of these leading technologies are in *Table 4.7*.

Table 4.7 Popular Batteries Technologies

S/N	Battery Science	General Characteristics
1	Lead (Pb) Acid-based	Wide range of proven applications and low cost of manufacturing
2	Lithium (Li) based	Lightweight and small size, as well as high energy density
3	Sodium (Na) based	High energy density and lightweight
4	Nickel (Ni) based	Longer life, suitable in the harsh environment, proven offshore or marine application.

4.7.1. Subsea Batteries (NiMH)

As shown in *Table 4.7*, Nickel (Ni) based battery technology is the most appropriate option for this application. The considerations that were made before selecting Nickel Metal Hydride (NiMH) as the potential energy storage subsea battery for this deepwater thermoelectric power system include the following:

Safety & Reliability: Nickel metal hydride (NiMH) is less prone to thermal runaway or safety hazards because it provides a higher level of chemical stability, unlike other battery chemistries. Hence, NiMH is resistant to overcharging and deep discharging, making it suitable for extreme ultra-deepwater conditions.

Environmental Friendliness: Nickel metal hydride batteries contain less toxic chemical compounds than other batteries. Additionally, NiMH is typically characterized by low self-discharge rates. Therefore, this type of battery allows prolonged storage without appreciable loss of charge.

Re-usability: NiMH is an eco-friendly chemistry; it is more recyclable than other chemistries. Hence, it reduces environmental impact and supports sustainability goals in underwater environments.

Cycle Life: Nickel metal hydride batteries can endure a considerable charge-discharge cycle and exhibit a good cycle life. These attributes are essential for long-term reliability in ultra-deepwater environments.

Commercial Practicality: Unlike other chemistries, NiMH offers a more cost-effective solution, thus making it viable and accessible for deepwater deployments.

Some companies involved in energy storage solutions include the below-listed organisations:

- Fluence
- Energy Vault
- ESS
- Hydrostor
- Form Energy
- Key Capture Energy
- Our Next Energy (ONE)
- Yotta Energy
- Noriker Power
- Plus Power
- Panasonic

Figure 4.21 Subsea Battery (Device-SBAT-101)

Any qualified company from the above list with expertise in the workings of subsea systems will be able to manufacture suitable subsea batteries for deepwater thermoelectric energy storage. Furthermore, the potential of Magnesium−Antimony Liquid Metal batteries (Chandler, 2009)(Bradwell *et al.*, 2012) in the subsea environment could be explored when such types of batteries are available in the market.

The subsea battery for this project is called Device-SBAT-101 from Manufacturer-K. (*Please note that trade names are not used in this project*). *Figure 4.21* is a pictural representation of Device-SBAT-101. It was assumed to be a stationary subsea battery for the deepwater power system. Essential information on the subsea battery specification is in *Table 4.8*.

Table 4.8 Device-SBAT-101 Specification

S/N	Item	Description
1	Subsea Battery Pack Rating	12 V / 90 Amp hours (Ah)
2	Discharge Current	100 Amps (A)
3	Minimum Operating Temperature	Minus (-) 20 °C
4	Maximum Operating Temperature	Plus (+) 60 °C
5	Dimensions (mm)	W x D x H (428 x 159 x 270)
6	Cells	Ten (10) numbers
7	Volume	18.4 L
8	Weight	23 Kg
9	Battery Chemistry	Nickel Metal Hydride (NiMH)

4.7.2. Battery Charge Controller

Standard electronic components are used in developing battery charge controllers (Kirn and Ha, 1997)(Kim *et al.*, 2009). In this deepwater power system design, the battery charge controller acts as the electronic interface between the Flex-DPP deepwater power source, the subsea battery, and power-demanding subsea equipment.

It is important to note that the DPPs or DPUs were not designed for battery charging only; instead, they were meant for exclusive power supply to subsea equipment and subsea battery charging on a need basis. Therefore, operating the DPPs or DPUs at the optimum operating point makes the energy harvester or power source capable of charging batteries and providing power to subsea equipment. Hence, the charge controller acts as a power interface that allows power flow management among the interfacing components. Thus, the charge controller design for this deepwater power system was expected to steer the flow of charge in three ways:

- Power flows from the Flex-DPP or DPU to the subsea equipment, as demonstrated in **Section 4.5**
- Power flow from Flex-DPP or DPU to the subsea battery when needed.
- Power flow from the subsea battery to subsea power demanding equipment.

Power flow in the various directions in the presence of the subsea temperature difference inputs, the Flex-250W-DPP, subsea DC-DC power converter, subsea battery, and subsea equipment is the subject of the following subsections:

4.7.2.1. Functional Logic of Charge Controller

In most battery system configurations, the battery voltage is often denoted as (V_{Bat}). A pre-set maximum voltage in such a battery system is referred to as (V_{max}), while the pre-determined minimum voltage is called (V_{min}). Unidirectional switches Q1, Q2, and Q3 are deployed in such power systems for electric current flow in a particular direction. A buffer capacitor (C_{buff}) is added to make such a controller circuit a complete system.

As shown in the conceptual illustration in *Figure 4.22*, if the battery voltage (V_{Bat}) is higher than the pre-set maximum voltage (V_{max}), that is, ($V_{Bat} > V_{max}$), then the battery is said to be in charged condition. Therefore, disconnecting the battery from the power source and linking it to the load or equipment becomes imperative. The battery, in turn, discharges to the load.

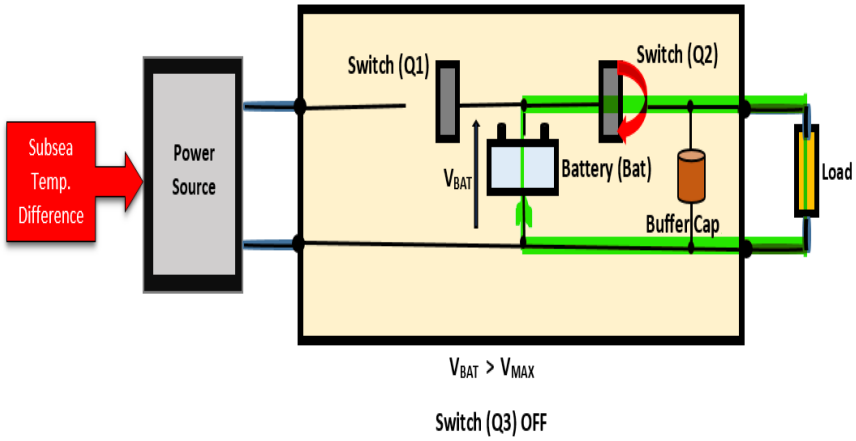

Figure 4.22 VBat is greater than Vmax

If the battery voltage (VBat) is below the pre-defined minimum voltage (V_{min}), that is, ($V_{Bat} < V_{min}$). The battery is disconnected from the equipment and connected to the power source because (V_{Bat}) is less than (V_{min}). The illustration in *Figure 4.23* further describes the idea.

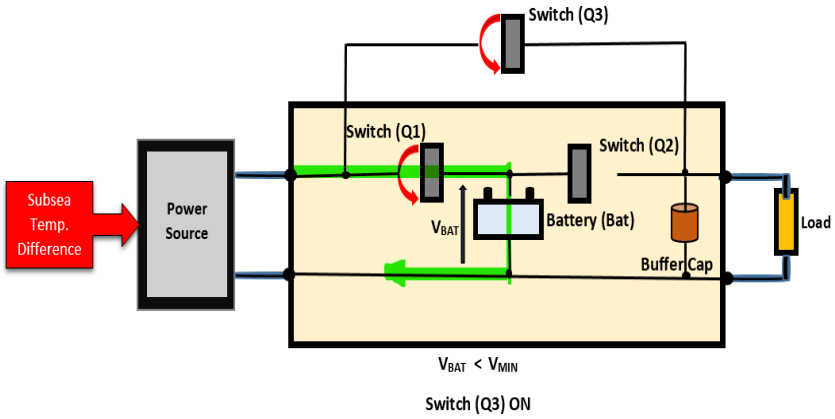

Figure 4.23 VBat is less than Vmax

If the battery voltage (V_{Bat}) is between the pre-determined minimum voltage (V_{min}) and pre-defined maximum voltage (V_{max}), that is, ($V_{min} \leq V_{Bat} \leq V_{max}$). The power source and equipment can then be connected to the battery, as shown in *Figure 4.24*. Additional details on the characteristics of the unidirectional converters and bi-directional converters are available (dos Santos, 2013)(Tan, Abe and Akagi, 2012).

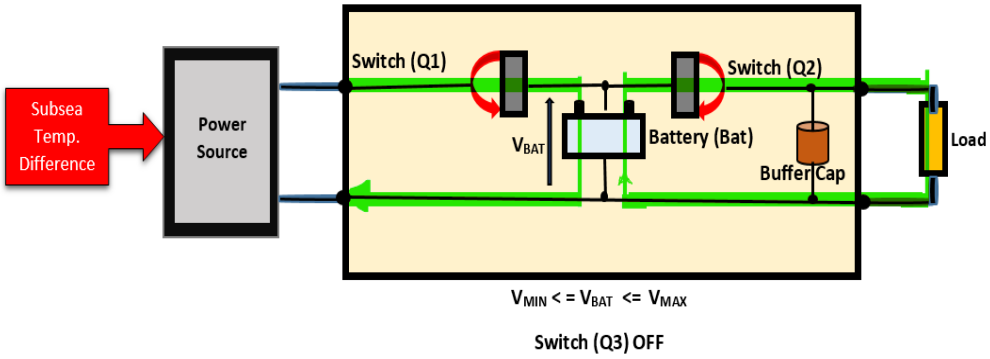

Figure 4.24 Vmin is less than or equal VBat

4.7.2.2. Subsea Battery Charge Controller

The obvious choice for implementing this deepwater power system was to use a bi-directional power converter as the charge controller circuitry. This type of charge controller circuitry can eliminate the one-directional power flow constraints described in **Subsection 4.7.2.1**. Another reason for this selection was the ability to remove and replenish charges at the buffer capacitor (C-buff), especially if multiple subsea equipment are connected to the deepwater power system. Therefore, the subsea charge controller's responsibilities include managing subsea battery charging, discharging, and power transfer to subsea equipment when the need for such service arises.

Additionally, several subsea batteries and bi-directional power converter arrangements can be connected in parallel to the buffer capacitor. In such an arrangement, power sourcing and power sinking are guaranteed at the seabed, thereby reducing ocean floor-based thermoelectric energy intermittency levels from minor to insignificant or non-existent.

Therefore, the conditions adopted for this system operation for a single subsea battery with a bi-directional power converter connected to a buffer capacitor were thus:

- If the power from the flexible 250W-DPP (power source or system power) is less than 15W (*Very Low Power condition*), the DPP is disconnected from the subsea equipment. Then, the subsea battery is connected to the subsea equipment.
- If the Flex-250W-DPP power was 15W but less than or equal to 90W (Low p*ower condition*), the DPP and the subsea battery should supply power to the subsea equipment.
- If power from the Flex-250W-DPP source is 90W but less or equal to 180W (*Medium Power condition*), then only the DPP should supply power to the subsea equipment.
- If the subsea battery level is low (less than 2.5A), the Flex-250W-DPP should be disconnected from the subsea equipment and connected to the subsea battery (*Battery Charging condition*).
- Only the DPP should supply power to subsea equipment if the Flex-250W-DPP source is 180W but less than or equal to 240W (*High-Power condition*).

- If the Flex-250W-DPP power source is between 240W and above (*Very High-Power condition*), the DPP should continuously supply power to subsea equipment.
- A fully charged subsea battery should be disconnected and be on standby (*Standby Condition*).

4.8. 250W-DPP & Subsea Energy Mgmt. Implementation

Based on the above subsea battery charge controller configuration, the deepwater thermoelectric power and subsea energy management (or subsea battery control) systems were performed in MATLAB/Simulink. The power system model is shown in *Figure 4.25*. The 250W-DPP power source, the subsea DC-DC boost converter, and the underwater power controller are on the left-hand side of the model. Centrally placed subsea equipment with a load resistance value of 20 Ohm is in the middle of the power harvesting and energy storage system. A bi-directional power converter, subsea battery, and battery output sensing/measuring devices are on the right-hand side of the power system model. The subsea energy management system or subsea battery control system is at the bottom right-hand side of the power system model.

The bi-directional power converter is the electronic interface between the subsea battery, battery control system, and the 250W-DPP power source, as described in **Section 4.7**. First, bus voltage (VBus) was generated through waste heat harvesting and harnessing from subsea oil-gas reservoirs and seawater via the flexible 250W-DPP. As previously discussed, the subsea DC-DC boost converter and the underwater power controller

assisted in converting heat to electricity when the subsea temperature difference was present.

In other words, the generated bus voltage was based on the optimum power point of the thermoelectric power source, the subsea temperature difference, and power electronics components, as discussed in **Section 4.5** and **Section 4.6**. Secondly, the VBus acted as the coupling point between the 250W-DPP power source segment of the circuit and the subsea energy management system.

The key components used for the bi-directional power converter design were 1000 e-6F (or 1000 μF) and 1e-4 Ohm buffer capacitor (Cap-Bat), 0.5 e-3H, a 0.1 Ohms inductor (Inductor-Bat), and two IGBT power switches (with capabilities for separate handling of positive control signals and negative control signals).

The subsea battery setting was 24V nominal voltage, the rated capacity was 50Ah, and the starting state of charge (SOC) was 45%. The other subsea battery parameters were 18V cut-off voltage, fully charged subsea battery voltage of 28V, nominal discharge current of 22A, capacity at nominal voltage of 45Ah, and subsea battery internal resistance of 0.0048 Ohms.

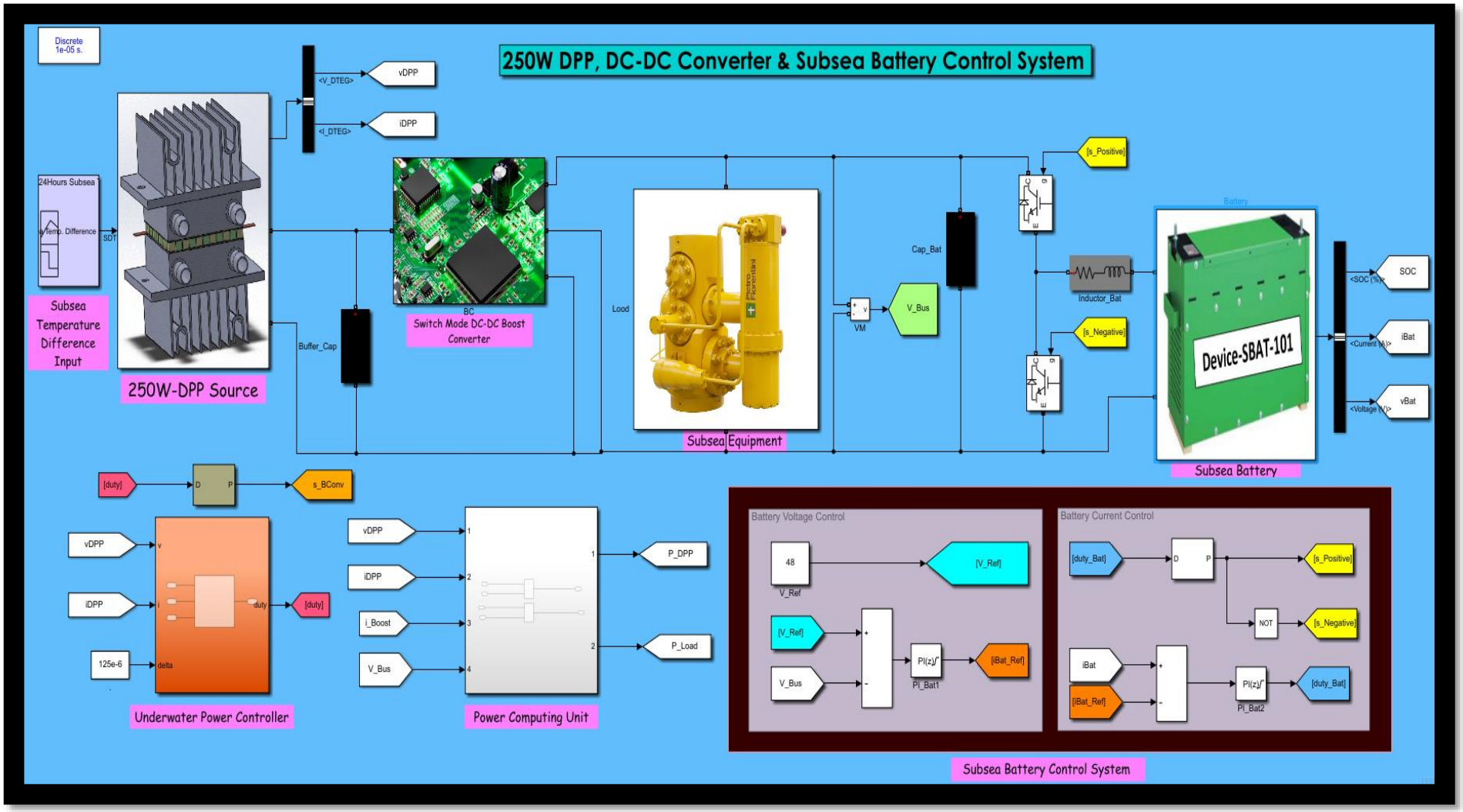

Figure 4.25 250W-DPP, Boost Converter, Subsea Energy Mgmt. System

4.8.1. Subsea Energy Management System

The energy management system was implemented via a two-stage energy management or control procedure. Therefore, the joint operations of the battery voltage and current management, shown in the bottom right-hand side of the power system model, was named the subsea battery control system or *Subsea Energy Management System*.

The voltage management system had a 48V reference voltage (V-Ref) setting. V-Ref was compared with VBus voltage (from the Flex-250W-DPP through the subsea DC-DC converter and underwater power controller) via a comparator arrangement, as shown on the left-hand side of the subsea energy management system. The output error signals of the comparator went through the PI-Bat1 (subsea battery Proportional-Integral controller). The output of the PI-Bat1 was battery reference current (iBat-Ref), as represented by an orange colour Goto block in the battery voltage management segment of the subsea energy management system in *Figure 4.25*. The PI-Bat1 parameters were obtained via trial-and-error technique. The P-value was 0.85, while the I-value was 10. The subsea battery discharge current values of +22A and -22A were the controller's output saturation limits.

The battery reference current (iBat-Ref) was compared with the battery current (iBat) at the current management stage of the subsea energy management system (right-hand side). The white-coloured battery current (iBat) Goto-block was compared with the orange-coloured (iBat-Ref) Goto-block in the battery current management portion of the model. The error output signals of the comparator went onto the second controller (PI-Bat2). The output of (PI-Bat2) was the battery duty cycle (duty-Bat). The blue-coloured Goto-block on the subsea energy management system represented the (duty-Bat). This controller's P

and I values were 0.01 and 10, respectively. Duty cycle values between 0 and 0.95 defined the output saturation limits of the (PI-Bat2) controller.

The subsea battery duty cycle (duty-Bat) went through the PWM generator within the current management stage. The output of the PWM generator was positive pulse width modulated signals (*Positive-PWM*). As shown in the battery current management segment, a NOT logical operator block converted part of the output positive pulse width modulated signals to negative pulse width modulated (*Negative-PWM*) signals, as shown in the power system model. The yellow Goto-blocks represent the positive signals (*s-Positive*), while the negative signals are (*s-Negative*).

The (*s-Positive*) and (*s-Negative*) signals were finally deployed at the gate terminals of the two (IGBT) power switches of the bi-directional power converter. *Figure 4.25* describes the parameters of the subsea battery and the subsea energy management system aspect of the DTEG power system. Further information on batteries, battery charger, charge controllers, and energy storage is available in (Liang-Rui Chen *et al.*, 2008)(Kisacikoglu, Ozpineci and Tolbert, 2010)(Sugimoto, 2015)(Hoque *et al.*, 2017)(Tashakor, Farjah and Ghanbari, 2017).

4.8.2. 250W-DPP & Subsea Energy Management Operations

Following the discussion on the subsea energy management system above, the stepwise sequence approach was adopted to operate the underwater power system. Therefore, the Flex-250W-DPP with its subsea temperature inputs, the subsea boost converter, the

underwater power controller, and the subsea battery control system were appropriately configured, and the subsea temperature difference was applied.

The subsea temperature difference input from *0 °C to 150 °C* denoted the *increment steps sequence*, while the subsea temperature difference input from *150 °C to 0 °C* represented the *decrement steps sequence*. As previously mentioned, the 250W-DPP power source is a single thermoelectric power plate mounted on a subsea structure for waste heat harnessing and harvesting from the subsea oil-gas reservoirs and cold seawater. Various subsea temperature difference settings operate the power system in *Figure 4.25*.

The following system outputs were sensed, measured, and calculated accordingly for each value of input subsea temperature difference applied to the Flex-250W-DPP:

1. Harvested waste heat to electrical output power (P-DPP), also known as power from the DPP through the subsea DC-DC converter and the underwater power controller
2. Power delivered to subsea equipment (P-Load or Subsea Equipment)
3. Bus voltage (VBus)
4. Subsea battery current (I-Bat)
5. Subsea battery voltage (V-Bat)
6. Subsea battery state of charge (SOC)

4.8.2.1. Stepwise Temp. Difference-Increment Sequence

The increment step sequence began with zero (0 °C) degree Celsius subsea temperature difference input to the power system model. Next, the power system was simulated with the abovementioned parameters and components in place, as discussed in Sections **4.7** and

Subsection 4.7.1. As a result, the Flex-250W-DPP power source generated no power or 0.00W.

Hence, the power output for Test-01 was designated *Very Low Power* because the output power value was less than 15W. Accordingly, the subsea equipment was disconnected from the Flex-250W-DPP power source per the system's pre-defined conditions in **Subsection 4.7.2.2**. That means power to subsea equipment was solely from the subsea battery. Thus, about 24.91W was delivered to the subsea equipment from the subsea battery. The bus voltage during this time was 47.93V. The measured battery current and voltage were 6.59A and 25.75V, respectively, while the subsea battery SOC was 44.94%. The summary results of Test-01 are in *Table 7.13*, while the detailed results are in **Appendix D (Table D.8)**.

Increment Step Sequence @ 10 °C Temperature Difference: Test-02

The subsea temperature difference was increased from 0 °C to 10 °C in Test-02. The power system was simulated as was done in Test-01. The recorded output power or P-DPP from the Flex-250W-DPP source was 15.88W. This output power was termed *Low Power* based on the system's pre-defined conditions. The Flex-250W-DPP and subsea battery at 25.04W jointly supplied power to the subsea equipment. The recorded bus voltage was 48.08V; the battery current was 5.41A, the battery voltage was 25.76V, and SOC was 44.95%. See *Table 7.13* for the summary results. Details on the results are in **Appendix D (Table D.8)**.

Increment Step Sequence @ 30 °C Temperature Difference: Test-03

In the third experiment, the subsea temperature difference was increased from 10 °C to 30 °C. The output power from the Flex-250W-DPP was described as *Low Power* because it was less than 50W. Again, the subsea equipment was powered by the Flex-250W-DPP and subsea battery at 24.84W. *Table 7.13* presents the summary results. Additional details are provided in **Appendix D (Table D.8)**.

Increment Step Sequence @ 60 °C Temperature Difference: Test-04

When the subsea temperature difference input was 60 °C, around 101.30W was generated through the Flex-250W-DPP power source. This output power value during this experiment was labelled as *Medium Power*. The subsea battery was connected to the system based on pre-defined conditions but did not contribute power to the subsea equipment. Therefore, the power supplied to subsea equipment was 24.59W from the Flex-250W-DPP power source alone. The summary results of Test-04 are in *Table 7.13*. Additional details are provided in **Appendix D (Table D.8)**.

Increment Step Sequence @ 70 °C and 90 °C Temperature Difference: Test-05 & 06

Power drawn from the Flex-250W-DPP power source was sufficient for subsea equipment when the subsea temperature difference input was 70 °C and 90 °C during the fifth and sixth experiments. Roughly 118.70W and 152.60W were obtained from the power generator at these subsea temperature difference inputs. The subsea battery current was at

2.55A. Hence, the subsea battery was still connected to the system when the subsea temperature difference was 70 °C. However, the subsea battery current dropped from 2.55A to 1.02A when the subsea temperature difference was 90 °C. At this time, the subsea battery was disconnected according to pre-defined conditions. See *Table 7.13* for the summary results. Further details are included in **Appendix D (Table D.8)**.

Increment Step Sequence @ 115 °C Temperature Difference: Test-07

During the seventh experiment, the subsea battery power level was *Low Power* (discharge current was -0.7442A). The Flex-250W-DPP source generated approximately 194.60W when the temperature difference was 115 °C. Consequently, the Flex-250W-DPP power source was disconnected from the subsea equipment and connected to the subsea battery for battery charging (*Battery Charging*). Hence, power was supplied to the subsea equipment from the subsea battery.

Increment Step Sequence @ 120 °C Temperature Difference: Test-08

Subsea battery charging continued in Test-08 when the subsea temperature difference input was 120 °C. The produced power from the Flex-250W-DPP was 202.80W; this was termed the *High-Power* condition, as defined in the power system settings. See *Table 7.13* for summary results on Test-08. Detailed results are in **Appendix D (Table D.8)**.

Increment Step Sequence @ 125 °C and 150 °C Temperature Difference: Test-09 & 10

When the subsea temperature difference input was 125 °C and 150 °C in the 9th and 10th experiments, the extracted power from the Flex-250W-DPP was 240.20W and 300.10W, respectively. The system's power was said to be in a *Very High-Power* state. The Flex-250W-DPP continued to supply power to the subsea equipment. During these times, the subsea battery was fully charged. It was disconnected and placed on *Standby*. The summary results obtained from the first to the tenth experiment are available in *Table 7.13* of ***Chapter 7***. Detailed results are in **Appendix D (Table D.8)**. *Figure 4.26* shows the power system bus voltage and subsea battery SOC during the subsea battery stepwise sequence operations.

4.8.2.2. Stepwise Temp. Difference-Decrement Sequence

During the eleventh experiment, the subsea temperature difference input was 130 °C (from the previous 150 °C in the tenth experiment). The power harvested through the Flex-250W-DPP thermoelectric power source was 249.50 W. Therefore, the system power was categorised as being *Very High Power*. The power supply to subsea equipment from the Flex-250W-DPP source was 24.89 W. The battery was fully charged, disconnected, and on *Standby*. See *Table 7.14* for the summary results. Additional details are in **Appendix D (Table D.8)**.

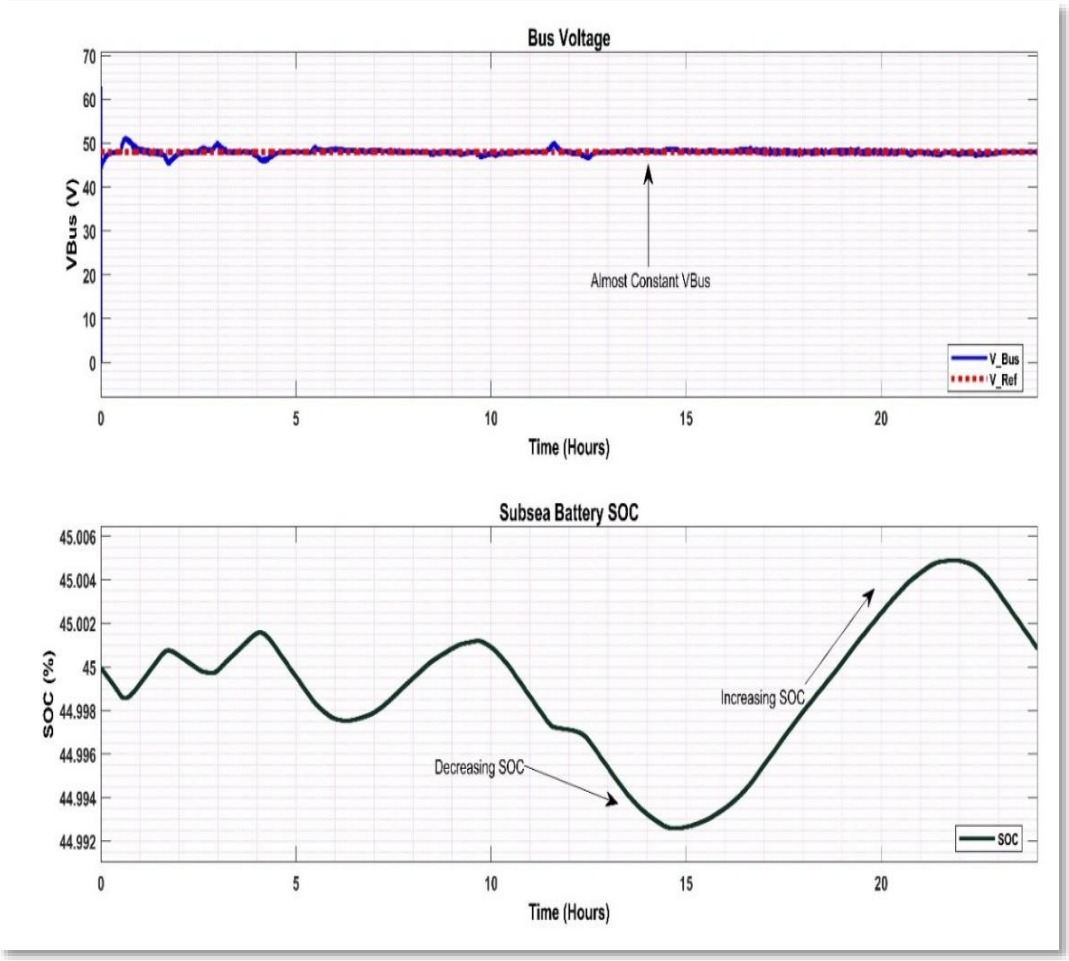

Figure 4.26 Power System Bus Voltage and Subsea Battery SOC

Decrement Step Sequence @ 118 °C Temperature Difference: Test-12

The subsea temperature difference was reduced from 130 °C to 118 °C. However, during which subsea battery power level was low, the discharge current was -0.3299A, and about 199.60W was harvested through the Flex-250W-DPP source. Therefore, the subsea equipment was disconnected from the power source. The Flex-250W-DPP was connected

to the subsea battery for battery charging, and the subsea equipment was connected to the battery. See *Table 7.14* for the summary results. Additional details are in **Appendix D (Table D.8)**.

Decrement Step Sequence @ 110 °C Temperature Difference: Test-13

The subsea battery level was low during the 13th experiment, while the Flex-250W-DPP power source generated 186.20W at 110 °C. The battery discharge current was -0.2967; hence, the charging process continued as Flex-250W-DPP was disconnected from the subsea equipment and connected to the battery.

Decrement Step Sequence @ 100 °C and 80 °C Temperature Difference: Test-14 & 15

When the subsea temperature difference was 100 °C and 80 °C, the subsea battery was disconnected from the subsea equipment. As a result, the power obtained through the Flex-250W-DPP source was 166.90W and 135.80W, respectively. During the 100 °C subsea temperature difference input, the power delivered to the subsea equipment was 24.62W, VBus was 47.85V, battery current was 0.26A, and VBat was 25.82 V, while SOC was 45.03%. See *Table 7.14* and **Appendix D (Table D.8)** for further details.

Decrement Step Sequence @ 50°C, 40°C, 20°C and 5 °C Temp. Diff: Test-16 to 19

System power through the thermoelectric power source declined from 83.99W to 67.19W and from 32.71W to 7.68W during the 16th, 17th, 18th, and 19th experiments when subsea temperature difference input was 50 °C, 40 °C, 20 °C, and 5 °C, respectively. As a result of the low power generation, the subsea equipment was powered jointly by the Flex-250W-DPP source and the subsea battery. Thus, the recorded power delivered to the subsea equipment was 24.76W, 24.86W, 24.83W, and 24.86W, respectively. The summary results from Test-16 to Test-19 are available in *Table 7.14*. See **Appendix D (Table D.8)** for further details.

Decrement Step Sequence @ 0 °C Temperature Difference: Test-20

Finally, when the subsea temperature difference input was 0 °C, no power was generated through the deepwater thermoelectric power source. The Flex-250W-DPP source was disconnected from the subsea equipment. The subsea equipment was powered singlehandedly by the subsea battery at 24.91W. The VBus was 47.93V, I-Bat was 6.59A, VBat was 25.75V, and SOC was 44.94% during the twentieth (20th) experiment. Additional details obtained from the stepwise decrement experiment are in the result section in *Table 7.14* and See **Appendix D (Table D.8)**. *Figure 4.27* shows subsea battery current and voltage plots during the deepwater power system battery stepwise operations.

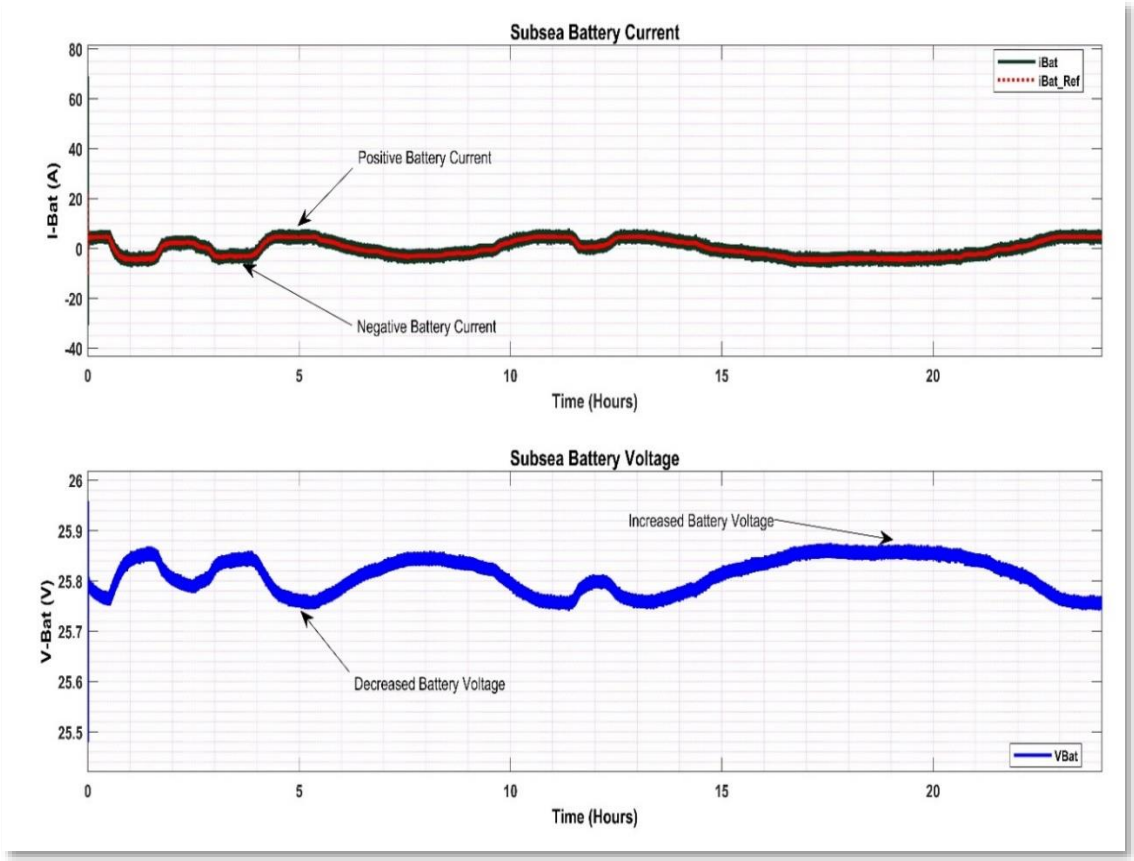

Figure 4.27 Subsea Battery Current and Voltage

4.9. Outcome of Stepwise Sequence Operations

As subsea temperature difference operated the Flex-250W-DPP from 0 °C to 150 °C (increment sequence) and from 150 °C to 0 °C (decrement sequence), waste heat from oil-gas reservoirs and surrounding seawater is converted to electrical energy. As shown in the plots in **Sections 4.8.2.1** to **4.8.2.2** and the bar chart in *Figure 4.28*, the generated electrical power was transferred to the subsea battery compartment through the centrally located VBus and the subsea energy management system at the lower part of the power system

model. Power was supplied to subsea equipment and used for subsea battery charging when needed.

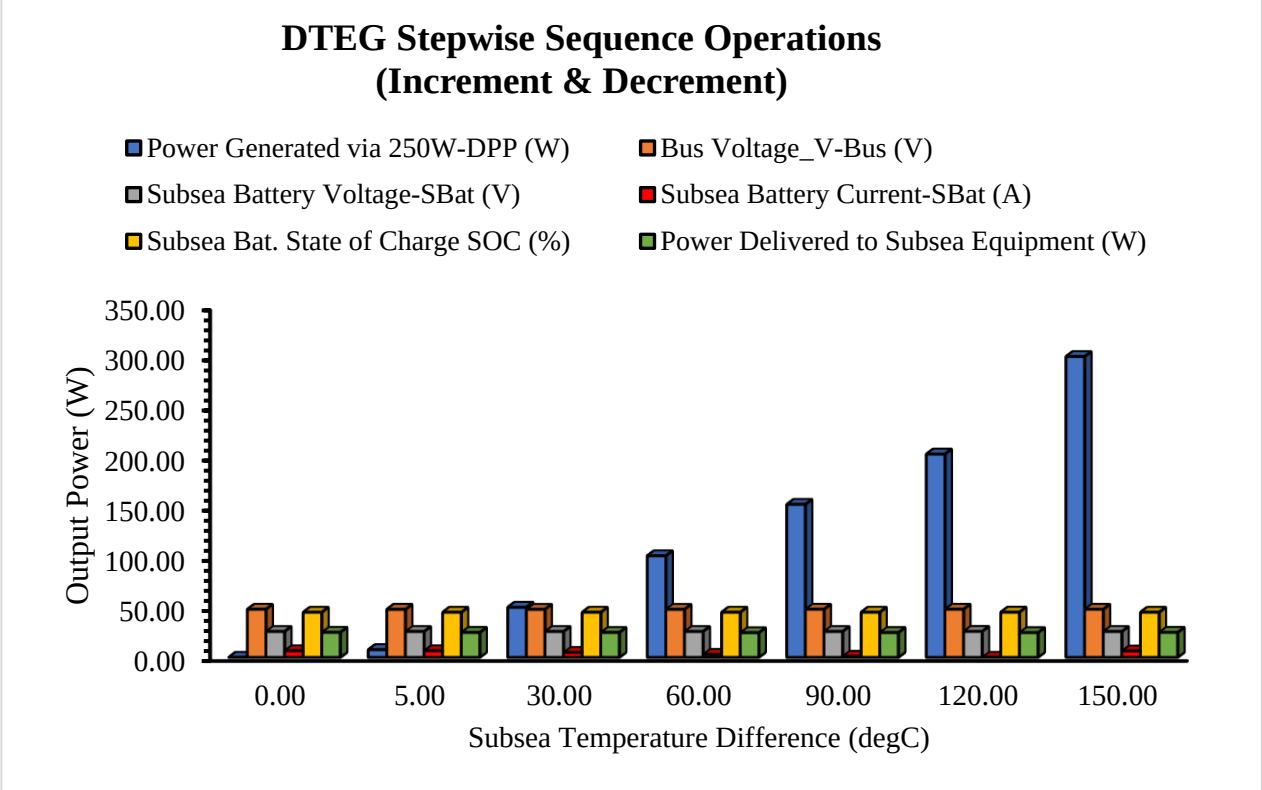

Figure 4.28 Stepwise Sequence Operations

When the subsea temperature difference was 0 °C, power was not generated by the Flex-250W-DPP. In such a scenario, the subsea battery was responsible for providing the required power needed by the subsea equipment. Furthermore, when the subsea temperature difference was up to 50 °C or less, the output power from the Flex-250W-DPP was low; hence, the subsea equipment was powered jointly by the Flex-250W-DPP and the subsea battery.

During the system operation, the generated power and the power supplied to subsea equipment were logged for every subsea temperature difference, as shown in **Appendix D (Table D.8)**. Also recorded are the bus voltage, the battery voltage, subsea battery current, and subsea battery state of charge (SOC). *Table 4.9* shows the mean, standard deviation, and standard error of the measured parameters during the experiment.

Table 4.9 Stepwise Sequence Operations-Calculated Data

Subsea Temperature Stepwise Sequence (Increment & Decrement)						
Attributes	**Power Generated via 250W-DPP (W)**	**Bus Voltage_V-Bus (V)**	**Subsea Battery Voltage-SBAT (V)**	**Subsea Battery Current-SBAT (A)**	**Subsea Bat. State of Charge SOC (%)**	**Power Supplied to Subsea Equipment (W)**
Mean:	133.328	47.945	25.785	3.438	44.965	24.806
Standard Deviation:	85.182	0.084	0.031	2.604	0.127	0.106
Standard Error:	10.997	0.011	0.004	0.336	0.016	0.014

The subsea battery state of charge (SOC) indicates the charge capacity currently available as a function of the rated battery capacity. Also, it can be described as counting the amps-in and amps-out of the subsea battery. Given that the designed state of charge (SOC) was 45%, the subsea battery state of charge (SOC) varied between 44.94% and 45.04% during the operations of the underwater system, proving the proficiency of the selected battery chemistry and rugged ability of the power system design. *Table 4.10* shows the confidence intervals of the measured SOC during the experiment.

Table 4.10 Subsea Battery SOC Confidence Intervals

Confidence Intervals - Subsea Bat. State of Charge SOC (%)	
Mean	44.96491525
Standard Error	0.016549825
Median	44.98
Mode	44.94
Standard Deviation	0.127121621
Sample Variance	0.016159906
Kurtosis	50.44267409
Skewness	-6.839405766
Range	1
Minimum	44.04
Maximum	45.04
Sum	2652.93
Count	59
Confidence Level (95.0%)	0.033128075
Upper CI (95%)	44.99804333
Lower CI (95%)	44.93178718

Additionally, the results from the stepwise sequence operations (Increment & Decrement) accurately depicted the subsea battery (NiMH) behaviour. The results showcased the inherent safety features and performance stability typical of battery chemistry.

Secondly, measured subsea battery outputs enabled the prediction of voltage, current, and state of charge responses, thus allowing proper evaluation of the battery's potential to meet the energy demands of a deepwater power system.

Thirdly, operating the power system at various subsea temperature gradients specific to ultra-deepwater environments has explored the effect of temperature on subsea battery

efficiency. Furthermore, the results provide insights into understanding the battery thermal performance.

Fourthly, the deepwater thermoelectric power system model has illustrated the subsea (NiMH) battery's ability to endure numerous charge and discharge cycles, thus predicting the battery system's reliability and durability in deepwater environments with limited access for maintenance.

Fifthly, the experiment's outcome has proven that nickel metal hydride (NiMH) has better environmental compatibility than other battery chemistries. However, one of NiMH's limitations is reduced energy density compared to new-generation chemistries like lithium-ion. Limited energy density potentially restricts energy storage capability for a deepwater thermoelectric power system. Another drawback of NiMH batteries is their relatively heavy weight. Weight and space constraints in deepwater applications might pose challenges during deployment.

The experiment and the results presented here revealed nickel metal hydride subsea battery strengths in safety, reliability, and environmental compatibility. Energy density, weight, and space constraints were highlighted. However, proven safety and reliability underscore any other characteristics. Hence, NiMH is the best-suited subsea battery for ultra-deepwater thermoelectric energy storage.

4.10. Marinising Subsea Electronics & Battery

Functionality and reliability in harsh underwater environments are paramount to subsea electronics and batteries. Therefore, the following requirements were considered essential for marinizing these components:

Corrosion-Resistant Materials: Subsea electronics and battery components were assumed to be coated with titanium stainless steel to withstand prolonged seawater exposure. Additionally, electronics were considered to be encased in a hermetically sealed housing, thereby preventing water ingress. Furthermore, the sealing protects against contamination, corrosion, and long-term functionality.

Pressure-Resistant & Compensation: It was assumed that subsea batteries and electronic enclosures were fitted with reinforced structures and robust seals to withstand high water pressure at over 3000-meter water depths. It was also presumed that pressure compensation was carried out to ensure internal and external pressure equilibrium, thus preventing pressure differential damage to the batteries and other components.

Waterproofing & Electrical Isolation: Protection against water intrusion into the subsea systems, it was assumed that electrical connections were waterproofed using specialized seals and potting compounds. Proper isolating of critical electrical components prevents short circuits, electrical shocks, and other forms of damage.

Remote Monitoring & Maintenance: Subsea battery and electronic systems' health, performance, and functionality were remotely monitored. As such, it was assumed that subsea sensors and systems were integrated into the thermoelectric power system for real-

time operations. Secondly, this deepwater thermoelectric power system was designed with ease of accessibility in mind. Hence, parts of the power system can easily be reached for inspection, maintenance, and repairs in severe ultra-deepwater conditions.

Testing & Certification: It was assumed that the deepwater thermoelectric power system's subsea battery and other electronic components were rigorously tested in simulated deepwater conditions. The test results validated the system's performance and reliability. Furthermore, test results and validations were assumed to align with industry standards and certifications for subsea equipment deployed in oil and gas fields.

4.11. Chapter Summary

The Flex-250W-DPP developed in ***Chapter 3*** was interfaced with power electronic components. As a result, stable and maximum power was drawn from oil-gas reservoirs through the thermoelectric power source at the optimum power point through a subsea DC-DC power converter and an underwater power controller. The power was delivered to subsea equipment. In the second half of ***Chapter 4***, additional electronic elements were connected to the deepwater thermoelectric power source with its subsea temperature difference inputs and subsea battery storage. These other elements served as connecting links between the Flex-250W-DPP, energy storage medium, and subsea equipment. The power system interfaces facilitated the conversion of electrical energy to chemical energy. Chemical energy was stored in the subsea battery; the stored energy was supplied to

subsea equipment as electrical power when needed. In ***Chapter 5***, the DTEG power system for conventional deepwater or ultra-deepwater oil-gas fields is brought to the fore.

Chapter 5

DTEG Power Systems Sizing

5.1. Introduction

The design and development of a DTEG power system for deepwater or ultra-deepwater oil-gas fields began in ***Chapter 3*** by creating DTEMs, DPPs, and DPUs. The deepwater power plate was interfaced with power electronic components for energy harnessing, storage, supply, and utilization in ***Chapter 4***. This Chapter delves into developing an ultra-deepwater oil-gas field and sizing the power system's major components, such as a deepwater power unit (DPU), subsea battery pack, and subsea battery bank. The DPU and subsea battery bank are meant to jointly supply electrical power to critical subsea equipment on the seafloor.

5.2. DTEG in the Oil and Gas Field

The essence of the deepwater thermoelectric generator (DTEG) or deepwater power system in an oil and gas field is harvesting and harnessing heat from oil-gas reservoirs,

using the surrounding seawater environment to convert heat to electricity. The generated electricity will supply electrical power to critical subsea equipment during exploration (drilling) and production. Unlike the other types of energy conversion technologies (renewable and non-renewable), thermoelectricity directly converts heat energy to electricity without intermediaries associated with the process, as demonstrated in ***Chapters 3*** and ***Chapter 4***.

Low system efficiency is the main drawback of thermoelectric generators compared to other technologies. That means less heat is inputted to a thermoelectric generator for the same quantity of heat to be converted to electricity. However, in a deepwater or ultra-deepwater oil-gas field, waste heat recovery application is less of a concern because geothermal heat is a by-product of exploration and production activities.

Figure 5.1 is an artistic impression of an oil-gas field undergoing exploration and production operations. Moho Nord Field is in Congo Brazzaville, Central Africa; the illustration shows a clustered subsea well arrangement on the seabed. The subsea equipment includes a drilling platform and riser, production risers, flowlines, pipelines, a floating production unit, a nearby offloading vessel, and some infrastructures typical of oil-gas exploration and production sites.

Higher initial cost per watt of electrical power might seem a cause for concern on a deepwater thermoelectric power system. Nonetheless, the DTEG power system's capital cost amortizes over time. Thus, the lifetime cost becomes lower than that of other technologies.

Depending on the oil and gas field at any location worldwide, the duration of drilling campaigns is often shorter than production operations. The subsea production life of most deepwater or ultra-deepwater fields in West Africa is over 20 years (Song, 2019)(Schoppa *et al.*, 2007)(Hovem *et al.*, 2014). Hence, a lower lifetime cost per watt is easily achievable in deepwater or ultra-deepwater production projects than in drilling programs. To this effect, this DTEG power system was sized for a deepwater or ultra-deepwater oil and gas production field.

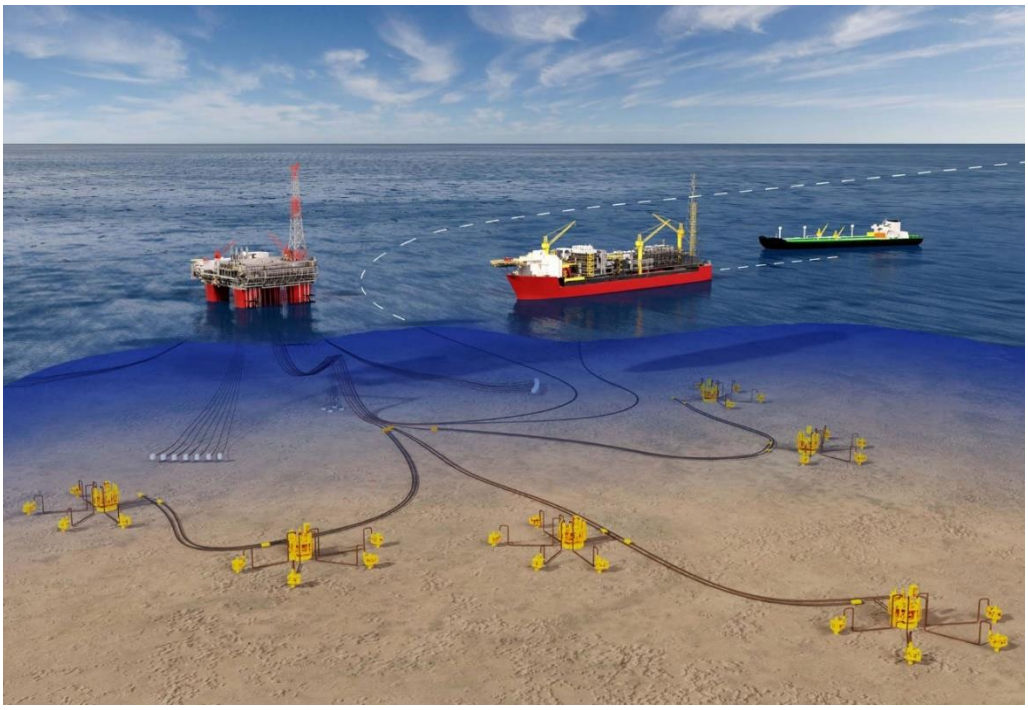

Figure 5.1 Moho Nord Field, Congo Brazzaville (Topsides64, 2012)

A close view of typical subsea production equipment located in a deepwater oil and gas field in Nigeria is illustrated in *Figure 5.2*. Some of the equipment includes subsea wellheads, subsea Christmas trees (XTrees), subsea flowlines, pipelines, subsea manifolds,

subsea sleds, production risers, etc. These are standard subsea equipment in a typical deepwater or ultra-deepwater oil-gas production field.

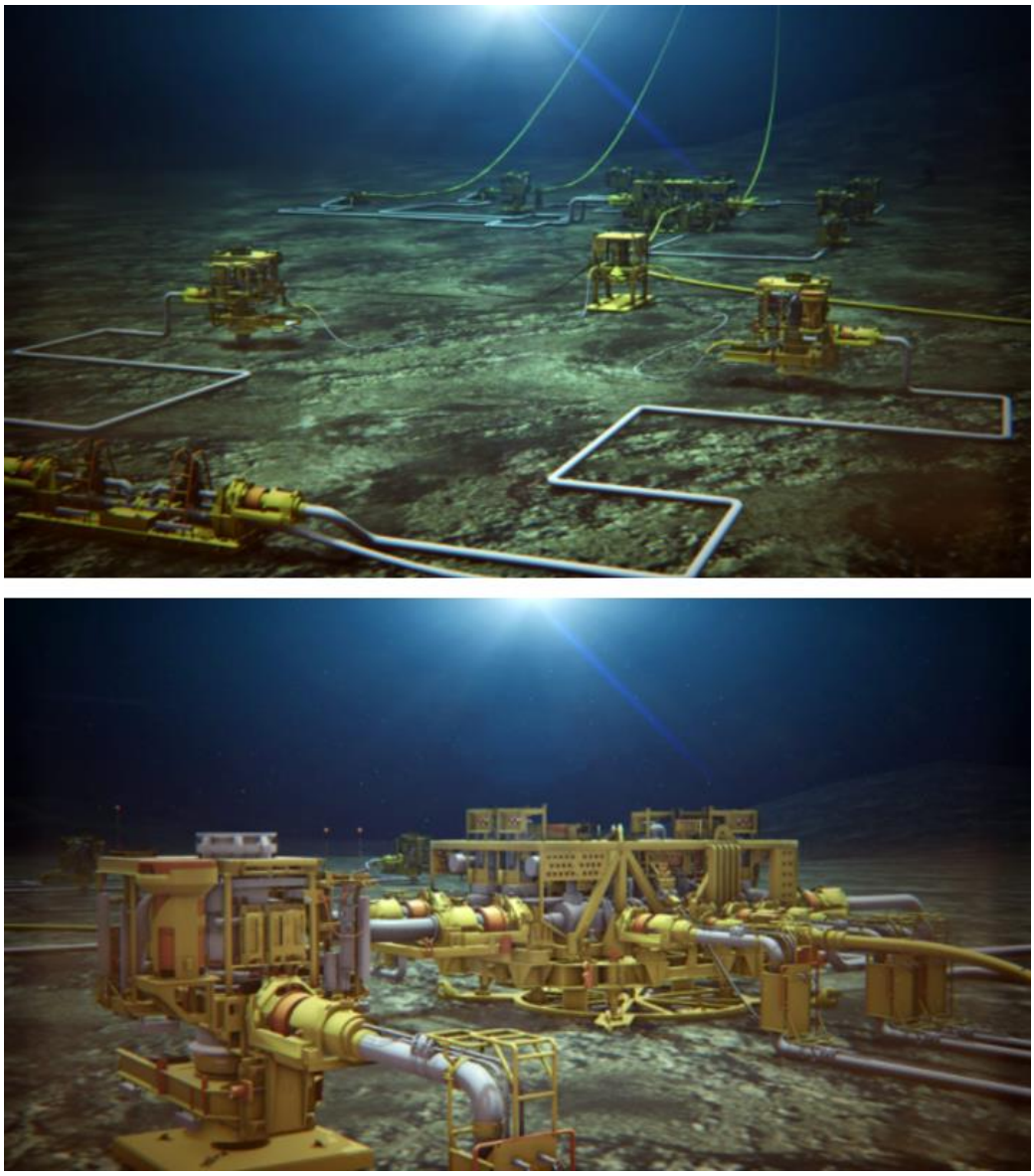

Figure 5.2 Egina Field, Offshore Nigeria (NorwayExportsNews, 2019)

5.3. Development of Deepwater Oil-Gas Production Field

The proposed ultra-deepwater oil and gas production field consists of subsea wells, XTrees, subsea manifolds, flowlines, pipelines, production risers, etc. These subsea systems are tied to a dedicated turret moored floating production storage and offloading (FPSO) structure in West Africa. ***Chapter 1*** briefly introduced this oil-gas production field and subsea equipment in such an environment.

The field's water depth ranges from 1500 to 3000 meters mean sea level (MSL). The area is about 70 square kilometers (in which North to South is about 10 km while East to West is approximately 7 km). The planned development has fifty-six (56) subsea wells comprising twenty-eight (28) oil and gas production wells, six (6) hot water production wells, and twenty-two (22) water injection wells located on the east and west sides of the field. The eastern part consists of 14 oil and gas production wells, three (3) production manifolds, three (3) hot water production wells, and eleven (11) water injectors. The western part of the field has a similar number of subsea wells and equipment arrangements, as shown in the field layout in *Figure 5.3*.

Chapters 1 to ***4*** indicate that fluids flowing from subsea wells are usually hot. Therefore, through the groups of flexible deepwater thermoelectric power plates (Flex-DPPs) mounted on subsea structures, geothermal energy from the hot oil-gas well from production wells can be converted to electrical energy by utilising the cold seawater environment. A deepwater thermoelectric power unit (DPU) of a particular power rating

is formed from groups of Flex-DPPs connected in a specified configuration, as discussed in **Sections 3.4.9** and **3.4.10**.

Therefore, the six (6) hot water production wells (Bybee, 2002) in *Figure 5.3* were assumed to be separately drilled and arranged for thermoelectric energy generation. Secondly, these hot water wells are independent subsea wells fitted with thermoelectric power-generating components to convert the hot water produced and the cold seawater environment to electricity. Thirdly, the hot water subsea production wells are solely for instant electrical energy generation from the produced hot water. These energy-generating subsea wells were classified as standby power stations. Fourthly, generated electricity from the six (6) subsea wells can supply electrical power to all subsea production control equipment in emergencies. Lastly, the hot water subsea wells were presumably designed to limit subsea temperature drops for fluids in subsea flowlines and pipelines. Thus, the function of hot water subsea wells or standby power stations includes improving flow assurance-related issues in the ultra-deepwater oil-gas field.

Furthermore, the two (2) million barrels of oil storage capacity FPSO in *Figure 5.3* was deemed capable of oil, gas, water, and fluid processing and handling. Processed oil was expected to be transferred to oil tankers via a tandem offloading system. Gas would be transported through pipelines and an intermediate deepwater gas gathering platform (DGGP) to a shore-based LNG (Liquefied Natural Gas) facility. Additionally, provisions were made on the site to accommodate an FLNG (Floating Liquefied Natural Gas).

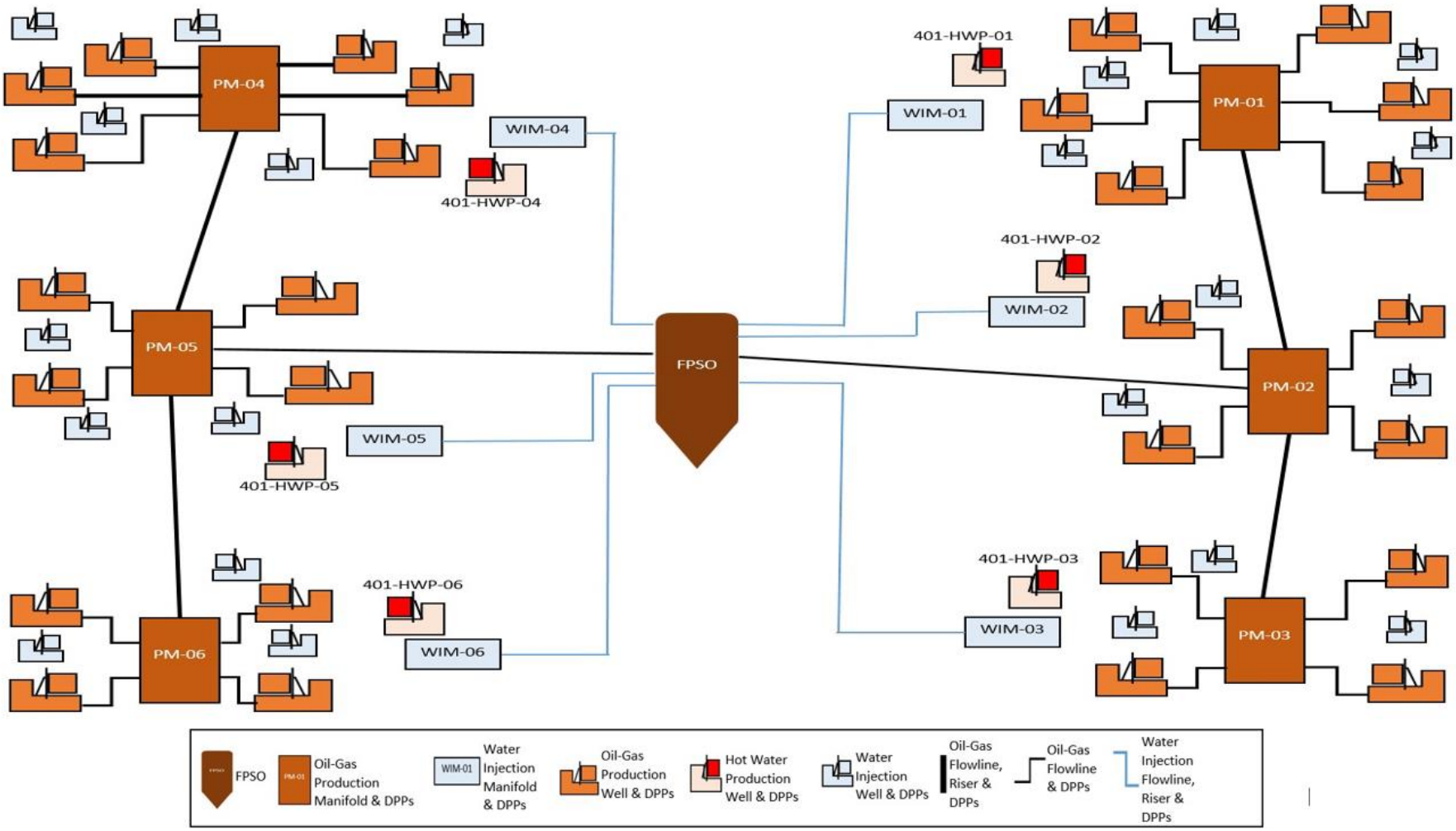

Figure 5.3 Field Layout of Ultra-Deepwater Oil & Gas Production Systems

Treated water at elevated temperatures and higher pressure would be re-injected into the deepwater reservoirs through subsea water injection manifolds and water injection Christmas Trees (XTrees), thereby increasing oil recovery. The ultra-deepwater oil and gas production field layout in *Figure 5.3* further describes the subsea system composition for concurrent oil-gas production and deepwater thermoelectric (DTEG) power generation, as discussed in the following sections.

5.4. Subsea Production Systems

Oil production from individual subsea wells (601-PFL-01 to 628-PFL-06) discussed above in **Section 5.3** was assumed to be 60 MBOPD. Gas production from each well was approximately 190 MMSCFD. The peak water produced from a single oil-gas production well was 55 MBWPD. The water injection rate per water injection well (501-WFL-01 to 522-WFL-06) was 55 MBWPD. These fluid flows were pumped out from subsea wells or back into the wells via the subsea production system. Hot water production wells (401-HWP-01 to 406-HWP-06) are standby energy generation wells, as shown in *Figure 5.3*. These subsea wells and production systems are itemized in *Table 5.1*.

The following subsections describe further some of the critical subsea production systems represented in the field layout. The oil-gas field layout goes further to discuss the DTEG power system for the ultra-deepwater development presented in this research:

5.4.1. Oil & Gas Production Flowlines and Riser Systems

The oil-gas field layout described above has provisions for flowlines, pipelines, and production risers. 10-inch by 14-inch production flowlines and riser systems were selected for the oil-gas field to transport fluids from the subsea-producing wells to the surface-located FPSO. The fluids produced from the subsea wells to the FPSO flowed through subsea wellheads, XTrees, manifolds, flowlines, flowline jumpers, flowline termination assemblies (sleds), and production risers. Each termination assembly was assumed to have suitable valves to allow flowline-operating functionality. The production flowline system was connected to the FPSO via shaped steel catenary risers (SSCRs) with vortex-induced vibration (VIV) suppression strakes. The production flowlines are single-insulated pipes, while production risers are pipe-in-pipe insulated (Qadir, Morris and Goodlad, 2016).

Additionally, Carbon steel was the selected flowline material for the production flowline and riser systems. The production flowline and riser systems were based on the following international standards: API RP 1111 (Design, Construction, Operation, and Maintenance of Offshore Hydrocarbon Pipelines), API RP 2RD (Design of Risers for Floating Production Systems and Tension-Leg Platforms (Kieran Kavanagh, Lou and Hays, 2003)(Stanton *et al.*, 2010).

The flowline system had provisions for bi-directional depressurisation, round-trip pigging, and intelligent pigging operations to remove wax, produced solids, and fluid displacement when necessary (Bernt and Smedsrud, 2007)(Taxy *et al.*, 2009). Furthermore, the flowline and riser systems were fitted with Flex-DPP power plates for waste heat harvesting and harnessing for electricity generation along the flow paths. Flowlines from the production

wells or producers are represented as 601-PFL-01 to 628-PFL-06 in *Table 5.1*. The field layout in *Figure 5.3* further demonstrates these production systems.

5.4.2. Water Injection Flowlines and Risers

The next item on the field layout is the water injection flowlines and riser systems. Like the production flowline and riser systems, the eastern and western parts of the oil-gas field had water injection flowline and riser systems. These systems transported treated water from the FPSO at elevated temperatures (Wu, Liu and Xing, 2015) back to the subsea injection wells or injectors via flowline termination assemblies (sleds), subsea manifolds, and flowline jumpers. Note that the treated water was initially a mixture of produced oil, gas, and water from the reservoirs to the storage FPSO. The standard practice is that produced water is treated before re-injection into the subsea well. Therefore, it was assumed that the water was treated on the FPSO and returned to the reservoirs through risers, flowlines, water injection manifolds, and water injection XTrees for enhanced oil recovery from the subsea wells.

The eastern and western lines are connected to the FPSO by SSCRs with VIV suppression strakes. The SSCRs are 10-inch line sizes for water injection systems. Provisions for thermal insulation and operational pigging routines are not required on water injection lines. Also, carbon steel was the selected flowline material. The water injection flowline and riser systems were based on API RP 1111 and API RP 2RD design codes. It was assumed that the water injection flowline and riser systems were fitted with Flex-DPP

power plates for harvesting and harnessing waste heat along the flow paths. Flowlines to the injectors are 501-WFL-01 to 522-WFL-06 (see *Table 5.1*), and the field layout in *Figure 5.3.*

5.4.3. Drilling/Well Engineering Systems

As shown in the field layout in *Figure 5.3,* cluster drilling arrangements with surrounding producers and injectors were adopted for the subsea well delivery. As a result, flowline congestion at various seabed infrastructures was avoided by drilling and completing the production and injection wells at separate clusters. Another benefit of this method was the improvement of subsea well operability and intervention capabilities, thus reducing maintenance or well-workover risk while increasing cost efficiency. Drill centers, referred to as drilling hubs (DHs) in this work, represent the cluster composition (Denney, 2007)(Marks, 2009). The drill centers or drilling hubs in this ultra-deepwater oil and gas field are denoted as DH-01, DH-02, and DH-03 in the eastern part of the field, while DH-04, DH-05, and DH-06 are on the western flank (as in *Figure 5.3* and *Table 5.1*).

5.4.4. Production Manifold and Flowline Sleds

Subsea manifolds and flowline sleds are the following items, as described on the field layout in *Figure 5.3.* The production flow loop in the east and west contains three (3) subsea manifolds on each side: PM-01, PM-02, PM-03 in the east while PM-04, PM-05, PM-06 in the west. PM-01 and PM-04 are six (6) slots subsea manifolds, while the rest

are four (4) slots subsea manifolds. Subsea control components were assumed to be housed/accommodated within the subsea manifolds. The field layout and table of information on the electrical power requirement clearly show the above-mentioned equipment.

As previously mentioned, Flex-DPP power plates are integrated into the fluid flow loops and paths within production manifolds, flowlines, and sleds to capture waste heat from the fluid flow paths. *Figure 5.4* is a typical subsea production manifold showing interconnected flow loops and paths that can accommodate Flex-DPP power plates.

Figure 5.4 Subsea Manifold, OneSubsea-Schlumberger (OneSubsea, 2019)

5.4.5. Water Injection Manifolds, Flowline Sleds

As depicted on the field layout, six separate water injection flowline systems are responsible for providing water injection services to subsea water injection wells in the western and eastern parts of the field. In the east, water injection manifolds (WIMs) are WIM-01, WIM-02, and WIM-03, while WIM-04, WIM-05, and WIM-06 are in the west (see *Table 5.1*). WIM-01 and WIM-04 are six (6) slots subsea manifolds, while WIM-02, WIM-03, WIM-05, and WIM-06 are four (4) slots subsea manifolds. In addition, Flex-DPP power plates were fitted/installed on the fluid flow structures within water injection systems, flowlines, and flowline sleds for waste heat harvesting and conversion to electricity along fluid flow paths.

5.4.6. Subsea Christmas Trees

Next on the field layout is the Christmas Trees. Subsea Christmas trees (XTrees) are installed on subsea wellheads. System configuration for oil and gas production trees differs from the composition of the hot water production XTrees. Furthermore, the water injection XTrees' design differs from the oil-gas production XTrees and hot water production trees. Nonetheless, subsea control components were assumed to be housed/accommodated within all the XTrees. Consideration was given to intelligent or smart well features on the subsea oil and gas production XTrees (Gao *et al.*, 2007)(York *et al.*, 2019).

Drilling hubs DH-01 and DH-04 consist of six (6) production XTrees, one (1) hot water production XTree, and five (5) water injection XTrees. DH-01 and DH-04 had twelve (12) subsea wells each. On the other hand, DH-02, DH-03, DH-05, and DH-06 have eight (8) subsea wells each. The composition of DH-02, DH-03, DH-05, and DH-06 are four (4) production XTrees, one (1) hot water production XTree, and three (3) water injection XTrees.

Flex-DPP power plates were equipped on fluid flow loops and paths on wellheads and within the Xmas trees for waste heat harvesting and conversion to electricity along fluid flow paths. *Figure 5.5* is a subsea XTree with potential fluid flow paths for hosting flexible DPP power plates.

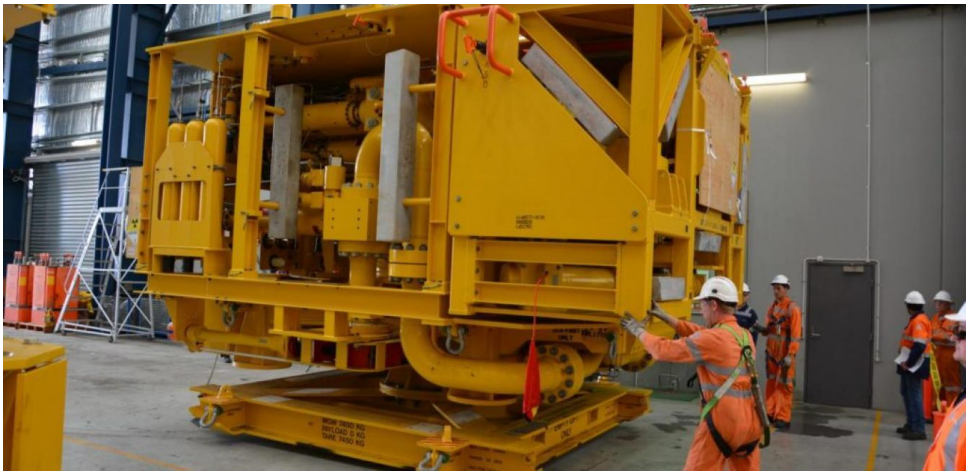

Figure 5.5 Subsea Christmas Tree, GE Oil & Gas (GE, 2014)

5.4.7. Subsea Controls

As mentioned in ***Chapter 2***, this project supports using control umbilicals vis-a-vis multiplexed electro-hydraulic, wired, and non-wired signal communication technologies. A multiplexed electro-hydraulic (MEH) control system (Goode, 2005) strategy was selected to monitor and control subsea wells and equipment. A significant difference from conventional MEH systems in this field development is that electrical power is locally sourced at the seabed, unlike traditional MEH systems in which electricity is transmitted from the topside, as described in ***Chapter 1***. This approach is poised to be a significant shift in the industry stock with old traditions.

The subsea control module (SCM) containing the subsea electronic module (SEM) is typically among the critical equipment at the seabed. Monitoring and controlling the field instrumentation and the instrumentation housed in subsea manifolds and subsea XTrees, including valves, choke, and measurement of physical properties of the process fluids, are done through the electro-hydraulic designed SCM. Among other things, the SCM reports on the status of subsea equipment. *Figure 5.6* illustrates a typical three-phase electrical distribution unit (EDU), electrical flying leads (EFL), ROV-based Tee-handle electrical connectors, terminations, SCMs (cylindrical structures), and hydraulic supply lines meant for critical subsea equipment.

Figure 5.6 Subsea Production Control System (Dril-Quip, 2018)

5.4.8. Subsea Equipment and Electrical Power Distribution

The generated electrical power via the DPPs mounted on subsea structures (the DTEG power system) will be distributed to the critical production control system on subsea wells, XTrees, subsea manifolds, downhole equipment, and associated subsea equipment. This work assumed that the critical subsea production control equipment were powered via the electric power drawn through the deepwater power unit (DPU), thus achieving the research aim.

As mentioned above, the DPU consists of groups of Flex-DPPs fitted on the flow paths of subsea structures. Some of the vital subsea instrumentation on the subsea wells, XTrees, and subsea manifolds considered are multiphase flow meters (MFMs), single-phase mass flow meters (SPFMs), cone flow meters (CFMs), wet gas flow meters (WGFM). Others

are corrosion monitors, sand monitors, combined production pressure and temperature transmitters, pressure transmitters, chemical injection metering valves (CIMVs), chokes, permanent downhole gauges (PDGs), etc.

Subsea wells' equipment are typically installed on the XTree, wellheads, and downhole (inside the subsea well). These equipment are electrically powered for telemetry, remote data collection, and transmission. Subsea well data enables monitoring, optimisation, control, and system automation. The subsea well devices measure real-time pressure, temperature, and fluid information. Other notable data required at the subsea well site include chemicals, solids detection, corrosion, leak detection, etc.

Furthermore, the downhole equipment mentioned above are specialised sensors for high-temperature and high-pressure operating conditions. These sensors send analog pulses to SEMs in the SCM, where analog-to-digital signal conversion occurs. Other components of the SEMs include logic controllers, ethernet, fiber optic, wireless communication components, and other communication devices. These wireless devices will be integrated with features capable of supporting the next generation of real-time 'seabed-to-cloud' infrastructure. Nonetheless, all these components and devices are electrical power-demanding equipment used in oil and gas production.

Table 5.1 Electrical Power Requirement-Production Control System

Location	Drilling Hubs	Production Wells, Flowlines & Production Manifolds	Power Requirement (W)	Hot Water Production Wells, Water Injection Wells, Flowlines & Water Injection Manifolds	Power Requirement (W)	Subtotal (W)	TOTAL Electrical Power (Watts)
East	DH-01	PM-01	700	401-HWP-01	552	1252	6392
		601-PFL-01		WIM-01			
		602-PFL-01		501-WFL-01			
		603-PFL-01		502-WFL-01			
		604-PFL-01		503-WFL-01			
		605-PFL-01		504-WFL-01			
		606-PFL-01		505-WFL-01			
	DH-02	PM-02	600	402-HWP-02	372	972	
		607-PFL-02		WIM-02			
		608-PFL-02		506-WFL-02			
		609-PFL-02		507-WFL-02			
		610-PFL-02		508-WFL-02			
	DH-03	PM-03	600	403-HWP-03	372	972	
		611-PFL-03		WIM-03			
		612-PFL-03		509-WFL-03			
		613-PFL-03		510-WFL-03			
		614-PFL-03		511-WFL-03			
West	DH-04	PM-04	700	404-HWP-04	552	1252	
		615-PFL-04		WIM-04			
		616-PFL-04		512-WFL-04			
		617-PFL-04		513-WFL-04			
		618-PFL-04		514-WFL-04			
		619-PFL-04		515-WFL-04			
		620-PFL-04		516-WFL-04			
	DH-05	PM-05	600	405-HWP-05	372	972	
		621-PFL-05		WIM-05			
		622-PFL-05		517-WFL-05			
		623-PFL-05		518-WFL-05			
		624-PFL-05		519-WFL-05			
	DH-06	PM-06	600	406-HWP-06	372	972	
		625-PFL-06		WIM-06			
		626-PFL-06		520-WFL-06			
		627-PFL-06		521-WFL-06			
		628-PFL-06		522-WFL-06			

Additionally, ‘smart or intelligent wells’ are subsea wells whose instrumentation inside and above the wells contains microprocessors and intelligent sensor algorithms that enable wired/wireless digital or remote network transmission. Some of the above subsea wells are smart/intelligent wells, while others are not. The subsea wells, XTrees, manifolds, flowlines/pipelines, and risers in this design were assumed to have specialised instrumentation. Further information on the characteristics and design of generic valves and other instrumentation is available (Lipták, 2006)(ISA, 2007).

The power calculations (*Table 5.1*) show the breakdown of the necessary subsea equipment considered in this field development and the estimated electrical power requirement of the subsea equipment. As illustrated, the critical production control systems in the field need 6392W or approximately 6.4 kW.

5.5. Sizing the DPU

The following sections concentrate on the main components of the deepwater thermoelectric power system, beginning with the DPU. Sizing the DPU (deepwater thermoelectric power generating unit) for the production control system was based on daily load (subsea equipment) requirements over twenty-four (24) hours, seven (7) days a week, and three hundred and sixty-five (365) days subsea operations. Furthermore, this deepwater thermoelectric power-generating system was considered more than a per-day load-consumption system due to uncertainties on the seafloor, the harshness, and the remoteness associated with the power unit installed on subsea equipment. Hence, worst-

case seabed conditions were considered during the system design. For these reasons, it was assumed that a single Flex-DPP within the DPU could generate an optimum power of 250W at 150 °C subsea temperature difference input in a minimum duration of 30 minutes (or half an hour). This minimum duration in hours for a Flex-DPP is denoted as ($H_{Opt-min}$). Additionally, a zero net energy arrangement was assumed. In such an arrangement, the day-to-day power consumed by subsea equipment ($Wh_{subsea\ Load}$) is the same as the electrical power delivered to the equipment through the DPU (Wh_{DPU}).

Secondly, the efficiency value (η_{TEG}) of thermoelectric power systems considered for this deepwater power system was 5% or 0.05 (Hi-Z_Technology, 2006). Therefore, *Equation (5.1)* and *Equation (5.2)* determine the intrinsic area ($A_{Intrinsic}$) or the calculated area in which the DPPs are installed/needed to generate the required electrical power for the subsea equipment within the ultra-deepwater oil-gas field.

$$\eta_{TEG} \quad \text{x} \quad A_{Intrinsic} \quad \text{x} \quad H_{Opt-min} = Wh_{DPU} \tag{5.1}$$

$$A_{Intrinsic} = \frac{Wh_{DPU}}{\eta_{TEG} \quad \text{x} \quad H_{Opt-min}} \tag{5.2}$$

Through *Equation (5.3)* and *Equation (5.4)*, the total area of subsea structures ($A_{Subsea\ Structures}$) in which the DPU occupies on the deepwater oil and gas field was obtained. A 30% spacing was provided in the design for system installation, remotely

operated underwater vehicle (ROV) troubleshooting, maintenance, and sundry allowances on subsea structures.

$$\mathrm{A}_{Subsea\ Structures} = A_{Intrinsic} \quad \mathrm{x} \quad A_{Maintenance} \tag{5.3}$$

$$\mathrm{A}_{Subsea\ Structures} = A_{Intrinsic} \quad \mathrm{x} \quad Approximately\ 30\%\ of\ A_{Intrinsic}$$

$$\mathrm{A}_{Subsea\ Structures} = A_{Intrinsic} \quad \mathrm{x} \quad (1.3A_{Intrinsic}) \tag{5.4}$$

From *Table 5.1,* the estimated mean daily energy consumption of the subsea production control equipment is approximately 6.4kW or 6400 units. Hence, setting up the DPU for net-zero energy is thus:

$$Wh_{subsea\ Load} = 6400\ units = 6.4\ kWh/day$$

$$Thermoelectric\ Efficiency\ (\eta_{TEG}) = 0.05$$

$$H_{Opt-min} = 0.5\ Hours$$

Therefore, the required intrinsic area or active power generation area on the subsea structure is derived by substituting the minimum duration, efficiency of thermoelectric power systems, and mean daily energy consumption values into *Equation (5.2)*:

$$A_{Intrinsic} = \frac{Wh_{DPU}}{\eta_{TEG} \quad \mathrm{x} \quad H_{Opt-mim}}$$

$$A_{Intrinsic} = \frac{6.4\ KWh/day}{0.05 \quad \mathrm{x} \quad 0.5} = 256\ m^2$$

From *Equation (5.4)*, the total area of subsea structures needed by the DPU or the required space in the deepwater oil and gas field ($A_{Subsea\ Structures}$) is thus:

$$A_{Subsea\ Structures} = 1.3 \quad x \quad A_{Intrinsic}$$

$$A_{Subsea\ Structures} = 1.3 \quad x \quad 256 = 332.80\ m^2$$

The above-calculated parameters and the information from **Sections 3.4.9** and **3.4.10** form the deepwater thermoelectric power generating unit (DPU) configuration requirement, as shown in *Table 5.2*. Further details on TEMs, Flex-DTEMs, Flex-DPPs, and DPUs are available in ***Chapter 3***.

Table 5.2 DPU Power Source Configuration

Item	**Rating/Description**
DPU Framework	5 nos.-Flex-DPPs Connected in Parallel, 6 nos.-Flex-DPP Connected in Series (5P x 6S)
Maximum Voltage of DPU	174.00 V
Maximum Current of DPU	36.75 A
Intrinsic or Active Power Generation Area	256 m^2
Total Subsea Systems Structural Area Requirement	332.80 or 333 m^2

5.6. Electrical Load Profile for a Subsea Well

This section focuses on estimating the electrical load profile for subsea wells. Therefore, minimising complex design errors was essential. The load profiling was carried out using the subsea equipment on one of the oil-gas production wells to represent all the subsea wells and equipment presented in *Figure 5.3*. The chosen subsea well was number #601 (same as in **Section 1.2**) to obtain the approximate power demand from a typical subsea well in the oil and gas field.

As mentioned in **Section 5.4.6**, subsea well #601 was integrated with intelligent well system (IWS) facilities (McLauchlan and Nielsen, 2004). Hence, the electrical power needs of this smart subsea well served as a reasonable estimate for the other subsea electrical loads. It was also assumed that all the subsea equipment installed on intelligent subsea wells had to operate continuously during the day and night.

Like the other oil and gas production wells in the field, subsea well #601 was equipped with instrumentation to monitor several subsea well parameters. Such parameters include temperature, pressure, flow measurements, XTree, and in-well-located servomechanisms that make changes according to the observations of the monitoring and control system. The other subsea well data considered were reservoir and production metrology information. Thereby providing valuable data to reservoir and production engineers in real time.

Figure 5.7 represents subsea electrical loads (in watts) and 24-hour (time) spread for the ultra-deepwater oil and gas field. The time axis was split into day and night loads. The

DPU and subsea battery supply electrical power to subsea loads 24 hours daily. As shown in the illustration on the equipment load profile representation, day load (Wh_{Day}) occurs from around 0600 hours to about 1800 hours. Night load (Wh_{Night}) is from 1800 hours to midnight and from midnight to approximately 0600 hours.

Apart from estimating day load and night load, this subsea well load profile assisted in establishing the peak subsea load current (I_{SLoad_Pk}) and average subsea load current (I_{SLoad_Avg}) for subsea batteries deployed at the ultra-deepwater oil and gas site.

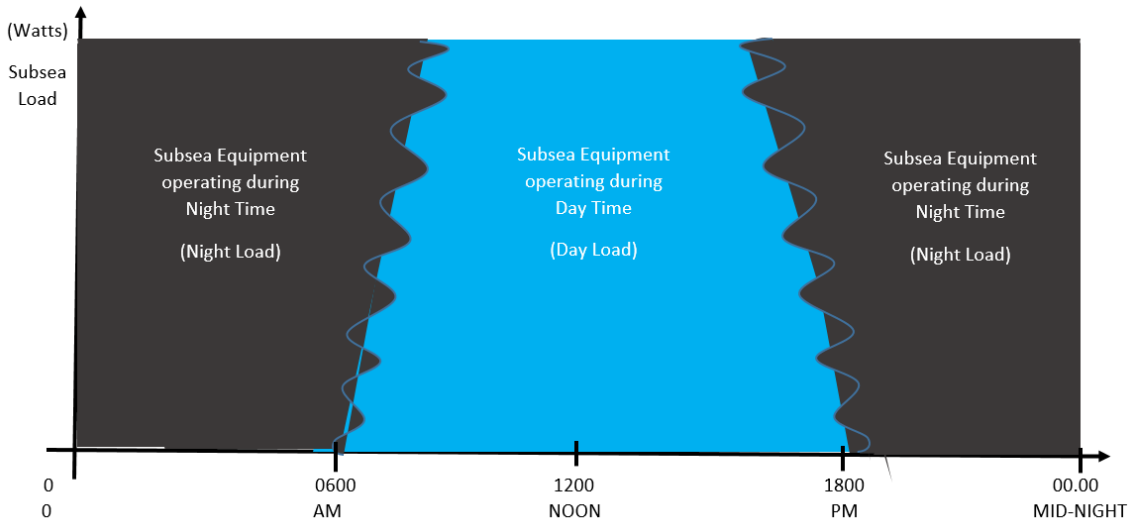

Figure 5.7 Load Profile of Subsea Equipment

From the intelligent subsea well #601 load profile in *Figure 5.8*, the day load (Wh_{Day}) occurs from 0700 hours (7 am) to 1700 hours (5 pm). Hence, this design considered ten (10) hours as a day load for subsea equipment operated during the daytime. Duration for night load (Wh_{Night}) started after 1700 hours (5 pm) to midnight (00.00 hours) and from

midnight to 0700 hours (7 am). The illustration shows that fourteen (14) hours was the total duration of the night load.

As explained above, subsea well #601 consists of various subsea equipment. However, for simplicity, three (3) pieces of equipment contributed to determining the production well's electrical load profile, as shown on the subsea well #601 load profile in *Figure 5.8*.

The operating characteristics of the equipment are discussed below:

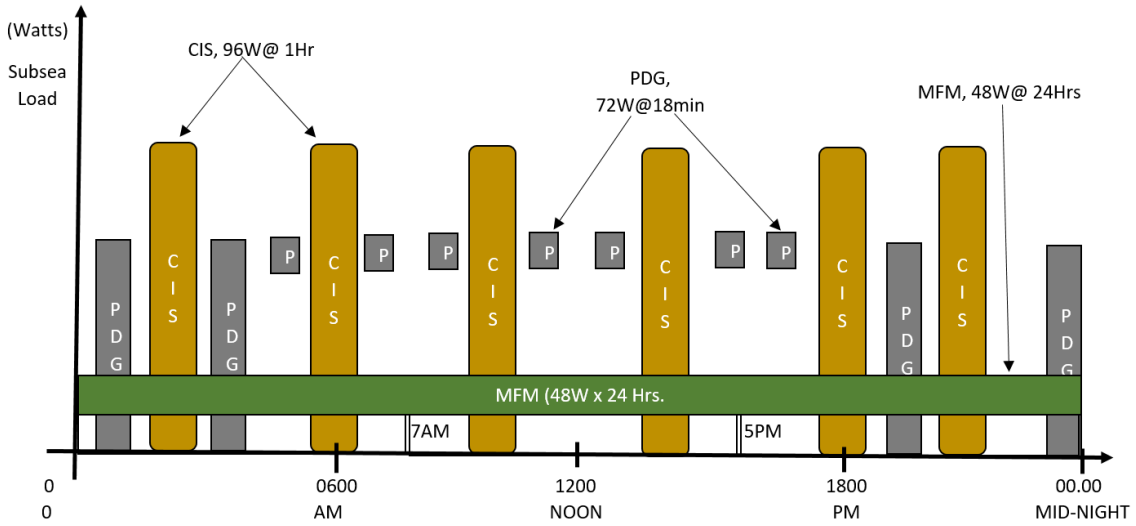

Figure 5.8 Load Profile for Smart Subsea Well-#601

- ***Subsea Load-01*** was a multiphase flow meter (MFM). The equipment operated at 24V DC and 48W day and night (24-hour operation). That means the MFM was regarded as day-and-night continuous or non-stop electrical load.

- ***Subsea Load-02*** was a chemical injection system (CIS) that was used to dose different chemical cocktails into the subsea well. CIS operated six (6) times daily for one (1) hour on each occasion. In other words, the daily working sequence for this equipment was twice before dawn, two times in the afternoon, and twice after dusk. The assumed average running current of the CIS was 4A at 24V DC.

- ***Subsea Load-03*** was a permanent downhole monitoring system and flow control gauge (PDG). (Note that the letter P represents the PDG in *Figure 5.8* to avoid crowding the diagram). The operating power rating of the PDG was 3A at 24V DC. This equipment was scheduled to work at intervals of two (2) hours for 18 minutes throughout the day.

Therefore, calculating the day load and night load is thus:

Day Load → Operated from 0700 to 1700 hours (10 hours of subsea operation time). The total day load from ***Subsea Load-01***, ***Subsea Load-02***, and ***Subsea Load-03***, respectively, was calculated as below:

$$Wh_{Day} = (48W \text{ x } 10hrs) + (96W \text{ x } 2hrs) + \left(72W \text{ x} \frac{18}{60} hrs \text{ x } 5\ cycles\right) \quad (5.5)$$

$$Wh_{Day} = 780\ Wh$$

Night Load → operated from 1700 hours to 00.00 hours and from 00.00 hours to 0700 hours (14 hours of subsea operation). The total night load from ***Subsea Load-1***, ***Subsea Load-02***, and ***Subsea Load-03***, respectively was calculated as below:

$$Wh_{Night} = (48W \text{ x} 14hrs) + (96W \text{ x } 4hrs) + \left(72W \text{ x} \frac{18}{60} hrs \text{ x } 7 \; cycles\right) \quad (5.6)$$

$$Wh_{Night} = 1207.20 \; Wh$$

The peak subsea load current (I_{SLoad_Pk}) and average subsea load current (I_{SLoad_Avg}) for the three subsea equipment on subsea well #601 is thus:

$$I_{SLoad\_Pk} = \frac{48W}{24V} + \frac{96W}{24V} + \frac{72W}{24V} \quad (5.7)$$

$$I_{SLoad\_Pk} = 2A + 4A + 3A = 9A$$

It was thought that in the worst case at the seafloor, all the subsea loads overlap, such that ***Subsea Load-01*** operates at 2A, ***Subsea Load-02*** functions at 4A, and ***Subsea Load-03*** works at 3A. Therefore, the peak operating current required at the subsea well was 9A. That is to say, the discharge current of the preferred subsea battery should be at least 9A or capable of withstanding 9A electrical current at normal and abnormal operating conditions.

Based on the duty ratio, the average subsea load current (I_{SLoad_Avg}) for the subsea well was calculated for individual loads in the following order:

- ***Subsea Load-01*** operates at 2A for 24 hours of the day
- ***Subsea Load-02*** operates at 4A for 6 hours in 24 hours

- ***Subsea Load-03*** works at 0.3 hours at 3A for 12 times in 24 hours.

Thus:

$$I_{SLoad\_Avg} = \left(2A \text{ x } \frac{24hrs}{24hrs}\right) + \left(4A \text{ x } \frac{6hrs}{24hrs}\right) + \left(3A \text{ x } \frac{\left(\frac{18}{60}\right)hrs}{24hrs} \text{ x } 12\ cycles\right) \quad (5.8)$$

$$I_{SLoad\_Avg} = \quad 2A \quad + \quad 1.0A \quad + \quad 0.45A = 3.45A$$

Therefore, during severe seabed conditions, if the subsea battery were the only electrical power source for the subsea equipment located on the ultra-deepwater oil-gas production well, the average subsea battery discharge current would be about 3.45A.

5.7. Days of Autonomy & Recharge at the Seabed

During abnormal sea states or severe flow assurance issues and a decrease in temperature along the fluids flow path, it was assumed that the DPU might not be capable of power generation. In such cases, the subsea equipment are meant to be supported by the subsea battery alone, as was demonstrated in **Sections 4.7**, **4.8**, and **4.9**. The days without support from the DPU are referred to as days of autonomy (n_{auto}). That means the subsea battery rating should be capable of accommodating seabed anomalies. When normalcy returns, the DPU resumes operation, and subsea batteries are recharged or replenished. Depending on the degree of abnormalities on the ocean floor, it was assumed that subsea battery replenishing might not be completed in a single day. Therefore, days of recharging or replenishing was represented by (n_{repl}) in this work.

As explained above, the hot water subsea production wells are the expected stopgap or emergency energy generation stations when anomalies occur on the seafloor. The inclusion of these emergency energy generation stations in this ultra-deepwater application nullifies abnormal sea effects, thus defining (n_{auto}) and (n_{repl}) as absent or zero (0) during poor seafloor conditions:

$$n_{auto} = 0$$

$$n_{repl} = 0$$

5.8. Sizing Subsea Battery

The hot water subsea production wells cancelled out abnormalities during unfavourable seabed conditions. Section 5.8 estimates the quantity and capabilities of the required subsea battery. Selecting a suitable subsea battery and battery capacity was crucial for this ultra-deepwater power system. Hence, the overall energy consumption for day load and night load (Wh_{SLoad_DN}) was calculated using *Equation (5.9)* and *Equation (5.10)*. Battery efficiency was denoted by (η_{BAT}):

$$Wh_{SLoad\_DN} = \left(\frac{Wh_{Night}}{\eta_{BAT}}\right) + \left(\frac{Wh_{Day} + Wh_{Night}}{\eta_{BAT}}\right) \text{ x } (n_{auto}) \qquad (5.9)$$

Simplifying *Equation (5.9)* gives:

$$Wh_{SLoad\_DN} = \left(\frac{Wh_{Night}}{\eta_{BAT}}\right) \text{ x } (n_{auto} + 1) + \left(\frac{Wh_{Day}}{\eta_{BAT}}\right) \text{ x } (n_{auto}) \qquad (5.10)$$

The selected battery chemistry was Nickel Metal Hydride (NiMH), as discussed in **Section 4.6.1**. This battery chemistry has deep discharge characteristics. The battery's depth of discharge (DoD) value typically ranges from 80% (0.8) to above 90% for continuous long-term power supply to subsea equipment. The DoD is the battery capacity discharged from the battery-rated ability. The battery efficiency was assumed to be 70% (0.7). Battery capacity (Ah_{BAT}) was calculated using *Equation (5.11)*:

$$\text{Ah}_{BAT} = \frac{Wh_{SLoad\_DN}}{(DoD) \quad \text{x} \quad (\text{V}_{BAT\_Nom})} \qquad (5.11)$$

From **Section 5.6**, the calculated day and night load from ***Subsea Load-01***, ***Subsea Load-02***, and ***Subsea Load-03*** for Subsea Well number #601 are 780Wh and 1207.20Wh, respectively. The night load value is higher than the day load value; therefore, the higher value was used to estimate the battery capacity.

Using a DOD of 80%, nominal battery voltage (V_{BAT_Nom}) of 24V, and (n_{auto}) = (n_{repl}) or zero (0), as stated above. Hence, the subsea day load (Wh_{Day}) and (n_{auto}) = (n_{repl}) terms were struck out from *Equation (5.10)*. Therefore, the required battery capacity was calculated as shown below using the simplified *Equation (5.10)*:

$$Wh_{SLoad\_DN} = \frac{Wh_{Night}}{\eta_{BAT}}$$

$$Wh_{SLoad\_DN} = \frac{1207.20}{0.7} = 1{,}724.57\ Wh$$

Substituting the value of the new day and night subsea load (Wh_{SLoad_DN}) into *Equation (5.11):*

$$\mathrm{Ah}_{BAT} = \frac{Wh_{SLoad\_DN}}{(DoD) \quad \mathrm{x} \quad (\mathrm{V}_{BAT\_Nom})}$$

$$\mathrm{Ah}_{BAT} = \frac{1{,}724.57\ Wh}{(0.8) \quad \mathrm{x} \quad (24V)} = 89.82 \cong 90\ Ah$$

From the above design calculations, the battery capacity for subsea well #601 was 90 Ah, while the peak operating current was 9A. Therefore, in conjunction with the DPU, the Device-SBAT-101 battery was considered suitable for supporting subsea equipment operating twenty-four (24) hours and seven (7) days a week. Further details on the selected battery are available in **Section 4.6**. *Table 5.3* shows the composition of the subsea battery pack for related subsea equipment on a subsea well. It equally means that two (2) numbers of Device-SBAT-101 make a battery pack.

Also, *Table 5.1* presented 68 associated items that require electrical power. As a result, *Table 5.4* provides information suitable for subsea battery-bank specifications for the deepwater oil and gas field. Additional details on stationary batteries are in (IEEE, 2020)(IEEE, 2014)(Doughty *et al.*, 2010)(Malhotra *et al.*, 2016).

Table 5.3 Subsea Battery-Pack Configuration

Item	**Rating/Description**
Subsea Battery-Set Configuration	2 Battery Modules Connected in Series (1P x 2S)
Subsea Battery-Set Voltage Rating	24 V
Subsea Battery-Set Voltage Nominal Capacity	90 Ah
Subsea Battery Model	Device-SBAT-101
Battery Chemistry	Nickel metal hydride (NiMH)

Table 5.4 Subsea Battery-Bank Configuration

Item	**Rating/Description**
Subsea Battery-Bank Configuration	1 x 68 Battery Packs Connected in Parallel (1Pack x 68P)
Subsea Battery-Bank Voltage Rating	24 V
Subsea Battery-Bank Capacity	68 x 90 or 6120 Ah
Subsea Battery Model	Device-SBAT-101
Battery Chemistry	Nickel metal hydride (NiMH)

5.9. Chapter Summary

The design and development of an ultra-deepwater oil and gas field were discussed in this Chapter. The oil and gas field contained 56 subsea wells and numerous subsea production equipment. The total structural area required by 6.4 kW-DPU was approximately 333 square metres. The 6.4 kW-DPU operated alongside a 6,120 Ah capacity subsea battery bank to provide electrical power to critical subsea production control equipment. While

oil and gas production were ongoing, deepwater thermoelectric power generation occurred day and night, 365 days, year in and year out, for at least 20 years. The 6.4 kW DC power derived from the ultra-deepwater oil-gas field through the DPU is transformed into AC power in ***Chapter 6***.

Chapter 6

DTEG & Underwater Power Grid System

6.1. Introduction

In the previous Chapter, a 6.4 kW-DPU energy harvesting-power source and subsea energy storage system were designed and developed for an ultra-deepwater oil and gas production field. In ***Chapter 6***, the 6.4 kW-DC power is transformed into AC power through a different combination of power electronic devices and delivered to an underwater combo power grid system. This deepwater thermoelectric power scheme for ocean floor-based electrical power is revolutionary and the first of its kind.

6.2. 6.4kW-DPU Input Parameters & Power Grid System

Designing and developing a deepwater thermoelectric power system for an ultra-deepwater oil/gas field involves intricate considerations. Fundamental thermoelectric equations like the Seebeck effect, electrical conductivity, thermal conductivity, heat transfer, power system models, equations, electronic systems, algorithms, and assumptions were discussed in ***Chapters 2***, ***3***, ***4***, and ***5***. These fundamental input parameters and assumptions are applicable in the design and development of this 6.4kW-

DPU. However, some modifications were made to accommodate the first-ever underwater power grid system integration in ***Chapters 6*** and ***7***. Hence, the factors considered in the design and development of the 6.4kW-DPU connected to the underwater power grid system were as follows:

Flex-250W-DPPs Configuration: Several flexible deepwater power plates were connected in series-parallel arrangements on subsea flowlines, pipelines, and other fluid-carrying structures to optimise power output and system efficiency.

Heat Source Management: The Flex-250W-DPPs consist of several flexible thermoelectric modules, and their heat exchangers were optimised to transfer heat from oil and gas reservoirs to the deepwater power unit (6.4kW-DPU) efficiently. Secondly, each Flex-250W-DPP was incorporated with insulation strategies to minimize heat loss throughout heat transfer. These strategies ensured that temperature differentials were maintained during system operation.

Underwater Electrical Power Grid: Subsea power converter and subsea power inverter designs were optimised to transform DC output power from the 6.4kW-DPU source to AC power suitable for underwater grid system integration. Secondly, the control algorithms were expanded and implemented for stable and synchronized AC output power compatible with underwater electrical power grid requirements. Thirdly, for the sake of the overall system's reliability, the topology and layout of the power grid system design considered load balancing, power transmission losses, voltage regulation, and redundancy.

Real-World Scenarios: Changes in seawater properties and ultra-deepwater characteristics such as salinity and low temperature were accounted for during the system design. Prolonged exposure to sea conditions that might impact the flexible thermoelectric modules at the seafloor was also assumed during the design and development. Other factors accounted for during system design were the depreciation of thermoelectric materials and the degradation of power system components. Furthermore, exposure to high pressure at the seabed and the corrosive nature of seawater over time are some of the real-world challenges that were also considered.

Limitations: This comprehensive deepwater thermoelectric power system and underwater electrical power grid system considered the intricacies of flexible thermoelectric modules, deepwater power plates, heat source management, subsea power converters, subsea power inverters, control algorithms, power grid system went through rigorous design and development effort. Secondly, real-life conditions, such as challenging ultra-deepwater environments, heat source inconsistencies, subsea temperature gradient fluctuations, oil/gas reservoir flow dynamics, water depth, salinity, and pressure impact, are some of the naturally occurring phenomena that are complicated and cumbersome to represent on the power system models. Thirdly, the technologies for precisely predicting some of these natural occurrences are not yet available. Therefore, available resources were used during the system design and development of the electrical power system presented in ***Chapters 6*** and ***7***. This deepwater thermoelectric system and the underwater electrical power grid systems are reliable, efficient, and adaptable for an ultra-deepwater oil and gas field.

6.3. Underwater Combo Power Grid System

An in-situ energy harvesting, harnessing, and power generation process with the aid of a Flex-250W-DPP and subsea battery was demonstrated in ***Chapter 4***. The configuration of sets of Flex-250W-DPP in parallel (5P) and series (6S), resulting in a 6.4kW-DPU power source in conjunction with a 6120 Ah capacity subsea battery bank, was established in ***Chapter 5***. Notably, converting electrical energy to chemical energy (or stored energy in batteries) and back to electrical power usually comes with energy losses. Such losses are detrimental to subsea operations. Secondly, DC-powered subsea equipment is not a standard norm in the subsea market (see **Sections 5.4.7** and **5.4.8**). Hence, converting the 6.4 kW DC power to AC power was imperative. Also, the transformation of DC power to AC power on the seafloor places the subsea sector of the oil and gas industry in an advantageous position towards alternative energy processing on the ocean floor.

Moreover, land-based utility power grid systems are typically AC electrical power sources. Hence, supplying land-based electrical power to subsea equipment is not new to the industry. One such example is Martin Linge, an offshore gas production field in the Norwegian sector of the North Sea. The step-out distance is about 170 km, and approximately 55MW is supplied to an offshore platform from a land-based power source (Thibaut and Leforgeais, 2012). Another instance is the Ormen Lange subsea gas compression system. Around 58 MW of electrical power and communication signals were deployed onshore to the seafloor at about 3,000 meters of water depth. The Ormen Lange subsea power umbilical was approximately 125 km long (Bjerkreim *et al.*, 2009). As such,

the assumption in this design was deploying submarine and umbilical power cables to an underwater electrical power grid system from onshore to the seafloor and back to onshore.

It is important to note that most deepwater or ultra-deepwater oil and gas field development solutions in West Africa and other parts of the world use offshore gas turbine power plants and diesel-driven power generators on board FPSOs or other floating structures. Some notable oil-gas fields at various stages of development in Nigeria, where electrical power is transmitted from the topside to the seafloor, are the Bonga deepwater, Agbami field, and the Egina oil field. Additional examples include Deepwater Tano/Cape Three in Ghana, the Zinia-2 development, and the Pazflor offshore field in Angola (Africa Oil Week, 2019). As mentioned earlier, the electrical power supply for these oil-gas fields is designed from the platforms/FPSOs to the subsea equipment.

Renewable energy sources are often not considered in most deepwater or ultra-deepwater oil and gas development, especially in Africa. In contrast to the conventional approach, this ultra-deepwater thermoelectric power system design assumed the reachability of shore-based facilities, as stated above. Furthermore, an open architecture approach was adopted. The approach allows the integration of non-renewable and other offshore-based renewable energy sources. Hence, in addition to shore-based facilities, FPSO/platform-based power sources and ocean thermal energy conversion (OTEC) formed an unconventional *'underwater combo power grid system*.' The modified *Figure 3.1* is seen below in *Figure 6.1*. OTEC and other offshore renewable potentials are available in West Africa (Song, 2019)(J. O. Ahaotu, B. Nkoi, 2018).

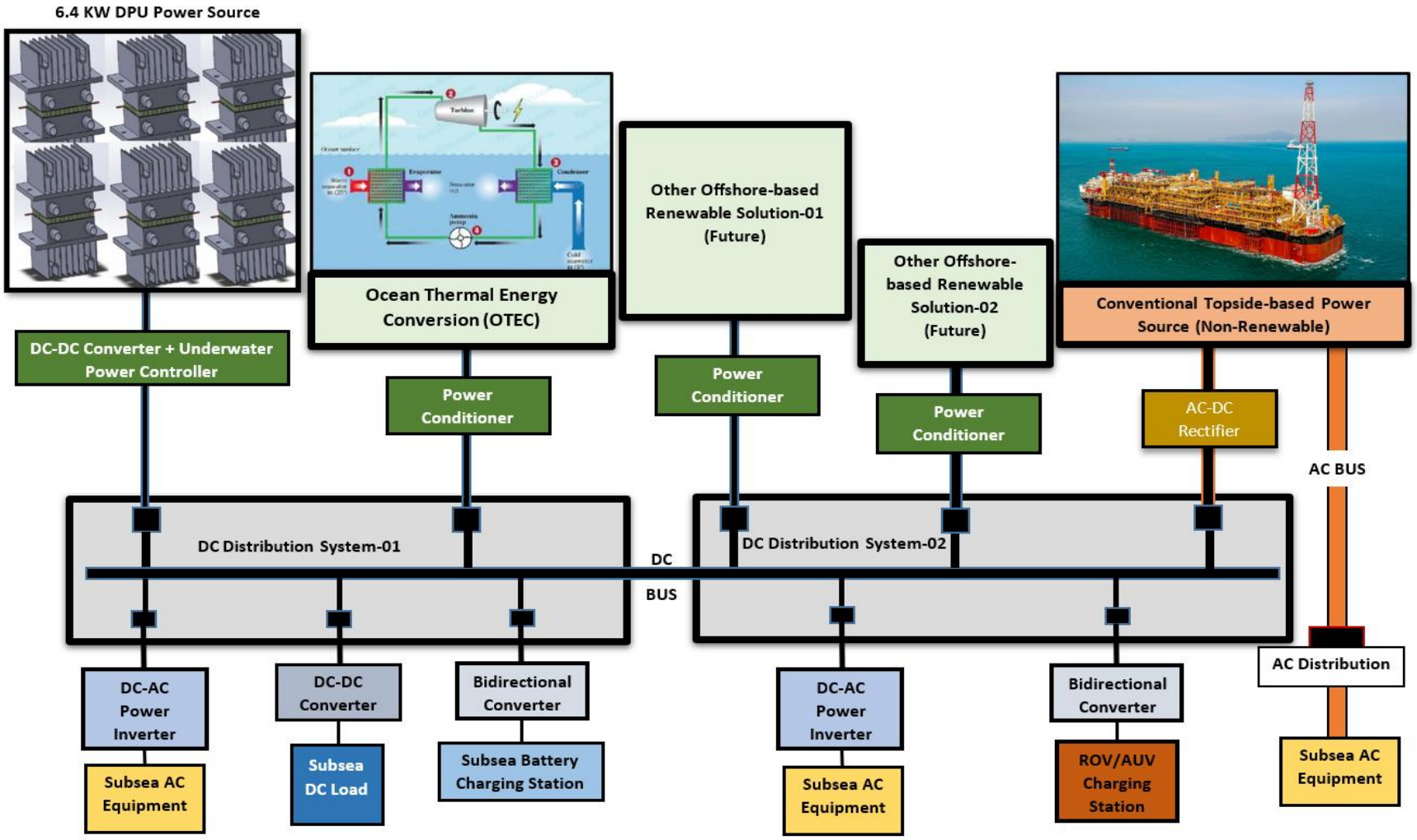

Figure 6.1 Ultra-Deepwater Power System Architecture-West Africa

Note that tie-in points for the platform-based sources, shore-based sources, and offshore-based power lines are not shown in the underwater combo power grid architecture; such details are outside the scope of the research. Furthermore, the system architecture shows that individual power sources can supply power to the underwater combo power grid system. However, if there is a decline in any power source, the other sources compensate for such a deficit. Excess-generated energy during normal sea operating times goes into the grid system. Thus, this power grid system acts as an underwater energy buffer or subsea energy storage medium.

This underwater combo power grid system will use an energy management strategy to supply electrical power to critical subsea controls and non-critical power-demanding equipment such as subsea pumps, subsea compressors, and other subsea processes (Ray *et al.*, 2019). Secondly, the combo power system has facilities for underwater charging stations for ROVs and AUVs (autonomous underwater vehicles) (Manikandan *et al.*, 2018)(Davis, 2011)(API, 2009). The intended power grid system offers possibilities not only for the wired but also for both wired and wireless charging stations (Lempidis *et al.*, 2014)(Mude, 2018).

However, it is essential to note that this work does not include electrical power supply from the underwater power grid system to individual subsea equipment such as ROVs, AUVs, subsea battery charging, and excess power transmission from the underwater combo power grid system back to shore. Beyond this point, there are no discussions on OTEC, other renewable sources, future offshore renewable sources, and non-renewables.

Instead, the focus is on incorporating the deepwater thermoelectric power source into the underwater power grid system in the following sections.

6.4. Power Grid Connection Principle

Like most renewable energy sources, the 6.4kW-DPU is a fluctuating power source requiring an energy storage device, as discussed in ***Chapters 4 and 5***. Furthermore, thermoelectric power systems depend on temperature differences, among other factors. Therefore, this 6.4kW-DPU relies on the subsea temperature difference input between hot-flowing fluids from oil-gas reservoirs and cold seawater as one of the main constituents for its functionality.

On the contrary, traditional shore-based power grid systems are infinite power sources capable of supplying power within reasonable limits. Thus, a power grid system seems to be an ideal power source with almost negligible output impedance. Therefore, converting 6.4 kW DC power to AC power and connecting it to the underwater combo power grid makes the proposed deepwater power system a viable supplementary power source for both power supply and power removal.

6.5. Topologies for Grid System Interface

Based on the discussions in **Sections 6.3 and 6.4**, connecting power sources to an electrical power grid system can be done in various ways or combinations of methods and topologies. Some of the techniques considered for such connections are:

- ***Isolation*** – The use of low-frequency and high-frequency transformers for electrical power isolation purposes
- ***Transformerless*** - The use of transformerless interfaces for connection to the electrical power grid system
- ***The number of electrical power stages*** – A one-stage power system has only one power converter, while two or three-stage systems have two and three-power converters, respectively.

The adopted approach for this ultra-deepwater application was the transformerless interface and two-stage power conversion method. The selected grid voltage for the power system was 380 VLL (line-to-line voltage). Given at least 20% losses across IGBT power switches, filter inductors, and other system losses, the estimated minimum DC Bus voltage (Karlsson and Svensson, 2003)(Dam and Lee, 2018) for the selected 380 VLL grid voltage was calculated using *Equation (6.1):*

$$Min\ DC\ Bus\ Voltage = V_{LL} \quad \text{x} \quad \sqrt{2} \quad \text{x} \quad 1.2 \tag{6.1}$$

$$Min\ DC\ Bus\ Voltage = 380 \quad \text{x} \quad 1.4142 \quad \text{x} \quad 1.2 \quad = 645V$$

Hence, the minimum DC Bus voltage is 645V, as shown in the above calculation. However, uncertainties at the seabed during severe sea conditions (as highlighted in

Section 5.3 and **Section 6.3**) were considered during the design phase. That means the 6.4kW-DPU power source might not be able to generate up to 645V in abnormal ocean floor conditions. Therefore, the selected minimum DC Bus voltage through the subsea DC-DC boost converter was 570V, as shown in *Figure 6.2.* Additional components, such as a three-phase subsea power inverter, AC filter inductors, and delivered power to the combo grid system, are represented in *Figure 6.2*.

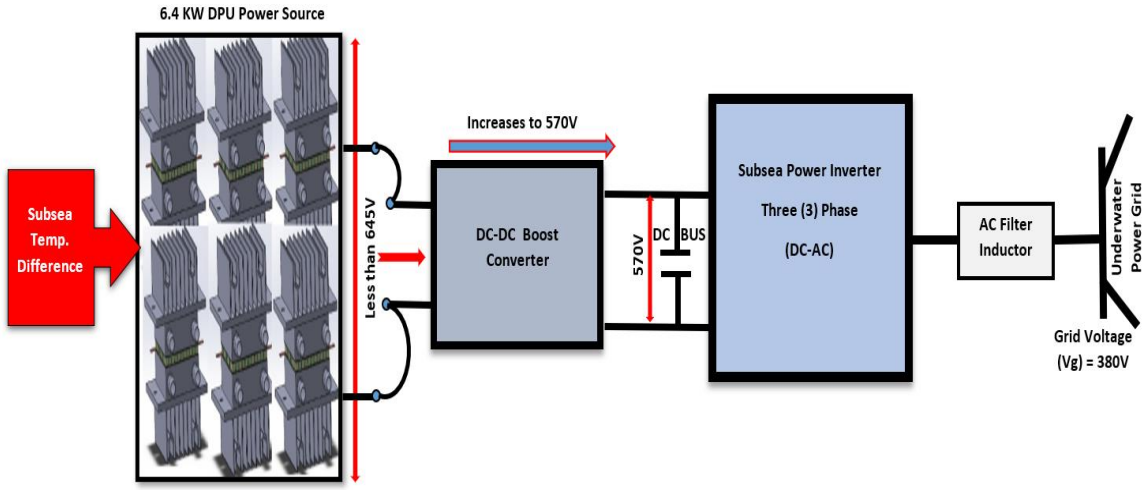

Figure 6.2 Two-Stage 3-Phase Deepwater Thermoelectric Power System

6.6. DPU & 3-Phase Combo Power Grid System

The expansion of the DC and AC segments of *Figure 6.2* is shown in *Figure 6.3*. The functionality of the subsea DC-DC power converter, the 6.4 kW-DPU with its subsea temperature difference profile, is the same as discussed in ***Chapter 4***. Control signals are generated through the underwater power controller, as explained in **Sections 4.3**, **4.4**, and

4.5. Hence, the reference signals generated by the underwater power controller dictate the power potentials delivered to the AC combo power grid system.

Furthermore, the illustration in *Figure 6.3* shows that the subsea power inverter consists of IGBT power switches in which the gate drive circuits are energised at the gate terminals. The outcome of the DC control signals from the underwater power controller, in conjunction with the gate drive control signals, are responsible for creating three-phase AC signals: a-phase, b-phase, and c-phase.

From the above discussions, the subsea power inverter's output voltage and current signals ([Va, Vb, Vc] and [Ia, Ib, Ic]) are sensed and manipulated by DC-to-AC conversion procedures. The AC-domain sinusoidal signals are transformed into DC-domain signals. Afterward, the DC signals are changed back to AC through a frame transformation process known as the (d-q) axis principle (Aktaibi *et al.*, 2014)(Ahmad *et al.*, 2020).

The (d-q) or direct and quadrature axis technique is a theoretical transformation technique in which a three-phase stationary coordinate system changes to a (d-q) rotating coordinate system (Aktaibi *et al.*, 2014). The three-phase components of AC signals (a, b, and c) are converted to DC quantities (d-q axis components) and operated upon, then changed back to AC signals in a forward and reverse transformation sequence (Kim *et al.*, 2002)(Kim, Blaabjerg and Bak-Jensen, 2002).

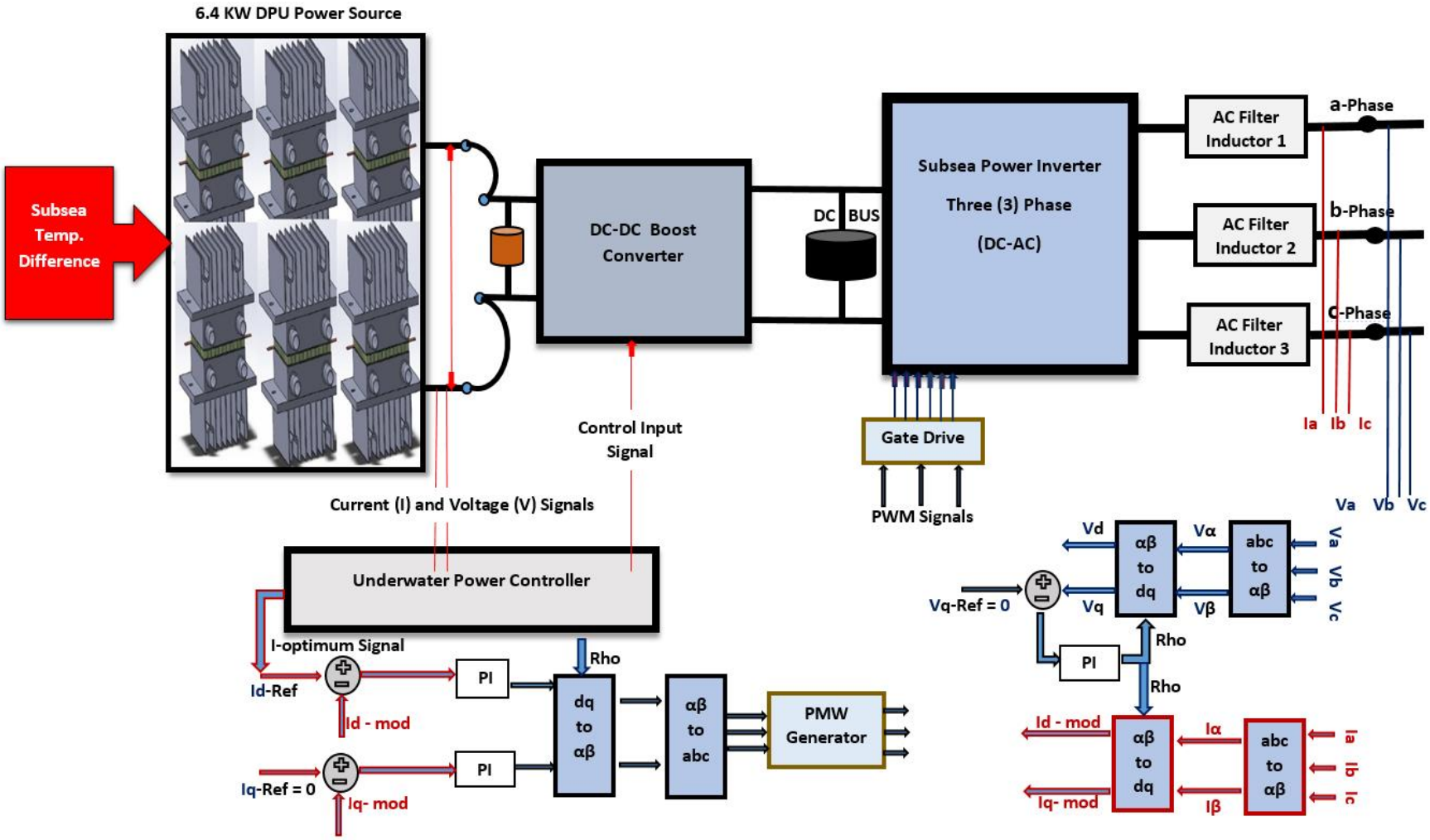

Figure 6.3 DC-AC Frame Transformation

The forward and reverse transformation processes are grouped into four stages. In the forward transformation, AC signals are converted to DC domain quantities. This means that three-phase AC sinusoidal signals are changed into two-phase AC signals or AC wave shapes during the first stage (abc to αβ). In the second stage, the two-phase AC signals are converted to two-phase DC signals (αβ to dq):

$$Stage-01 \quad a\ b\ c \quad to \quad \alpha\beta \quad \rightarrow \quad 3\emptyset\ AC \quad to \quad 2\emptyset\ AC$$

$$Stage-02 \quad \alpha\beta \quad to \quad dq \quad \rightarrow \quad 2\emptyset\ AC \quad to \quad 2\emptyset\ DC$$

During the reverse transformation step, DC-domain quantities are converted back to AC quantities. Hence, in the third stage of the transformation process, two-phase DC signals are changed to two-phase AC (dq to αβ). Finally, in the fourth stage, two-phase AC signals are converted back to three-phase AC signals (αβ to abc):

$$Stage-03 \quad dq \quad to \quad \alpha\beta \quad \rightarrow \quad 2\emptyset\ DC \quad to \quad 2\emptyset\ AC$$

$$Stage-04 \quad \alpha\beta \quad to \quad a\ b\ c \quad \rightarrow \quad 2\emptyset\ AC \quad to \quad 3\emptyset\ AC$$

6.7. DPU & 3-Phase Combo Grid Implementation

From the discussions above, the design and implementation of two-stage power conversion for the underwater combo grid-connected 6.4kW-DPU power source

(illustrated in *Figure 6.2* and *Figure 6.3*) was realised in MATLAB/Simulink. The power system model is shown in *Figure 6.4.*

The power system model was partitioned as DC and AC parts for easy understanding. The subsea temperature difference input (STD) side of the model to the DC Bus was labeled as part-A. The underwater power controller section is labeled as part-B. (See *Figure 6.4*)

Part-C is the AC output portion of the power system. The system model shows that the subsea power inverter, AC filter, voltage-current sensor/measurement block (representing a Hall-effect sensor), and a 380V power grid block are components in part-C. Through the 3-phase sensor/measurement block, AC voltage and current signals were sensed and measured. These AC signals were converted to DC quantities and operated upon in part-D and part-E sections of the power system model.

A 100 μF terminal capacitor (DPU terminal-capacitor) was interfaced between the 6.4 kW-DPU power unit and the subsea DC-DC boost converter. The outlet of the subsea boost converter was a DC link or DC Bus (a 1000 μF capacitor represents the DC Bus). Beyond the DC Bus point is the AC segment of the power circuit. Therefore, the DC Bus offered a common connection point between the DC and AC segments of the power system.

The subsea power inverter used in the power system model was a three-phase universal bridge power inverter system with IGBT and diodes as power electronic devices.

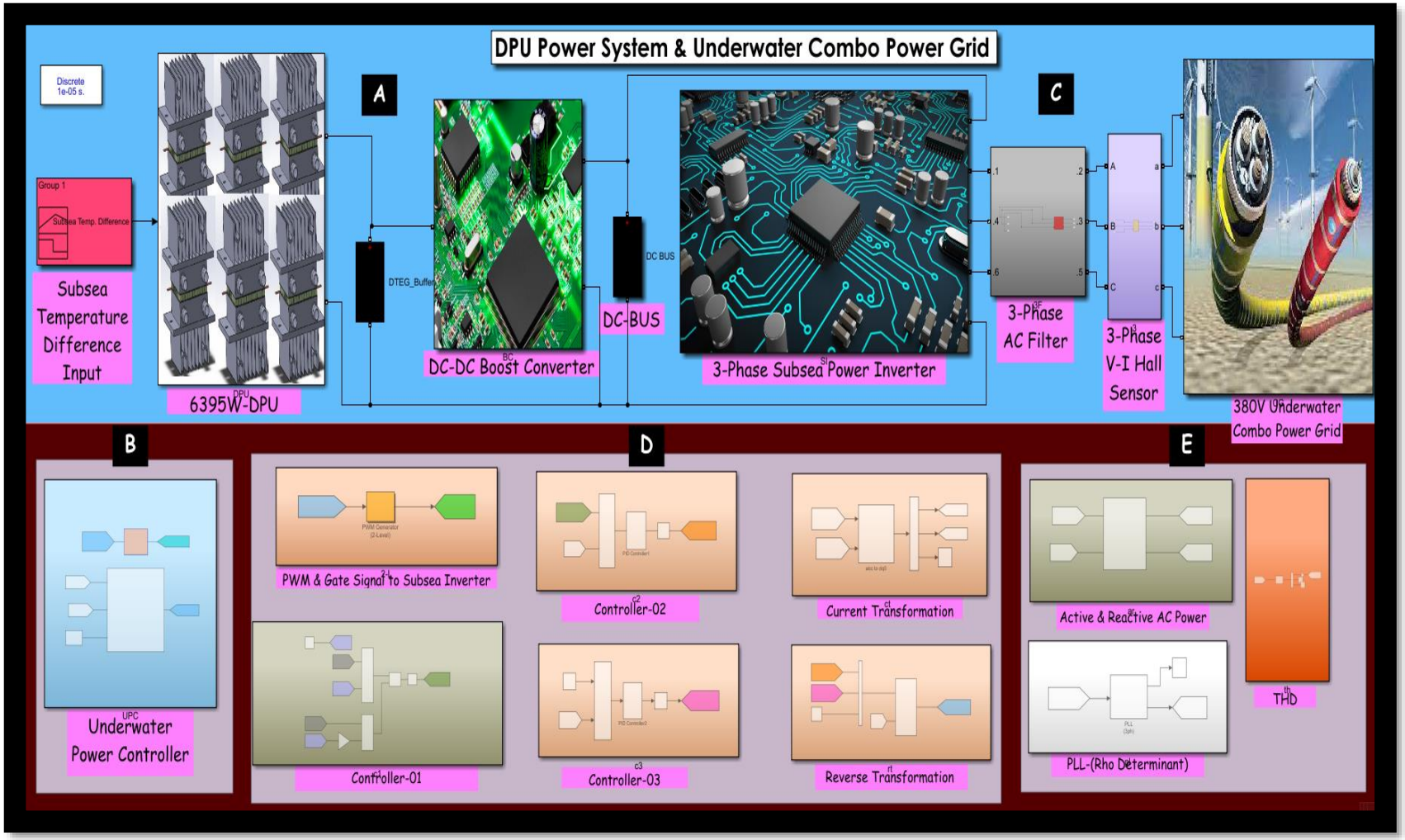

*Figure 6.4 6.4*kW*-DPU Power Source & Underwater Power Grid System*

A three-phase AC filter (Series RLC with Inductance as branch type) connects the output of the subsea power inverter. The power system model shows a grid voltage source represented by the underwater combo power grid system. The parameter setting on the three (3) phase grid voltage-source block was 380 Vrms phase-to-phase and 50 Hz frequency.

The sample time for system simulation was ten (10) microseconds (μS). Other design parameters for the deepwater power system, including the DPU power rating, subsea DC-DC boost converter component rating, the underwater power controller composition, selected bus voltage, subsea power inverter rating, AC filter, etc., are available as a MATLAB script file in **Appendix E (Algorithm E.1)**. Further information on grid-connected renewable energy systems is in (Yasmeena and Das, 2015)(Al-Shetwi *et al.*, 2020)(Basit *et al.*, 2020)(Gurrola-Corral *et al.*, 2020).

The deepwater power system was operated by subsea temperature difference input from 0 °C to 150 °C through the 6.4kW-DPU energy harvesting, harnessing, and power-generating source. A multiplexer block and associated components (not shown in Figure 6.4) were used for sensing, measuring, and computing the output voltage and current from the DPU power unit when a subsea temperature difference was applied to the power unit.

6.8. Two-Stage Power System

As mentioned in **Section 6.5**, the transformerless interface and two-stage power conversion method were selected for the grid-connected underwater power system. The two-stage control strategy of this ultra-deepwater power system had two control system loops logically connected as a single physical system (Li *et al.*, 2016)(Bae *et al.*, 2005). The first control system loop consists of the underwater power controller, subsea DC-DC boost converter, and the 6.4kW-DPU power unit with subsea temperature difference input. The second control system loop managed the DC-AC frame transformation process, as explained in **Section 6.6**. The product of the two-stage scheme is the AC output voltage and current delivered to the underwater combo power grid system.

As discussed in ***Chapter 4***, the subsea DC-DC boost converter and the underwater power controller aided in extracting power at the optimum power point via the 6.4kW-DPU power unit through a Hill-Climbing control algorithm. The system operated based on the subsea temperature difference input between hot fluids from subsea oil-gas reservoirs flowing through subsea structures and cold seawater environment. The generated DC power via the 6.4kW-DPU passes onto the AC segment through the DC Bus (bus voltage or VBus) to the subsea power inverter.

Sections 4.3 to 4.6 explained how the flexible 250W-DPP, the subsea DC-DC boost converter, and the underwater power controller worked in tandem. The working principle is the same for the 6.4kW-DPU power source, subsea DC-DC boost converter, and underwater power controller. However, minor modifications to the DPU power source

were made to account for a large power rating during the system design. To that end, the following sections provide glimpses of the activities at the subsystems contained in part-C, part-D & part-E of the AC segment in *Figure 6.4*. The power and control system narrative is made with regard to *Figure 6.2* and *Figure 6.3* to facilitate an understanding of the grid-connected thermoelectric power system.

6.8.1. Subsea Power Inverter System

The subsea power inverter is placed in part-C of the power system model. The subsea power inverter control system ensured the stability of the power system. Additionally, the control initiative within the subsea power inverter ascertained that the generated power from the 6.4kW-DPU power source was supplied to the underwater combo power grid.

As the DPU voltage increases in the system arrangement, power is transferred to the grid system through the subsea power inverter. System stability was achieved through control algorithms inside the power inverter, thus maintaining a consistent DC-Bus voltage supply from the DC segment to the AC segment. As a result, a stable DC-Bus affirmed power transfer in the overall power system network.

As discussed above, the AC subdivision of the power system model begins from the subsea power inverter. Other AC-related components of the power system are placed on the right-hand side of the DC-Bus. Therefore, apart from the blocks in part-A and part-B, the subsea power inverter control algorithm occupies the lower portion of the power system model.

Part-D components within the control algorithm are PMW signals to the subsea power inverter, controller-01, controller-02, controller-03, current transformation, and the reverse transformation block. Part-E comprises the real (active) and reactive power block, PLL (phase locked loop), and the THD (total harmonic distortion) computing units.

In *Figure 6.2* and *Figure 6.3*, three (3) phase voltage and current signals from the subsea power inverter and AC filter inductors to the power grid are sensed, measured, and delivered to the power grid. That process is represented in the power system model (*Figure 6.4*) by the 3-phase subsea power inverter, the 3-phase AC filter, the 3-phase V-I Hall-effect sensor, and the 380V underwater combo power grid.

6.8.2. PLL and Angle ‘Rho’ Formation

The phase-locked loop (PLL) concept (Karimi-Ghartemani *et al.*, 2001)(Limongi *et al.*, 2007) was applied on the 3-phase subsea power inverter for the delivery of active (or real) and reactive power to the underwater power grid system. Power delivery to the grid system means transmitting active current to the underwater combo power grid system. Inferable electric current transmission to the grid system translates to the marking or shaping of the grid voltage. Therefore, the required grid current must be in phase with the marked grid voltage.

The PLL link generated a reference signal in phase with the actual voltage to deliver the needed current. The reference signal's magnitude was assumed to be between (+1) and (-1), as illustrated in *Figure 6.5*. Therefore, one of the functions of the PLL in the power

system model, as shown in *Figure 6.4*, was the generation of a reference signal. The generated reference signal operates the controllers within the subsea power inverter, ensuring that the required current and voltage are delivered to the underwater combo power grid system.

Apart from the active power, delivering reactive power to the power grid system was also the PLL's responsibility. Thus, the PLL-generated reference signals were 90 degrees out of phase with the active voltage, as shown in the reactive power part of *Figure 6.5*.

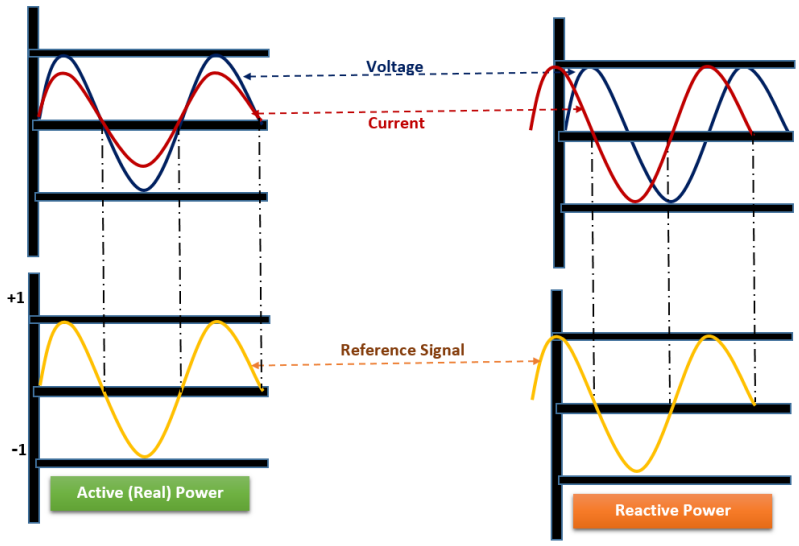

Figure 6.5 Active & Reactive Power Components of Power Grid System

Furthermore, the PLL unit was thought to operate in a closed-loop mode. Systems with close-loop capabilities can withstand ambiguities on the ocean floor. *Figure 6.6* describes the adopted control operating mode within the PLL unit.

Also, in *Figure 6.6*, 3-phase AC voltage (Vabc) signals are transformed into 2-phase alpha and beta voltage signals (Vα and Vβ). Voltage signals (Vα and Vβ) are converted to DC domain voltage quantities (Vd and Vq) through the (αβ to dq) transformation block.

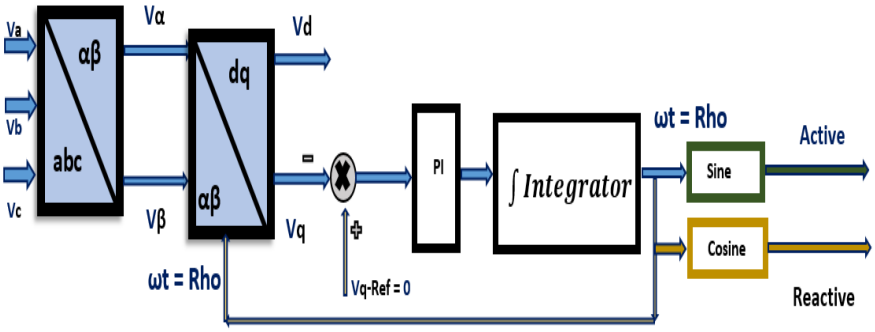

Figure 6.6 Robust PLL Scheme

The phasor representation of the underwater combo-power grid system voltage (Vg), the voltage along the alpha axis (Vα), and the voltage along the beta axis (Vβ) are described in *Figure 6.7*. Also shown in the phasor diagram are the (D-axis) and (Q-axis).

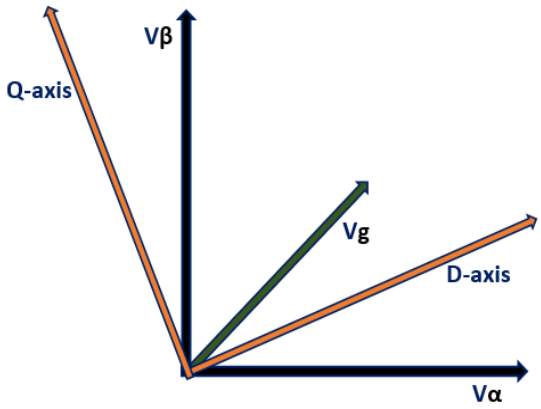

Figure 6.7 D-axis, Q-axis, Grid-Voltage, Alpha-Voltage, & Beta-Voltage

It is evident from the vector representation that grid voltage (Vg) is not aligned with the (D-axis). Consequently, a non-zero value of the (D-axis) and (Q-axis) voltages, (Vd) and (Vq), are obtained on the phasor description in *Figure 6.8*. Hence, an angular displacement between the V-alpha axis (Vα) and (D-axis) denoted by (ωt) exists, as represented below. The control strategy deployed in the PLL block enables the value of (Vq) always to remain zero (0) irrespective of system dynamics at the seabed.

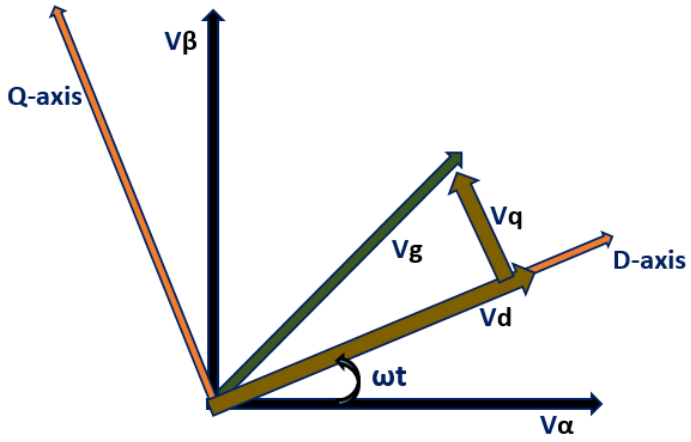

Figure 6.8 Non-zero Voltages (Vd and Vq) and Angular Displacement

Thus, allowing the alignment of (Vd) and (Vg) on the (D-axis), thereby ensuring that (Vq) becomes zero (0). By so doing, the angle (ωt) between (Vα) and (D-axis) changes to a new value called 'Rho,' as shown in *Figure 6.9*.

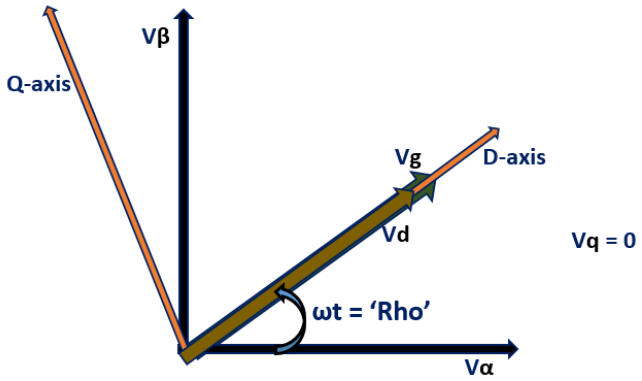

Figure 6.9 Alignment of (Vd), (Vg), and 'Rho' Angle Formation

Therefore, the deepwater power system model had a robust overall plan of action capable of withstanding system instability at the seabed. Also, the PLL system can stand against harmonics, surges, system noise, spikes, and other unpredictable conditions that might warrant drifting or generating wrong angle information.

Rho angle generation is one of the several functions of the PLL unit. The unit is at the bottom section of part-E on the power system model. An appropriate Rho angle was computed by passing three-phase AC voltage signals (Vabc) through the 3-phase PLL block at a sample time setting of 10e-6 seconds. On the DC-AC frame transformation diagram in *Figure 6.3*, the Rho angle determination points are at three different spots associated with PI-Controllers.

The formation of the Rho angle while maintaining the q-reference voltage (Vq-ref) signal as zero (0) through a feedback mechanism, as depicted in the PLL scheme above (*Figure 6.6*), helped the system to accomplish active and reactive power components.

6.8.2.1. Controller-01 Unit

The controller-01 unit is the second block in part-D of the power system model (see *Figure 6.4*). This unit defined a constant reference bus voltage (VBus-Ref) of 570V, as explained in **Section 6.5**. The system bus voltage (VBus) was compared with (VBus-Ref). The error signals between the (VBus) and (VBus-Ref) were applied to a PI-Controller-01. The P-value of the controller was 0.15, while the I-value was 80, and the selected sample time setting was (20 x 10e-6) seconds.

Transferred system power depended on voltage signal as explained in **Section 6.7.1**; thus, the output current reference signals (Id-Ref) from PI-Controller-01 represented the transferred power component. An upper saturation parameter (+13.8A) and a lower boundary at (0A) were the set controls at the output of PI-Controller-01.

6.8.2.2. Current Transformation Unit

Rho angle input and three-phase AC signals (Iabc) were converted to DC domain signals through the (Iabc to dq0) transformation block. As a result, the output of the transformation process was active (or the real) power and reactive power components labelled (Id) and (Iq) current signals, respectively. These current signals are represented as (Id-mod) and (Iq-mod) in *Figure 6.3*.

Generally, the three forms of electrical power often associated with power transfer are real (active), reactive, and apparent. As the name suggests, real/active power is regarded as the needed or essential power component. Also, real/active power can be likened to a vital

power component that requires a sort of container (representing the apparent power) and packaging or supporting materials (representing the reactive power) for smooth transportation from one place to another.

The unit for active power is (W), while the unit for reactive power is (VAR), and apparent power is denoted by (VA). This deepwater power system only considered the active and reactive power components transferred from the 6.4kW-DPU through the subsea power inverter to the underwater combo power grid system. The current transformation block is placed in part-D of the power system model shown in *Figure 6.4*.

6.8.2.3. Controller-02 Unit

The Controller-02 unit is also in part-D of *Figure 6.4*. A comparator compared the output reference current signal (Id-Ref) with the active power component or transferred current signal (Id-mod) obtained from the current transformation process and passed to the PI-Controller, as shown in *Figure 6.3*.

The output of PI-Controller-02 was a modulation signal represented as (d-mod) in the control algorithm of the power system model. The output of this unit is depicted in an orange-coloured Goto-block in the Controller-02 unit. The sample time setting for this controller was 10e-6 seconds, while P-and-I parameters were 0.005 and 1.0, respectively. The upper saturation limit for the modulating signal output was (+1.2), while the lower boundary was at (-1.2).

6.8.2.4. Controller-03 Unit

The reactive power component or transferred current signal (Iq) from the current transformation process of **Section 6.8.2.2** and the reference current signal of zero (0) amp were compared. The error signal output of the comparator passes through PI-controller-03. Reactive power components are described by reactive current elements (Iq-mod) and (Iq-Ref), as shown in *Figure 6.3*. The output of PI-Controller-03 was a modulation signal represented as (q-mod) in a pink-coloured Goto-block in the power system model. The sample time value was (20 x 10e-6 seconds), while the P-and-I parameters of PI-Controller-03 were 0.01 and 1.0, respectively. The upper saturation parameter setting for the (q-mod) modulating signal was 1.2, while the lower boundary was -1.2. The Controller-03 unit is in the part-D portion of the power system model in *Figure 6.4*.

6.8.2.5. Reverse Transformation Unit

DC domain signals or modulating signals (d-mod) and (q-mod) at Rho angle input were transformed into three-phase quantities via (dq0 to abc) transformation block. The output of the transformation block was voltage modulation signals (Vabc) denoted by (mod) on the control algorithm. A light blue coloured Goto-block represents the modulated voltage signals or (mod). The reverse transformation unit is the 6th unit in part-D of the power system model (*Figure 6.4*). Rho angle input, ($dq\ to\ \alpha\beta$)block, ($\alpha\beta\ to\ abc$)block, and (Va, Vb, Vc) outputs of PMW generator block are represented in the frame transformation illustration or *Figure 6.3*.

6.8.2.6. Gate Signal to Subsea Inverter Unit

Also, in part-D of *Figure 6.4*, the first unit (orange colour) is the gate signal to the subsea power inverter. The same unit is called the gate drive block with PWM signal inputs below the subsea power inverter in *Figure 6.3*.

The output from the reverse transformation process is reference voltage signals (Va), (Vb), and (Vc). These signals are required to generate the necessary PWM signals for the gate drive circuit ON and OFF switching of the IGBT power switches inside the subsea power inverter. Therefore, in the control algorithm (*Figure 6.4*), the final modulation signal (mod) was passed through a 2-Level PWM generator block at a frequency of 5000 Hz (5e3) and a sample time setting of 10e-6 seconds. The PWM & Gate Signal unit's outcomes (light green Goto-block) were PWM signals sent to the gate terminals of the subsea power inverter.

6.8.2.7. Real and Reactive Power Unit

The active and reactive power unit occupies the first spot in part-E (dark green colour) of the power system model in *Figure 6.4*. An explanation was given using the electrical power transport analogy to understand better real power (active), apparent, and reactive power concepts in **Section 6.8.2.2**. This unit determined the instantaneous power of the deepwater power system. Instantaneous power is obtainable at any instance (Kim and Akagi, 1999)(Terzija *et al.*, 2011). The value can be either positive or negative at a given time.

However, the active power does not contain negative (-ve) quantities. An active or real power never changes direction; it always remains positive (+ve). On the other hand, the reactive power generally oscillates back and forth and never gets used up. Therefore, it can be positive or negative; moreover, it does no valuable (practical) work.

In this unit, three-phase voltage (Vabc) signals and current (Iabc) signals derived from the transformation process were interfaced with a 3-phase instantaneous power block for computing the instantaneous power delivered to the underwater combo power grid system.

6.8.2.8. THD Unit

Total harmonic distortion (THD) describes the noise or distortion relative to the fundamental or original signal (Shmilovitz, 2005). THD is unitless and can be evaluated in voltage and current signals. THD is zero (0) for a perfect sinusoid or clean waveform. A minimal THD effect on power quality is one of the essential characteristics of any power inverter system (Sinvula *et al.*, 2019). Power inverters generally mimic the sine wave by generating jumpy, stepwise, or triangular waveforms that might resemble sinusoidal waveforms. The extent to which the power inverter output differs from a perfect waveform or a typical sinusoidal waveform is the measure of THD. Thus, the lower the THD value, the better the subsea power inverter design. The THD block on the deepwater power system model estimated the total harmonic distortion in the mains current (Iabc) on a single phase at 50 Hz frequency and 10e-6 seconds sample time. The THD is the last unit (orange colour) in part-E of the power system model in *Figure 6.4.*

6.9. Safety Mechanism & Systems Operation

Critically considered in the design was the safe operation of the deepwater thermoelectric power system and underwater combo grid system. As a result, a safety algorithm was incorporated into the power system model.

Power was not generated from the power system when the subsea temperature difference input to the 6.4kW-DPU power source was zero degrees Celsius (0°C). Therefore, power transfer from the DPU power source through the subsea DC-DC converter to the DC-Bus (VBus) did not occur. Consequently, the VBus could not transfer power to the subsea power inverter. Unpredictable conditions at the seafloor can prolong zero power delivery to the underwater combo power grid. Therefore, zero power transmission was an essential consideration during system design.

However, when normalcy returned, the subsea temperature difference was presented as input to the 6.4kW-DPU power source, resulting in power generation. Power was transferred to the VBus via the subsea DC-DC converter. For this reason, the VBus voltage steadily increases. Notably, there was a tendency for VBus voltage to rise beyond the set point limit, thereby causing system upset or instability.

Pre-defined conditions were set up on PI-Controller-01 (in the controller-01 unit in part-D of the power system model in *Figure 6.4*) to prevent such system disturbance at the seabed. The first condition was creating a reset mechanism using a rising edge trigger to avoid over-saturation of the controller. Secondly, a reference bus voltage (VBus-Ref) scheme was introduced. VBus and VBus-Ref were constantly monitored through a system

comprising a comparator and associated blocks. Based on the built-in control and safety system algorithm, when the VBus voltage was 5% greater than the VBus reference voltages, the output signal from the comparator activated the rising edge trigger on the controller, thus triggering a system reset to the original state. Hence, the system returned to its initial conditions; the deepwater power system and underwater combo-power grid system operations safely resumed without damage to any part of the system. Further info on safety and alarm management practices in process industries, which can be extended to power systems, is available (ISA, 2010). The operation of the deepwater power unit and the underwater combo power grid system are outlined in the following subsections:

6.9.1. Safety Mechanism Test & System Operations

The first test was performed when the power system had no safety control mechanism integrated into the system. Under this condition, the power system model was operated via the 4-hour subsea operations template for subsea temperature difference input to the 6.4kW-DPU power unit ranging from zero (0 °C) degree Celsius to 150 °C and 150 °C back to 0 °C. (Note that the 4-hour subsea operations template is described in **Section 7.3**).

The results of the experiment through the oscilloscope (scope) are shown in *Figure 6.10*. From the results, power was transferred from the 6.4kW-DPU source through the subsea DC-DC boost converter in tandem with the underwater power controller to the DC Bus (VBus) and beyond. However, the system became unstable at about 1.3 hours. Systems instability continued until the 3.8th hour before the operation ended in the 4th hour.

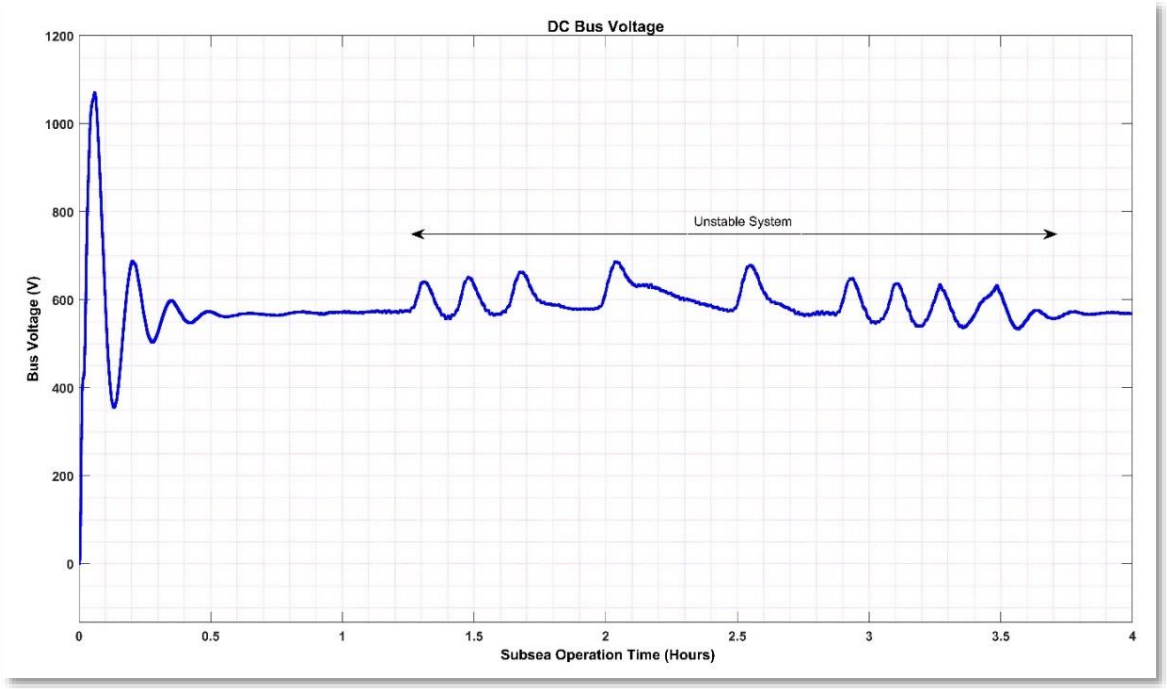

Figure 6.10 Power System without Safety Control Mechanism

The control safety mechanism was configured on the power system via the Controller-01 block, as explained in **Section 6.9,** and the experiment was repeated. The results obtained through the scope are shown in *Figure 6.11*.

There was a power build-up at the start of system operations. After that, system voltage steadily increases beyond 590V. Around the 35th minute, 598.50V was recorded; consequently, the pre-configured safety control algorithm immediately activated a system reset, thus mandating the power system return to the safety zone, as shown in *Figure 6.11*, *Figure 6.12,* and **Appendix E (Table E.3***)*. Further details on safety systems and functional safety used within oil and gas facilities include (IEC-61508, 2010)(IEC-61511, 2016).

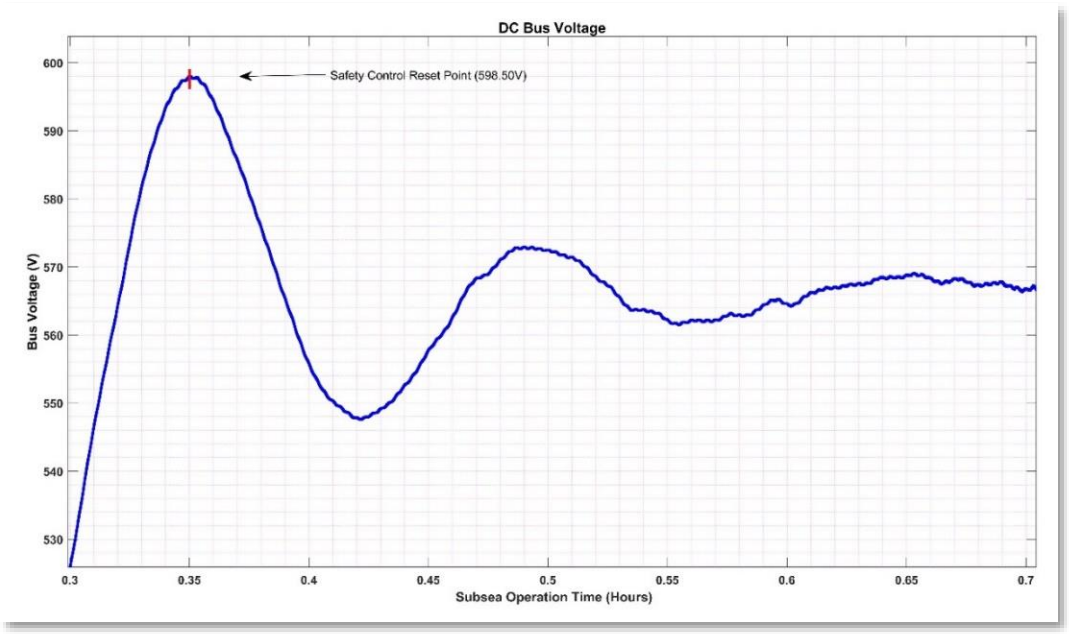

Figure 6.11 Power System with Safety Control Mechanism

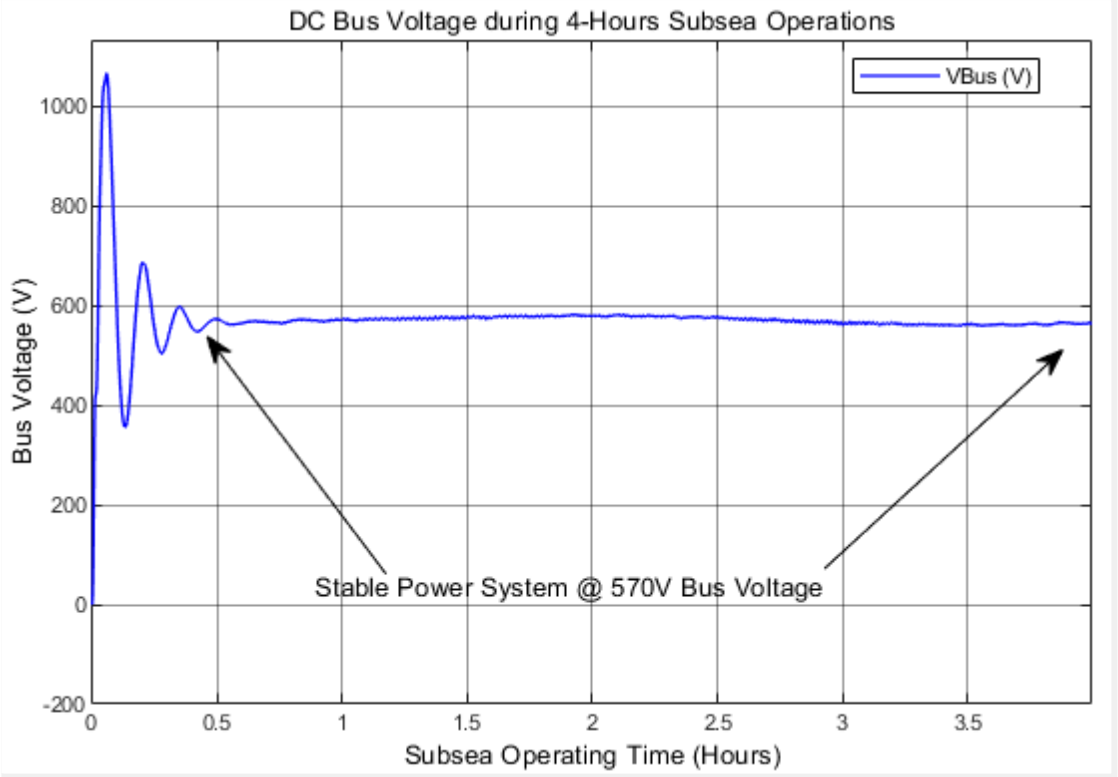

Figure 6.12 Stable Power System

6.9.2. DC Electric Current Flow from DPU

From this point onward, the power system was operated with the safety system in place, as discussed in **Section 6.9.1**. Therefore, waste heat harvesting, harnessing, and conversion to electricity continued due to the subsea temperature difference input to the 6.4kW-DPU. The result of the DC electric current flow from the DPU power source to the rest of the power system is shown in *Figure 6.13*. The recorded electric current flow from the 6.4kW-DPU was nearly 45A when the subsea temperature difference was 150 °C.

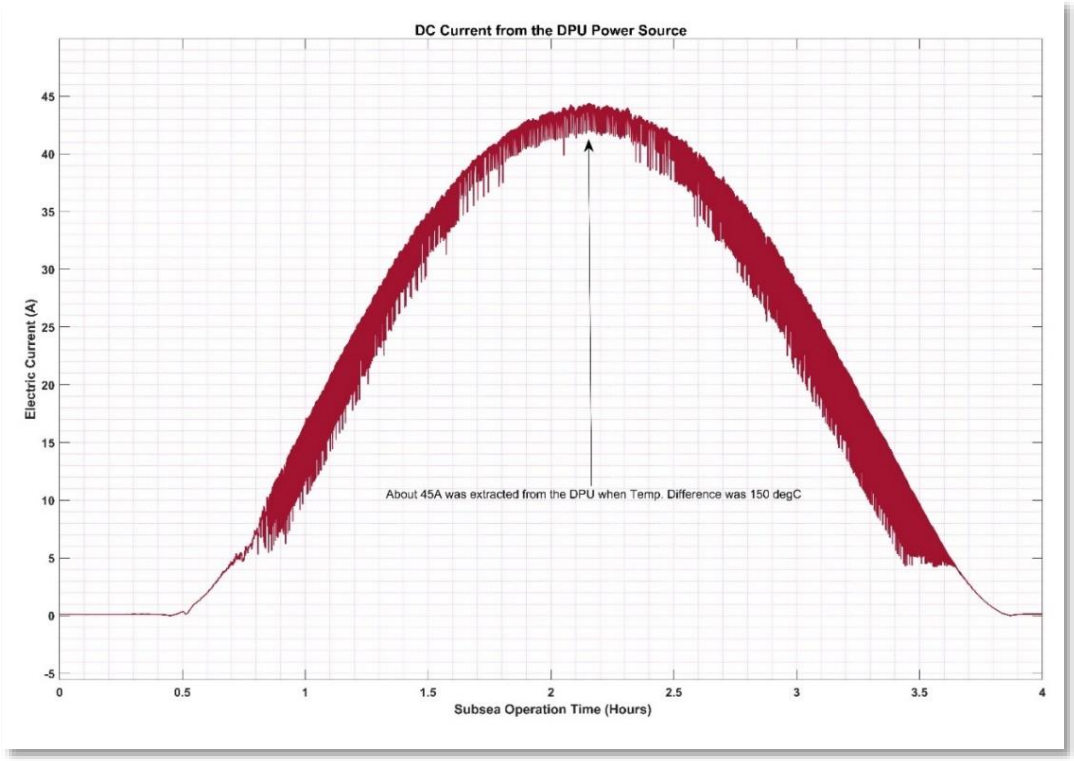

Figure 6.13 Electric Current from DPU

A closer look at sections of the current flow (*Figure 6.14*) indicated that the upper and lower current flow boundaries were 44.40A and 41.70A, respectively. Therefore, the current ripple from the 6.4kW-DPU power source was 2.70A.

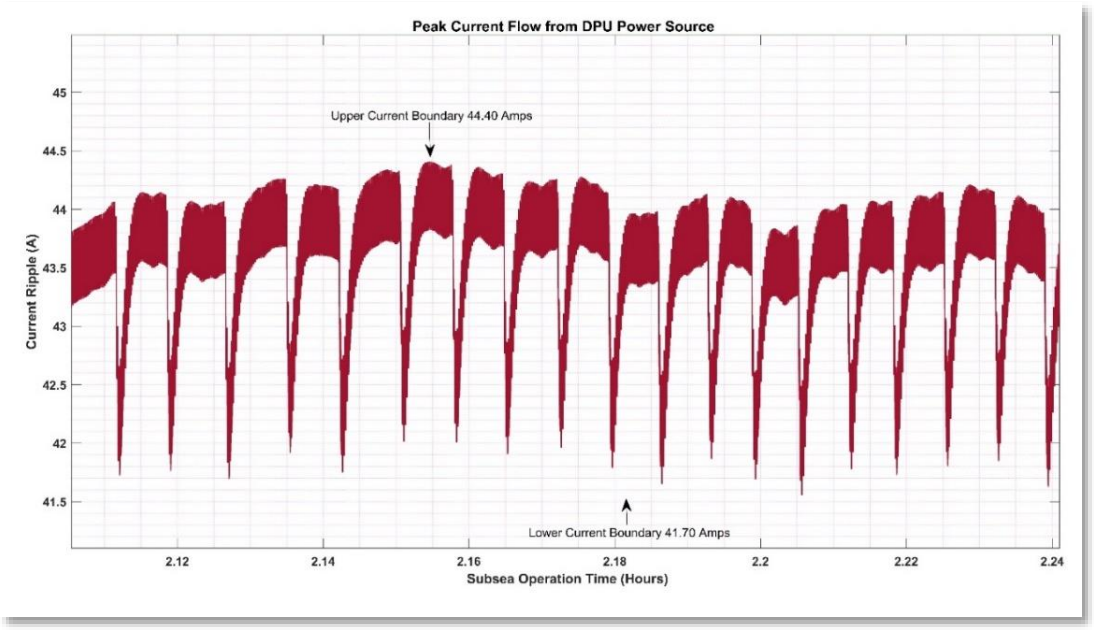

Figure 6.14 Electric Current Ripple

6.9.3. DC Power Derived through the DPU

Through the subsea DC-DC boost converter and the underwater power controller, the DC power obtained via the 6.4kW-DPU power source and the tracked power at optimum power points are presented in *Figure 6.15*. The operating subsea temperature difference input was from 0 to 150 °C and 150 to 0 °C.

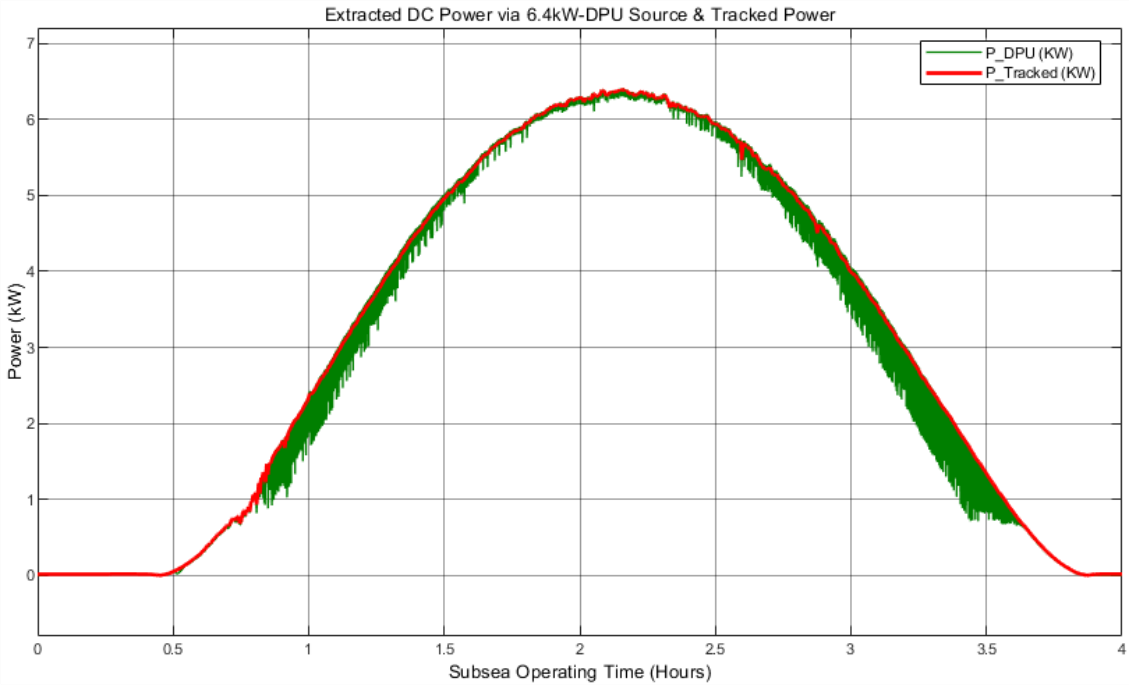

*Figure 6.15 DC Power from 6.4*kW*-DPU Source and Tracked Power*

Irrespective of the fluctuating subsea temperature difference at the seabed, maximum power at every point was extracted from the oil and gas reservoir through the 6.4kW-DPU unit. The highest power level obtained from the system was almost 6.4 kW at 150 °C.

A zoom-in section of the results through the scope revealed that at 2.148 hours, 6.395 kW DC power was tracked with the aid of the underwater power controller, as indicated in *Figure 6.16*. See **Appendix E (Table E.2)** for additional information.

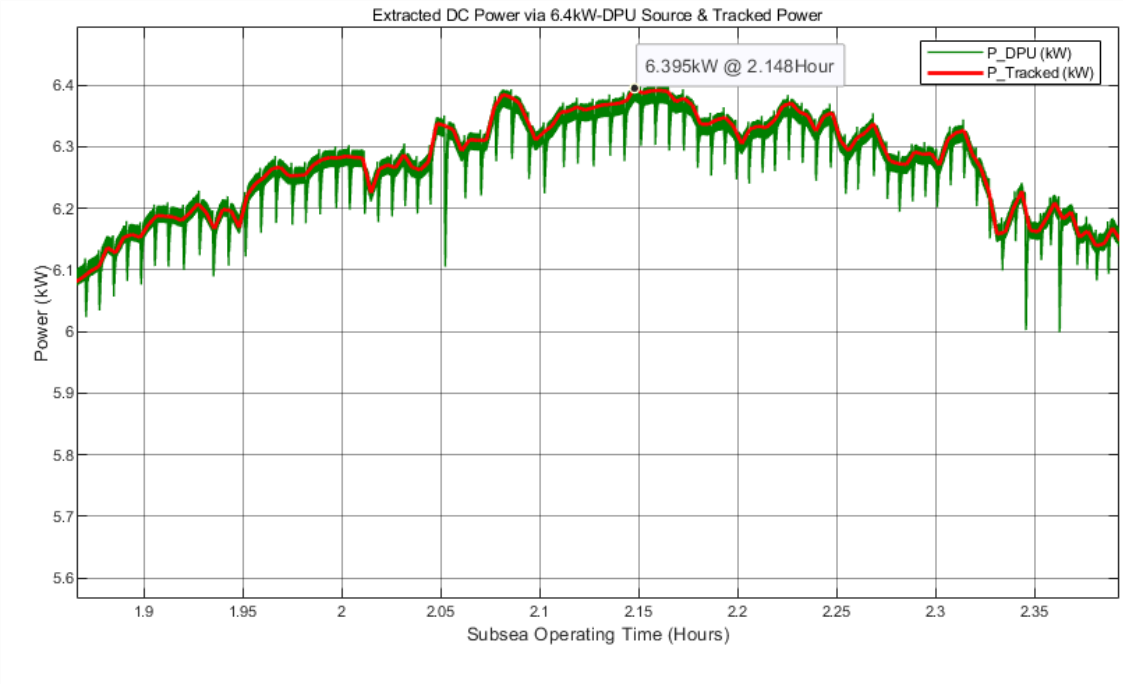

Figure 6.16 DC Power via 6.4kW-DPU Source & Tracked Power(zoom-in)

6.9.4. Three (3) Phase AC Current

The DC power at optimum power points was transferred to the AC side via the DC Bus and subsea power inverter. Through the subsea power inverter and accompanying control algorithm, the three (3) phase output current from the subsea power inverter, as documented through the scope, is shown in *Figure 6.17*.

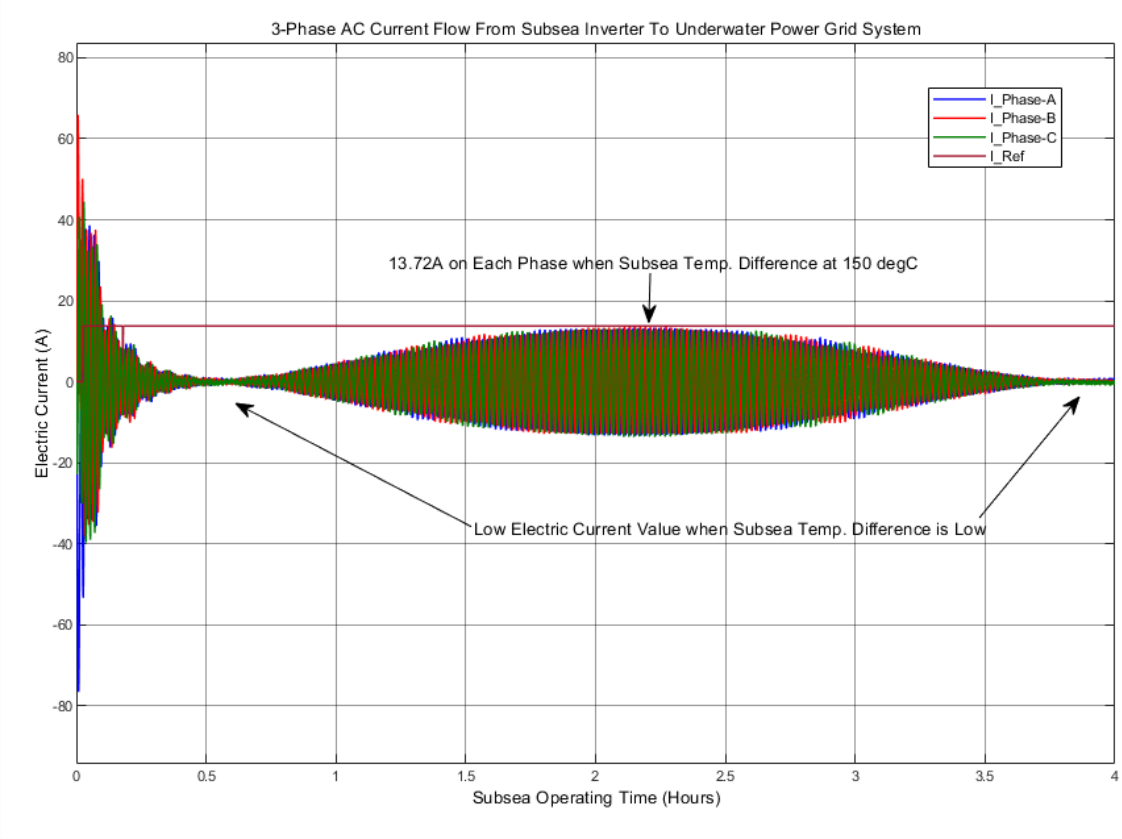

Figure 6.17 Three-Phase AC Current from Subsea Inverter

When the subsea temperature difference input at the 6.4kW-DPU power source was 150 °C, the current on each phase was 13.72A. Low current values ranging from -1A to +1A on each of the three (3) phases were recorded on the scope when the subsea temperature difference input was at its lowest levels, as depicted in *Figure 6.18*. See **Appendix E (Table E.4)** for additional information.

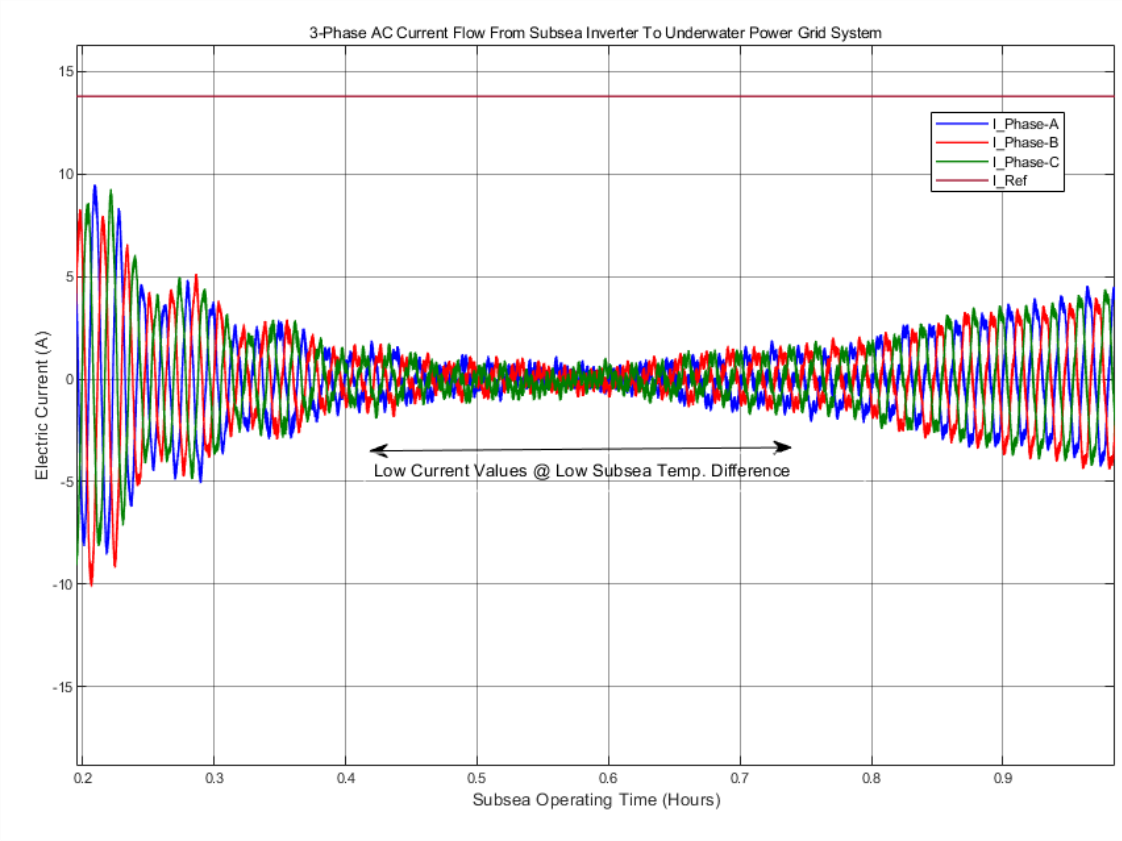

Figure 6.18 Low AC Current from Subsea Power Inverter

6.9.5. AC Power Delivered at Underwater Power Grid System

DC power was generated as the subsea temperature difference input was fed through the 6.4kW-DPU source. The generated DC power passes through the DC Bus to the subsea power inverter. DC power was transformed to AC power at the subsea power inverter and delivered to the underwater combo power grid system. *Figure 6.19* shows the active and reactive power contents supplied to the power grid system. About 6.4 kW of active power was delivered at the underwater combo power grid system when the subsea temperature difference input was 150 °C. The reactive power was about 0 kW throughout the

experiment. The real (active) power delivered at the power grid system at the 2.148th hour was 6.389 kW, as presented in *Figure 6.20*. The conversion loss from DC to AC power was about 0.006 kW or 0.1%.

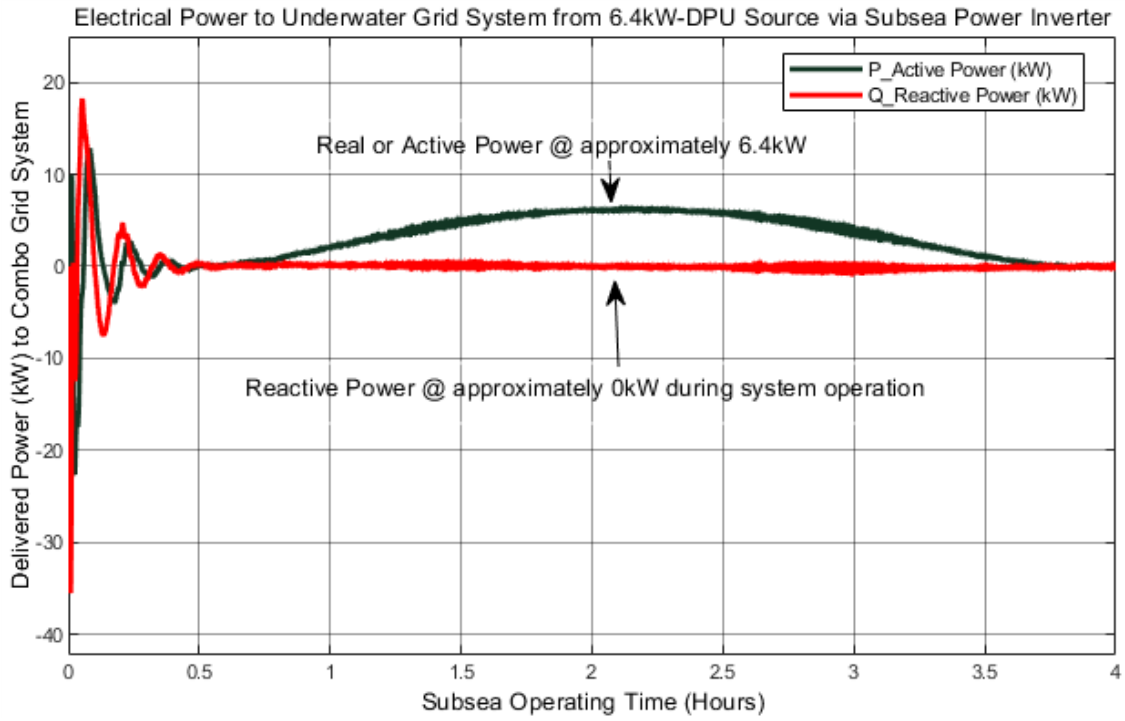

Figure 6.19 Delivered AC Power at Underwater Power Grid System

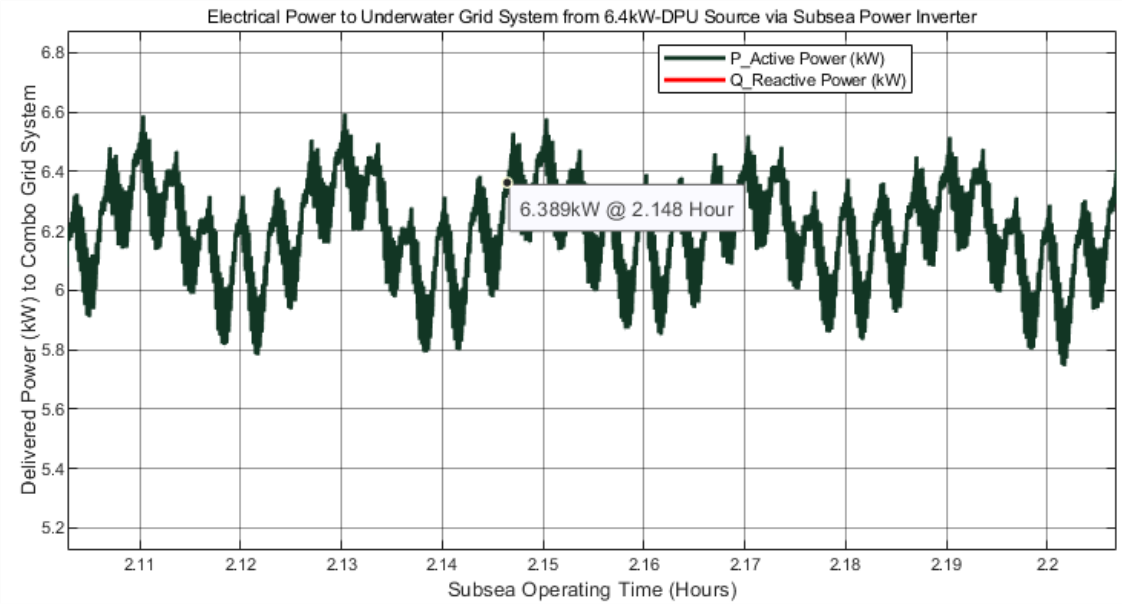

Figure 6.20 Active Power Delivered at the Power Grid System

6.9.6. THD of Underwater Power Grid System

Depending on the power quality sent to the underwater combo power grid, the total harmonic distortion (THD) values reported at the scope slowly decrease from 15 to 14. After that, it went on from 14 to 12, 10, 8, 6, and 4, remaining roughly stationary between 4 and 2. The value of THD for the deepwater power system was 2.7. *Figure 6.21* is the screen capture of the oscilloscope. Additional information is available in **Appendix E (Table E.4)**.

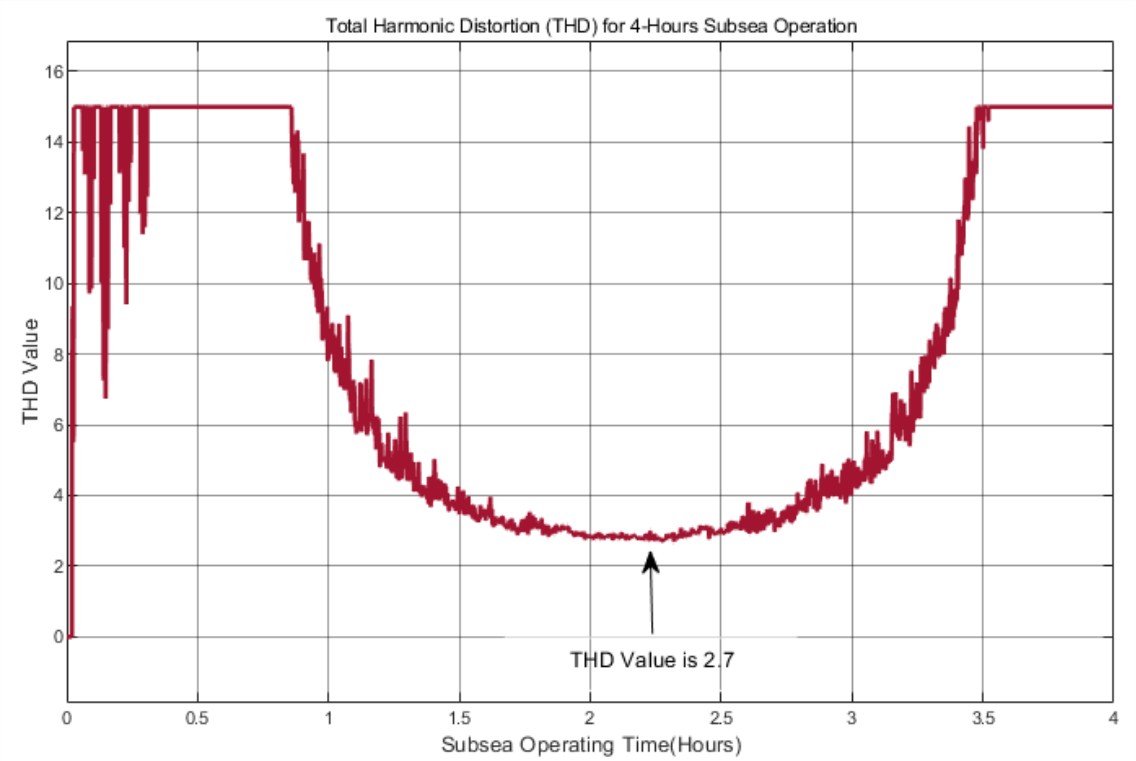

Figure 6.21 Total Harmonic Distortion of Power System

6.10. 4-Hour Operations & Grid System Outcome

Sections 6.4 to **6.9** illustrated the 6.4kW-DPU power source and the underwater power Grid System operations via a 4-hour subsea operation template. The formation of the short-duration subsea operations template is discussed in ***Chapter 7***. This section analyzes, validates, and critically analyzes the ultra-deepwater thermoelectric power system results. *Figure 6.22* represents the subsea temperature difference against the DC output current, the DC output power of the DPU power source, and tracked power (power output through the combined action of the subsea DC-DC Converter and underwater controller). *Table 6.1* contains the computed mean, standard deviation, and the standard error of the current,

6.4kW-DPU-Source power and the tracked power based on the data in **Appendix E (Table E.2)**. Error bars for the three DC outputs are shown in *Figure 6.23*.

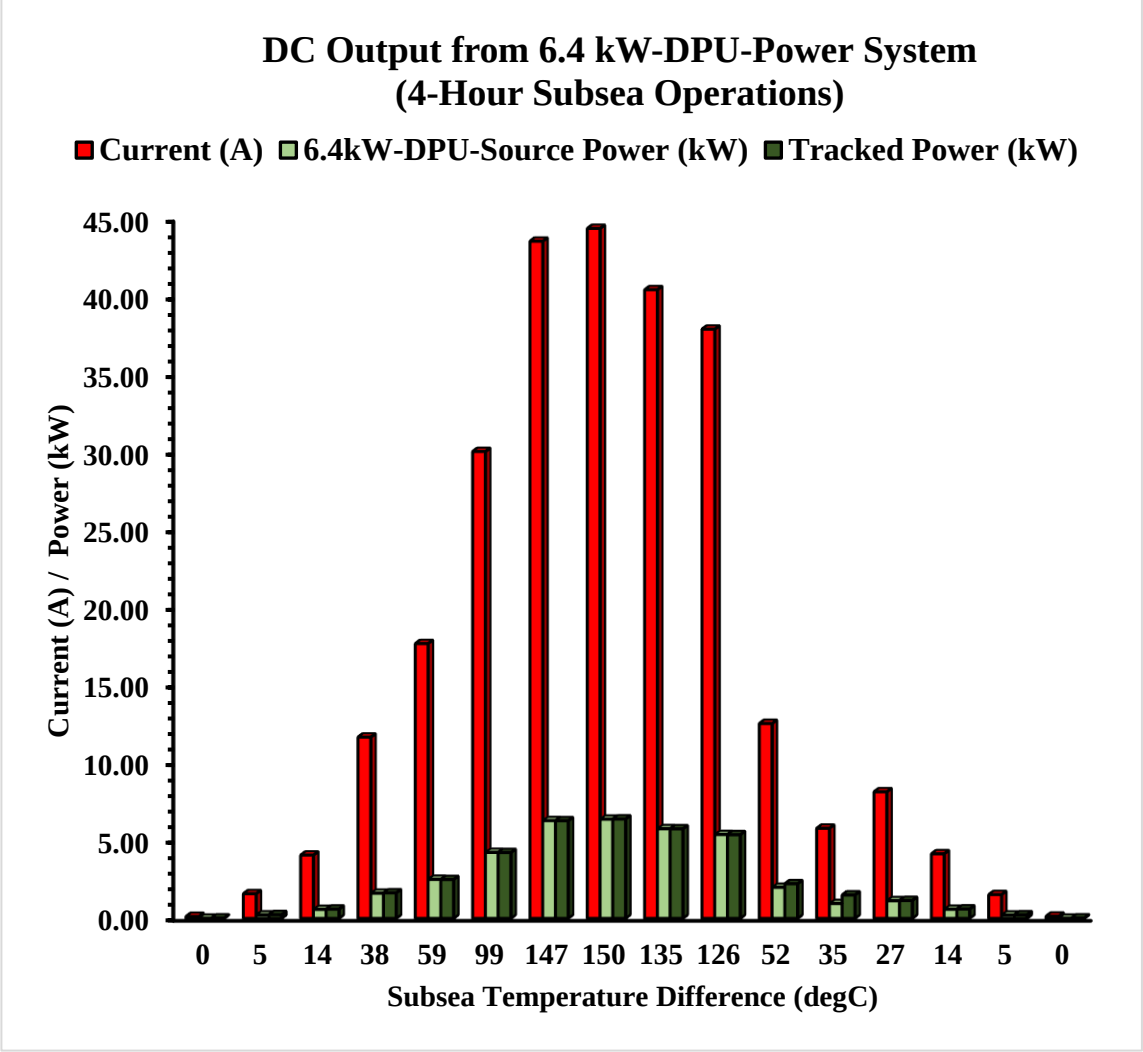

*Figure 6.22 DC Outputs-6.4*kW*-DPU Power System(4-Hour Subsea Operations)*

Table 6.1 Computed DC-Output Attributes

DC Output from 6.4 kW-DPU-Power System (4-Hours Subsea Operations)			
Attributes	**Current (A)**	**6.4kW-DPU-Source Power (kW)**	**Tracked Power (kW)**
Mean	21.1727964	3.077710935	3.109325474
Standard Deviation	16.51544518	2.397249371	2.381187108
Standard Error	1.066067402	0.154741782	0.153704967

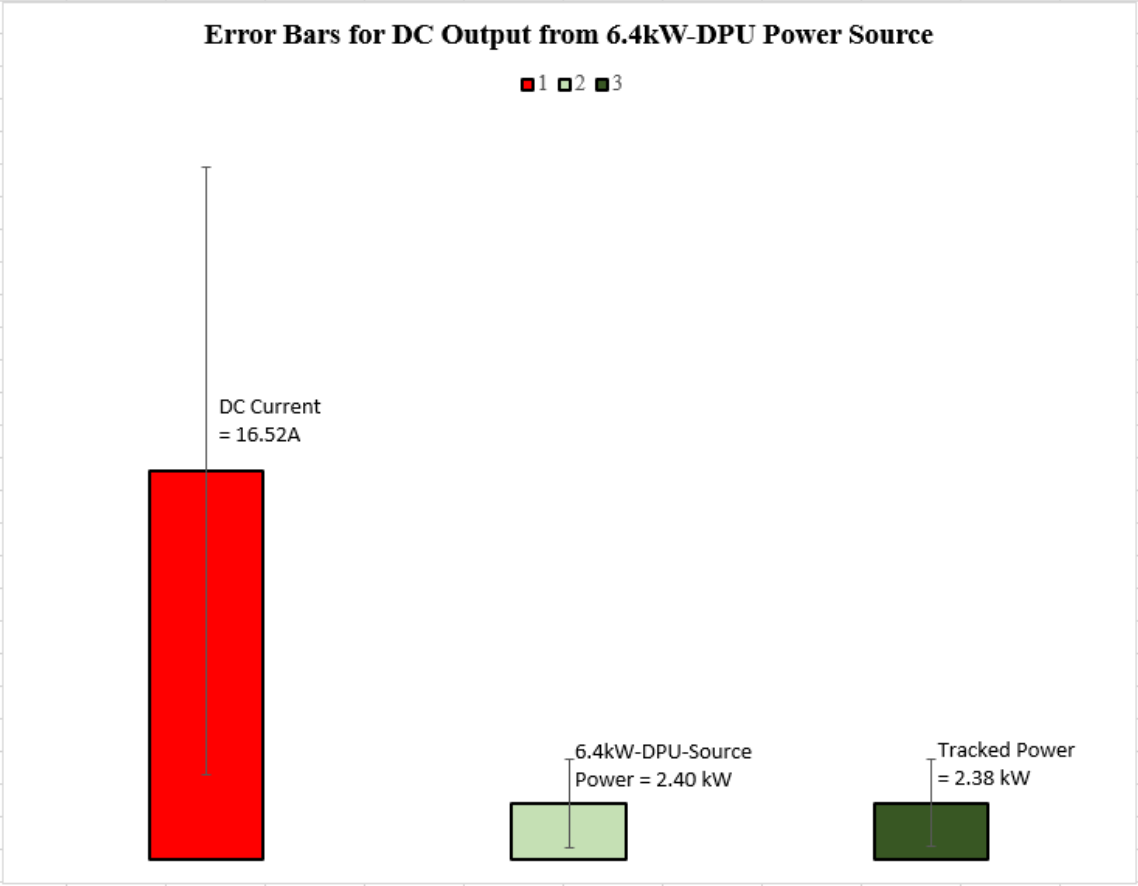

Figure 6.23 Error Bars of Computed DC Output Attributes

The DC outputs of the 6.4kW-DPU power system operated through the 4-hour subsea operation template were transferred to the AC side of the power system through the DC-BUS. The BUS-Voltage determines the stability of the power system, as explained in **Sections 6.5**, **6.6**, **6.8**, and **6.9**. *Table 6.2* has the computed mean, standard deviation, and standard error of the measurements obtained from the DC-BUS (See **Appendix E** (**Table E.3 for details**)). Furthermore, *Table 6.3* presents the power stabilisation process of the deepwater power system for multiple timestamp intervals.

Table 6.2 Computed DC-BUS Attributes (4-Hour Subsea Operations)

4-Hours Subsea Operations	
Attributes	**Voltage (V)**
Mean	572.0343
Standard Deviation	66.9541
Standard Error	4.3219

Table 6.3 Power Stabilisation Process (4-Hour Subsea Operations)

Power Stability (4-Hours Subsea Operating)		
Time Stamp (Hours)	**Subsea Temp. Diff. (degC)**	**BUS-Voltage (V)**
T024 - 0.3818H	0.3707	573.7726
T048 - 0.7802H	20.4640	566.8796
T072 - 1.1786H	78.3322	575.5222
T096 - 1.5770H	122.7138	573.8224
T120 - 1.9754H	146.6727	580.0937
T144 - 2.3738H	144.4006	576.6371
T168 - 2.7722H	118.4753	568.3492
T192 - 3.1706H	72.9480	563.4899
T216 - 3.5690H	23.1232	560.3526
T240 - 3.9986H	0.4234	565.3379

The 10% equal power stabilization across the board during the system's operation, as shown in *Figure 6.24*, suggests that DC power was successfully transferred from the DC side to the AC side, thus validating the underwater power system design.

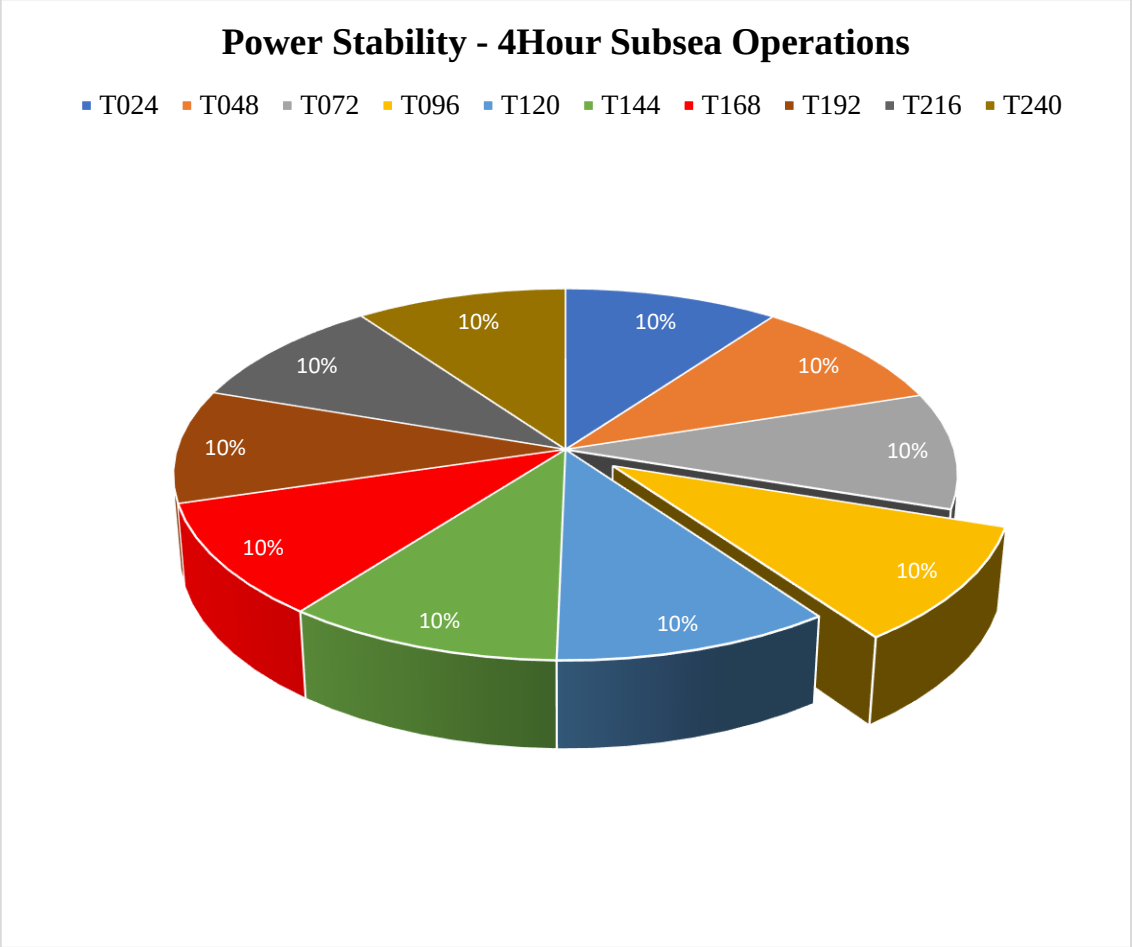

Figure 6.24 Power Stability Plots (4-Hour Subsea Operations)

DC power components were transferred to the AC side. These DC power parameters were transformed from DC to AC via a three-phase subsea power inverter. The AC output power of the thermoelectric power system was delivered to an underwater power grid

system. The AC outputs to the underwater power grid system during the 4-hour subsea operations, such as AC current, active (real power), reactive power, and total harmonic distortion, are presented in *Figure 6.25*.

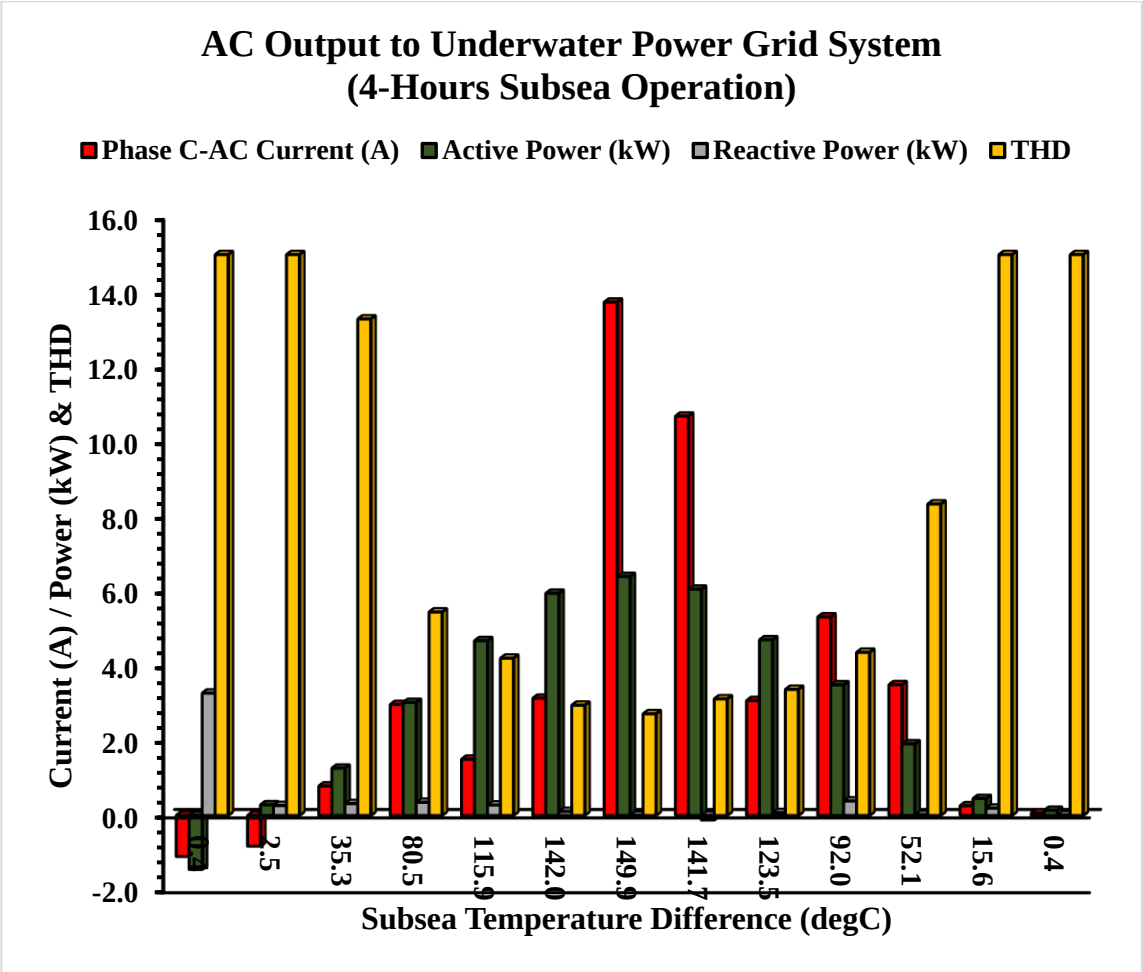

*Figure 6.25 AC Outputs-6.4*kW*-DPU Power System (4-Hour Subsea Operations)*

Based on the data in **Appendix E (Table E.4)**, *Table 6.4* contains the computed mean, standard deviation, and standard error of the AC current, active power, reactive power, and total harmonic distortion (THD). As mentioned above, the THD represents the power

quality delivered to the underwater power grid system. The smaller the THD value of any electrical power grid system, the higher the power quality. 2.7 was the recorded THD value for this operation; thus, high-quality power was sent to the power grid system.

Table 6.4 Computed Attributes-AC Output to Power Grid System

AC Output to Underwater Power Grid System				
Attributes	**Phase C-AC Current (A)**	**Active Power (kW)**	**Reactive Power (kW)**	**THD**
Mean	0.2728	2.9737	0.1101	8.1446
Standard Deviation	6.3083	2.8637	1.7343	5.2278
Standard Error	0.4072	0.1849	0.1119	0.3375

The computed confidence interval, upper confidence interval, and lower confidence interval at 95% of the active power delivered to the power grid system are presented in *Table 6.5*. Further analysis was carried out, and *Table 6.6* shows Pearson's correlation for output DC power against the output AC power during the 4-hour subsea operations. *Figure 6.26* is the scatter plot that corroborates the DC output power from the 6.4kW-DPU thermoelectric power system during 4-hour subsea operations, which was transformed into AC power and delivered to an underwater power grid system.

A significant positive correlation was found between DC and AC output power from the 6.4kW-DPU thermoelectric power system during 4-hour subsea operations, $r(238) = 0.807$, $p < 0.001$.

Table 6.5 Confidence Intervals-AC Power to Grid(4Hour Operations)

Confidence Intervals for AC Power Delivered to Underwater Power Grid (4-Hours Subsea Operation)

Mean	2.97374206
Standard Error	0.184851374
Median	3.104363166
Mode	#N/A
Standard Deviation	2.863705178
Sample Variance	8.200807348
Kurtosis	9.381685761
Skewness	-1.403516872
Range	30.00619829
Minimum	-17.24099871
Maximum	12.76519958
Sum	713.6980943
Count	240
Confidence Level (95.0%)	0.364146007
Upper CI (95%)	3.337888066
Lower CI (95%)	2.609596053

Table 6.6 Pearson's Correlation (4-Hour Subsea Operations)

Pearson's Correlations (4-Hour Subsea Operations)

	n	Pearson's r	p
DC Power (kW) - AC Power (kW)	240	0.807	< .001

As shown by Pearson's correlation and the scatter plots above, the p-value from the results of the experiments is less than 0.05. Therefore, a statistical relationship exists between the DC and AC output power. Consequently, it can be concluded that the experiments are repeatable, the outcomes are valid, and the results are validated.

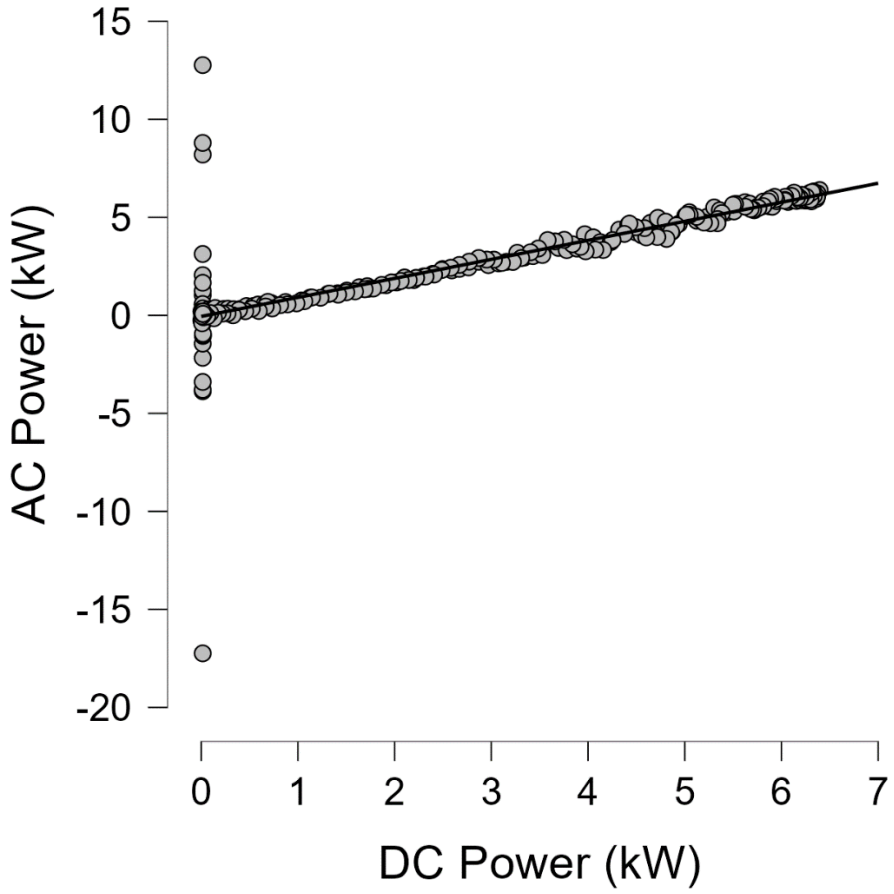

Figure 6.26 Scatter Plots-DC Power vs. AC Power (4-Hour Subsea Operations)

The power system stability test attempted to understand the system's stress-induced behaviour by applying engineering principles as explained in **Sections 6.5**, **6.6**, **6.8**, and **6.9**. The results from the experiments predict the robustness of the ultra-deepwater and underwater power grid systems. In other words, the outcome of the power system stability test verifies the system's energy conversion efficiency from heat to electrical power. Secondly, the test confirms that the delivered AC power, voltage, and frequency met electrical power grid system requirements. Thirdly, the power quality of the grid system

after transformation was high, hence authenticating the overall system. Fourthly, the statistical correlation between the DC output power and AC output power established a high level of agreement for the underwater power system design. This agreement ensures the accuracy and reliability of the system's ability to predict real-world performance.

However, heat transfer patterns and temperature distributions around the Flex-250W-DPPs in underwater conditions were not carried out. Also, the structural integrity of the system components against high pressures and stress at 3000 meters of water depth and beyond was not done. Existing information from past studies is not available to show a correlation between output power from any deepwater thermoelectric power system and an underwater power grid system. Future research can further address these shortfalls. Long-term field trials in conditions imitating continuous ultra-deepwater environments can be carried out to validate system performance, stability, reliability, and degradation over an extended period and compared with these simulated projections.

A 6.4kW-DPU thermoelectric power system had been operated via a 4-hour subsea operations template and integrated into an underwater combo power grid system. The results from the ultra-deepwater power system had been validated, and recommendations for future work to enhance the system's predictive capabilities for real-world application had been made.

6.11. Chapter Summary

In ***Chapter 6***, a 6.4kW-DPU and an underwater combo power grid system were designed, developed, and implemented. Harvested waste heat from ultra-deepwater oil-gas reservoirs and seawater through the DPU thermoelectric power source mounted on subsea structures converted waste heat to electricity. DC power was transformed into AC power via a three-phase subsea power inverter and associated control algorithm. The AC output power from the subsea power inverter was delivered to the underwater combo power grid system. ***Chapter 7*** discusses how the characteristics of ultra-deepwater oil-gas fields in West Africa were expanded to accommodate a new type of offshore energy harvesting and power generation scheme. Also, the validity of the results obtained from this novel deepwater thermoelectric power system, the underwater combo power grid, and related issues are evaluated in the next Chapter.

Chapter 7

Deepwater Characteristics in West Africa

7.1. Introduction

Chapter 7 discusses the ocean floor characteristics in West Africa, emphasising offshore Nigeria in the Gulf of Guinea portion of the Atlantic Ocean. Next, it explains waves, wind, ocean currents, temperatures, seabed-marine environment, and petroleum engineering information. Details on how the subsea temperature difference data used in this work was obtained are also presented. Furthermore, the results of experiments are examined, and findings are interpreted. The outcomes of this first deepwater thermoelectric power scheme connected to an underwater combo power grid system for providing electricity to subsea equipment are analysed, recommendations are made, and results are validated.

7.2. Deepwater Characteristics in the Gulf of Guinea

Some data and parameters used in this deepwater or ultra-deepwater oil-gas power system were presumptive. At the same time, the information represents the views and opinions of the author based on his experience in West Africa; hence, some data are precise, while others are not. The presumptive data added relevance to the subject matter of this research

towards actualising offshore renewable and non-renewable possibilities. The essence of this approach was to achieve seafloor electrical power and underwater power grid systems in an area of study where research data is almost non-existent.

7.2.1. Wave, Wind, and Ocean Current

The ocean wave environment in West African waters is relatively mild. However, it was assumed that this work's oil and gas field location was rarely calm. Therefore, the presumed wave height was approximately 1.0 meters for about 6 seconds (Olugbenga, Gudmestad and Agbakwuru, 2017)(Nwaokocha and Layeni, 2013). Extreme wind events are a regular occurrence in this part of the world; therefore, the expected wind speed was 15 m/s. Ocean current speed is typically around 0.1 m/s to 0.3 m/s, flowing to the southern region for a hundred meters of the water column (Asiegbu, 2021)(Olaniyan and Afiesimama, 2002). In this design, extreme local waves, wind, and current were supposed to have insignificant effects. Additionally, fouling occurs all year round in West Africa (E Oug, A Tobiesen, 2003)(Ateme, 2021). The presumed marine growth projection at the seafloor is in *Table 7.1*. Also, the seawater temperature against water depth (Song, 2019)(J. O. Ahaotu, B. Nkoi, 2018) for this work is in *Table 7.2*.

Table 7.1 Seabed-Marine Growth Profile

Water Depth in Meters (m) below Mean Sea Level	**Thickness in Millimeters (mm)**	**Weight in Air (Kg/m^2)**	**Weight in Seawater (Kg/m^2)**
Plus (+) 2	100.00	9.50	3.20
Minus (-) 10	100.00	9.50	3.20
Minus (-) 65	25.00	2.40	0.80
Minus (-) 65	0.00	0.00	0.00
Seabed	0.00	0.00	0.00

7.2.2. Petroleum Engineering and Related Information

Hydrocarbons in Nigeria generally occur at a depth of between 1500 and 3000 metres. The porosities of formation sands are often between 28 % to 40 %. Different types of crude oil occur throughout the complex delta region of Nigeria, typically ranging from heavy crude of 16 API to light crudes of 50 API. Nearly 1000 standard cubic feet (SCF) of gas are produced with every barrel of oil in Nigeria. Hence, with 3.0 million barrels per day (BPD), almost 3.0 billion SCF of associated gas is also produced. These oil and gas reservoirs have multiple characteristics.

Table 7.2 Water Depth against Seawater Temperature

Water Depth in Meters (m)	**Average Temperature (°C)**	**Minimum Temperature (°C)**	**Maximum Temperature (°C)**
0	27.50	22.10	30.60
10	27.20	18.90	29.90
20	26.60	17.80	29.70
50	20.50	15.30	28.70
100	16.30	14.60	20.00
200	14.50	13.20	16.90
400	8.70	7.30	11.30
600	6.20	5.20	7.70
800	4.90	4.50	5.80
1000	4.50	4.00	5.30
1500+	4.20	3.80	4.90

The reservoir temperature of some deepwater or ultra-deepwater developments such as Bonga, Erha, Erha-North, Akpo, and Agbami fields ranges from 40 to 116 °C. Also, the shut-in bottom hole pressure (BHP) varies between 3000 to 5000 PSI. (Schoppa *et al.*, 2007)(Ekejiuba, 2021)(Li *et al.*, 2020)(Rafin and Laine, 2010)(Sankaran *et al.*, 2011)(Kelly and Strauss, 2009)(Nolop *et al.*, 2007).

Based on the above information, hydrocarbon accumulation in the ultra-deepwater oil-gas field developed in this research was assumed to be on horizons with varying fluid characteristics. Injected water was expected to maintain reservoir pressure from the start of production. Oil production from the individual well was considered as 60 MBOPD.

Gas production from each well was approximately 190 MMSCFD. Peak water produced from a single well was around 55 MBWPD, while the water injection rate per well was 55 MBWPD. Other assumptions considered in this deepwater or ultra-deepwater thermoelectric power system are in *Table 7.3*, *Table 7.4*, *Table 7.5*, *Table 7.6*, and *Table 7.7*.

Table 7.3 Subsea Wells and Completions Parameters

System	**Characteristics/Comments**
Subsurface Targets/Total Subsea Wells	56 Subsea wells and 18 Subsea Manifolds: (28 Oil & Gas Producers, 6 Hot-water Producers, 22 Water Injectors, 12 Production Manifold, and 6 Water Injection Manifolds)
Subsea Well Capability	Intelligent (smart) wells, commingled completions
Subsea Well Instrumentation	Downhole Pressure and Temperature Sensors, Multiphase Meters on Oil & Gas Producers, Flow Meters on Water Injectors and Hot Water Producers

Table 7.4 Subsea Production Well Parameters

System	**Characteristics/Comments**
Depth	Deepest development well at 3000 meters
Reservoir Pressure	7600 psi (524 bar)
Tubing Head Pressure	6500 psi (448 bar)
Max. Arrival Pressure at FPSO	4300 psi (297 bar)
Max. Reservoir Temperature	165 °C
Max. Flowing Wellhead Temp.	150 °C

Table 7.5 Subsea Water Injection Well Parameters

System	**Characteristics/Comments**
Injection Water	Nitrate in Water stream
Injection Water Quality	15-Microns
Max. Pressure at Flowline Sled	5360 psi (369 bar)
Max. Pressure at Riser-base	6000 psi (413 bar)
Max. Temperature Injection Water	100 °C

Table 7.6 Deepwater Flowline Capacity & System Parameters

System	**Characteristics/Comments**
Average flow condition Wellhead Temperature	4.0 °C to 150 °C
Downstream of Subsea Choke Minimum Temperature	Minus (-) 40 °C
Gas Lift Riser Requirement	20 MMSCFD of gas-assisted blowdown of the individual riser. 60 MMSCFD for production improvement and slug suppression

Table 7.7 Parameters for Subsea Flowlines, Risers, & Pipeline

System	**Characteristics/Comments**
Production Flowlines	A 10-inch x 14-inch pipe-in-pipe was configured in 2 flowline pair loops for the East and West parts of the field. Production flowlines and associated components fitted with Flex-DPP power plates
Design pressure and temperature of production flowlines	6000 psi and 150 °C
Water Injection Flowlines	10-inch is configured in flowline loops for the eastern and western parts of the field. Water Injection Flowlines and associated components fitted with Flex-DPP power plates
Design Pressure and Temperature of Water Injection Flowlines	6000 psi and 100 °C
Gas Lift Riser System	Two (2) 5.5-inch Gas-Lift-Riser systems, one is on the eastern production flowline, while the other is on the western part.
Design Pressure and Temperature of the Gas Lift Riser System	3000 psi, 90 °C at the Topside and 6000 psi, 100 °C at the Subsea Manifold
Minimum Design Temperature for Production Flowlines and Risers Arrangement	Minus (-)10°C at the Top of the Riser. Minus (-) 20°C at the Riser base
Gas Export Pipeline	16-inch outer diameter Gas Export Pipeline and associated components fitted with Flex-DPP power plates
Pressure and Temperature of Deepwater Gas Gathering System (DGGS)	Max. Pressure = 3000 psi, Max. Temperature = 100 °C.

7.3. The 6.4kW-DPU Power Source

From the data in **Section 7.2**, the assumption was that marinised/flexible deepwater thermoelectric modules (Flex-DTEMs) were assembled as deepwater thermoelectric power plates (Flex-DPPs). Flex-DPPs were appropriately connected in series-parallel configuration into a deepwater power unit (DPU). Hence, Flex-DPPs were installed on the flow paths of subsea wellheads, XTrees, manifolds, and sleds. Flex-DPPs were also on subsea flowlines, pipelines, and risers. Therefore, groups of Flex-DPPs constructed on subsea structures resulted in a 6.4 kW deepwater thermoelectric power unit (DPU).

Furthermore, the 6.4kW-DPU can withstand maximum seabed pressure rated at 6000 psi (413 bar). The assumed minimum and maximum temperatures of the Flex-DTEM, Flex-DPP, and DPU were 0 °C and 150 °C, respectively, while the operating pressure rating was 6000 psi. See ***Chapters 3***, ***4***, ***5***, and ***6*** for further details on Flex-DTEMs, Flex-DPP, and DPU.

Compiling tentative temperature values from 0 °C to 150 °C for various day and night times was done using Microsoft Excel. These temperature and time values represented twenty-four (24) hours, seven (7) days a week, and 365 days of operations typical for oil-gas activities. MATLAB Script was developed from the Microsoft Excel data representing the subsea temperature difference profile used in this work. The subsea temperature difference data (Subsea Temp. Diff. data or STD) were loaded onto the MATLAB/Simulink signal builder block. The data were simulated thus, representing a short subsea operations model of four (4) hours and an extended or long subsea operations

model of twenty-four (24) hours. The subsea temperature difference templates are shown in *Figure 7.1* and *Figure 7.2*.

Currently (when writing this thesis), no known technology accurately predicts the exact characteristics of subsea oil and gas reservoirs. Similarly, definite forecasts on seabed conditions, ultra-deepwater characteristics, and sea state are unavailable for a specific time, day, week, month, or year. Therefore, the outcome from the subsea temperature difference profile via Microsoft Excel and MATLAB/Simulink, as shown in *Figure 7.1* and *Figure 7.2*, represents subsea temperature difference data or subsea operation paradigms used in this research.

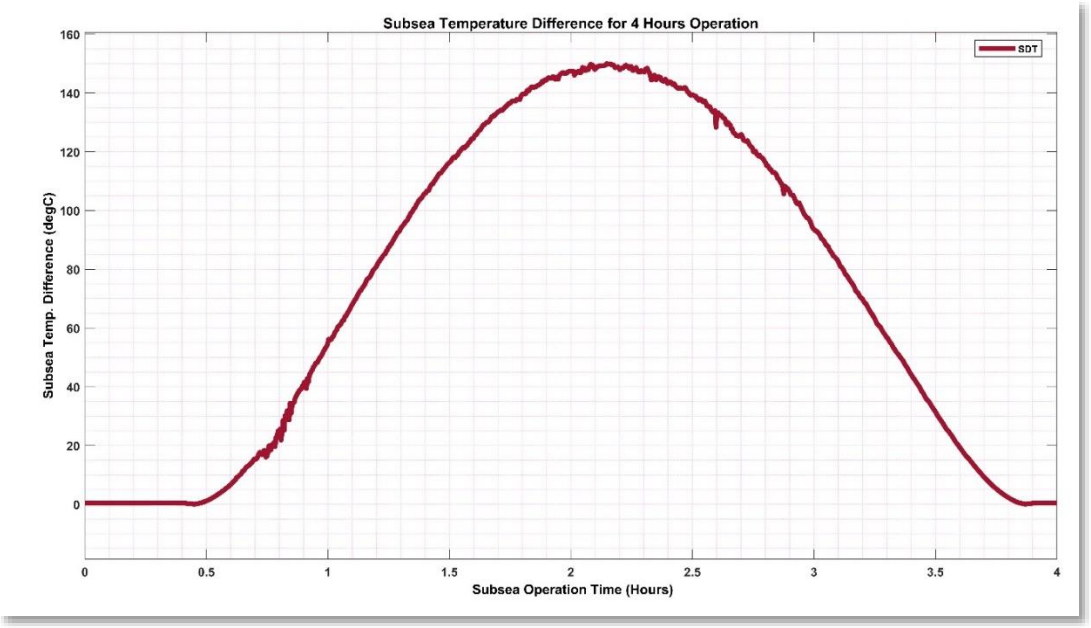

Figure 7.1 Short Duration Subsea Operations (4-hour) Template

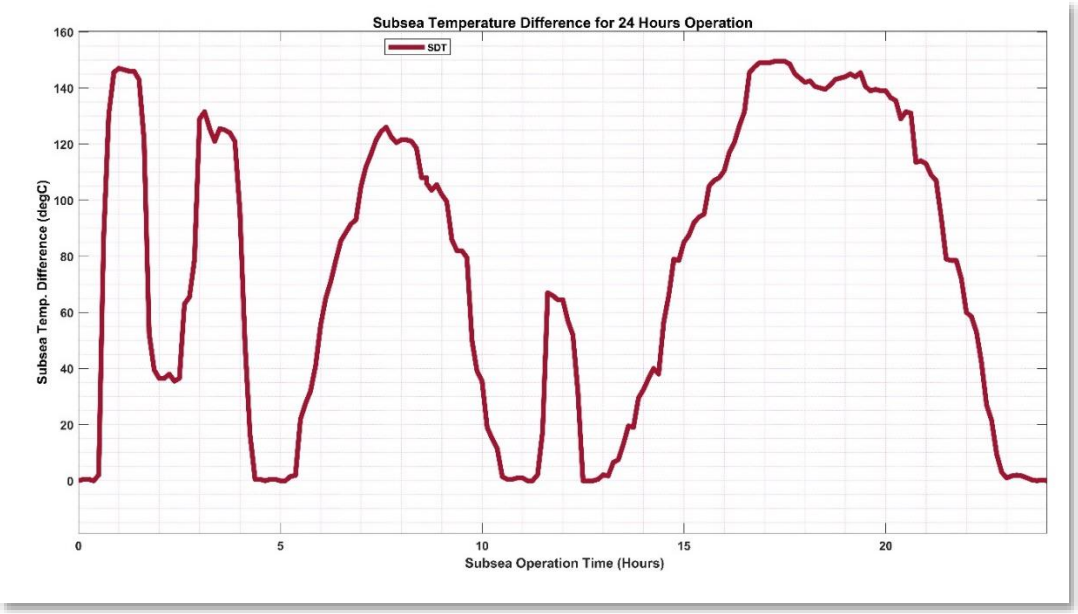

Figure 7.2 Long Duration Subsea Operations (24-hour) Template

7.4. Results of the Experiments

The following subsections further evaluate the results of experiments in ***Chapters 3, 4,*** and ***6***. It is important to note that some of the ultra-deepwater oil-gas field design and the DTEG power system components sizing outcomes in ***Chapter 5*** were applied in ***Chapter 6***. Thereby providing valuable insights into the deepwater or ultra-deepwater thermoelectric power system in West Africa as discussed below:

7.4.1. TEMs Test, DTEM, DPP & DPU Development

As discussed in ***Chapter 3***, off-the-shelf thermoelectric generator modules (TEMs) and other components used in this project were not designed for a deepwater environment.

However, tests were carried out on three (3) different types of commercial TEMs: Device-TEM-01, Device-TEM-02, and Device-TEM-03, from Manufacturer-B. The electricity generation potential of thermoelectric modules, as in *Table 3.5* and **Appendix A (Table A.1)**, verifies that waste heat from hot oil-gas reservoirs and cold seawater can be converted to electricity.

The test results in *Table 3.5* led to the selection of Device-TEM-03 as the potential deepwater thermoelectric module for this work. One of the reasons for the highest output power value of 1.06W at 70 °C temperature difference input was the larger surface area (4cm x 4cm) of thermocouples inside the Device-TEM-03 compared to the other TEMs. The dimensions for Device-TEM-02 were (3cm x 3cm), while Device-TEM-01 was (2cm x 2cm). Details on the three TEMs are in *Table 3.2*. Therefore, the large surface area occupied by the selected TEM on the Hotplate-HPL-X01 translated to high output power from Device-TEM-03. The large surface area also means that higher output power is achievable if the Flex-DTEMs in the DPPs (or the DPU) occupy a large surface area on subsea structures.

Additionally, a considerable amount of power/energy (or surplus energy) is achievable at the seafloor if DPPs are installed on the numerous subsea structures in West Africa. On the other hand, the mounting or installation of the Flex-DPPs on subsea structures must align with the latest (modern) offshore installation guidelines. The new guideline shall have provisions for renewable energy sources and non-renewable sources.

Furthermore, the selected Device-TEM-03 was configured for power boosting. *Table 7.8* and *Table 7.9* are the test rig results obtained from the six (6) Device-TEM-03 in series

and parallel configurations. Additionally, thermoelectric modules (Device-TEM-03) were marinised. The datasheet of the marinised Flex-DTEM is available in *Table 3.9*. Manufacturing of flexible thermoelectric modules is now possible due to advances in research and development efforts (Zhu, Xu and Jia, 2018)(Park *et al.*, 2017). Hence, thirty-six (36) Flex-DTEMs were connected in a combined parallel-series arrangement with six (6) bypass diodes and two (2) blocking diodes to form a Flex-250W-DPP.

Table 7.8 Six (6) Device-TEM-03 in Series Arrangements

Six (6) Device-TEM-03	**Parallel (P)-Series (S)-Configuration**	**4 Ohms Load Resistance, 70 °C Temp. Difference, at 1000 L/h Cold water Flow Rate**		
		Voltage (V)	**Current (A)**	**Power (W)**
Device-TEM-03	Single Module, VOC = 2.95 V	Nil	Nil	Nil
Modules in Series Arrangement				
Mod-A, Mod-B, Mod-C, Mod-D, Mod-E, Mod-F	6 Good, 1P + 6S	9.96	0.61	6.08
Mod-A, Mod-B, Mod-C, Mod-D, Mod-E, Mod-F	5 Good + 1Bad	7.98	0.00	0.00
Mod-A, Mod-B, Mod-C, Mod-D, Mod-E, Mod-F	3 Good + 2 Inactive +1 Bad	5.13	0.60	3.08

Table 7.9 Six (6) Device-TEM-03 in Parallel Arrangements

Six (6) Device-TEM-03	Parallel (P)-Series (S) Configuration	4 Ohms Load Resistance, 70 °C Temp. Difference, at 1000 L/h Cold water Flow Rate		
		Voltage (V)	Current (A)	Power (W)
Device-TEM-03	Single Module, VOC = 2.95 V	Nil	Nil	Nil
Modules in Parallel Arrangement				
Mod-A, Mod-B, Mod-C, Mod-D, Mod-E, Mod-F	6 Good, 3P + 3P	5.12	1.22	6.25
Mod-A, Mod-B, Mod-C, Mod-D, Mod-E, Mod-F	3 Good + 2 Inactive + 1Bad	2.56	0.59	1.51
Mod-A, Mod-B, Mod-C, Mod-D, Mod-E, Mod-F	5 Good + 1Bad	8.52	0.60	5.11

Using MATLAB/Simulink, a power tool for computing thermoelectric power parameters was created. The electrical power computing tool instrumented the establishment of 250W-DPP and 350W-DPP configurations; details are in **Section 3.5.8** and **Section 3.5.9**. The 250W-DPP was the selected DPP formation for the project. Several Flex-DPPs connected in parallel-series configuration produced nine (9) different deepwater

thermoelectric power unit (DPUs) frameworks. The power ratings of the 9 DPUs were from 1279 W to 10440 W; see **Section 3.5.10**.

7.4.2. Flex-250W-DPP & Power Electronics Interfaces

In ***Chapter 4***, power electronics devices were interfaced between the Flex-250W-DPP and subsea equipment. The description of the power interface is in **Sections 4.3** to **4.6.1** and **Sections 4.7** to **4.8**. Therefore, only the results from the Flex-250W-DPP power source and power control system experiments in **Section 4.6.1.1** are available here.

Secondly, the plots of the output power through the Flex-250W-DPP power source and the tracked power via the underwater power controller and DC-DC power converter are shown in *Figure 4.17*. The results indicate effective waste heat harvesting from oil-gas reservoirs and cold seawater. Also, the results show appropriate harnessing and conversion of waste heat to electrical power.

Thirdly, the efficiency of the subsea DC-DC power converter and the underwater power controller was almost 98%. Additionally, the overall system efficiency, comprising the Flex-250W-DPP integrated with subsea temperature difference input, the subsea DC-DC converter, and the underwater controller, was nearly 95%, thus providing a high degree of confidence in the power system design.

Fourthly, irrespective of the load resistance values on the subsea equipment, maximum power was obtained through the Flex-250W-DPP and the subsea temperature difference inputs. The results were achieved through continuous adjustments on the duty cycle values

over a Hill-Climbing algorithm-based underwater power controller. Therefore, a guaranteed approach is established to supply stable DC power derived from waste heat and cold seawater to subsea equipment.

Furthermore, *Table 7.10* shows the results obtained when the load resistance of 20 Ohms on subsea equipment was connected to the Flex-250W-DPP power source, underwater power controller, and subsea DC-DC converter experiments. Similarly, *Table 7.11* shows the results obtained when a 50 Ohm load resistance on subsea equipment replaced the previous 20 Ohm load resistance on subsea equipment. Finally, *Table 7.12* shows the results when the load resistance on subsea equipment was 100 Ohms.

The results reaffirmed the appropriate configuration of power electronic components. The power electronic devices exploited electrical power at maximum potential from waste heat from deepwater oil and gas reservoirs in West Africa via thermoelectric generators on subsea structures, as depicted in the system architecture in **Section 3.1** and **Section 6.3**.

Table 7.10 DC Power-20 Ohms Load Resist. on Subsea Equipment

Subsea Temp. Diff. (°C)	**20 Ohms Load Resistance on Subsea Equipment**				
	DPP-Power (W)	**Converter-Vo(V)**	**Converter-Io(A)**	**Converter-Po(W)**	**Tracked Power(W)**
20	15.62	17.73	0.89	15.72	**33.33**
50	83.51	41.47	2.07	85.97	**83.33**
70	118.20	48.13	2.41	115.85	**116.70**
90	149.60	53.83	2.69	144.86	**150.00**
110	183.90	61.33	3.07	188.04	**183.30**
130	114.50	47.80	2.39	114.24	**216.70**
150	273.90	41.51	2.08	86.13	**250.00**

Table 7.11 DC Power-50 Ohms Load Resist. On Subsea Equipment

Subsea Temp. Diff. (°C)	50 Ohms Load Resistance on Subsea Equipment				
	DPP-Power (W)	Converter-Vo(V)	Converter-Io(A)	Converter-Po(W)	Tracked Power(W)
20	32.72	40.33	0.81	32.53	**33.33**
50	81.99	64.62	1.29	83.49	**83.33**
70	117.50	74.44	1.49	110.77	**116.70**
90	152.00	85.67	1.71	146.75	**150.00**
110	174.70	42.47	0.85	36.08	**183.30**
130	240.50	42.20	0.84	35.62	**216.70**
150	293.20	41.91	0.84	35.13	**250.00**

Table 7.12 DC Power-100 Ohms Load Resist. On Subsea Equipment

Subsea Temp. Diff. (°C)	100 Ohms Load Resistance on Subsea Equipment				
	DPP-Power(W)	Conv-Vo(V)	Conv-Io (A)	Power-(W)	Tracked Power(W)
20	32.82	55.21	0.55	30.48	**33.33**
50	72.60	85.60	0.86	73.27	**83.33**
70	113.20	105.90	1.06	112.15	**116.70**
90	66.39	42.27	0.42	17.87	**150.00**
110	188.50	42.62	0.43	18.16	**183.30**
130	247.50	42.34	0.42	17.93	**216.70**
150	297.40	42.05	0.42	17.68	**250.00**

7.4.3. 250W-DPP & Subsea Energy Mgmt. System

In the second part of ***Chapter 4***, additional electronic components were added to the system to convert electrical power to chemical energy. Chemical energy was stored in a subsea battery and supplied as electrical power to subsea equipment when the need arose,

as explained in **Section 4.7**. The subsea energy management system generated the required switching signals depending on bus voltage, as discussed in **Section 4.8**. During the stepwise subsea temperature difference increment and decrement experiments, bus voltage (VBus) remained almost constant, as shown in *Figure 4.26*. As expected, there were up-and-down movements in the battery state of charge (SOC) or the charge level relative to the subsea battery capacity following the output power through the Flex-250W-DPP source. The plots in *Figure 4.26* show the increase and decrease in the SOC values (between 44.992% and 45.002%). In the 15th hour, a steady increase from 44.992% to around 45.005% in the 22nd hour was observed. Lastly, there was a decline to less than 45.002% in the 24th hour.

Similarly, there was a continuous rise and fall in subsea battery current and voltage, as obtained in the plots in *Figure 4.27*. During the experiments, the recorded maximum battery current was around 6.72A, while the minimum value was about –0.28A. The highest battery voltage value was less than 25.85V, while the lowest was 25.74V.

Electrical energy was converted to stored chemical energy. When there were shortfalls in the power supply from the Flex-250W-DPP source, the subsea battery provided complementary power to the subsea equipment. Additionally, when the battery level was low, the Flex-250W-DPP power source charged the subsea battery. As a result, the intermittent effect, typical in most renewable sources, was further reduced in this thermoelectric power system. *Table 7.13* and *Table 7.14* provide additional information on the stepwise increment and decrement in subsea temperature difference.

The purpose of power electronic devices, in the first instance in this deepwater thermoelectric power system, was to enhance power generation at the optimum power point from a varying energy source (varying subsea temperature input). In the second instance, additional power electronic devices and subsea batteries further reduce the low intermittent effect in the thermoelectric system to near or non-existence in a deepwater environment.

Therefore, it can be inferred that deploying power electronic components and suitable control strategies at the seabed in West Africa could seamlessly supply electrical power to subsea equipment while storing electrical energy in subsea batteries. This energy harvesting, conversion, supply, and storage approach minimizes intermittent seafloor energy. A 6.4kW-DPU power system on subsea structures for DC power generation, energy storage, and supply to subsea equipment via charging stations is depicted in the system architecture in **Section 6.3**.

Table 7.13 Stepwise Increment in Subsea Temp. Difference Inputs

Subsea Temp.Diff (degC)	DPP-Power (W)	Delivered Power to Subsea Load (W)	V-Bus (V)	I-Bat (A)	V-Bat (V)	SOC (%)	System Status	Remarks
0	0.00	24.91	47.93	6.59	25.75	44.94	Very Low Power. DPP Disconnected from Load. Battery Connected to Load + Battery Power supply to Load	Chemical Energy (CE) Conversion to Electrical Energy (EE)
10	15.88	25.04	48.08	5.41	25.76	44.95	Low Power. DPP and Battery Power supply to Load	Combine Power supply: Direct Electric + Chemical Energy to EE
30	49.93	24.84	47.87	4.83	25.77	44.96	Low Power. DPP and Battery Power supply to Load	Combine Power supply: Direct Electric + Chemical Energy to EE
60	101.30	24.59	47.86	2.92	25.79	44.99	Medium Power. DPP supply to Load. (Battery Connected but not contributting)	Direct Electric Power supply to Load
70	118.70	24.76	47.98	2.55	25.80	45.00	Medium Power. DPP supply to Load (Battery Connected but not contributting)	Direct Electric Power to Load
90	152.60	24.74	47.93	1.02	25.81	45.01	Medium Power. DPP supply to Load (Battery Disconnected)	Direct Electric Power to Load
115	194.60	24.66	48.03	minus(-) 0.7442	25.83	45.03	High Power. Low Battery Level. DPP Disconnected from Load and connected to Battery(Battery Charging)	Conversion of Electrical Energy (EE) to Chemical Energy (CE)
120	202.80	24.65	47.98	minus (-) 1.336	25.84	45.04	High Power. Low Battery Level. DPP Disconnected from Load and connected to Battery(Battery Charging)	Conversion of Electrical Energy (EE) to Chemical Energy (CE)
125	240.20	24.88	47.91	6.63	25.74	44.94	Very High Power. DPP continuous supply to Load/Fully Charge Battery Disconnected & Standby	Chemical Energy (CE) on Standby
150	300.10	24.89	47.91	6.29	25.75	44.94	Very High Power. DPP continuous supply to Load/Fully Charge Battery Disconnected & Standby	Chemical Energy (CE) on Standby

Table 7.14 Stepwise Decrement in Subsea Temp. Difference Inputs

Subsea Temp.Diff (degC)	DPP-Power (W)	Delivered Power to Subsea Load (W)	V-Bus (V)	I-Bat (A)	V-Bat (V)	SOC (%)	System Status	Remarks
130	249.50	24.89	47.93	6.71	25.75	44.94	Very High Power. DPP continuous supply to Load/Fully Charge Battery Disconnected & Standby	Chemical Energy (CE) on Standby
118	199.60	24.90	48.03	minus (-) 0.3299	25.83	45.04	High Power. Low Battery Level. DPP Disconnected from Load and connected to Battery(Battery Charging)	Conversion of Electrical Energy (EE) to Chemical Energy (CE)
110	186.20	24.76	48.12	minus (-) 0.2967	25.83	45.03	High Power. Low Battery Level. DPP Disconnected from Load and connected to Battery(Battery Charging)	Conversion of Electrical Energy (EE) to Chemical Energy (CE)
100	166.90	24.62	47.85	0.26	25.82	45.02	Medium Power. DPP supply to Load (Battery Disconnected)	Direct Electric Power supply to Load
80	135.80	24.78	47.97	1.27	25.81	45.01	Medium Power. DPP supply to Load (Battery Disconnected)	Direct Electric Power supply to Load
50	83.99	24.76	47.87	3.44	25.79	44.98	Low Power. DPP and Battery Power supply to Load	Combine Power supply: Direct Electric + Chemical Energy to EE
40	67.19	24.86	47.97	4.45	25.78	44.97	Low Power. DPP and Battery Power supply to Load	Combine Power supply: Direct Electric + Chemical Energy to EE
20	32.71	24.83	47.88	4.90	25.76	44.95	Low Power. DPP and Battery Power supply to Load	Combine Power supply: Direct Electric + Chemical Energy to EE
5	7.68	24.86	47.89	6.57	25.75	44.94	Very Low Power. DPP Disconnected from Load. Battery Connected to Load + Battery Power supply to Load	Chemical Energy (CE) Conversion to Electrical Energy (EE)
0	0.00	24.91	47.93	6.59	25.75	44.94	Very Low Power. DPP Disconnected from Load. Battery Connected to Load + Battery Power supply to Load	Chemical Energy (CE) Conversion to Electrical Energy (EE)

7.5. Validating the 6.4kW-DPU & Power Grid System

An ultra-deepwater oil and gas production field in West Africa was designed and developed in ***Chapter 5***. The subsea production field contained 56 subsea wells and several other power-demanding subsea equipment at water depths ranging from 1500 meters to 3000 meters. A 6.4 kW-DPU thermoelectric power system required an area of 332.80 square meters at the seafloor to support subsea operations. Refer to ***Chapter 5***, *Table 5.1,* and *Table 5.2* for additional details on the power system composition.

Furthermore, intermittent characteristics often associated with most renewable energy sources led to obtaining 136 pieces of Device-SBAT-101 subsea batteries, thus forming a 6,120Ah capacity subsea battery bank for day and night operation along with the 6.4kW-DPU power unit. As a result, electrical power was efficiently drawn from oil-gas reservoirs' waste heat and the cold sea environment through the deepwater thermoelectric power source and delivered to critical subsea control equipment; see *Table 5.3* and *Table 5.4*.

However, DC-powered subsea equipment is not the trend in the subsea market (at the time of this writing). Secondly, conversion losses are often associated with converting electrical energy to chemical energy and from chemical energy back to electrical power. These and other factors led to the transformation of DC power to AC power in ***Chapter 6***.

The Flex-250W-DPP power system model developed in ***Chapter 4*** was modified and upgraded to a larger power system. Some of the main components of the extended power system were the 6.4 kW-DPU energy harvester and power source, the subsea DC-DC

boost converter, a DC Bus, and a three-phase subsea power inverter. Thus, DC power was transformed into AC power through a frame transformation process. The AC power was supplied to the first-of-its-kind underwater combo power grid system, as demonstrated in ***Chapter 6***.

The underwater combo power grid system of renewable and non-renewable sources opened energy possibilities in West Africa. Alternative energy opportunities are enormous in the region; however, the supporting infrastructures are either in short supply or non-existent. Based on this innovative deepwater or ultra-deepwater power system, the subsea oil and gas equipment are expected to be the first beneficiaries of the power system. Secondly, this unconventional power system can potentially transmit ocean floor or offshore base electric power supply back to shore.

In ***Chapter 6***, the 6.4kW-DPU power unit was operated via subsea temperature difference input ranging from 0 °C to 150 °C by applying the 4-hour subsea operations template (see *Figure 7.1*), as demonstrated in **Section 6.9.1** to **Section 6.9.6**. Therefore, the remaining part of ***Chapter 7*** is focused on operating the underwater power system using the 24-hour operating template. The new sets of experiments will provide valuable insight into the system's performance.

Hence, in this deepwater power system and validity test, the 6.4kW-DPU power unit was operated through subsea temperature difference input from 0 °C to 150 °C by applying the 24-hour subsea operations model described above in **Section 7.3** (see *Figure 7.2*).

As discussed in ***Chapter 5*** and the preceding ***Chapters***, subsea operations are typically twenty-four (24) hours and seven (7) days a week. Thus, it was considered that the results obtained from a 24-hour operating system comprising multiple peaks and troughs should be benchmarked with results obtained from a 4-hour subsea operation that has a single peak point. The experiment's outcome predicted the performance and integrity of the deepwater power system, among other things.

7.5.1. Safety Mechanism Test & 24-Hour Operations

The 24-hour subsea operations template was connected to the power system while the safety control mechanism was in place (**Sections 6.9 and 6.9.1**). Subsea temperature difference input to the 6.4kW-DPU power source started from zero (0) °C and rose to 147 °C. From 147 °C, the temperature difference fell to approximately 40 °C at about the 2nd and 3rd hour. Then, the subsea temperature difference slowly increased from 40 °C to about 131 °C. From 131 °C, the temperature difference dropped to 126 °C at 3.5 hours and slowly fell to 0 °C at about the 4.7th hour. Next, the subsea temperature difference slowly rises from 0 °C to 126 °C at the 7.6th hour (see *Figure 7.2*).

From 126 °C, the subsea temperature difference slowly fell to 0 °C around the 11.20th hour. Afterward, the temperature difference around the 11.9th hour had risen to nearly 70 °C. From 64 °C at the 12th hour, it came down to 0 °C at the 12.5th hour. The peak subsea temperature difference of 150 °C was attained near the 17th hour. After that, the temperature difference slowly decreases from 150 °C to about 142 °C at the 18th hour.

Later, the subsea temperature difference increased to 145 °C and around 140 °C at the 20th hour. By the 23rd hour, the subsea temperature difference was between 1°C and 2 °C. Next, the temperature difference was less than 2 °C till the end of the experiment at the 24th hour. The long-duration (24-hour) subsea temperature profile is in *Figure 7.2*.

The behaviour of the safety control mechanism and the overall system performance are discussed below:

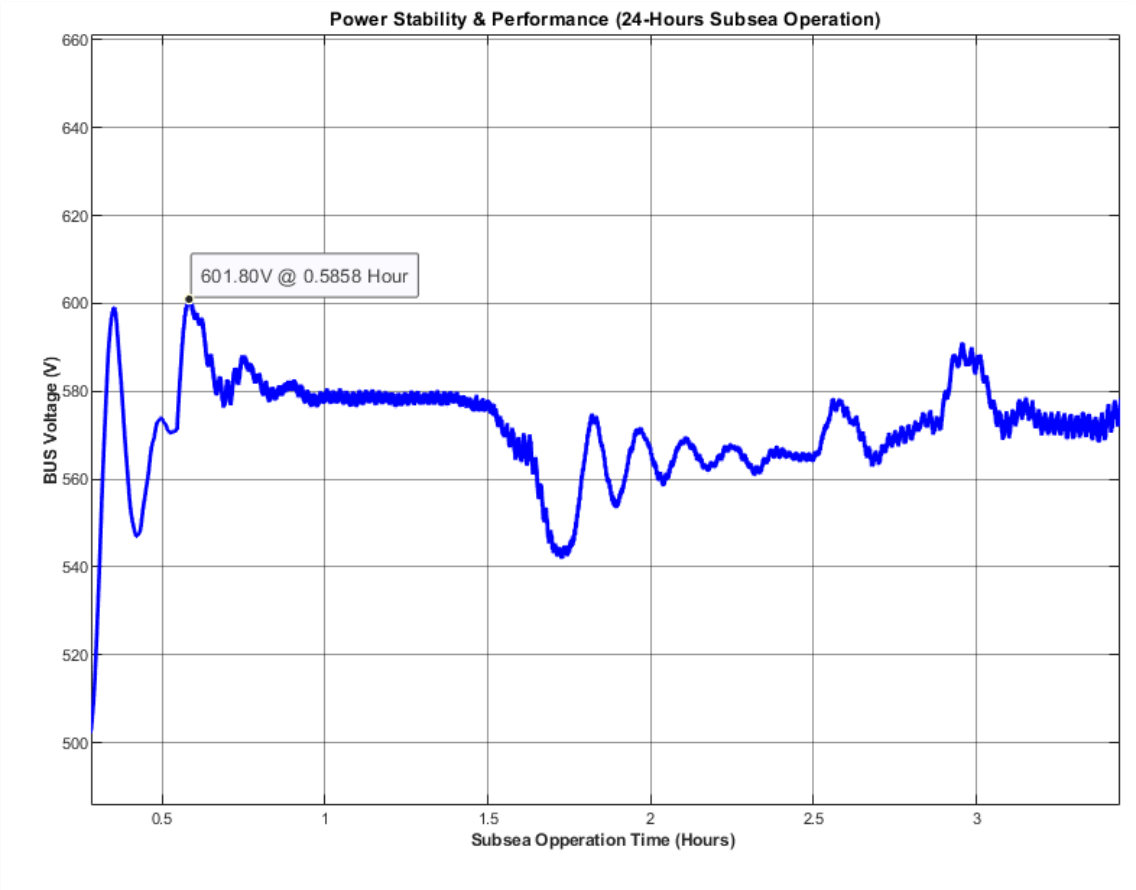

Figure 7.3 Power System with Safety Mechanism (24-Hour Operations)

In the subsea power inverter control system (subsea power inverter algorithm), the power system was programmed for a system reset when the value of VBus voltage was 5% above (or greater than) the original setting, as discussed in **Section 6.9**. Hence, a system reset was expected when the VBus voltage was 598.5V at 0.3501 hours.

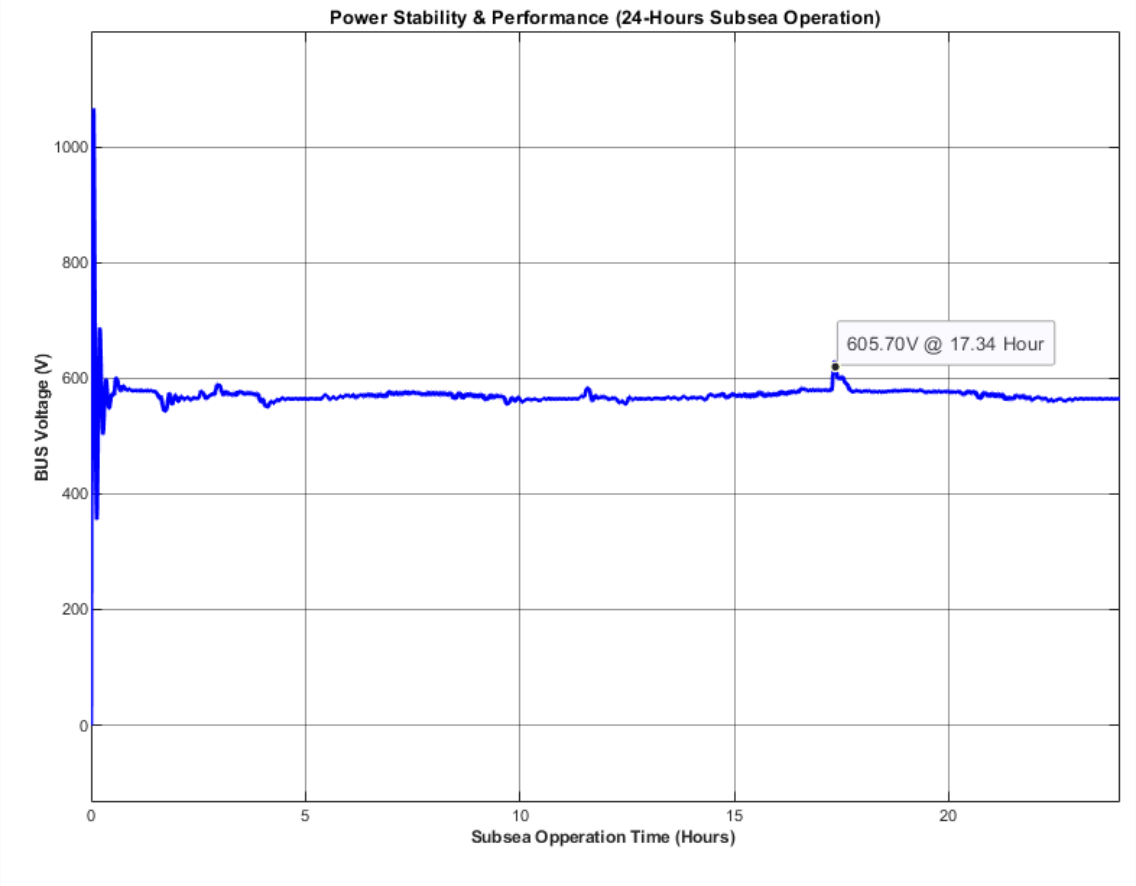

Figure 7.4 Power Stability & Performance (24-Hour Operations)

However, the system reset was activated when VBus was 599.10V, as shown in *Figure 7.3*. After the reset at 0.3501 hours, VBus slowly increased to a high value of 601.80V at the 0.5858th hour before the second system reset occurred. As can be seen in *Figure 7.4*,

another safety incident or system upset took place at 17.34 hours. Again, a third reset was triggered when the VBus voltage was 605.70V instead of 598.5V.

From the above results, the safety mechanism responded during system-critical scenarios or system upsets; however, safety targets were not precisely met. Several reasons may have been attributed to the system's behaviour leading to the power system's disturbances and the safety system's failure to respond appropriately. The selection of individual components and parameter settings at the early design stage might have been one of the several problems. Secondly, parasitic resistances on the individual components in the power system might have contributed to the issues, thereby affecting the system efficiency, as discussed in **Section 4.6.1.2**.

Hence, control system reconfiguration and parameter tuning would improve the safety performance of the power system. The response actions of the safety mechanism during system upsets verified the functionality of the safety system design in the 4-hour subsea operation discussed in **Section 6.9.1** and the 24-hour operation. **Appendix F (Table F.2)** provides additional information on the DC BUS during the 24-hour subsea operations.

7.5.2. DC Current Flow from 6.4kW-DPU Source

Section 7.5.1 shows '*a better-than-average stable power system*' during the 24-hour subsea operations, in which the bus voltage was roughly 570V throughout the power system operation. In this section, *Figure 7.5* represents the electric current (DC) drawn

via the 6.4kW-DPU power source as hot fluids from oil-gas reservoirs flow through subsea structures in a cold seabed environment.

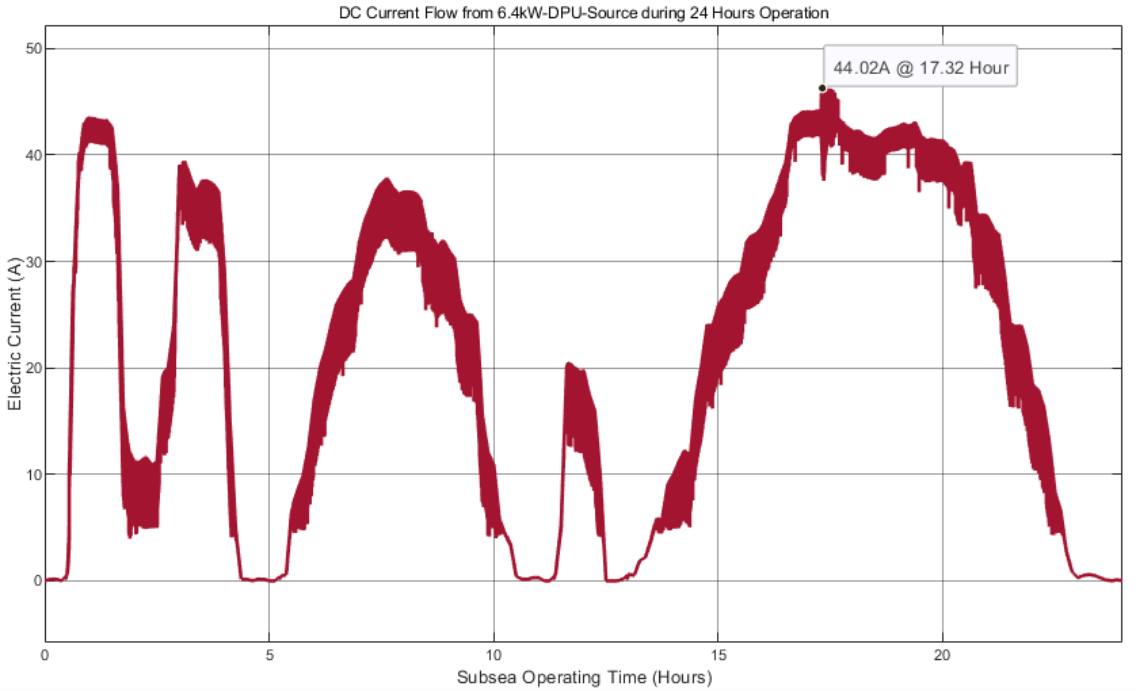

*Figure 7.5 Electric Current from 6.4*kW*-DPU Source (24-Hour Operations)*

The electric current flowed from the 6.4kW-DPU power source to the rest of the power circuit via the actions of the subsea DC-DC boost converter and the underwater power controller.

The electric current value was between 0A and 0.5A at the start and slowly rose to about 44A. Next, there was a drop from 44A to less than 12A between the 1.80th and 2.50th hour. Between the 7th and 8th hour, the electric current value was nearly 38A. Later, the highest electric current value between the 11th and 12th hour was less than 22A, while between the 12.5th and 13.5th hour, the electric current value was between 0A and slightly

less than 4A. As shown in the plots in *Figure 7.5*, around the 17th and the 17.5th hour, the highest electric current value was over 44A. After that, there was a decrease at the 20th hour, from less than 42A, slowly decreasing to 0A and less than 0.5A at the 23rd hour. The electrical current values were between 0A and below 1A till the end of the experiment.

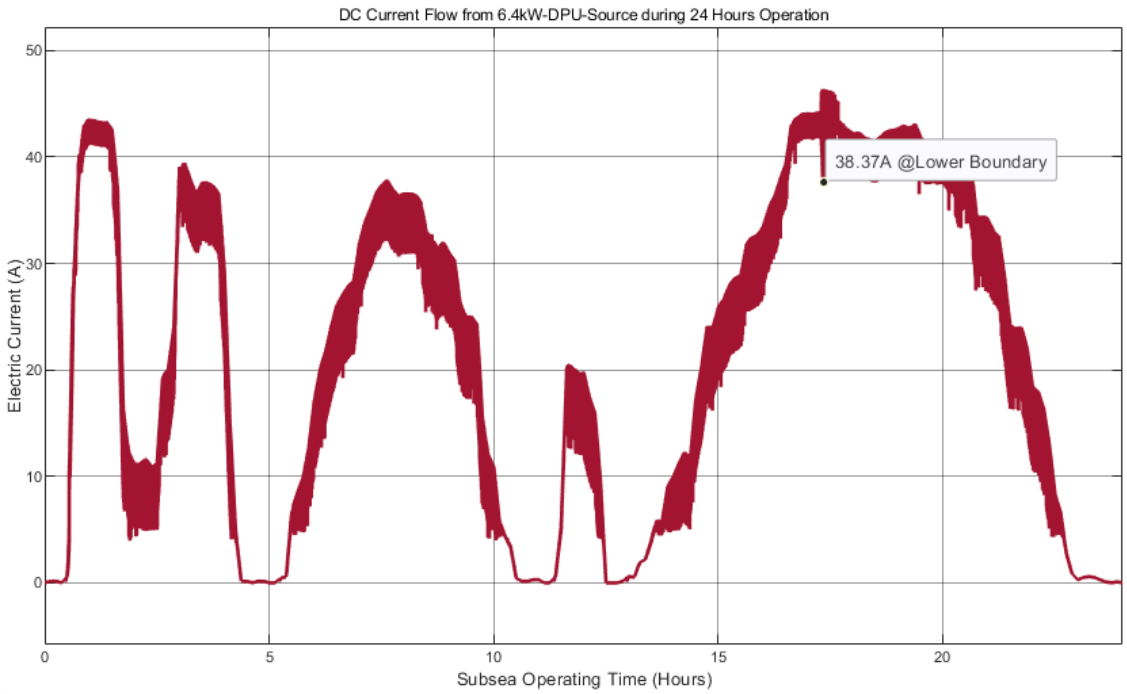

Figure 7.6 Electric Current Ripple (24-Hour Operations)

Compared with the previous results obtained from the 4-hour subsea operation in **Section 6.9.2**, the highest electric current (DC) value obtained from the power system was 44.41A. The plots in *Figure 7.6* show that the peak current drawn through the 6.4kW-DPU power source during the 24-hour operation was 44.02A.

The difference between the peak electric current values from the two results (the 4-hour subsea operations and the 24-hour operations) was 0.39A at a maximum subsea

temperature difference of 150 °C. The resultant electric current (from both system operations) has a minimal error of less than 1A. Hence, the outcome of both experiments indicates sound system design.

However, there were variations in the results obtained from the electric current ripple, as shown in *Figure 7.6* and *Figure 6.17*. The current ripple value was 5.65A during the 24-hour operation, while the 4-hour system operation had a current ripple value of 2.70A. The margin of error between the two results is slightly oversized. The power system design current was 47.04A; therefore, the expected value of the electric current ripple should not have been higher than 10% of the design current. The current ripple (during the 24-hour operation) would somewhat negatively affect some of the power circuit components. In such a situation, the inductive and capacitive features are likely to be impacted by the current ripple flowing from the 6.4kW-DPU power source to other parts of the power circuit. Therefore, design parameter adjustment would reduce the system's electric current ripples. However, further design revision was unnecessary since the current ripple value could not have severe consequences on the power system.

7.5.3. DC Power Flow from 6.4kW-DPU Source

During the 24-hour subsea operations, the calculated DC power derived through the 6.4kW-DPU power source was logged. In addition, electric power via the combined effort of the underwater power controller and subsea DC-DC boost converter was simultaneously tracked at the same time, as shown below:

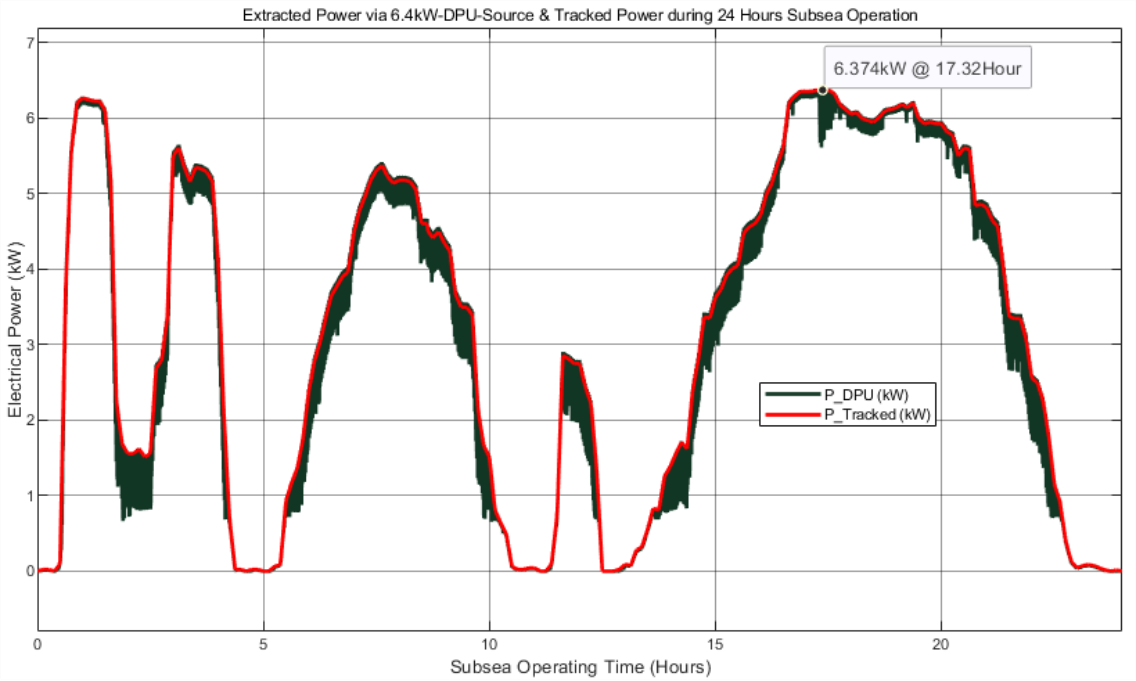

*Figure 7.7 6.4*kW*-DPU Source Power & Tracked Power (24-Hour Ops)*

The dark green plots in *Figure 7.7* represented the calculated electrical power harvested through the 6.4kW-DPU generator. In contrast, the red colour plots concurrently tracked power via the combined actions of the underwater power controller and the subsea DC-DC power converter. As indicated in the results, between the 17.2nd and the 17.5th hour, about 6.374 kW (DC power) was obtained when the subsea temperature difference input was 150 °C. Comparing this result with the 6.395 kW obtained from the 4-hour operating system (see *Figure 6.15* and *Figure 6.16*) in **Section 6.9.3** suggests the credibility of the deepwater power system design. **Appendix F (Table F.1)** provides further information on the DC outputs of the deepwater power system during the 24-hour subsea operations.

7.5.4. The 3-Phase AC Current in 24-Hour Operations

The DC voltage and electric current outputs from the 6.4kW-DPU were transformed to three (3) phase AC voltage and current through pre-defined control strategies or control algorithms in the subsea power inverter.

Figure 7.8 Three-Phase AC Current via Subsea Inverter (24-Hour Ops)

In other words, the derived DC power (in **Section 7.4.3**) was routed to a 3-phase subsea power inverter through the DC Bus (see *Figure 6.3* and *Figure 6.4*). The 3-phase output current from the subsea power inverter during the 24-hour operations is shown in *Figure 7.8*.

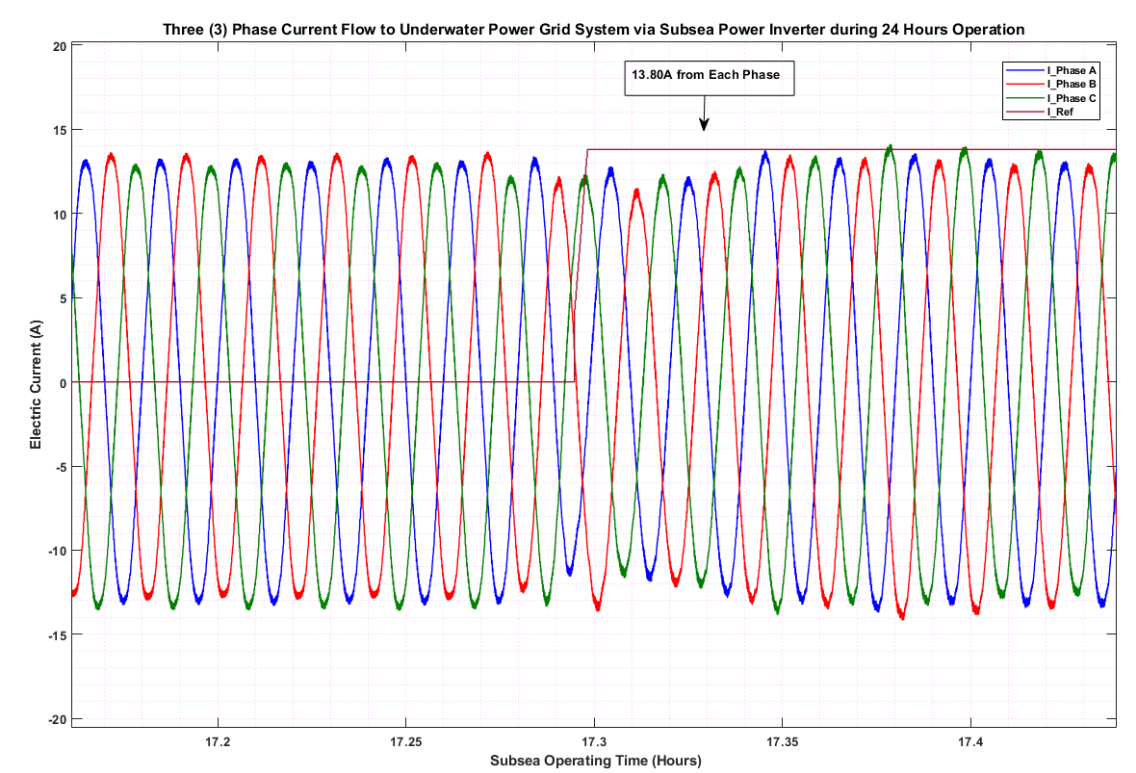

Figure 7.9 AC Current on Each Phase via Subsea Inverter (24-Hour Ops)

The results in *Figure 7.9* indicate that when the subsea temperature difference was 150 °C, 13.80A was recorded in the three phases. Compared with *Figure 6.17* in **Section 6.9.4**, the (AC) current obtained from each phase was 13.73A when the subsea temperature difference input was at its maximum during the 4-hour operation. The results from both operations confirm the efficacy of the subsea power inverter design.

7.5.5. Delivered AC Power to the Power Grid System

As presented in *Figure 7.10*, the AC power supplied to the underwater combo power grid system when the subsea temperature difference input was 150 °C was 6.342 kW.

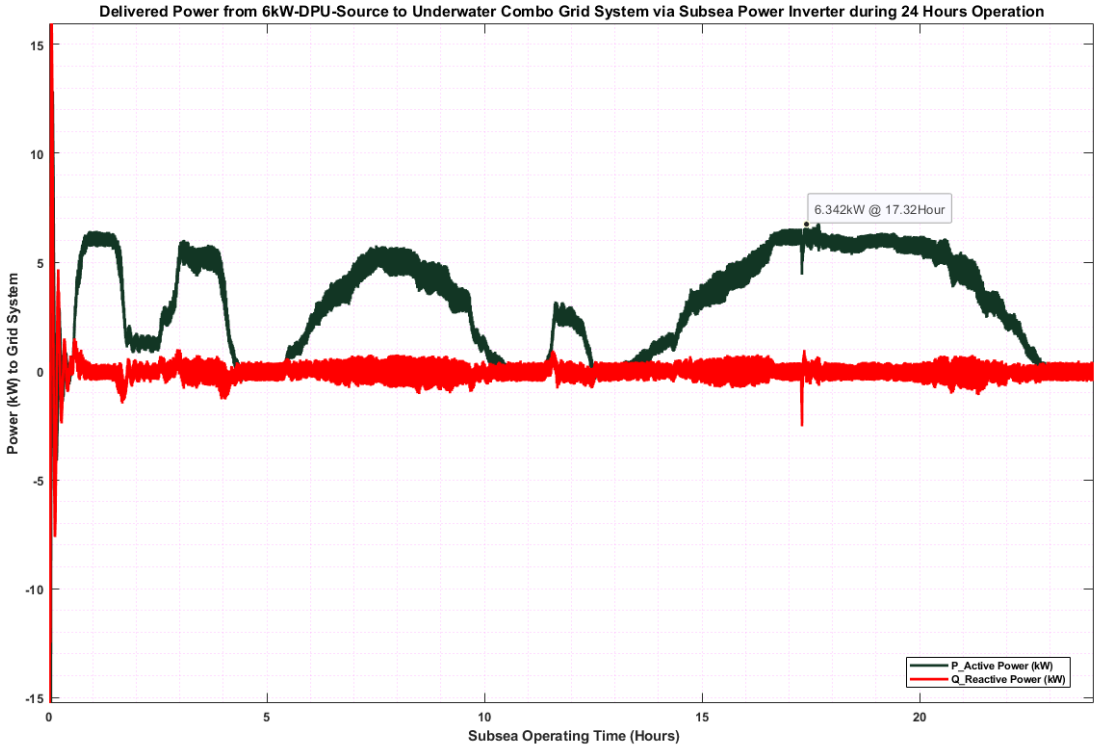

Figure 7.10 Delivered Power at Underwater Power Grid (24-Hour Ops)

On the other hand, when the subsea temperature difference was at maximum, the output DC power tracked through the underwater power controller and the subsea DC-DC converter was 6.374 kW. Therefore, the difference between the DC and AC outputs (during 24-hour operation) could be called power conversion losses. The calculated DC to AC power loss or power conversion loss is 0.032 kW. Conversely, the conversion loss

during the 4-hour subsea operations, as discussed in **Section 6.9.5**, was 0.006 kW. These results validate the capability of the deepwater power system.

7.5.6. THD in Underwater Combo Power Grid System

As revealed in *Figure 7.11*, the total harmonic distortion (THD) unit discussed in **Section 6.9.6** computed the quality of the AC power supplied to the underwater combo power grid system through the AC filters. The cumulative THD during the 24-hour subsea operations was roughly 2.8.

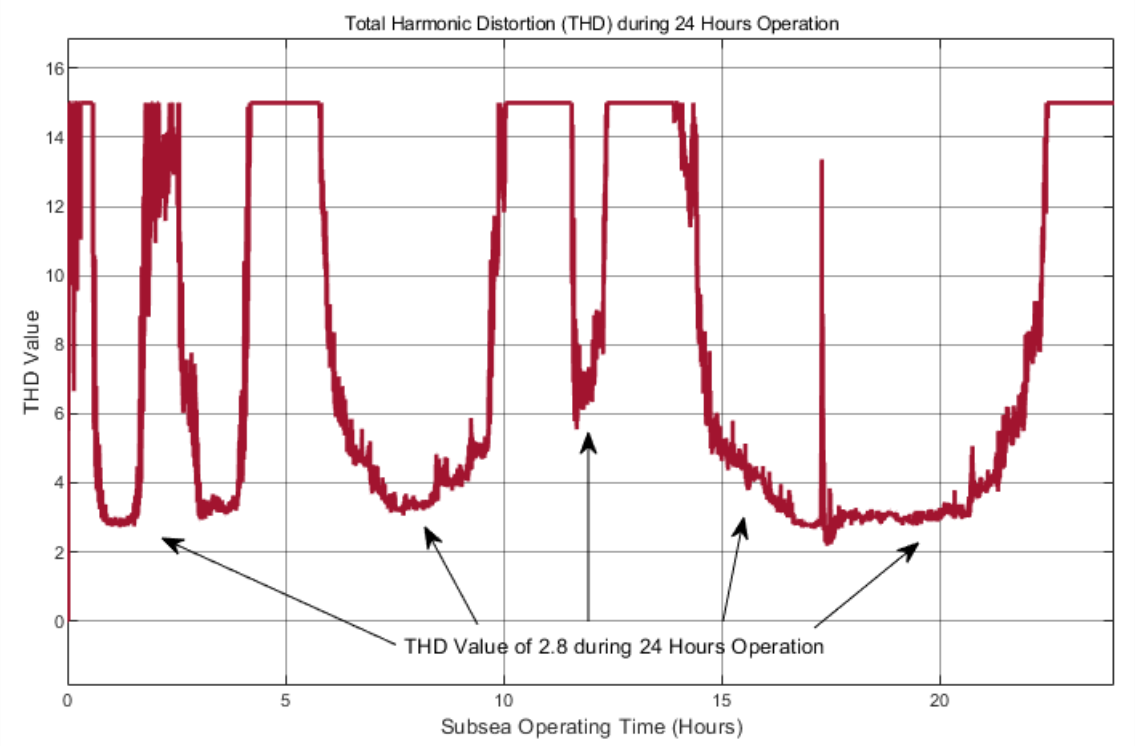

Figure 7.11 THD of Deepwater Power System (24-Hour Operations)

Generally, voltage and current harmonics exist in electrical power systems with integral multiples of the fundamental power frequency. These voltage and current harmonics are detrimental to the power system or equipment as they can cause disruption to the power system or damage the power equipment. Therefore, the lower the harmonics value, the higher the power quality.

Considering the factor above, a lower THD value could be attained by redesigning the AC filters (see *Figure 6.3* and *Figure 6.4*), a lower THD value could have been achieved. However, the savings from such a reduction would have affected the overall performance of the power system. Nevertheless, the low THD value of 2.8 corroborates the low THD of 2.7 obtained during the 4-hour subsea operation in *Figure 6.21*. Additional information on the AC outputs of the deepwater power system to the underwater power system during the 24-hour subsea operations is available in **Appendix F (Table F.3)**.

7.6. 24-Hour Operations & Grid System Outcome

Sections 6.4 to **6.9** demonstrated the 6.4kW-DPU power source and the underwater power Grid System via a 4-hour subsea operation template. In ***Chapter 7***, the discussion is focused on the 6.4kW-DPU power source and the underwater power grid system operation via the 24-hour subsea template or long-duration subsea operation.

The formation of the long-duration subsea operations template is discussed in **Sections 7.3** and **7.5**. This section analyses, validates, and critically analyses the ultra-deepwater thermoelectric power system results. *Figure 7.12* represents the subsea temperature

difference against the DC output current, the DC output power of the DPU power source, and tracked power (power output through the combined action of the subsea DC-DC Converter and underwater controller). *Table 7.15* contains the computed mean, standard deviation, and the standard error of the current, 6.4kW-DPU-Source power and the tracked power based on the data in **Appendix F (Table F.1)**.

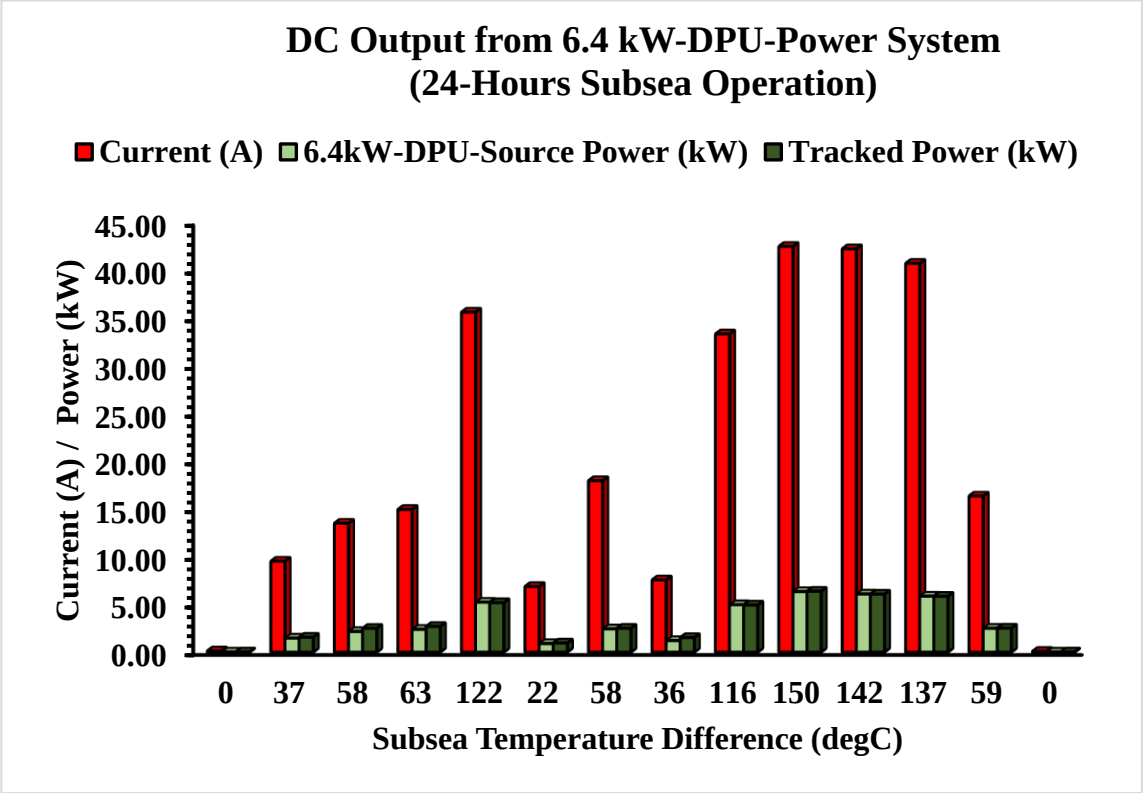

Figure 7.12 DC Outputs-6.4 kW-*DPU-Power System (24-Hours Subsea Operation)*

The DC outputs of the 6.4kW-DPU power system operated through the 24-hour subsea operation template were transferred to the AC side of the power system through the DC-BUS.

Table 7.15 Computed DC-Outputs Attributes (24-Hours Subsea Operation)

DC Output from 6.4 kW-DPU-Power System (24-Hours Subsea Operations)			
Attributes	**Current (A)**	**6.4kW-DPU-Source Power (kW)**	**Tracked Power (kW)**
Mean	21.67792292	3.15933973	3.193371559
Standard Deviation	15.75057688	2.28866313	2.271325991
Standard Error	1.016695366	0.14773257	0.146613462

The BUS-Voltage determines the stability of the power system, as explained in **Sections 6.5**, **6.6**, **6.8**, **6.9**, and **7.5**. *Table 7.16* has the computed mean, standard deviation, and standard error of the measurements obtained from the DC-BUS (See **Appendix F** (**Table F.2** for details)).

Table 7.16 Computed DC-BUS Attributes (24-Hours Subsea Operating)

Power Stability (24-Hours Subsea Operating)	
Attributes	**BUS-Voltage (V)**
Mean	569.3400915
Standard Deviation	38.6762604
Standard Error	2.496541874

Table 7.17 Power Stabilisation Process (24-Hours Subsea Operating)

Power Stability (24-Hours Subsea Operating)		
Time (Hours)	**Subsea Temp. Diff. (degC)**	**BUS-Voltage (V)**
T02.30H	37	563.7723061
T04.70H	0	564.5035268
T07.10H	111	576.6714551
T09.50H	82	570.8729652
T11.90H	65	567.0619267
T14.30H	39	563.4737102
T16.70H	147	578.5898398
T19.10H	145	579.7530376
T21.50H	79	567.3806947
T24.00H	0	564.3991374

Furthermore, *Table 7.17* presents the power stabilisation process of the deepwater power system based on timestamp intervals. The 10% equal power stabilization across the board during the system's operation, as shown in *Figure 7.13*, provides evidence that DC power was successfully transferred from the DC side to the AC side, validating the underwater power system design. Also, these results corroborate with the results obtained through the 4-hour subsea template in ***Chapter 6***.

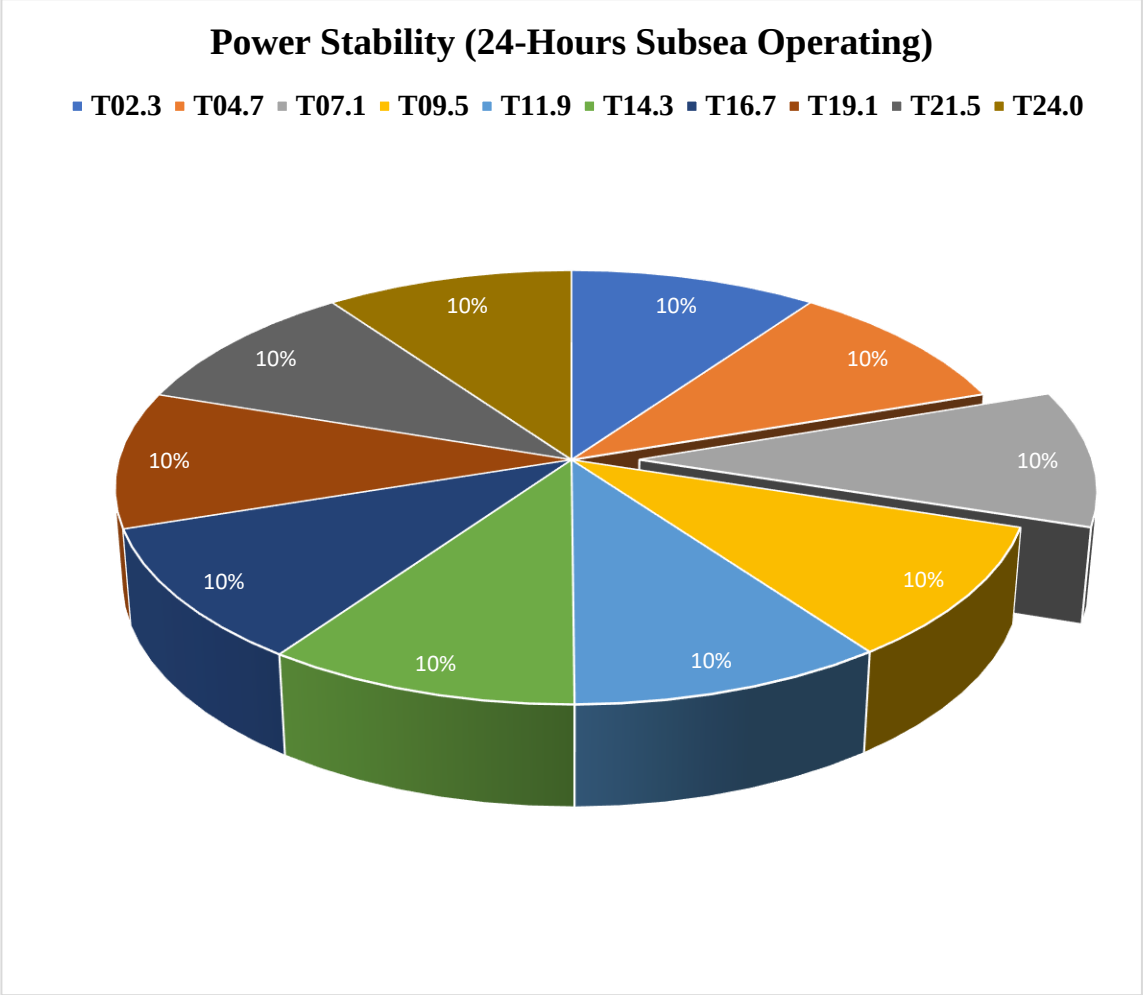

Figure 7.13 Power Stability Plots- 24Hour Subsea Operations

DC power components were transferred to the AC side. These DC power parameters were transformed from DC to AC via a three-phase subsea power inverter. The AC output power of the thermoelectric power system was delivered to an underwater power grid system. The AC output to the underwater power grid system during the 24-hour subsea operations, such as AC current, active (real power), reactive power, and total harmonic distortion, are shown in *Figure 7.14*.

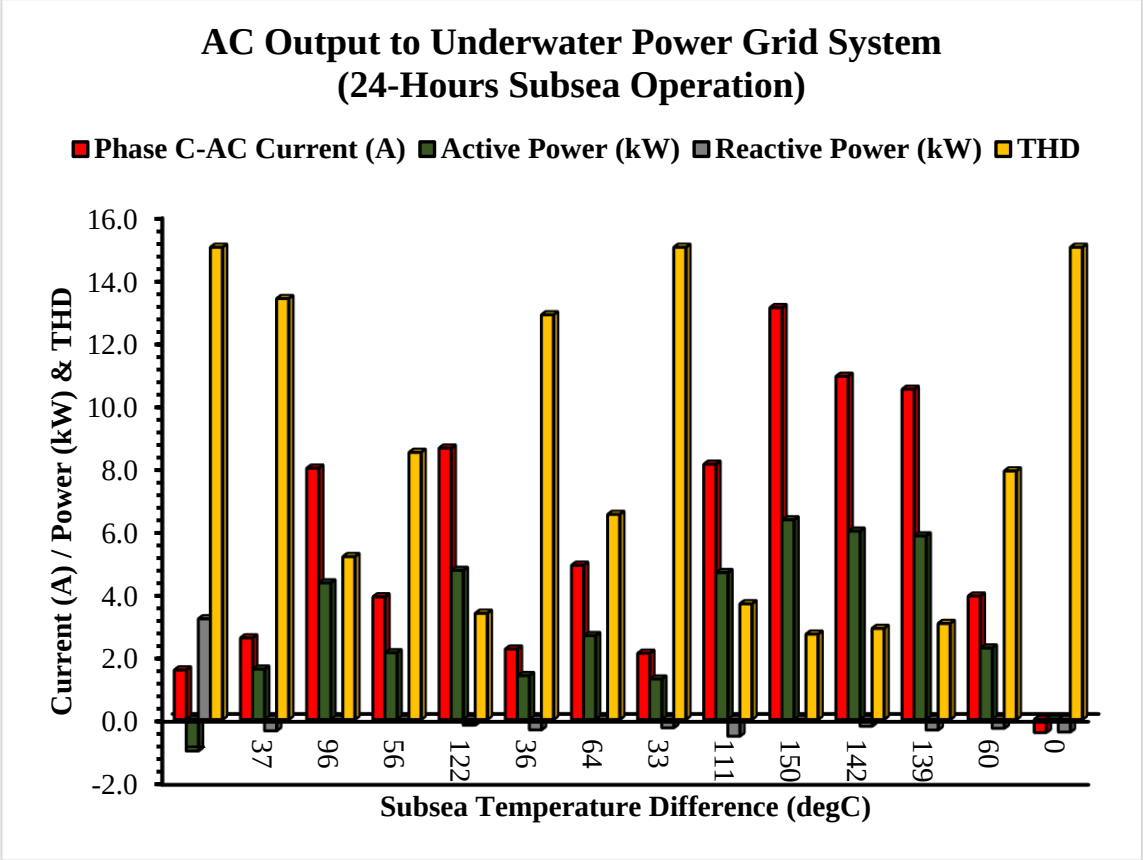

Figure 7.14 AC Outputs-6.4 kW-*DPU-Power System (24-Hours Subsea Operation)*

From the data in **Appendix F (Table F.3)**, *Table 7.18* contains the computed mean, standard deviation, and standard error of the AC current, active power, reactive power, and total harmonic distortion (THD). As mentioned, the THD represents the power quality delivered to the underwater power grid system. The smaller the THD value of any electrical power grid system, the higher the power quality. 2.8 was the recorded THD value for this operation when the subsea temperature difference was at its maximum; thus, high-quality power was sent to the power grid system.

Table 7.18 Computed Attributes-AC Output to Power Grid System

AC Output to Underwater Power Grid System (24-Hours Subsea Operation)				
Attributes	**Phase C-AC Current (A)**	**Active Power (kW)**	**Reactive Power (kW)**	**THD**
Mean	5.561494761	3.123515569	-0.234433953	8.029758995
Standard Deviation	4.415605138	2.312379447	0.3398614	5.156765621
Standard Error	0.284434131	0.149263451	0.021892397	0.332176475

The computed confidence interval, upper confidence interval, and lower confidence interval at 95% of the active power delivered to the power grid system are reported in *Table 7.19*. Further analysis was carried out, and *Table 7.20* shows Pearson's correlation for output DC power against the output AC power during the 24-hour subsea operations. *Figure 7.15* is the scatter plots that confirm the DC output power from the 6.4kW-DPU thermoelectric power system during 24-hour subsea operations, which was transformed into AC power and delivered to an underwater power grid system.

A significant positive correlation was found between DC output power and AC output power from the 6.4kW-DPU thermoelectric power system during 24-hour subsea operations, $r(238) = 0.966$, $p < 0.001$. As shown by Pearson's correlation and the scatter plots, the p-value from the results of the experiments is less than 0.05. Therefore, a statistical relationship exists between the DC and AC output power. Consequently, it can be concluded that the experiments are repeatable, the outcomes are valid, and the results are validated.

Table 7.19 Confidence Intervals-AC Power to Grid (24-Hour Operations)

Confidence Interval for AC Power Delivered to Underwater Power Grid (24-Hours Subsea Operation)	
Mean	3.123515569
Standard Error	0.149263451
Median	3.241059357
Mode	#N/A
Standard Deviation	2.312379447
Sample Variance	5.347098709
Kurtosis	-1.39119638
Skewness	-0.072617674
Range	9.72950487
Minimum	-1.0290157
Maximum	8.700489169
Sum	749.6437367
Count	240
Confidence Level (95.0%)	0.294039955
Upper CI (95%)	3.417555524
Lower CI (95%)	2.829475614

Table 7.20 Pearson's Correlation (24-Hour Subsea Operations)

Pearson's Correlations (24-Hour Subsea Operation)

	n	**Pearson's r**	**p**
DC Power (kW) - AC Power (kW)	240	0.966	< .001

The power system stability investigation attempted to understand the system's behavior under stress by applying engineering principles as explained in ***Chapter 6*** and **Section 7.5.1**. The results from the experiments predicted the robustness of the ultra-deepwater and underwater power grid systems. That is, the outcome of the power system stability test verifies the system's energy conversion efficiency from heat to electrical power.

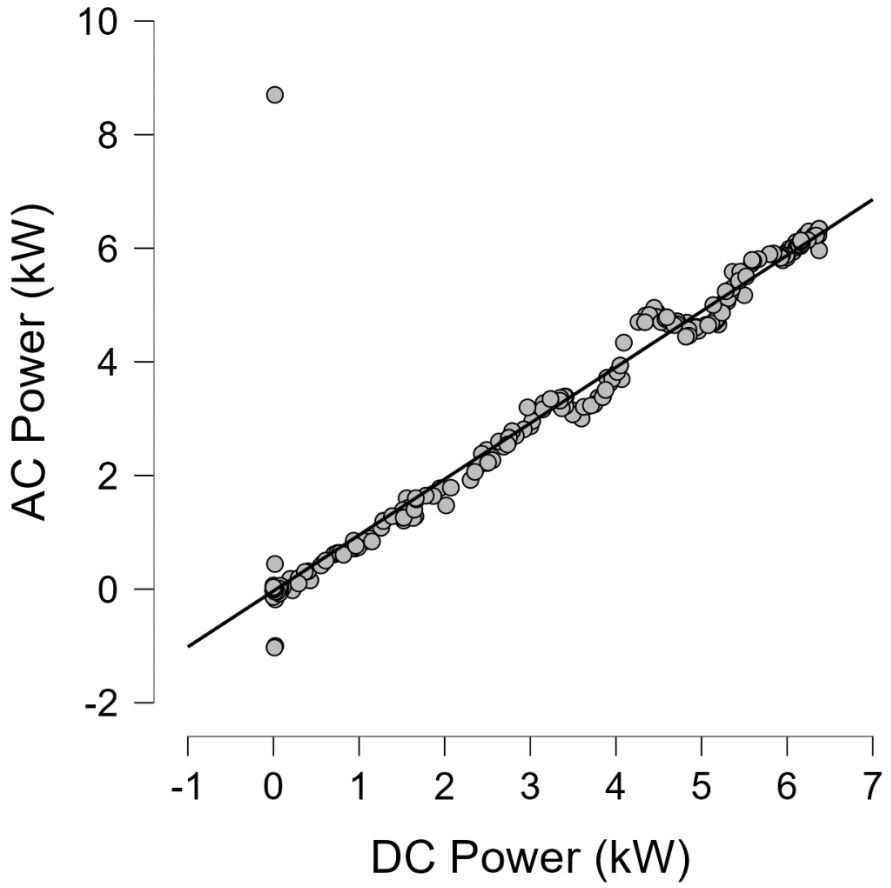

Figure 7.15 Scatter Plots – DC Power vs AC Power (24-Hour Subsea Operations)

The test reaffirms that the delivered AC power, voltage, and frequency met electrical power grid system requirements. Thirdly, the power quality of the grid system after transformation was high, hence validating the overall system. Fourthly, the statistical correlation between the DC output power and AC output power established a high level of agreement for the underwater power system design. This agreement certifies the accuracy and reliability of the system's ability to predict real-world performance.

The long-duration subsea operation experiments that had multiple peaks and troughs applied to the deepwater power system had significant achievements. However, the remarkable feats from this research were not compared with theoretical expectations or subsea oil and gas industry benchmarks because such information is not available. Future research can further address these shortcomings and collaborate with industry partners to conduct joint field trials, thereby validating the power system's functionalities in an oil-gas exploration and production environment. Be that as it may, the validation process employed above provided a thorough insight into the underwater power system performance, reliability, and adaptability in challenging ultra-deepwater environments.

7.7. Chapter Summary

A reference frame was given to an ultra-deepwater oil and gas field in West Africa through the field's systems design and development in ***Chapters 5*** and ***6***. ***Chapter 7*** defined the characteristics of the oil-gas field for the inclusivity of thermoelectricity. This Chapter further analysed the results of experiments in ***Chapters 3***, ***4***, and ***6***. It is important to note that the oil-gas field systems design and DTEG power system component sizing from ***Chapter 5*** were used in ***Chapter 6***. Emphasis was provided on transforming DC outputs from the 6.4 kW-DPU thermoelectric power source into three (3) phase AC outputs. The transformed AC power was supplied to an underwater combo power grid system of renewable and non-renewable sources in ***Chapter 6***. The transformed DC to AC outputs delivered to the seafloor power grid system were validated in ***Chapters 6*** and ***7***. This

Chapter finalises the main body of work in this project. Next, the achievements and benefits of this study are discussed. Furthermore, the limitations encountered during this research, as well as upcoming plans and conclusions, are discussed in ***Chapter 8***.

Chapter 8

Discussions & Conclusions

8.1. Discussions and Conclusions

This Chapter focuses on two sections: the discussions and conclusions. ***Chapter 8*** highlights the milestones, research accomplishments, and impediments. The research aim and question are restated at the start of this Chapter. The key findings, innovations, and contributions are discussed. Furthermore, new ideas are brought to the fore. The limitations are acknowledged, recommendations and future plans are also made.

8.2. Discussions

8.2.1. The Research Aim and Question

The research aim and research question are stated as follows:

Research Aim

This research aimed to design an ultra or deepwater thermoelectric power-generating system capable of harnessing geothermal heat from oil and gas reservoirs and converting it to electricity.

Research Question

How best can energy be generated at the seafloor to provide electrical power to critical subsea control equipment during deepwater or ultra-deepwater oil-gas exploration and production activities?

8.2.2. The Key Findings

In this research, a temperature difference was applied across the surfaces of commercially available thermoelectric modules (Device-TEM-03), and electricity was generated. The underwater power system process was initiated when thirty-six (36) Device-TEM-03 integrated with subsea electronic systems, marinised at 6000 psi, and subsea operating temperature difference ranging from 0 to 150 degrees Celsius was applied on the system. The flexible deepwater power plate (Flex-250W-DPP) on a subsea wellhead harvested waste heat from subsea oil and gas reservoirs and converted it into electricity. The electricity was supplied to subsea equipment and stored for future use in subsea battery (Device-SBAT-101).

Thirty (30) flexible deepwater power plates (Flex-250W-DPP) were configured into 6.4kW-DPU (deepwater thermoelectric power unit) on 333 square meters of subsea flow system infrastructure. The 6.4kW-DPU was rated at 174 V and 36.75 A for a 70 square kilometers oil-gas field at water depths ranging from 1500 to 3000 meters mean sea level (MSL). The 6.4kW-DPU operation was supported by a 6120 Ah capacity subsea battery-bank for 24 hours a day, 7 days a week, and 365 days a year. Furthermore, the DC power

output from 6.4kW-DPU was transformed into high-quality AC power and delivered to an underwater combo power grid system. The combo power grid system is an underwater infinite energy storage system of renewable and non-renewable energy sources.

8.2.3. Novelty of the Research

1. A new and simplified concept for thermoelectric power system tests is now available for testing single and multiple commercial thermoelectric modules (TEMs). The test bench developed during the research is portable; thermoelectric generator components can be easily assembled and disassembled. The innovative test system is a significant shift from the old method of machining thermoelectric modules on pipelines and fluid-flowing structures, which often leads to damaging thermoelectric modules and a reduction in the structural integrity of the flowline or pipeline. This test system can be modified and upgraded to accommodate more TEMs by adding more sensing, measurement, monitoring, and control devices. This test bench is the first modern thermoelectric power-generating system representing a subsea oil and gas environment in a laboratory setting before proceeding on field tests or offshore trials.

2. A tool for determining electrical power parameters from a thermoelectric power system has emerged. The power tool can compute specifications such as open circuit voltage, short circuit current, output voltage, output current, and output power. This unique tool is the first deepwater power system framework that

accepts the input for the number of series and parallel connected thermoelectric modules and instantly determines the system performance metrics. The power tool can establish suitable deepwater power plate (DPPs) configurations and, by extension, a deepwater power unit (DPU) composition. Furthermore, the power system tool can estimate electrical power requirements for critical and non-critical subsea equipment of any deepwater or ultra-deepwater oil-gas installation.

3. Development of a power interface system using power electronic components for optimal heat conversion from deepwater oil and gas reservoirs to electrical power. This power system interface utilises underwater control system algorithms for waste heat harvesting, harnessing, and conversion to electrical power generation. The power system interface is the first for any underwater application.

4. Subsea battery control system for electric current and voltage through DC-DC converters and bi-directional power converters are now possible on the seafloor. The battery power system presented in this work is the first energy management system for converting electrical energy through a deepwater thermoelectric power system to chemical energy stored in the subsea battery. Through the control system or energy management system, subsea batteries can supply electrical power to critical seabed equipment and equipment inside subsea wells.

5. The absence of technology for precisely predicting the sea state at a particular time of the day, night, week, month, or year led to the development of the first short-duration (4-hour) and long-duration (24-hour) subsea operation templates for deepwater thermoelectric power generation. These subsea temperature difference templates can operate deepwater thermoelectric power systems of any size or power rating at any time, irrespective of the sea conditions or seasons of the year.

6. Deepwater thermoelectric power-driven oil and gas fields are now feasible. Thermoelectric-powered oil-gas fields can be applied anywhere across the globe. This first ultra-deepwater oil-gas field comprises 56 subsea wells (producers and injectors) in a cluster arrangement. The 6.4 kW capacity-powered oil-gas infrastructure has subsea wellheads, subsea Christmas trees (XTrees), manifolds, pressure and temperature transmitters, multiphase flow meters (MFMs), chemical injection systems, downhole equipment, flowlines, pipelines, production risers, and other subsea systems.

7. DC power was transformed to AC power through a two-stage power conversion control strategy and frame-transformation procedure. This research provided the first DC-to-AC power reconstruction and delivery of three-phase power to the first underwater combo power grid system comprising renewable and non-renewable power sources.

8.2.4. Original Contributions

First, electricity was generated through a thermoelectric power system from the by-product of oil-gas reservoirs during ultra-deepwater production operations. This in-situ-based power system design considerably reduces the dependence on the topside or platform-based electrical power transmission to the sea floor, especially if there is an emergency on such topside or platform. Also, the response time for power supply to critical subsea equipment via deepwater thermoelectricity offers considerable improvement compared to the traditional method of platform-to-seabed power transmission.

Secondly, this work's deepwater thermoelectric power system for electricity generation and distribution applies to deepwater or ultra-deepwater oil-gas exploration (drilling) and production fields worldwide. As such, if flexible deepwater power plates (Flex-DPPs) were a part of Deepwater Horizon, the electricity generated on the ocean floor would have been sufficient to operate the Deepwater Horizon's BOP at maximum capacity in the US Gulf of Mexico. Likewise, if there had been a deepwater power unit (DPU) on site, the Macondo subsea oil well would have been promptly sealed, thus preventing the emergency that happened on the 20th of April 2010. Perhaps the explosion would not have happened, and about 5 million barrels of oil wouldn't have spilled if Flex-DPPs had been on the drilling riser or drilling fluids flow paths into and out of the Macondo subsea well. Again, if this were the case, sufficient electrical power would have been generated and supplied to the subsea BOP when required. Hence, there would have been no explosion

or fire incident on the offshore drilling rig. Therefore, there would have been no loss of lives, environmental pollution, or ill reputation in the industry. Furthermore, this approach of deepwater power generation and supply to subsea equipment has not been used elsewhere.

Thirdly, West Africa has many offshore renewable energy opportunities; however, the region's lack of the necessary infrastructure is of concern. Generally, oil and gas from shallow water, deepwater, and ultra-deepwater fields are predominant in Africa. This deepwater thermoelectric power system and the underwater combo power grid system combine multiple power sources on the backbone of oil-gas infrastructure. The work has demonstrated electrical power generation, storage, and supply to subsea equipment. It has also revealed that delivering electrical power to an underwater power grid system is possible on the seafloor. Subsea equipment are the expected beneficiary of the deepwater power scheme, thus paving the way for surplus energy from the seafloor back to shore. This initiative is poised to be a win-win for the oil-gas industry and sub-Saharan African communities.

8.2.5. Additional Information

A new approach has been created for waste heat to electricity generation, energy storage, utilisation, and delivery to an underwater power grid system. The new concept is an addition to the body of knowledge. Besides, the methods in this research aim to eliminate intermittent power (intermittency) issues typical in most renewable energy resources.

Secondly, electrical energy sufficiency at the seafloor through the deepwater thermoelectric power system is determined to end the seabed power rationing concept among subsea systems. The proposed deepwater power system suggests changing the type of components installed on the seafloor. An example is the seabed deployment of very low-power microcontrollers and low-scale processors in subsea electronics modules (SEMs) instead of high-power gadgets (such as Quad Pentium processors or higher devices) with enormous computing capability. Therefore, introducing DTEG power systems on the seabed is synonymous with introducing high-end electrical and electronic appliances capable of improving the quality and performance of future subsea systems. Additionally, the design, manufacturing, and implementation of subsea systems will be significantly enhanced when there is a sufficient power supply on the seafloor for the new generation of subsea components.

Furthermore, deploying state-of-the-art subsea devices will bring about automated engineering workflows between personnel and subsea equipment on the seafloor. The proposed DTEG power system and state-of-the-art subsea machines will consistently establish direct communications with cutting-edge equipment for drilling, production, and other operations. The new approach will augment cooperation among offshore staff and onshore or land-based personnel. In addition, the information exchange strategy can potentially foster revolutionary ‘seabed-to-cloud’ reservoir engineering and computing technologies. The envisioned seabed-to-cloud technique will strengthen team

collaboration and deliver the right data to the relevant people at the right time for effective asset decision-making while maximizing oil-gas recovery. Similarly, information flow will enhance operational efficiency and enthronement of a modern deepwater or ultra-deepwater digital oil-gas field (DOGF).

8.2.6. Limitations

The manufacturer's (specified) maximum output power from the thermoelectric module (Device-TEM-03) at 220 °C temperature difference was 6.99 W. However, the output power of the same Device-TEM-03 via the test rig was 1.06 W at a temperature difference of 70 °C. Therefore, the derived low output power was attributed to the low-temperature difference applied to the device during the bench test. Low-temperature difference was used because deepwater oil and gas reservoirs temperature at the seabed is generally less than 220 °C. It also means that the thermoelectric modules used in this work were underutilised; hence, the power-generating capability of Device-TEM-03 was not at its maximum. Under-utilisation is a drawback. It is important to note that the use of non-specified devices, components, and methods recommended by the TEM manufacturer directly and indirectly impacted the outcome of the experiments.

Secondly, measuring the precise temperatures of the hot and cold sides of the thermoelectric modules (Device-TEM-03) during the test was challenging. Therefore, pieces of flat metals fitted between the thermoelectric modules, the hotside-blocks, and

the coldside-blocks facilitated hotside and coldside temperature sensing and measurement through Temperature Data Recorder-ADN-03 and Temperature Data Recorder-ADN-04 instead of direct measurements from the surfaces of the thermoelectric modules. Additionally, these flat pieces of metals on both sides of the modules made the coupling of the TEM assemblies not seamless, thus introducing heat loss from the heat source (Hotplate-HPL-X01) to the thermoelectric modules. Lost heat was a setback in the power system experiments. However, the losses were minimised using foam wrapped around the power system assemblies. Be that as it may, the heat losses introduced inefficiency, thus impacting the accuracy of the results.

Thirdly, the proposed deepwater thermoelectric modules (Flex-DTEMs) will be flexible devices. These flexible DTEMs will be incorporated into deepwater power plates (DPPs). The Flex-DPPs will be directly mounted on subsea flowlines or fluid flow structures to prevent heat losses and maximize power generation at the ocean floor. Moreover, the operating temperature and pressure ratings of Flex-DTEMs will be location/site-specific, with provisions for temperature allowances. For instance, the temperature of flowing crude oil, gas, and water mixture from subsea reservoirs in Brazil, Agbami-Nigeria, Cherbourg-France, and Cascade-Chinook in the US Gulf of Mexico is up to 60 °C, 116 °C, 120 °C, and 126 °C, respectively. Therefore, the specified maximum operating temperature (plus 20% allowance) of the intended Flex-DTEMs for each of these locations will be approximately 72 °C, 139.2 °C, 144 °C and 151.2 °C, respectively. Furthermore, subsea pressure, corrosion resistance, marine growth, and other local/site or sea influences

should be factored into the engineering, manufacturing, and installation of the proposed Flex-DTEMs, Flex-DPPs, DPU, and other DTEG power system components.

Finally, some drawbacks during the study included limited access to high-end research equipment and data access. The lack of access to research data from oil-gas corporations and the absence of advanced equipment, tools, etc., were among the factors that impacted the project. Additionally, funding constraints from start to finish of this project had a negative effect on this research. Despite these limitations, a new method of energy harvesting, power generation, and electrical power supply to subsea equipment on the seafloor and beyond the deep seafloor has been born.

8.2.7. Future Research

Commercially available thermoelectric modules used in this project (Device-TEM-01, Device-TEM-02, and Device-TEM-03) were tested by applying temperature difference to the power-generating devices. The test provided a physical demonstration and proof of direct conversion of heat to electricity. Developed computer models and simulation results agreed with those obtained from parameter design and calculations. Furthermore, the outcomes of the experiments were in line with results from standard electrical power systems. Thus, this study's experiments and power system models have shown potential for further evaluation and investments in deepwater thermoelectric power generation. The technology's enormous potential requires additional appraisal and funding of deepwater

thermoelectricity because no deepwater or ultra-deepwater thermoelectric power system or power plant exists worldwide.

The deepwater thermoelectric power system can maximize geothermal and ocean-floor energy capabilities in a safe, affordable, sustainable, and environmentally sensitive manner. Conversely, developing third-generation or nanotechnology-driven thermoelectric devices is an ongoing area of research. Likewise, the next phase of this research is the testing for the onward supply of electricity from this unique underwater power grid system to critical, non-critical subsea equipment and beyond.

8.3. Conclusions

The oil and gas industry has been powering the world economically and otherwise for nearly a century. However, there is a shortfall in the technique for providing electricity to subsea equipment during deepwater or ultra-deepwater exploration and production. This Ph.D. work presented a new approach to electricity generation and distribution to subsea equipment on the seafloor through a Deepwater thermoelectric power system (DTEG).

In this work, waste heat from ultra-deepwater oil and gas reservoirs was converted to electrical power. Generated electricity was stored in subsea batteries as chemical energy and supplied as electrical power to critical subsea equipment. Subsequently, 6.4 kW DC-generated electrical power was transformed into AC power and delivered to the first underwater combo power grid system of renewable and non-renewable energy systems.

The DTEG power system has the potential to supply subsea equipment and transmit electrical power from the seafloor back to shore.

This investigation was necessary because research findings show the overbearing dependence on power transmission from topsides/platforms to the seabed. Historical evidence shows that unplanned power failures on platforms or topsides of these oil and gas installations have led to explosions. Such catastrophes often lead to the loss of lives, environmental damage, and the loss of assets. This innovative deepwater power system can prevent electrical power failure during vital subsea operations. Furthermore, the technique in this report is poised to change the narrative while opening up new frontiers in offshore sustainable energy.

This work has provided sufficient evidence to conclude that waste heat from deepwater or ultra-deepwater oil and gas reservoirs can be harvested, harnessed, and converted to electrical energy through Flex-DTEMs, Flex-DPPs, and DPUs. Thus, deepwater thermoelectric power systems are the future.

References

Achparaki, M. *et al.* (2012) 'Automotive Waste Heat Recovery by Thermoelectric Generator Technology. Chapter 9', *Intechopen. ISSN:18734359*, p. 13. Available at: http://dx.doi.org/10.5772/intechopen.75443.

Africa Oil Week (2019) *Africa oil & Gas Project Watch: West Africa, 5 must-see West African oil & gas developments*. Available at: https://africa-oilweek.com/Articles (Accessed: 10 May 2020).

Ahiska, R. and Dişlitaş, S. (2006) 'Microcontroller Based Thermoelectric Generator Application. 19(2): 135-141 (2006)', *G.U. Journal of Science*, pp. 135–141. Available at: www.gujs.org.

Ahmad, S., Mekhilef, S. and Mokhlis, H. (2020) 'DQ-axis Synchronous Reference Frame based P-Q Control of Grid Connected AC Microgrid', in *2020 IEEE International Conference on Computing, Power and Communication Technologies (GUCON). ISBN:978-1-7281-5070-3*. IEEE, pp. 842–847.

Aktaibi, A., Rahman, M. A. and Razali, A. M. (2014) 'An Experimental Implementation of the dq-Axis Wavelet Packet Transform Hybrid Technique for Three-Phase Power Transformer Protection', *IEEE Transactions on Industry Applications. ISSN:0093-9994*, 50(4), pp. 2919–2927. doi: 10.1109/TIA.2013.2292999.

Al-Shetwi, A. Q. *et al.* (2020) 'Grid-connected renewable energy sources: Review of the recent integration requirements and control methods', *Journal of Cleaner Production*. Elsevier Ltd, 253, p. 119831. doi: 10.1016/j.jclepro.2019.119831.

Aljaghtham, M. and Celik, E. (2020) 'Design optimization of oil pan thermoelectric generator to recover waste heat from internal combustion engines', *Energy*. Elsevier Ltd, 200, p. 117547. doi: 10.1016/j.energy.2020.117547.

Amar, A., Kouki, A. and Cao, H. (2015) 'Power Approaches for Implantable Medical Devices. ISBN:2888928914', *Sensors*, 15(11), pp. 28889–28914. doi: 10.3390/s151128889.

API (2009) *ANSI/API Recommended Practice 17H. ISO 13628-8:2002 (Identical), Petroleum and natural gas industries. Remotely Operated Vehicle (ROV) Interfaces on Subsea Production Systems*.

Araiz, M. *et al.* (2020) 'Prospects of waste-heat recovery from a real industry using thermoelectric generators: Economic and power output analysis', *Energy Conversion and Management*. Elsevier, 205(September 2019), p. 112376. doi: 10.1016/j.enconman.2019.112376.

Asiegbu, N. M. (2021) 'Design of a Combined Offshore Renewable Energy System for Bonny Nigeria Based on Comparative Feasibility Analysis', *International Journal of*

Renewable Energy Research, 11(3), pp. 967–980. doi: 10.20508/ijrer.v11i3.11674.g8229.

Ateme, M. E. (2021) 'Developing marine and coastal resources in Nigeria: Prospects and challenges', *Maritime Technology and Research*, 3(4), pp. 335–347. doi: 10.33175/mtr.2021.244473.

Bae, H. S. *et al.* (2005) 'New control strategy for 2-stage utility-connected photovoltaic power conditioning system with a low cost digital processor', *PESC Record - IEEE Annual Power Electronics Specialists Conference*, 2005, pp. 2925–2929. doi: 10.1109/PESC.2005.1582049.

Bai, Y. and Bai, Q. (2019) 'Heat Transfer and Thermal Insulation', in *Subsea Engineering Handbook. ISBN:978-0-12-812622-6*. Second Edi. Gulf Professional Publishing. Elsevier Inc., pp. 364–408.

Basit, M. A. *et al.* (2020) 'Limitations, challenges, and solution approaches in grid-connected renewable energy systems', *International Journal of Energy Research*, 44(6), pp. 4132–4162. doi: 10.1002/er.5033.

Bernt, T. and Smedsrud, E. (2007) 'Ormen Lange Subsea Production System. OTC-18965-MS. ISBN: 978-1-55563-254-0', (April 2007).

Biswas, K. *et al.* (2012) 'High-performance bulk thermoelectrics with all-scale hierarchical architectures. ISSN: 14764687', *Nature*, 489(7416), pp. 414–418. doi: 10.1038/nature11439.

Bjerkreim, B. *et al.* (2009) 'Ormen Lange Subsea Compression Pilot System', in *Proceedings of Offshore Technology Conference, DOI:10.4043/OTC-20028-MS*. The Offshore Technology Conference. doi: 10.4043/OTC-20028-MS.

Bradwell, D. J. *et al.* (2012) 'Magnesium–Antimony Liquid Metal Battery for Stationary Energy Storage', *Journal of the American Chemical Society*, 134(4), pp. 1895–1897. doi: 10.1021/ja209759s.

Brown, S. R. *et al.* (2006) 'Yb 14MnSb 11: New high efficiency thermoelectric material for power generation. ISSN: 08974756', *Chemistry of Materials*, 18(7), pp. 1873–1877. doi: 10.1021/cm060261t.

Bunn, D. W. and Muñoz, J. I. (2016) 'Supporting the externality of intermittency in policies for renewable energy', *Energy Policy*. Elsevier Ltd, 88, pp. 594–602. doi: 10.1016/j.enpol.2015.07.036.

Bybee, K. (2002) 'Geothermal-Hot-Water Waterflood', *Journal of Petroleum Technol 54 (01): 49. Paper Number: SPE-0102-0049-JPT. https://doi.org/10.2118/0102-0049-JPT*.

Byrne, S., Juguet, J. P. and Dubourdieu, P. (1998) 'APAC concept: A new umbilical-less subsea control system', in *Subsea Controls and Data Acquisition 1998: Cost Effective Challenges for a Geographically Expanding Industry, SCADA 1998*, pp. 119–135. doi: 0 906940 32 X.

Caillat, T., Borshchevsky, A. and Fleurial, J. P. (1996) 'Properties of single crystalline semiconducting CoSb3. ISSN: 00218979', *Journal of Applied Physics*, 80(8), pp. 4442–4449. doi: 10.1063/1.363405.

Cao, Q., Luan, W. and Wang, T. (2018) 'Performance enhancement of heat pipes assisted thermoelectric generator for automobile exhaust heat recovery. ISSN:13594311', *Applied Thermal Engineering*. Elsevier Ltd, 130, pp. 1472–1479. doi: 10.1016/j.applthermaleng.2017.09.134.

Casi, Á. *et al.* (2021) 'Thermoelectric heat recovery in a real industry: From laboratory optimization to reality', *Applied Thermal Engineering*, 184(September 2020). doi: 10.1016/j.applthermaleng.2020.116275.

Cavallo, A. (2007) 'Controllable and affordable utility-scale electricity from intermittent wind resources and compressed air energy storage (CAES)', *Energy*, 32(2), pp. 120–127. doi: 10.1016/j.energy.2006.03.018.

Chakrabarti, S. K. (2005a) *Handbook of Offshore Engineering. ISBN-13: 978-0-08-044568-7*. Volume 1. Elsevier Ltd.

Chakrabarti, S. K. (2005b) *Handbook of Offshore Engineering. ISBN-13: 978-0-08-044569-4*. Volume 2. Elsevier Ltd.

Champier, D. (2017) 'Thermoelectric generators: A review of applications', *Energy Conversion and Management*. Elsevier Ltd, 140, pp. 167–181. doi: 10.1016/j.enconman.2017.02.070.

Chandler, D. L. (2009) 'Liquid battery big enough for the electric grid ?', *MIT News Office, Massachusetts Institute of Technology*, (November 19, 2009), pp. 1–3. Available at: https://news.mit.edu/2009/liquid-battery.

Chen, Z.-G. *et al.* (2012) 'Nanostructured thermoelectric materials: Current research and future challenge.', *Progress in Natural Science: Materials International*. Elsevier, 22(6), pp. 535–549. doi: 10.1016/j.pnsc.2012.11.011.

Choi, B. (2013) 'Pulsewidth Modulated DC-to-DC Power Conversion Circuits, Dynamics, and Control Designs', in *ISBN 978-1-118-18063-1*. IEEE PRESS, WILEY.

Crane, D., Jackson, G. and Holloway, D. (2001) 'Towards optimization of automotive waste heat recovery using thermoelectrics', *SAE Technical Papers*, p. 7191. doi: 10.4271/2001-01-1021.

Crane, D. T. and Lagrandeur, J. W. (2010) 'Progress Report on BSST-Led US Department of Energy Automotive Waste Heat Recovery Program.', *Journal of ELECTRONIC MATERIALS*, 39(9), pp. 2142–2148. doi: 10.1007/s11664-009-0991-0.

Dam, D. H. and Lee, H. H. (2018) 'A Power Distributed Control Method for Proportional Load Power Sharing and Bus Voltage Restoration in a DC Microgrid', *IEEE Transactions on Industry Applications*. IEEE, 54(4), pp. 3616–3625. doi: 10.1109/TIA.2018.2815661.

Davis, J. E. (2011) ‘ROV: Improving Remotely Operated(ROV) Intervention Capabilities for Blowout Preventer Override Systems’, in *Offshore Technology Conference, OTC-21322-MS. ISBN: 978-1-61399-117-6*. OTC, pp. 1–5. doi: 10.4043/21322-MS.

Deepwater-Horizon-56C17 (2010) *Deepwater_Horizon Image*, *Deepwater-Horizon*. Available at: www.deepwater.com (Accessed: 10 July 2016).

Denney, D. (2007) ‘Erha and Erha North development’, *JPT, Journal of Petroleum Technology*, 59(6), pp. 54–57. doi: 10.2118/0607-0054-JPT.

Dilhac, J. M. *et al.* (2014) ‘Implementation of thermoelectric generators in airliners for powering battery-free wireless sensor networks’, *Journal of Electronic Materials*, 43(6), pp. 2444–2451. doi: 10.1007/s11664-014-3150-1.

Dismukes, J. P. *et al.* (1964) ‘Thermal and electrical properties of heavily doped Ge-Si alloys up to 1300°K. ISSN: 00218979’, *Journal of Applied Physics*, 35(10), pp. 2899–2907. doi: 10.1063/1.1713126.

Doughty, D. H. *et al.* (2010) ‘Batteries for Large-Scale Stationary Electrical Energy Storage’, *The Electrochemical Society Interface*, 19(3), pp. 49–53. doi: 10.1149/2.F05103if.

Dril-Quip (2018) *Production Control System*, *Multiplex Control System*. Available at: www.dril-quip.com (Accessed: 14 March 2019).

Dubourdieu, P., Tribou, G. and Byrne, S. (1997) ‘Thermoelectric Generator for Underwater Wellhead. ISBN:0780340574’, *International Conference on Thermoelectrics, ICT, Proceedings*, pp. 603–606. doi: 10.1109/ict.1997.667603.

E Oug, A Tobiesen, T. M. (2003) *Marine growth in cooling plant at drilling installation, Nigeria. S/No. 4641, Report No.O-21349. Statoil ASA, Contract 4500462433*. Available at: www.niva.no.

Ekejiuba, A. I. B. (2021) ‘Cumulative Potential Petroleum Deposit in the Provincial Geology of Nigeria. Durson Associations. http://www.rdursonassociations.com’, *INTER-WORLD JOURNAL OF SCIENCE AND TECHNOLOGY*, 4(2), pp. 150–176.

Elankovan, R. *et al.* (2019) ‘Evaluation of thermoelectric power generated through waste heat recovery from long ducts and different thermal system configurations’, *Energy*. Elsevier Ltd, 185, pp. 477–491. doi: 10.1016/j.energy.2019.07.039.

Elmoughni, H. M. *et al.* (2019) ‘A Textile-Integrated Polymer Thermoelectric Generator for Body Heat Harvesting’, *Advanced Materials Technologies*, 4(7), p. 1800708. doi: 10.1002/admt.201800708.

Engineer, H. R. *et al.* (2015) ‘A review on the potential sources for producing electricity with thermoelectric generators and different configurations’, *International Journal of Energy and Statistics. ISSN: 2335-6804*, 03(04), pp. 15500 1–19. doi: 10.1142/S2335680415500192.

Esram, T. and Chapman, P. L. (2007) 'Comparison of Photovoltaic Array Maximum Power Point Tracking Techniques', *IEEE Transactions on Energy Conversion*, 22(2), pp. 439–449. doi: 10.1109/TEC.2006.874230.

European-Commission (2019) *North Seas Energy Cooperation (NSEC), Annex 1-Work programme. NSEC Ministerial Meeting on 4 December 2019. https://energy.ec.europa.eu. Accessed: 13th, Dec. 2020*.

Ferrotec (2001) *Power Generation, Power Generation-Thermoelectric Technical Reference*. Available at: www.ferrotec.com Access on 14 September 2016.

G. S. Nolas, G. A. S. (2001) 'Thermoelectric Clathrates: Cagelike crystals may soon help to pump heat with electricity and to create electricity with heat. ISSN 0003-0996', *American Scientist*, Vol. 89, N, pp. 136-141 (6 pages). Available at: https://www.jstor.org/stable/27857436.

Gao, C. H., Rajeswaran, R. T. and Nakagawa, E. Y. (2007) 'A Literature Review on Smart Well Technology.', in *Production and Operations Symposium. ISBN: 978-1-55563-194-9*. SPE. doi: 10.2118/106011-MS.

Garbuglia, E., Calore, D. and Guaita, P. (1997) 'Future Developments in Subsea Autonomous Control Systems', in *Society of Petroleum Engineers (SPE)*. SPE. doi: 10.2118/38517-MS.

García-Cañadas, J. *et al.* (2013) 'Fabrication and Evaluation of a Skutterudite-Based Thermoelectric Module for High-Temperature Applications. ISSN:0361-5235', *Journal of Electronic Materials*, 42(7), pp. 1369–1374. doi: 10.1007/s11664-012-2241-0.

GE (2014) *Christmas Tree, What the GEek?.The GE Christmas tree.* Available at: https://www.ge.com (Accessed: 10 April 2019).

Goode, P. (2005) 'Progress towards the digital oilfield: Evolution or revolution?', *Proceedings of the Annual Offshore Technology Conference*, 2005-May(May), pp. 2294–2299. doi: 10.4043/17728-ms.

Goodfellow, R., Webb, A. and Harbonn, J. (1974) 'Subsea experience gained at Zakum. ISSN:01603663', *Proceedings of the Annual Offshore Technology Conference*, 1974-May(April), pp. 79–86. doi: 10.4043/1942-ms.

Gurrola-Corral, C. *et al.* (2020) 'Optimal LCL-filter design method for grid-connected renewable energy sources', *International Journal of Electrical Power and Energy Systems*. Elsevier, 120(8), p. 105998. doi: 10.1016/j.ijepes.2020.105998.

Haddad, Z. *et al.* (2011) 'The design and execution of frac jobs in the ultra deepwater lower tertiary wilcox formation', *Proceedings - SPE Annual Technical Conference and Exhibition*, 5, pp. 3859–3880. doi: 10.2118/147237-ms.

Han, C., Li, Z. and Dou, S. (2014) 'Recent progress in thermoelectric materials', *Chinese Science Bulletin*, 59(18), pp. 2073–2091. doi: 10.1007/s11434-014-0237-2.

Hardisty, J. (2008) ‘Power intermittency, redundancy and tidal phasing around the United Kingdom’, *Geographical Journal*, 174(1), pp. 76–84. doi: 10.1111/j.1475-4959.2007.00263.x.

Hasaneen, B. M. and Mohammed, A. A. E. (2008) ‘DESIGN AND SIMULATION OF DC / DC BOOST CONVERTER. ISBN:9781424419333’, *IEEE, 978-1-4244-1933-3/08/2008*. IEEE, pp. 335–340.

Hatzikraniotis, E. *et al.* (2010) ‘Efficiency study of a commercial thermoelectric power generator (TEG) under thermal cycling. ISSN:03615235’, *Journal of Electronic Materials*, 39(9), pp. 2112–2116. doi: 10.1007/s11664-009-0988-8.

Hébert, S. (2014) ‘The search for new thermoelectric materials.’, *Reflections phys.*, (41), pp. 18–22. doi: 10.1051/refdp/201441018.

Heuberger, C. F. *et al.* (2017) ‘A systems approach to quantifying the value of power generation and energy storage technologies in future electricity networks’, *Computers and Chemical Engineering*. Elsevier Ltd, 107, pp. 247–256. doi: 10.1016/j.compchemeng.2017.05.012.

Hi-Z_Technology (2006) *Thermoelectric Generator Modules (TEM). HZ-20HV, 20W TEG Module Data Sheet*. Available at: www.hi-z.com (Accessed: 12 January 2018).

Holand, P. (1996) *Offshore Blowouts, Causes and Trends. Doctoral Dissertation*. Norwegian Institute of Technology, NTNU: Norwegian University of Science and Technology. Available at: www.ntnu.edu.

Hoque, M. M. *et al.* (2017) ‘Battery charge equalization controller in electric vehicle applications: A review’, *Renewable and Sustainable Energy Reviews*. Elsevier Ltd, 75(November 2016), pp. 1363–1385. doi: 10.1016/j.rser.2016.11.126.

Hovem, L. A. *et al.* (2014) ‘Managing risk in deepwater frontiers - Key learnings from five continents’, *World Petroleum Congress Proceedings. ISBN:9781510825673*, 2, pp. 949–958.

Howimanporn, S. and Bunlaksananusorn, C. (2003) ‘Performance comparison of continuous conduction mode (CCM) and discontinuous conduction mode (DCM) flyback converters’, *Proceedings of the International Conference on Power Electronics and Drive Systems. ISSN: 0780378857*, 2(Ccm), pp. 1434–1438. doi: 10.1109/PEDS.2003.1283194.

IEC-61508 (2010) *International Electrotechnical Commission. Functional safety of electrical/electronic/programmable electronic safety-related systems - Part 1: General requirements. TC 65/SC 65A. International Standard. Publication date 30-04-2010. Edition 2.0.*

IEC-61511 (2016) *International Electrotechnical Commission. Functional safety - Safety instrumented systems for the process industry sector - Part 1: Framework, definitions, system, hardware and application programming requirements. TC 65/SC 65A. International Standard. P*.

IEEE (2014) *Draft Recommended Practice for Sizing Nickel-Cadmium Batteries for Stationary Applications Date of Publication. The Institute of Electrical and Electronics Engineers. e-ISBN:978-0-7381-8532-3*.

IEEE (2020) *Recommended Practice for Sizing Lead-Acid Batteries for Stationary Applications. The Institute of Electrical and Electronics Engineers. e-ISBN:978-1-5044-6703-2*.

Iezzi, B. *et al.* (2017) 'Printed, metallic thermoelectric generators integrated with pipe insulation for powering wireless sensors', *Applied Energy*. Elsevier, 208(May), pp. 758–765. doi: 10.1016/j.apenergy.2017.09.073.

Indragandhi, V., Subramaniyaswamy, V. and Logesh, R. (2017) 'Topological review and analysis of DC-DC boost converters', *Journal of Engineering Science and Technology, ISSN: 18234690*, 12(6), pp. 1541–1567.

Ioffe A.F. (1957) 'Semiconductor Thermoelements and Thermo-Electric Cooling', *London-Infosearch*, 4(3), p. 27. doi: 10.1016/0038-092X(60)90073-6.

ISA (2007) *Flow Equations for Sizing Control Valves. The International Society of Automation.* Research Triangle Park, USA.

ISA (2010) *Recommended Practice-Fossil Fuel Power Plant Human-Machine Interface: Hard Panel Alarms. The International Society of Automation. ISBN: 978-1-936007-68-4*.

J. O. Ahaotu, B. Nkoi, B. T. A. (2018) 'Thermodynamic Design and Economic Analysis of Ocean Thermal Energy Conversion for Coastal Nigeria. E-ISSN: 2320-0847 p-ISSN: 2320-0936', *American Journal of Engineering Research (AJER)*, (12), pp. 120–128.

Jeon, H.-W. *et al.* (1991) 'Electrical and thermoelectrical properties of undoped Bi2Te3-Sb2Te3 and Bi2Te3-Sb2Te3-Sb2Se3 single crystals. ISSN: 00223697', *Journal of Physics and Chemistry of Solids*, 52(4), pp. 579–585. doi: 10.1016/0022-3697(91)90151-O.

Johnson, F. C. (Pat) (1967) 'The Underwater Power. SOCIETY OF PETROLEUM ENGINEERS OF AIME', *Society of Petroleum Engineers OF AIME*, SPE1911, pp. 1–11.

Kaibe, H. *et al.* (2012) 'Thermoelectric generating system attached to a carburizing furnace at Komatsu Ltd., Awazu Plant', *AIP Conference Proceedings*, 1449(June 2012), pp. 524–527. doi: 10.1063/1.4731609.

Kamala Devi, V. *et al.* (2017) 'A modified Perturb & Observe MPPT technique to tackle steady state and rapidly varying atmospheric conditions', *Solar Energy*. Elsevier, 157(August), pp. 419–426. doi: 10.1016/j.solener.2017.08.059.

Kanatzidis, M. G.; Dravid, V. P.; Zhao, L.-D. (2014) 'The panoscopic approach to high performance thermoelectrics. ISSN:1754-5692', *Energy Environ. Sci.*, 7(1), pp. 251–268. doi: 10.1039/C3EE43099E.

Kao, P. H. *et al.* (2010) 'Fabrication and characterization of CMOS-MEMS thermoelectric

micro generators', *Sensors*, 10(2), pp. 1315–1325. doi: 10.3390/s100201315.

Karimi-Ghartemani, M. and Iravani, M. R. (2001) 'A new phase-locked loop (PLL) system', in *Proceedings of the 44th IEEE 2001 Midwest Symposium on Circuits and Systems. MWSCAS 2001 (Cat. No.01CH37257)*. IEEE, pp. 421–424. doi: 10.1109/MWSCAS.2001.986202.

Karlsson, P. and Svensson, J. (2003) 'DC Bus Voltage Control for a Distributed Power System', *IEEE Transactions on Power Electronics*, 18(6), pp. 1405–1412. doi: 10.1109/TPEL.2003.818872.

Karthick, K. *et al.* (2019) 'Evaluation of solar thermal system configurations for thermoelectric generator applications: A critical review', *Solar Energy*. Elsevier, 188(March), pp. 111–142. doi: 10.1016/j.solener.2019.05.075.

Kazimierczuk, M. K. and Ayachit, A. (2015) 'Pulse-Width Modulated DC-DC Power Converters', in *Laboratory Manual for Pulse-Width Modulated DC-DC Power Converters. ISBN 13: 9781119052760*. 1st edn. John Wiley & Sons, Ltd.

Kelly, T. and Strauss, R. (2009) 'Agbami Field Development—Subsea Equipment Systems, Trees, Manifolds and Controls', in *Proceedings of Offshore Technology Conference*. The Offshore Technology Conference, p. 35872. doi: 10.4043/OTC-19919-MS.

Kieran Kavanagh, W., Lou, J. and Hays, P. (2003) 'Design of steel risers in ultra deep water-the influence of recent code requirements on wall thickness design for 10,000ft water depth', *Proceedings of the Annual Offshore Technology Conference*, 2003-May, pp. 419–428. doi: 10.4043/15101-ms.

Kim, H. *et al.* (2002) 'Instantaneous power compensation in three-phase systems by using p-q-r theory', *IEEE Transactions on Power Electronics*. IEEE, 17(5), pp. 701–710. doi: 10.1109/TPEL.2002.802185.

Kim, H. and Akagi, H. (1999) 'Instantaneous power theory on the rotating p-q-r reference frames', in *Proceedings of the International Conference on Power Electronics and Drive Systems*, pp. 422–427. doi: 10.1109/peds.1999.794600.

Kim, H., Blaabjerg, F. and Bak-Jensen, B. (2002) 'Spectral analysis of instantaneous powers in single-phase and three-phase systems with use of p-q-r theory', *IEEE Transactions on Power Electronics*. IEEE, 17(5), pp. 711–720. doi: 10.1109/TPEL.2002.802188.

Kim, H. S. *et al.* (2015) 'Relationship between thermoelectric figure of merit and energy conversion efficiency. ISSN: 10916490', *Proceedings of the National Academy of Sciences of the United States of America*, 112(27), pp. 8205–8210. doi: 10.1073/pnas.1510231112.

Kim, R. Y. *et al.* (2009) 'Analysis and design of maximum power point tracking scheme for thermoelectric battery energy storage system', *IEEE Transactions on Industrial*

Electronics. ISSN: 02780046. IEEE, 56(9), pp. 3709–3716. doi: 10.1109/TIE.2009.2025717.

Kirn, Y. H. and Ha, H. D. (1997) 'Design of interface circuits with electrical battery models', *IEEE Transactions on Industrial Electronics. ISSN: 02780046*, 44(1), pp. 81–86. doi: 10.1109/41.557502.

Kisacikoglu, M. C., Ozpineci, B. and Tolbert, L. M. (2010) 'Examination of a PHEV bidirectional charger system for V2G reactive power compensation', *Conference Proceedings - IEEE Applied Power Electronics Conference and Exposition - APEC*. IEEE, pp. 458–465. doi: 10.1109/APEC.2010.5433629.

Kraemer, D., Poudel, B., Feng, H., *et al.* (2011) 'High-performance flat-panel solar thermoelectric generators with high thermal concentration. DOI: 10.1038/NMAT3013', *Nature Materials*. Nature Publishing Group, 10(7), pp. 532–538. doi: 10.1038/nmat3013.

Kraemer, D., Poudel, B., Feng, H. P., *et al.* (2011) 'High-performance flat-panel solar thermoelectric generators with high thermal concentration', *Nature Materials*, 10(7), pp. 532–538. doi: 10.1038/nmat3013.

Kuroki, T. *et al.* (2015) 'Research and Development for Thermoelectric Generation Technology Using Waste Heat from Steelmaking Process', *Journal of Electronic Materials*, 44(6), pp. 2151–2156. doi: 10.1007/s11664-015-3722-8.

Lay-Ekuakille, A. *et al.* (2009) 'Thermoelectric generator design based on power from body heat for biomedical autonomous devices', *2009 IEEE International Workshop on Medical Measurements and Applications, MeMeA 2009*. IEEE, pp. 1–4. doi: 10.1109/MEMEA.2009.5167942.

Lee, J.-Y., Jeong, Y.-S. and Han, B.-M. (2011) 'An Isolated DC/DC Converter Using High-Frequency Unregulated LLC Resonant Converter for Fuel Cell Applications', *IEEE Transactions on Industrial Electronics. ISSN: 0278-0046*, 58(7), pp. 2926–2934. doi: 10.1109/TIE.2010.2076311.

Lempidis, G. *et al.* (2014) 'Wired and wireless charging of electric vehicles: A system approach', in *2014 4th International Electric Drives Production Conference (EDPC). ISBN 978-1-4799-5008-9*. IEEE, pp. 1–7. doi: 10.1109/EDPC.2014.6984421.

Leonov, V. *et al.* (2007) 'Small-size BiTe thermopiles and a thermoelectric generator for wearable sensor nodes', *Proc 6th Eur Conf*, (January 2014).

Leonov, V. *et al.* (2009) 'Thermal matching of a thermoelectric energy harvester with the environment and its application in wearable self-powered wireless medical sensors', *15th International Workshop on Thermal Investigations of ICs and Systems, THERMINIC 2009*. IEEE, 1(October), pp. 95–100.

Li, H. *et al.* (2020) 'China's deepwater development: subsurface challenges and opportunities', *Journal of Petroleum Science and Engineering*. Elsevier B.V., 195(August), p. 107761. doi: 10.1016/j.petrol.2020.107761.

Li, Z. *et al.* (2016) 'Two-stage stochastic programming based model predictive control strategy for microgrid energy management under uncertainties', *2016 International Conference on Probabilistic Methods Applied to Power Systems, PMAPS 2016 - Proceedings*. IEEE, pp. 0–5. doi: 10.1109/PMAPS.2016.7764076.

Liang-Rui Chen *et al.* (2008) 'Current-Pumped Battery Charger', *IEEE Transactions on Industrial Electronics.*, 55(6), pp. 2482–2488. doi: 10.1109/TIE.2008.921685.

Limongi, L. R. *et al.* (2007) 'Analysis and Comparison of Phase Locked Loop Techniques for Grid Utility Applications', in *2007 Power Conversion Conference - Nagoya. ISBN:1-4244-0843-1*. IEEE, pp. 674–681. doi: 10.1109/PCCON.2007.373038.

Lipták, B. G. (2006) *Instrument Engineers' Handbook. ISBN-13: 978-0-8493-1081-2. Vol.2*. 4th ed. ISA/CRC Press.

Liu, K. *et al.* (2017) 'Experimental prototype and simulation optimization of micro-radial milliwatt-power radioisotope thermoelectric generator. ISSN: 13594311', *Applied Thermal Engineering*. Elsevier Ltd, 125, pp. 425–431. doi: 10.1016/j.applthermaleng.2017.07.022.

Loth, W. D. (1995) 'Lower cost control systems for marginal fields. ISSN: 01603663', *Proceedings of the Annual Offshore Technology Conference*, 1995-May(May), pp. 581–591. doi: 10.4043/7870-ms.

Lowd, J. D., Burrus, B. S. and Hill, E. G. (1969) 'Production processing prototype for submerged operational test. ISBN:9781555638177', *Proceedings of the Annual Offshore Technology Conference*, 1969-May, pp. 123–128. doi: 10.4043/1083-ms.

Luff, A C; Auckland, D.W.; Shuttleworth, R.; Axcell, B. P.; Rahman, M. (1995) 'Design of a semiconductor thermoelectric generator for remote subsea wellheads', *IEE Proc.-Elecrr. Power Appl*, 142(2).

Malhotra, A. *et al.* (2016) 'Use cases for stationary battery technologies: A review of the literature and existing projects', *Renewable and Sustainable Energy Reviews*. Elsevier Ltd, 56, pp. 705–721. doi: 10.1016/j.rser.2015.11.085.

Manikandan, J., Vishwanath, A. and Korulla, M. (2018) 'Design of a 1kW

Underwater Wireless Charging Station for Underwater Data Gathering Systems', in *International Conference on Advances in Computing, Communications and Informatics. ISBN:9781538653142*. IEEE, pp. 211–216. doi: 10.1109/ICACCI.2018.8554936.

Markowski, P. and Dziedzic, A. (2008) 'Planar and three-dimensional thick-film thermoelectric microgenerators. DOI:10.1016/j.microrel.2008.03.008. ISSN 1356-5362', *Microelectronics Reliability*, 48(6), pp. 890–896. doi: 10.1016/j.microrel.2008.03.008.

Markowski, P. M. (2016) 'Multilayer thick-film thermoelectric microgenerator based on LTCC technology', *Microelectronics International*, 33(3), pp. 155–161. doi: 10.1108/MI-05-2016-0038.

Marks, H. (2009) ‘Betting big on Africa’, *JPT, Journal of Petroleum Technology. ISSN:01492136*, 61(11), pp. 36–38. doi: 10.2118/1109-0036-jpt.

Marlow-Industries (2016) *How Do Thermoelectric Generator (TEGS) Work ?* Available at: www.ii-vi.com Access on 11 Febuary 2018.

Mattos, D. M. *et al.* (2013) ‘Development and Production of Cascade and Chinook Fields in the Gulf of Mexico: An Overview’, p. 37650. doi: 10.4043/24156-ms.

May, A. F., Fleurial, J. P. and Snyder, G. J. (2010) ‘Optimizing thermoelectric efficiency in La3-xTe4 via Yb substitution. ISSN: 08974756’, *Chemistry of Materials*, 22(9), pp. 2995–2999. doi: 10.1021/cm1004054.

McLauchlan, A. and Nielsen, V. J. (2004) ‘Intelligent completions: Lessons learned from 7 years of installation and operational experience’, *Proceedings - SPE Annual Technical Conference and Exhibition*, pp. 3207–3214. doi: 10.2118/90566-ms.

MDL2179 PSC and Avansic (2015) *BOP Control System-AMF/Deadman Function, MDL 2179 Trial Docs. Demonstrative. BP Reviewed GCCF Claim Methodology. Source: TREX-003169, 0043*. Available at: www.mdl2179trialdocs.com (Accessed: 16 November 2016).

Mohammadnia, A. *et al.* (2020) ‘Hybrid energy harvesting system to maximize power generation from solar energy’, *Energy Conversion and Management*. Elsevier, 205(August 2019), p. 112352. doi: 10.1016/j.enconman.2019.112352.

Montecucco, A., Siviter, J. and Knox, A. R. (2017) ‘Combined heat and power system for stoves with thermoelectric generators’, *Applied Energy*. Elsevier Ltd, 185, pp. 1336–1342. doi: 10.1016/j.apenergy.2015.10.132.

Mude, K. N. (2018) ‘Battery charging method for electric vehicles: From wired to on-road wireless charging’, *Chinese Journal of Electrical Engineering. ISSN: :20961529*, 4(4), pp. 1–15. doi: 10.23919/CJEE.2018.8606784.

NanowerkNews (2014) *Thermoelectric nanomaterials for future green tech devices, Nanotechnology-News*. Available at: https://www.nanowerk.com (Accessed: 10 March 2017).

National-Geographic (2020) *We still don’t know the full impacts of the BP oil spill, 10 years later, The Deepwater Horizon spill started 10 years ago. Its effects are still playing out.* Available at: www.nationalgeographic.com (Accessed: 19 July 2020).

Nguyen Huu, T., Nguyen Van, T. and Takahito, O. (2018) ‘Flexible thermoelectric power generator with Y-type structure using electrochemical deposition process’, *Applied Energy*. Elsevier Ltd, 210, pp. 467–476. doi: 10.1016/j.apenergy.2017.05.005.

Ni, L. X. *et al.* (2011) ‘A power conditioning system for thermoelectric generator based on interleaved Boost converter with MPPT control’, *2011 International Conference on Electrical Machines and Systems, ICEMS 2011. ISBN: 9781457710445*. IEEE. doi: 10.1109/ICEMS.2011.6073395.

Nolop, N. C. *et al.* (2007) 'Erha and Erha North Development : Steel Catenary Risers and Offloading System', *Offshore Technology Conference. ISBN: 978-1-55563-254-0*, (OTC-18657-MS), pp. 11–12.

NorwayExportsNews (2019) *Egina starts production with TechnipFMC's subsea systems, Aquaculture, News*. Available at: www.norwayexports.no (Accessed: 29 April 2020).

Nwaokocha, C. N. and Layeni, A. T. (2013) 'Ocean Wave Energy: An Option for Nigerian Power Situation', *Scientific Research & Essay*, 8(25), pp. 1547–1552. doi: DOI: 10.5897/SRE10.1023.

Olaniyan, E. and Afiesimama, E. A. (2002) 'On marine winds, waves and swells over West African coast for effective coastal management - A case study of Victoria Island beach in Nigeria', *Oceans Conference Record (IEEE)*, 1, pp. 561–568. doi: 10.1109/OCEANS.2002.1193329.

Olsen, M. L. *et al.* (2014) 'A High-temperature, High-efficiency Solar Thermoelectric Generator Prototype. ISSN:18766102', *Energy Procedia*. Elsevier B.V., 49, pp. 1460–1469. doi: 10.1016/j.egypro.2014.03.155.

Olugbenga, A. A., Gudmestad, O. T. and Agbakwuru, J. (2017) 'Swell description for Bonga offshore Nigeria location', *Ocean Systems Engineering*, 7(4), pp. 345–369. doi: 10.12989/ose.2017.7.4.345.

Olvera, A. A. *et al.* (2017) 'Partial indium solubility induces chemical stability and colossal thermoelectric figure of merit in Cu2Se. ISSN: 17545706', *Energy and Environmental Science*. Royal Society of Chemistry, 10(7), pp. 1668–1676. doi: 10.1039/c7ee01193h.

OneSubsea (2019) *Subsea Oil & Gas Production Systems Manifold, Key role in well testing, isolation, sampling, and allocation management*. Available at: https://www.onesubsea.slb.com (Accessed: 19 October 2019).

Orr, B. *et al.* (2016) 'A review of car waste heat recovery systems utilising thermoelectric generators and heat pipes.', *Applied Thermal Engineering*. Elsevier Ltd, 101, pp. 490–495. doi: 10.1016/j.applthermaleng.2015.10.081.

Park, T. *et al.* (2017) 'Roll type conducting polymer legs for rigid-flexible thermoelectric generator. doi.org/10.1063/1.4979873. ISSN: 2166532X', *APL Materials*, 5(7). doi: 10.1063/1.4979873.

Pasquale, G. (2013) *Energy harvesters for powering wireless systems. Handbook of Mems for Wireless and Mobile Applications., Handbook of Mems for Wireless and Mobile Applications.* Woodhead Publishing Limited. doi: 10.1533/9780857098610.2.345.

Phil Davis, Bill Dunford, M. B. (2018) 'Radioisotope Thermoelectric Generators (RTGs). Cassini-NASA Solar System Exploration', *Planetary Science Communications team . Jet Propulsion Laboratory for NASA's Science Mission Directorate*. Available at: https://solarsystem.nasa.gov.

Poudel, B. *et al.* (2008) 'High-thermoelectric performance of nanostructured bismuth antimony telluride bulk alloys. ISSN: 00368075', *Science*, 320(5876), pp. 634–638. doi: 10.1126/science.1156446.

Qadir, K. S., Morris, K. and Goodlad, M. (2016) 'Pre-tensioned pipeline bundles design challenges and solutions for HPHT field development', *Offshore Technology Conference Asia 2016, OTCA 2016*, pp. 3440–3459. doi: 10.4043/26517-ms.

Rafin, F. and Laine, A. (2010) 'AKPO: Early completion of a giant Nigerian deep offshore development', *Proceedings of the Annual Offshore Technology Conference*, 4, pp. 3087–3094. doi: 10.4043/20989-ms.

Ray, A., Rajashekara, K. and Krishnamoorthy, H. (2019) 'Novel HVDC Power Transmission Architectures for Subsea Grid', in *Offshore Technology Conference, OTC-29412-MS. ISBN:9781613996416*. OTC. doi: 10.4043/29412-MS.

Richard R. Furlong and Earl J. Wahlquist (1999) 'U . S . Space Missions using Radioisotope Power Systems. Nuclear News. 42 (4): 26–34.', *NuclearNews, Radioisotope Power Systems in Space.*, (April Issue).

Rowe, D.M.; Bhandari, C. M. (1983) *Modern Thermoelectrics. Holt, Rinehart and Winston Ltd. ISBN 0-8359-4593-6, Electronics and Power*. Reston Publishing Company. doi: 10.1049/ep.1984.0389.

Rowe, D. M. (1991) 'Applications of nuclear-powered thermoelectric generators in space. ISSN: 03062619', *Applied Energy*, 40(4), pp. 241–271. doi: 10.1016/0306-2619(91)90020-X.

Rowe, D. M. (1994) 'Thermoelectric generators as alternative sources of low power', *Renewable Energy*, 5(5–8), pp. 1470–1478. doi: 10.1016/0960-1481(94)90191-0.

S&PF MODUL. (2007) *Thermoelectric Generators, Principle of operation of a thermoelectric generator*. Available at: www.spf-modul.com Access on 24 November 2019.

Sanders, W. *et al.* (2012) 'Efficient Perforation Of High-Pressure Deepwater Wells', in *Journal of Petroleum Technology. DOI:10.4043/21758-MS*. OTC, pp. 1–2. doi: 10.4043/21758-MS.

Sankaran, S. *et al.* (2011) 'Realizing value from implementing i-field^{TM} in Agbami - A deepwater greenfield in an offshore Nigeria development', *SPE Economics and Management*, 3(1), pp. 31–44. doi: 10.2118/127691-pa.

dos Santos, E. C. (2013) 'Dual-output dc-dc buck converters with bidirectional and unidirectional characteristics', *IET Power Electronics. ISSN: 17554535*, 6(5), pp. 999–1009. doi: 10.1049/iet-pel.2012.0731.

Schaltz, E. and Man, E. A. (2017) 'Power Electronic Converters and Their Control in Thermoelectric Applications', in Diana Dávila Pineda, A. R. (ed.) *Thermoelectric Energy Conversion Basic Concepts and Device Applications. ISBN: 10.1002/9783527698110.ch9*,

pp. 177–203. doi: 10.1002/9783527698110.ch9.

Schoppa, W. *et al.* (2007) 'Bonga-Flow Assurance Benchmarking via Field Surveillance', (April), pp. 11–12. doi: 10.4043/18949-ms.

Shmilovitz, D. (2005) 'On the definition of total harmonic distortion and its effect on measurement interpretation', *IEEE Transactions on Power Delivery. ISSN:0885-8977*, 20(1), pp. 526–528. doi: 10.1109/TPWRD.2004.839744.

Shu, G. *et al.* (2018) 'Configuration optimization of the segmented modules in an exhaust-based thermoelectric generator for engine waste heat recovery. ISSN:03605442', *Energy*. Elsevier Ltd, 160, pp. 612–624. doi: 10.1016/j.energy.2018.06.175.

Singh, D. *et al.* (2018) 'Thermoelectric Generators: Strain-Induced Rolled Thin Films for Lightweight Tubular Thermoelectric Generators (Adv. Mater. Technol. 1/2018)', *Advanced Materials Technologies*, 3(1). doi: 10.1002/admt.201870002.

Sinvula, R., Abo-Al-Ez, K. M. and Kahn, M. T. (2019) 'Total harmonics distortion (THD) with PV system integration in smart grids: Case study', *Proceedings of the 27th International Conference on the Domestic Use of Energy, DUE 2019. ISBN:9780639964737*. cape peninsula university of technology, pp. 102–108.

Snyder, G. and Jones, M. R. (2017) 'The role of mirror neurons relative to the core stuttering pathology and compensatory stuttering behaviors. ISSN: 25085948', *Clinical Archives of Communication Disorders*, 2(1), pp. 1–6. doi: 10.21849/cacd.2017.00059.

Solbrekken, G. L. *et al.* (2004) 'Thermal management of portable electronic equipment using thermoelectric energy conversion.', *IEEE, Inter Society Conference on Thermal Phenomena*, (0-18Q3-8351–5IQ4/2004 IEEE), pp. 276–283.

Song, Y. (2019) 'A study of OTEC application on deep-sea FPSOs', *Journal of Marine Science and Technology (Japan)*. Springer Japan, 24(2), pp. 466–478. doi: 10.1007/s00773-018-0567-x.

Stanton, P. *et al.* (2010) 'New code for the design of dynamic risers for floating production installations', *Proceedings of the Annual Offshore Technology Conference*, 3(January 2001), pp. 2235–2243. doi: 10.4043/20816-ms.

Sugimoto, Y. (2015) 'The solar cells and the battery charger system using the fast and precise analog maximum power point tracking circuits', *Proceedings of IEEE Computer Society Annual Symposium on VLSI, ISVLSI*. IEEE, 07-10-July, pp. 597–602. doi: 10.1109/ISVLSI.2015.36.

Tan, N. M. L., Abe, T. and Akagi, H. (2012) 'Design and performance of a bidirectional isolated DC-DC converter for a battery energy storage system', *IEEE Transactions on Power Electronics. ISSN: 08858993*. IEEE, 27(3), pp. 1237–1248. doi: 10.1109/TPEL.2011.2108317.

Tang, X. *et al.* (2005) 'Synthesis and thermoelectric properties of p -type- and n -type-filled skutterudite R yM xCo 4-xSb 12 (R: Ce, Ba, Y; M: Fe, Ni). ISSN: 00218979',

Journal of Applied Physics, 97(9). doi: 10.1063/1.1888048.

Tashakor, N., Farjah, E. and Ghanbari, T. (2017) 'A Bidirectional Battery Charger With Modular Integrated Charge Equalization Circuit', *IEEE Transactions on Power Electronics*. IEEE, 32(3), pp. 2133–2145. doi: 10.1109/TPEL.2016.2569541.

Taxy, S. *et al.* (2009) 'Pigging Operation of Single Production Lines in Deepwater Fields', pp. 1–2. doi: 10.4043/otc-19941-ms.

Terzija, V. *et al.* (2011) 'Frequency and power components estimation from instantaneous power signal', *IEEE Transactions on Instrumentation and Measurement*. IEEE, 60(11), pp. 3640–3649. doi: 10.1109/TIM.2011.2138190.

Tethys (2009) *Ocean Current, Capturing energy from ocean currents*. Available at: www.tethys.pnnl.gov (Accessed: 20 March 2018).

The U. S. Chemical Safety and Hazard Investigation Board (2014) *Macondo Blowout and Explosion Investigation, Deepwater Horizon RBS 8D BOP MUX Control System Report*. Available at: www.csb.gov (Accessed: 12 November 2016).

Theobald, M. FSSL Limited, L. (1993) 'Autonomous Control System (SPARCS) For Low Cost Subsea Production System. ArXiv ID: 1310.3244v1', *Society for Underwater Technology*, 30(Subsea International '93), pp. 125–148.

Theobald, M. C. (1994) 'SPARCS autonomous control system. 1994 Society for Underwater Technology. Printed in the Netherlands', *Society for Underwater Technology*, 32, pp. 155–170.

Thibaut, E. and Leforgeais, B. (2012) 'Martin Linge Electric Power from Shore', in *Society of Petroleum Engineers (SPE),SPE 161960, DOI: 10.2118/161960-MS, ISBN:9781622768745*. SPE, pp. 3013–3023. doi: 10.2118/161960-MS.

Thielen, M. *et al.* (2017) 'Human body heat for powering wearable devices: From thermal energy to application. ISSN:01968904', *Energy Conversion and Management*. Elsevier Ltd, 131, pp. 44–54. doi: 10.1016/j.enconman.2016.11.005.

Topsides64 (2012) *Moho Nord Project, Amec-SHI, Doris-HH, Saipem-STX in competition*. Available at: www.topsides64.rssing.com (Accessed: 17 November 2016).

Ueno, T. *et al.* (2018) 'Development and demonstration test for floating type ocean current turbine system conducted in kuroshio current', *2018 OCEANS - MTS/IEEE Kobe Techno-Oceans, OCEANS - Kobe 2018*. IEEE. doi: 10.1109/OCEANSKOBE.2018.8558792.

US-Energy-Information-Administration-(EIA) (2017a) *Geothermal explained, What is geothermal energy?* Available at: www.eia.gov (Accessed: 20 February 2018).

US-Energy-Information-Administration-(EIA) (2017b) *Ocean thermal energy conversion, Hydropower explained*. Available at: www.eia.gov (Accessed: 20 February 2018).

Wang, W. *et al.* (2013) 'Thermoelectric energy harvesting for building energy

management wireless sensor networks', *International Journal of Distributed Sensor Networks*, 2013. doi: 10.1155/2013/232438.

Wang, X. W. *et al.* (2008) 'Enhanced thermoelectric figure of merit in nanostructured n - type silicon germanium bulk alloy. ISSN: 00036951', *Applied Physics Letters*, 93(19), pp. 1–4. doi: 10.1063/1.3027060.

von der Weid, J. P., da Silva, J. A.P., *et al.* (1993) 'Subsea Electric Generator. ISBN:0780313860', *Proceedings of the Conference on Oceans '93*, (November 1993), pp. 172–176. doi: 10.1109/oceans.1993.326086.

von der Weid, J. P., da Silva, J. A. P., *et al.* (1993) 'Subsea electric generator', *OCEANS '93. Engineering in Harmony with Ocean. Proceedings*, p. II/172-II/176 vol.2. doi: 10.1109/OCEANS.1993.326086.

Wilbrecht, S. and Beitelschmidt, M. (2018) 'The Potential of a Cascaded TEG System for Waste Heat Usage in Railway Vehicles', *Journal of Electronic Materials*. Springer US, 47(6), pp. 3358–3369. doi: 10.1007/s11664-018-6094-z.

Wu, H. *et al.* (2014) 'Mechanical behavior of interface between composite geomembrane and permeable cushion material. ISSN:16878442', *Advances in Materials Science and Engineering*, 2014. doi: 10.1155/2014/184359.

Wu, K. C. (2006) 'Switch-Mode Power Converters Design and Analysis', in *Isolated Step-Down (Buck) Converter. Push Pull Converter with Current-Mode Control and Slope Compensation. Nonisolated Forward Converter. Full-Bridge Converter. Flyback Converters ISBN 0-12-088795-9*. Elsevier Academic Press.

Wu, Y., Liu, X. and Xing, D. (2015) 'Case study of hot water foam flooding in deep heavy oil reservoirs', *Society of Petroleum Engineers - SPE Asia Pacific Enhanced Oil Recovery Conference, EORC 2015*, pp. 449–460. doi: 10.2118/174606-ms.

Yan, X. *et al.* (2010) 'Experimental studies on anisotropic thermoelectric properties and structures of n-type Bi2Te2.7Se0.3. ISSN: 15306984', *Nano Letters*, 10(9), pp. 3373–3378. doi: 10.1021/nl101156v.

Yan, Z. and Chen, J. (2008) 'The load matching of a thermoelectric device at maximum power output', *American Institute of Physics. AIP Conference Proceedings 316, 343 (1994)*, 343(May 2008), pp. 343–344. doi: 10.1063/1.46828.

Yang, M. Z. *et al.* (2013) 'Energy harvesting thermoelectric generators manufactured using the complementary metal oxide semiconductor process. ISSN 1424-8220', *Sensors (Switzerland)*, 13(2), pp. 2359–2367. doi: 10.3390/s130202359.

Yang, S. H. *et al.* (2008) 'Nanostructures in high-performance (GeTe)x(AgSbTe 2)100-x thermoelectric materials', *Nanotechnology*, 19(24), pp. 11–16. doi: 10.1088/0957-4484/19/24/245707.

Yasmeena, S. and Das, G. T. (2015) 'A Review of Technical Issues for Grid Connected Renewable Energy Sources', *International Journal of Energy and Power Engineering*

International Journal of Energy and Power Engineering. Special Issue: Energy Systems and Developments, 4(5), pp. 22–32. doi: 10.11648/j.ijepe.s.2015040501.14.

Yazawa, K., Shakouri, A. and Hendricks, T. J. (2017) 'Thermoelectric heat recovery from glass melt processes', *Energy*. Elsevier Ltd, 118, pp. 1035–1043. doi: 10.1016/j.energy.2016.10.136.

Yazdani, S. and Pettes, M. T. (2018) 'Nanoscale self-assembly of thermoelectric materials: A review of chemistry-based approaches', *Nanotechnology. ISSN:13616528*. IOP Publishing, 29(43). doi: 10.1088/1361-6528/aad673.

York, M. *et al.* (2019) 'Subsea Smart Electric Control Unit for Building Smarter and Cheaper Subsea Hardware', in *Offshore Techn. Conference.ISBN: 978-1-61399-641-6*. OTC. doi: 10.4043/29639-MS.

YOUNG, H. L. (1989) 'Development in subsea controls. John Brown Engineers & Constructors Limited', *Society of Petroleum Engineers*, SPE19225-. doi: SPE19225 - l.

Yuan, Z. *et al.* (2018) 'Screen-Printed Radial Structure Micro Radioisotope Thermoelectric Generator.', *Applied Energy*. Elsevier, 225(May), pp. 746–754. doi: 10.1016/j.apenergy.2018.05.073.

Zhang, Q. H. *et al.* (2016) 'Thermoelectric Devices for Power Generation: Recent Progress and Future Challenges', *Advanced Engineering Materials*, 18(2), pp. 194–213. doi: 10.1002/adem.201500333.

Zhang, Y. *et al.* (2016) 'High-performance nanostructured thermoelectric generators for micro combined heat and power systems', *Applied Thermal Engineering*. Elsevier Ltd, 96, pp. 83–87. doi: 10.1016/j.applthermaleng.2015.11.064.

Zhao, L. D., Dravid, V. P. and Kanatzidis, M. G. (2014) 'The panoscopic approach to high performance thermoelectrics. ISSN: 17545706', *Energy and Environmental Science*, 7(1), pp. 251–268. doi: 10.1039/c3ee43099e.

Zhou, Y., Paul, S. and Bhunia, S. (2008) 'Harvesting Wasted Heat in a Microprocessor Using Thermoelectric Generators : Modeling , Analysis and Measurement. ISBN:9783981080131', *IEEE, EDAA*, (978-3-9810801-3–1/2008), pp. 3–8.

Zhu, J., Xu, Z. and Jia, L. (2018) 'Design and fabrication of 3D flexible thermoelectric energy generator using chemical vapor deposition method based on paper substrate. ISBN: 9781538656389', *ISSI 2018*. IEEE, pp. 1–4. doi: 10.1109/ISSI.2018.8538256.

Appendix A

Table A.1 - Detailed Results of Device-TEMs Test

Derivation A.2 -Thermoelectric Module System Assembly

Table A.1 - Detailed Results of Device-TEMs Test

Temperature Difference (degC)	Device-TEM-01 on 0.5 Ohms Load			Device-TEM-02 on 7 Ohms Load			Device-TEM-03 on 4 Ohms Load_Test1			Device-TEM-03 on 4 Ohms Load_Test2		
	Voltage (V)	Current (A)	Power (W)	Voltage (V)	Current (A)	Power (W)	Voltage (V)	Current (A)	Power (W)	Voltage (V)	Current (A)	Power (W)
50.00	0.22	1.48	0.33	1.79	0.43	0.77	1.53	0.49	0.75	1.53	0.49	0.75
50.50	0.23	1.45	0.33	1.78	0.44	0.78	1.54	0.49	0.76	1.54	0.49	0.76
51.00	0.24	1.49	0.36	1.79	0.42	0.75	1.53	0.50	0.77	1.54	0.49	0.76
51.50	0.22	1.47	0.32	1.79	0.44	0.79	1.54	0.49	0.76	1.52	0.49	0.75
52.00	0.25	1.46	0.37	1.80	0.43	0.77	1.53	0.50	0.77	1.53	0.50	0.77
52.50	0.24	1.46	0.35	1.81	0.44	0.80	1.54	0.50	0.77	1.54	0.50	0.77
53.00	0.26	1.45	0.38	1.80	0.44	0.79	1.52	0.51	0.76	1.53	0.49	0.75
53.50	0.25	1.46	0.37	1.82	0.42	0.76	1.54	0.52	0.80	1.54	0.52	0.80
54.00	0.26	1.47	0.38	1.83	0.43	0.79	1.53	0.49	0.75	1.55	0.49	0.76
54.50	0.27	1.47	0.40	1.85	0.44	0.81	1.55	0.49	0.76	1.54	0.49	0.76
55.00	0.27	1.52	0.41	1.87	0.46	0.86	1.55	0.50	0.78	1.55	0.50	0.78
55.50	0.28	1.52	0.43	1.86	0.46	0.86	1.54	0.50	0.77	1.54	0.50	0.77
56.00	0.28	1.51	0.42	1.87	0.45	0.84	1.55	0.49	0.76	1.55	0.49	0.76
56.50	0.27	1.53	0.41	1.88	0.46	0.87	1.56	0.49	0.77	1.54	0.51	0.79
57.00	0.27	1.54	0.42	1.88	0.47	0.88	1.56	0.50	0.78	1.55	0.51	0.79
57.50	0.28	1.54	0.43	1.87	0.47	0.88	1.55	0.50	0.78	1.55	0.50	0.78
58.00	0.28	1.55	0.43	1.88	0.48	0.90	1.56	0.51	0.80	1.56	0.48	0.75
58.50	0.29	1.54	0.45	1.87	0.48	0.90	1.56	0.50	0.78	1.57	0.49	0.77
59.00	0.28	1.54	0.43	1.89	0.49	0.93	1.57	0.51	0.80	1.57	0.51	0.80
59.50	0.29	1.53	0.44	1.89	0.49	0.93	1.58	0.51	0.81	1.58	0.51	0.81
60.00	0.29	1.55	0.45	1.90	0.49	0.93	1.59	0.50	0.80	1.59	0.50	0.80
60.50	0.29	1.54	0.45	1.90	0.48	0.91	1.59	0.51	0.81	1.59	0.51	0.81
61.00	0.29	1.53	0.44	1.89	0.49	0.93	1.58	0.52	0.82	1.58	0.52	0.82
61.50	0.30	1.53	0.46	1.90	0.49	0.93	1.58	0.53	0.84	1.58	0.53	0.84
62.00	0.30	1.52	0.46	1.91	0.48	0.92	1.59	0.53	0.84	1.59	0.53	0.84
62.50	0.31	1.52	0.47	1.91	0.49	0.94	1.60	0.52	0.83	1.60	0.54	0.86
63.00	0.29	1.53	0.44	1.91	0.49	0.94	1.59	0.54	0.86	1.59	0.54	0.86
63.50	0.30	1.53	0.46	1.92	0.48	0.92	1.59	0.55	0.88	1.61	0.56	0.90
64.00	0.29	1.55	0.45	1.93	0.49	0.95	1.60	0.56	0.90	1.60	0.56	0.90
64.50	0.31	1.57	0.49	1.94	0.50	0.97	1.60	0.58	0.93	1.61	0.57	0.92
65.00	0.31	1.58	0.49	1.95	0.51	0.99	1.61	0.59	0.95	1.61	0.59	0.95
65.50	0.30	1.58	0.47	1.95	0.50	0.96	1.60	0.59	0.94	1.61	0.60	0.97
66.00	0.30	1.58	0.47	1.95	0.51	0.99	1.60	0.58	0.93	1.60	0.58	0.93
66.50	0.31	1.57	0.49	1.94	0.50	0.97	1.61	0.58	0.93	1.61	0.61	0.98
67.00	0.31	1.56	0.48	1.95	0.50	0.98	1.61	0.58	0.93	1.61	0.58	0.93
67.50	0.30	1.56	0.47	1.96	0.50	0.98	1.62	0.58	0.94	1.68	0.60	1.00
68.00	0.32	1.56	0.50	1.96	0.51	1.00	1.63	0.59	0.96	1.67	0.61	1.01
68.50	0.31	1.58	0.49	1.97	0.50	0.99	1.66	0.60	1.00	1.66	0.60	1.00
69.00	0.32	1.57	0.50	1.96	0.51	1.00	1.69	0.61	1.03	1.69	0.61	1.03
69.50	0.31	1.59	0.49	1.96	0.52	1.02	1.70	0.63	1.07	1.72	0.62	1.07
70.00	0.32	1.60	0.51	1.97	0.52	1.02	1.71	0.62	1.06	1.71	0.62	1.06

Derivation A.2 -Thermoelectric Module System Assembly

Thermoelectric module system assembly involves clamping the thermoelectric modules between the hot heat source and the cold heat exchangers. The compression or clamping load required by Device-TEM-01 is 1.0 Mpa (Mega-Pascal). Device-TEM-02 required 1.2 Mpa, while Device-TEM-03 needed 1.2 Mpa. The bolt tightening process was to a specific torque for each thermoelectric module. The torque value to attain an expected clamping force (T_q) can be calculated using the equation below:

$$T_q = \frac{C_{Tq} \text{ x } B_{size} \text{ x } P_C \text{ x } A_{TEM}}{N_{Screw}}$$

Where the terms are as follows:

- C_{Tq} = Torque Coefficient
- B_{size} = Bolt Size
- P_C = Compression Pressure
- A_{TEM} = TEM Area
- N_{Screw} = Number of Screws

The torque coefficient (C_{Tq}) and nominal bolt size (B_{size}) for the two M5 steel bolts are 0.2 and 5.2mm, respectively. Therefore, the clamping force (T_{q1}, T_{q2}, and T_{q3}) for the three thermoelectric modules was calculated by substituting their parameters with the above equation.

Device-TEM-01 module was (0.02 meters x 0.02 meters) and had a compression or clamping load of 1.0 Mpa thus:

$$T_{q1} = \frac{0.2 \text{ x } 0.0052 \text{ x } 1000000 \text{ x } 0.02 \text{ x } 0.02}{2} = 0.208\, N.m$$

Device-TEM-02 was (0.03 m x 0.03 m) and has a compression or clamping load of 1.2 Mpa, hence:

$$T_{q2} = \frac{0.2 \text{ x } 0.0052 \text{ x } 1200000 \text{ x } 0.03 \text{ x } 0.03}{2} = 0.5616\, N.m$$

Device-TEM-03 module was (0.04 m x 0.04 m) and had a clamping load of 1.2 Mpa, therefore:

$$T_{q3} = \frac{0.2 \text{ x } 0.0052 \text{ x } 1200000 \text{ x } 0.04 \text{ x } 0.04}{2} = 0.9984\, N.m$$

Appendix B

Error Analysis – Series Parallel Thermoelectric Power System Configuration.

Table B.1 – STAGE A

Table B.2 – STAGE B

Table B.1 – STAGE A

TE-MODULES	Voltage(V)	Current (A)	Voltage (V) Per String	Total Circuit Voltage (V)	Current (A) Per String	Total Circuit Current (A)
TEM-1	3	1				
TEM-2	3					
TEM-3	3					
TEM-4	3	1				
TEM-5	3					
TEM-6	3					
String-01 (TEM-1+TEM-2+TEM-3)			9	9	1	2
String-02 (TEM-4+TEM-5+TEM-6)			9		1	

Table B.2 – STAGE B

TE-MODULES	Voltage(V)	Current (A)	Voltage (V) Per String	Total Circuit Voltage (V)	Current (A) Per String	Total Circuit Current (A)
TEM-1	3	1				
TEM-2	3					
TEM-3	2.5					
TEM-4	3	0.5				
TEM-5	3					
TEM-6	3					
String-01 (TEM-1+TEM-2+TEM-3)			8.5	9	1	1.5
String-02 (TEM-4+TEM-5+TEM-6)			9		0.5	

Appendix C

Derivation C.1 - Deepwater Thermoelectric Power Unit (DPU)

The 6.4kW-DPU Framework Calculations

For a 6395 W rated DPU, the desired maximum output voltage at the terminals of the power unit was set as 174V. Therefore, the maximum power point current was calculated using the DC power equation below:

$$P_{Max}^{DPU} = (V_{Max}^{DPU} \text{ x } I_{Max}^{DPU})$$

Hence,

The 6395 W rated DPU consists of a combination of Flex-250W-DPP connected in series and parallel configuration. The selected maximum power point voltage of the Flex-250W-DPP was 29V, while the maximum power point current was 7.35A. Therefore, the Flex-250W-DPP power at maximum power point is calculated as:

$$P_{Max}^{DPP} = (V_{Max}^{DPP}) \text{ x } (I_{Max}^{DPP}) = 29\text{V} \text{ x } 7.35\text{A} = 213.15\text{W}$$

The number of Flex-250W-DPP connected in the series string (Ns) and parallel string (Np) is calculated below:

$$N_S = \left(\frac{V_{Max}^{DPU}}{V_{Max}^{DPP}}\right)$$

$$N_S = \left(\frac{174\,V}{29\,\text{V}}\right) = 6$$

$$N_P \quad = \quad \left(\frac{I_{Max}^{DPU}}{I_{Max}^{DPP}}\right)$$

$$N_P \quad = \quad \left(\frac{36.75\ A}{7.35\ \text{A}}\right) \ = 5$$

Therefore, the maximum power of a DPU of desired DPU is calculated below:

$$P_{Max}^{DPU} \ = \ (N_S \quad \text{x} \quad N_P \quad \text{x} \quad P_{Max}^{DPP})$$

$$P_{Max}^{DPU} \ = \ 6\ X\ \ 5\ X\ \ 213.15\text{W} = \ 6{,}394.5\ W$$

Appendix D

Derivation D.1 – Minimum Operating Inductance

Minimum Operating Inductance (L_{min})

Some other assumptions considered for power system implementation include the maximum subsea load or equipment resistance capability of up to 50 kilo-Ohms. A switching frequency (f_s) of 100 kHz and a minimum duty cycle (d_{min}) of 0.1 for the functionality of the power system. Thus, the minimum operating inductance was calculated as follows:

$$L_{min} = \frac{R_{Lmax} \text{ x } d_{min} \ (1 - d_{min})^2}{2 \text{ x } f_s}$$

$$L_{min} = \frac{(50 \text{ x } 10^3) \text{ x } 0.1 \ (1 - 0.1)^2}{2 \text{ x } (100 \text{ x } 10^3)}$$

$$L_{min} = 0.02025 = 20.25\, mH$$

The calculated minimum inductance was 20.25mH or 0.02025H. Nonetheless, the value of the operating inductance used for this power system model was 2e-3 H (or 0.002 H) and 0.1 Ohms internal resistance (also known as equivalent series resistance (ESR)).

Derivation D.2 - Minimum Operating Capacitance

Minimum Operating Capacitance (C_{min})

The power circuit's minimum capacitance (C_{min}) was estimated on the assumption that ripple voltage ($V_r = 2V$) was equally divided between ESR and the capacitance. Additionally, a maximum output voltage (V_O) of 370V was assumed. Other assumptions considered in calculating the minimum system capacitance were maximum duty cycle (d_{max}) value of 0.9 and minimum load resistance (R_{Lmin}) value of 10 ohms. The calculated minimum capacitance was as follows:

$$C_{min} = \frac{d_{max} \text{ x } V_O}{f_s \text{ x } R_{Lmin} \text{ x } V_r}$$

$$C_{min} = \frac{0.9 \text{ x } 370}{(100 \text{ x } 10^3) \text{ x } 10 \text{ x } 2}$$

$$C_{min} = 1.7 \text{ x } 10^{-4}\, F$$

The calculated minimum capacitance was 170 μF. Though, a capacitance value of 100 μF and 1e-4 Ohm resistance was used for the buffer capacitor (at the output of the Flex-250W-DPP) and the output capacitor (at the power outlet side of the step-up converter).

Algorithm D.3 - MATLAB Script: Hill-Climbing Algorithm

MATLAB Script – Hill-Climbing Algorithm

```
%%%%%%%%%%%%%%%%%%%%%%%%%%%%%%%%%%%%%%%%%%%%%%%%%%%%%%%%%%%%%%%%%%%%%%%%
%                                                                      %
%   Dept. of Naval Architecture, Ocean & Marine Engineering            %
%   University of Strathclyde, Glasgow, Scotland, United Kingdom.      %
%                                                                      %
%   Project Name:   Deepwater Thermoelectricity                        %
%                              in                                      %
%                   Underwater Combo Power Grid                        %
%                                                                      %
%                                                                      %
%                                                                      %
%   File Description: Optimum Power Point Tracking                     %
%                     Hill-Climbing Algorithm                          %
%                     Underwater Power Controller                      %
%                     Switch Mode DC-DC Boost Converter                %
%                     Design Parameters                                %
%                                                                      %
%                                                                      %
%  Inputs:              Voltage, Current, Duty Cycle                   %
%  Components:          250W-DPP Source, IGBT, Diode, Inductor, Capacitor %
%                                                                      %
%   Author:         Austin Asuquo                                      %
%   Date:           15th May, 2018                                     %
%                                                                      %
%%%%%%%%%%%%%%%%%%%%%%%%%%%%%%%%%%%%%%%%%%%%%%%%%%%%%%%%%%%%%%%%%%%%%%%%
%
%         Optimum Power Point Tracking, switch mode DC-DC Converter, Underwater Power Controller
%
%
function duty = Opp_algorithm(vDPP,iDPP,delta)
%
% Optimum power point tracking algorithm was used in MATLAB for operating Underwater Power Controller
% Through DC-DC BoostConverter, the Underwater Power Controller algorithm assisted in harnessing maximum
% Power from thermoelctric power source (250W-DPP)
%
%
duty_init = 0.1;
% The minimum and maximum setting for duty cycle was 0 and 0.95, respectively.
%
%
duty_min=0;
duty_max=0.95;

persistent Vold Pold duty_old;
% persistent variable type of data were stored at this stage
% The difference between the old data and new data was required going forward
%
if isempty(Vold)
   Vold=0;
   Pold=0;
   duty_old=duty_init;
```

```
end
P= vDPP*iDPP;                                   % power calculation
dV= vDPP - Vold;                                % Subtracting old voltage from the new voltage value of the DPP
dP= P - Pold;                                   % Subtracting old power value from new power value of the DPP

%   At this point, the power controller algorithm begins a search for derivative of Power and voltage (dP/dV=0)
% There is no change in duty cycle if the value of dP/dV is equal to zero (0)
% Also, an initial voltage setting of 30V was introduce, the algorithm was fully activated when vDPP was greater than 30V
% if old and new power not equal
%
%
%
if dP ~= 0 && vDPP>30
   if dP < 0
      if dV < 0
         duty = duty_old - delta;
      else
         duty = duty_old + delta;
      end
   else
      if dV < 0
         duty = duty_old + delta;
      else
         duty = duty_old - delta;
      end
   end
else
   duty = duty_old;
end

%At this point, the minimum and maximum duty cycle value is determined.
if duty >= duty_max
   duty=duty_max;
elseif duty<duty_min
   duty=duty_min;
end

%  data storage for new iterration takes place here
duty_old=duty;
Vold=vDPP;
Pold=P;
```

Table D.4 – 20-Ohms Load Resistance on Subsea Equipment

20-Ohms Load Resistance on Subsea Equipment					
Subsea Temp. Diff. (degC)	DPP-250W-Power(W)	Converter-Vo(V)	Converter-Io(A)	Converter-Power_Po(W)	Tracked-Power(W)
2.50	0.32	2.23	0.11	0.25	4.17
5.00	1.11	4.45	0.22	0.99	8.33
7.50	2.37	6.67	0.33	2.23	12.50
10.00	4.10	8.89	0.44	3.95	16.67
12.50	6.28	11.10	0.56	6.17	20.83
15.00	8.93	13.32	0.67	8.87	25.00
17.50	12.05	15.52	0.78	12.05	29.17
20.00	15.62	17.73	0.89	15.72	33.33
22.50	19.64	19.93	0.99	19.87	37.50
25.00	24.13	22.13	1.11	24.49	41.67
27.50	29.06	24.33	1.22	29.58	45.83
30.00	34.45	26.52	1.33	35.16	50.00
32.50	40.28	28.70	1.44	41.19	54.17
35.00	48.61	30.72	1.54	47.20	58.33
37.50	62.74	34.82	1.74	60.64	62.50
40.00	67.00	36.46	1.82	66.47	66.67
42.50	71.37	37.25	1.86	69.39	70.83
45.00	75.66	38.39	1.92	73.68	75.00
47.50	79.96	39.55	1.98	78.21	79.17
50.00	83.51	41.47	2.07	85.97	83.33
52.50	87.38	42.66	2.13	90.98	87.50
55.00	92.89	42.52	2.13	90.39	91.67
57.50	96.99	43.38	2.17	94.10	95.83
60.00	100.60	45.39	2.27	103.00	100.00
62.50	105.70	45.19	2.26	102.10	104.20
65.00	109.80	46.22	2.31	106.80	108.30
67.50	112.70	46.29	2.32	107.10	112.50
70.00	118.20	48.13	2.41	115.85	116.70
72.50	119.40	47.93	2.40	114.80	120.80
75.00	126.60	49.71	2.49	123.50	125.00
77.50	130.70	51.42	2.57	132.20	129.20
80.00	135.10	51.37	2.57	131.90	133.30
82.50	139.40	52.50	2.63	137.80	137.50
85.00	143.60	53.74	2.69	144.40	141.70
87.50	147.80	53.86	2.69	145.00	145.80
90.00	149.60	53.83	2.69	144.86	150.00
92.50	156.50	55.76	2.79	155.40	154.20
95.00	158.80	56.88	2.84	161.80	158.30
97.50	163.70	56.81	2.84	161.40	162.50
100.00	169.00	57.90	2.90	167.60	166.70
102.50	172.70	59.02	2.95	174.20	170.80
105.00	176.30	58.49	2.92	171.00	175.00
107.50	181.40	60.02	3.00	180.10	179.20
110.00	183.90	61.33	3.07	188.04	183.30
112.50	187.00	60.74	3.04	184.50	187.50
115.00	190.20	61.48	3.07	189.00	191.70
117.50	197.90	62.84	3.14	197.50	195.80
120.00	200.00	63.78	3.19	203.40	200.00
122.50	205.00	63.80	3.19	203.50	204.20
125.00	210.10	64.31	3.22	207.50	208.30
127.50	213.60	65.13	3.26	212.10	212.50
130.00	114.50	47.80	2.39	114.24	216.70
132.50	213.20	41.74	2.09	87.11	220.80
135.00	223.30	41.71	2.09	86.98	225.00
137.50	232.80	41.67	2.08	86.84	229.20
140.00	241.70	41.64	2.08	86.70	233.30
142.50	250.20	41.61	2.08	86.56	237.50
145.00	258.40	41.57	2.08	86.42	241.70
147.50	266.30	41.54	2.08	86.28	245.80
150.00	273.90	41.51	2.08	86.13	250.00

Table D.5 – 50-Ohms Load Resistance on Subsea Equipment

50-Ohms Load Resistance on Subsea Equipment					
Subsea Temp. Diff. (degC)	DPP-250W-Power(W)	Converter-Vo(V)	Converter-Io(A)	Converter-Power_Po(W)	Tracked-Power(W)
2.50	0.67	5.49	0.11	0.60	4.17
5.00	2.49	11.00	0.22	2.42	8.33
7.50	5.44	16.49	0.33	5.44	12.50
10.00	9.52	21.97	0.44	9.65	16.67
12.50	14.72	27.41	0.55	15.03	20.83
15.00	24.32	33.11	0.66	21.93	25.00
17.50	28.48	37.08	0.74	27.49	29.19
20.00	32.72	40.33	0.81	32.53	33.33
22.50	36.89	42.36	0.85	35.88	37.50
25.00	40.22	45.89	0.92	42.11	41.67
27.50	45.42	46.78	0.94	43.77	45.83
30.00	49.72	49.58	0.99	49.17	50.00
32.50	53.43	52.13	1.04	54.35	54.17
35.00	58.26	53.66	1.07	57.59	58.33
37.50	62.12	55.93	1.20	62.56	62.50
40.00	64.72	57.78	1.16	66.77	66.67
42.50	66.62	56.61	1.13	64.08	70.83
45.00	74.68	59.71	1.19	71.32	75.00
47.50	73.74	59.92	1.20	71.80	79.17
50.00	81.99	64.62	1.29	83.49	83.33
52.50	86.23	65.95	1.32	86.98	87.50
55.00	90.97	67.68	1.35	91.61	91.67
57.50	89.54	66.62	1.33	88.75	95.83
60.00	101.40	69.76	1.40	97.34	100.00
62.50	103.90	71.42	1.43	102.00	104.20
65.00	108.60	72.28	1.45	104.50	108.30
67.50	110.70	74.90	1.50	112.20	112.50
70.00	117.50	74.44	1.49	110.77	116.70
72.50	122.70	76.70	1.53	117.60	120.80
75.00	126.60	77.23	1.55	119.30	125.00
77.50	128.00	80.04	1.60	128.10	129.20
80.00	134.90	80.80	1.62	130.60	133.30
82.50	139.40	82.22	1.64	135.20	137.50
85.00	142.30	82.01	1.64	134.50	141.70
87.50	142.90	84.03	1.68	141.20	145.80
90.00	152.00	85.67	1.71	146.75	150.00
92.50	156.10	87.15	1.74	151.90	154.20
95.00	157.30	88.09	1.76	155.20	158.30
97.50	164.70	88.52	1.77	156.70	162.50
100.00	63.02	43.80	0.88	38.37	166.70
102.50	141.80	42.57	0.85	36.25	170.80
105.00	153.70	42.54	0.85	36.19	175.00
107.50	164.60	42.51	0.85	36.14	179.20
110.00	174.70	42.47	0.85	36.08	183.30
112.50	184.30	42.44	0.85	36.03	187.50
115.00	193.30	42.41	0.84	35.97	191.70
117.50	201.90	42.37	0.85	35.91	195.80
120.00	210.10	42.34	0.85	35.85	200.00
122.50	218.10	42.31	0.85	35.80	204.20
125.00	225.80	42.27	0.85	35.74	208.30
127.50	233.30	42.24	0.85	35.68	212.50
130.00	240.50	42.20	0.84	35.62	216.70
132.50	247.60	42.17	0.84	35.56	220.80
135.00	254.50	42.13	0.84	35.50	225.00
137.50	261.30	42.10	0.84	35.44	229.20
140.00	267.90	42.06	0.84	35.38	233.30
142.50	274.40	42.02	0.84	35.32	237.50
145.00	280.80	41.99	0.84	35.26	241.70
147.50	287.00	41.95	0.84	35.20	245.80
150.00	293.20	41.91	0.84	35.13	250.00

Table D.6 – 100-Ohms Load Resistance on Subsea Equipment

100-Ohms Load Resistance on Subsea Equipment					
Subsea Temp. Diff. (degC)	DPP-250W-Power(W)	Converter-Vo(V)	Converter-Io(A)	Converter-Power_Po(W)	Tracked-Power(W)
2.50	1.25	10.69	0.11	1.14	4.17
5.00	4.80	21.33	0.21	4.55	8.33
7.50	10.81	32.12	0.32	10.32	12.50
10.00	15.82	38.28	0.38	14.65	16.67
12.50	20.02	44.14	0.44	19.49	20.83
15.00	24.12	47.25	0.47	22.32	25.00
17.50	28.45	52.34	0.52	27.40	29.17
20.00	32.82	55.21	0.55	30.48	33.33
22.50	36.79	58.40	0.58	34.10	37.50
25.00	41.30	61.91	0.62	38.32	41.67
27.50	44.17	64.22	0.64	41.24	45.83
30.00	48.54	69.31	0.69	48.04	50.00
32.50	54.09	70.20	0.70	49.28	54.17
35.00	53.13	71.72	0.72	51.44	58.33
37.50	61.44	75.48	0.76	56.97	62.50
40.00	67.21	77.83	0.78	60.57	66.67
42.50	71.28	80.59	0.81	64.95	70.83
45.00	72.98	83.52	0.83	69.75	75.00
47.50	76.06	84.57	0.85	71.51	79.17
50.00	72.60	85.60	0.86	73.27	83.33
52.50	88.62	91.15	0.91	83.09	87.50
55.00	85.02	90.89	0.91	82.60	91.67
57.50	93.62	94.45	0.95	89.21	95.83
60.00	100.60	97.17	0.97	94.42	100.00
62.50	105.50	98.40	0.98	96.82	104.20
65.00	107.40	100.30	1.00	100.70	108.30
67.50	114.20	104.00	1.04	108.20	112.50
70.00	113.20	105.90	1.06	112.15	116.70
72.50	115.20	107.10	1.07	114.60	120.80
75.00	125.80	107.60	1.08	115.70	125.00
77.50	131.20	111.50	1.12	124.30	129.20
80.00	134.60	112.30	1.12	126.10	133.30
82.50	139.60	113.10	1.13	128.00	137.50
85.00	140.00	115.50	1.16	133.30	141.70
87.50	142.10	116.50	1.17	135.80	145.80
90.00	66.39	42.27	0.42	17.87	150.00
92.50	52.56	45.14	0.45	20.37	154.20
95.00	130.00	42.82	0.43	18.34	158.30
97.50	141.40	42.79	0.43	18.31	162.50
100.00	151.90	42.76	0.43	18.28	166.70
102.50	161.80	42.72	0.43	18.25	170.80
105.00	171.10	42.69	0.43	18.22	175.00
107.50	175.60	44.28	0.44	19.60	179.20
110.00	188.50	42.62	0.43	18.16	183.30
112.50	196.70	42.59	0.43	18.14	187.50
115.00	204.50	42.55	0.43	18.11	191.70
117.50	212.20	42.52	0.43	18.08	195.80
120.00	219.60	42.48	0.43	18.05	200.00
122.50	226.80	42.45	0.43	18.02	204.20
125.00	233.90	42.41	0.42	17.99	208.30
127.50	240.70	42.38	0.42	17.96	212.50
130.00	247.50	42.34	0.42	17.93	216.70
132.50	254.10	42.31	0.42	17.90	220.80
135.00	260.60	42.27	0.42	17.87	225.00
137.50	267.00	42.23	0.42	17.84	229.20
140.00	273.20	42.20	0.42	17.80	233.30
142.50	279.40	42.16	0.42	17.77	237.50
145.00	285.50	42.12	0.42	17.74	241.70
147.50	291.50	42.08	0.42	17.71	245.80
150.00	297.40	42.05	0.42	17.68	250.00

Table D.7 – System Efficiency & Overall Systems Efficiency

Time (Hours)	System_Efficiency_(%)	Overall Systems_Efficiency_(%)
1	0.020671749	0.004480133
2	0.020736993	0.009488504
3	0.02075819	0.004723337
4	0.020699509	0.001606032
5	0.020752042	0.041190612
6	0.020784594	0.972790761
7	0.020774021	0.964155617
8	0.02072075	0.951501449
9	0.020730993	0.95121663
10	0.020739491	0.949181776
11	0.020746812	0.950057752
12	0.020777544	0.949721989
13	0.020791158	0.94923583
14	0.020808382	0.951066017
15	0.021823996	0.953951335
16	0.024578219	0.960242833
17	0.024744362	0.973503993
18	0.024759572	0.964610874
19	0.024725238	0.960305448
20	0.024739268	0.965266106
21	0.02353128	0.971351205
22	0.020890245	0.974028895
23	0.020693114	0.942603402
24	0.015439524	0.962686975
25	0.006660996	0.969826971
26	0.004146839	0.967756683
27	0.020574032	0.969933742
28	0.0393886	0.975962007
29	0.054775552	0.968923663
30	0.073041064	0.955749982
31	0.094433141	0.958171661
32	0.119291211	0.960185848
33	0.145859866	0.957783993
34	0.17459896	0.957809
35	0.208482226	0.956770363
36	0.247676802	0.95642958
37	0.286620749	0.956392071
38	0.327519431	0.956593592
39	0.36245524	0.964521522
40	0.399424875	0.969229735
41	0.435020475	0.973770885
42	0.464188316	0.92742766
43	0.463922418	0.359031826
44	0.51244353	0.013616653
45	0.555821803	0.012122857
46	0.618915351	0.001205127
47	0.681417657	0.002910559
48	0.77560002	0.012122776
49	0.85678918	0.010068477
50	0.986428312	0.000177448

Time (Hours)	System_Efficiency_(%)	Overall Systems_Efficiency_(%)
51	0.983941201	0.000177448
52	0.991906474	0.019982947
53	0.993714931	0.046795841
54	0.992545177	0.093097865
55	0.991420375	0.550014275
56	0.99191978	0.732929027
57	0.991353639	0.840872396
58	0.990152226	0.945626425
59	0.991682793	0.954220317
60	0.990156398	0.835889241
61	0.990591928	0.969837527
62	0.990109901	0.964789727
63	0.989713426	0.967990748
64	0.990308657	0.973293081
65	0.988478347	0.968069961
66	0.990012933	0.971020917
67	0.991528854	0.965289898
68	0.988583972	0.975480825
69	0.991981041	0.969894782
70	0.990867526	0.962705345
71	0.988541254	0.966649852
72	0.992588751	0.959798188
73	0.991331186	0.964700363
74	0.989116248	0.959037088
75	0.992957834	0.956490998
76	0.992404912	0.956592951
77	0.989948132	0.95626395
78	0.991982597	0.959087763
79	0.994103715	0.960132187
80	0.994744674	0.958505219
81	0.992276323	0.95847705
82	0.992205369	0.958992136
83	0.99540137	0.960421501
84	0.994879374	0.964440062
85	0.994990231	0.967542938
86	0.99442937	0.968339215
87	0.993628345	0.962683918
88	0.995347337	0.962651748
89	0.996612671	0.963590232
90	0.995673094	0.965283773
91	0.994902809	0.972032153
92	0.995530999	0.974617117
93	0.996430292	0.97476533
94	0.996657211	0.969151259
95	0.997718147	0.968222696
96	0.997246506	0.978454108
97	0.995562355	0.972467372
98	0.994350065	0.963450266
99	0.993849969	0.953531344
100	0.993817459	0.966956156

Time (Hours)	System_Efficiency_(%)	Overall Systems_Efficiency_(%)
100	0.993817459	0.966956156
101	0.994745833	0.707204082
102	0.995835762	0.494634621
103	0.996609669	0.4069922
104	0.998528543	0.315860342
105	0.998773176	0.085405054
106	0.997600472	0.023994996
107	0.996799823	0.012122858
108	0.995347331	0.018281938
109	0.993533624	0.029042596
110	0.993053018	0.029094713
111	0.992633079	0.00482485
112	0.992527807	0.981975096
113	0.991216351	0.015828629
114	0.99043151	0.089854224
115	0.990563683	0.44107827
116	0.990789379	0.847720517
117	0.990537573	0.968444681
118	0.990396918	0.978767221
119	0.990775607	0.987352759
120	0.990278903	0.981975096
121	0.990183735	0.962966695
122	0.989921658	0.969624995
123	0.989789407	0.963432975
124	0.99048259	0.835390557
125	0.990483007	0.14630659
126	0.990187024	0.843277047
127	0.99000469	0.903252368
128	0.990002204	0.957683695
129	0.990157918	0.97602427
130	0.990418581	0.961656263
131	0.99061704	0.956738151
132	0.990604229	0.967080259
133	0.990226789	0.963005173
134	0.99092675	0.96602044
135	0.992153706	0.972504424
136	0.992506165	0.973460834
137	0.993048419	0.967096131
138	0.993614807	0.974357392
139	0.994261233	0.965152538
140	0.995183727	0.975307365
141	0.997384374	0.969805852
142	0.997621028	0.967878773
143	0.998274791	0.966924727
144	0.998864597	0.963294947
145	0.998406621	0.967679975
146	0.996734973	0.96834371
147	0.995816833	0.965454473
148	0.994297342	0.9600639
149	0.994167307	0.96456199

Time (Hours)	System_Efficiency_(%)	Overall Systems_Efficiency_(%)
150	0.995112221	0.957548633
151	0.994715032	0.959627628
152	0.996618151	0.957521946
153	0.998086326	0.956456931
154	0.99635153	0.949393901
155	0.996645123	0.949355016
156	0.996783031	0.94904428
157	0.995400387	0.948774066
158	0.995053317	0.948761943
159	0.995950826	0.948929844
160	0.996110069	0.949453549
161	0.994638948	0.948970605
162	0.993519767	0.949517541
163	0.994876596	0.949899954
164	0.994906213	0.94961493
165	0.995132741	0.951679185
166	0.992256556	0.953695985
167	0.990708902	0.956254315
168	0.991845602	0.956327422
169	0.993761278	0.956605402
170	0.994073332	0.957100289
171	0.990041478	0.957167368
172	0.990445533	0.957103374
173	0.994042432	0.956789512
174	0.992266875	0.956841772
175	0.987980912	0.954184147
176	0.990874202	0.953772209
177	0.992516868	0.952725758
178	0.987688739	0.951379489
179	0.988280866	0.952008137
180	0.992158369	0.952000385
181	0.986594299	0.951637461
182	0.989733088	0.955995778
183	0.989449528	0.95704722
184	0.987467196	0.956699438
185	0.991497226	0.957485717
186	0.987007713	0.95647649
187	0.991160465	0.957076254
188	0.98870312	0.953516295
189	0.991844272	0.953277638
190	0.989149335	0.953341312
191	0.990911753	0.959979177
192	0.990076582	0.956902687
193	0.990447208	0.957909261
194	0.992707505	0.959341345
195	0.992342683	0.959231569
196	0.993522352	0.959915473
197	0.993988381	0.959476099
198	0.994542879	0.966624439
199	0.99535215	0.968338251
200	0.996598749	0.965418554

Time (Hours)	System_Efficiency_(%)	Overall Systems_Efficiency_(%)
201	0.993554948	0.975284986
202	0.973677784	0.977227294
203	0.929280681	0.969022987
204	0.89451925	0.96860121
205	0.83813194	0.968186734
206	0.782725041	0.973654337
207	0.7176916	0.980420299
208	0.655559912	0.961850493
209	0.592731383	0.960644397
210	0.536884372	0.970403054
211	0.483907059	0.961003806
212	0.42839361	0.803907398
213	0.375901555	0.63699968
214	0.323699551	0.438380671
215	0.275788474	0.215388893
216	0.231983822	0.080000808
217	0.191728763	0.035516351
218	0.155306242	0.040404071
219	0.121611845	0.050774117
220	0.092857982	0.05307532
221	0.067411274	0.045923128
222	0.043077689	0.030352946
223	0.014573557	0.012110776
224	0.005761422	0.001024235
225	0.016738538	0.000328265
226	0.023965681	0.003234558
227	0.027360021	0.003234558
228	0.028887212	0.003234558
229	0.028927305	0.003234558
230	0.028928942	0.003234558
231	0.015829105	0.003234558

Table D.8 – DTEG Stepwise Sequence Operation

(Increment & Decrement)

Subsea Temperature Stepwise Sequence (Increment & Decrement)						
Subsea Temp.Diff (degC)	**Power Generated via 250W-DPP (W)**	**Bus Voltage_V-Bus (V)**	**Subsea Battery Voltage-SBat (V)**	**Subsea Battery Current-SBat (A)**	**Subsea Bat. State of Charge SOC (%)**	**Power Delivered to Subsea Equipment (W)**
0.00	0.00	47.93	25.75	6.59	44.94	24.91
3.50	4.54	47.92	25.75	6.38	44.94	24.89
5.00	7.68	47.89	25.75	6.57	44.94	24.86
7.00	10.94	47.88	25.75	5.95	44.94	24.82
10.00	15.88	48.08	25.76	5.41	44.95	25.04
10.50	16.74	48.02	25.75	6.29	44.95	25.00
14.00	22.59	47.87	25.75	6.36	44.95	24.82
17.50	28.54	47.88	25.76	6.18	44.95	24.82
20.00	32.71	47.88	25.76	4.90	44.95	24.83
21.00	34.51	47.90	25.76	5.30	44.96	24.85
24.50	40.46	47.94	25.77	5.00	44.96	24.82
28.00	46.50	47.90	25.77	5.21	44.96	24.77
30.00	49.93	47.87	25.77	4.83	44.96	24.84
31.50	52.26	47.81	25.77	4.30	44.96	24.77
35.00	58.57	47.93	25.77	4.93	44.97	24.81
38.50	64.51	47.93	25.78	4.07	44.97	24.81
40.00	67.19	47.97	25.78	4.45	44.97	24.86
42.00	70.62	47.92	25.78	4.25	44.97	24.82
45.50	76.11	48.15	25.78	3.75	44.98	24.93
49.00	82.40	47.88	25.78	3.54	44.98	24.77
50.00	83.99	47.87	25.79	3.44	44.98	24.76
52.50	88.73	48.00	25.79	2.88	44.98	24.93
56.00	94.70	47.92	25.79	3.21	44.99	24.83
59.50	100.80	48.00	25.79	3.04	44.99	24.75
60.00	101.30	47.86	25.79	2.92	44.99	24.59
63.00	106.60	48.13	25.80	2.48	44.99	24.93
66.50	111.60	47.76	25.80	2.65	45.00	24.67
70.00	118.70	47.98	25.80	2.55	45.00	24.76

Subsea Temperature Stepwise Sequence (Increment & Decrement)						
Subsea Temp.Diff (degC)	Power Generated via 250W-DPP (W)	Bus Voltage_V-Bus (V)	Subsea Battery Voltage-SBat (V)	Subsea Battery Current-SBat (A)	Subsea Bat. State of Charge SOC (%)	Power Delivered to Subsea Equipment (W)
73.50	124.70	47.96	25.81	1.59	45.00	24.72
77.00	130.70	47.99	25.81	1.73	45.00	24.77
80.00	135.80	47.97	25.81	1.27	45.01	24.78
80.50	136.70	48.05	25.81	1.29	45.01	24.86
84.00	141.90	47.88	25.81	1.19	45.01	24.64
87.50	147.60	48.17	25.81	1.66	45.01	24.77
90.00	152.60	47.93	25.81	1.02	45.01	24.74
91.00	154.40	48.05	25.82	0.57	45.02	24.85
94.50	158.80	47.90	25.82	0.62	45.02	24.68
98.00	163.30	47.81	25.82	0.74	45.02	24.56
100.00	166.90	47.85	25.82	0.26	45.02	24.62
101.50	170.50	47.96	25.82	0.25	45.02	24.76
105.00	173.60	47.83	25.83	-0.14	45.03	24.59
108.50	183.20	47.96	25.83	-0.13	45.03	24.63
110.00	186.20	48.12	25.83	-0.30	45.03	24.76
112.00	189.50	48.08	25.83	-0.06	45.03	24.72
115.00	194.60	48.03	25.83	-0.74	45.03	24.66
115.50	195.40	47.98	25.83	-0.94	45.04	24.69
118.00	199.60	47.99	25.83	-0.33	44.04	24.89
119.00	201.20	48.04	25.83	-0.48	45.04	24.98
120.00	202.80	47.98	25.84	-1.34	45.04	24.65
122.50	232.80	47.87	25.75	6.05	44.94	24.84
125.00	240.20	47.91	25.74	6.63	44.94	24.88
126.00	242.80	47.95	25.75	6.32	44.94	24.92
129.50	250.90	47.93	25.75	6.31	44.94	24.91
130.00	249.50	47.93	25.75	6.71	44.94	24.89
133.00	260.50	47.94	25.75	6.41	44.94	24.91
136.50	269.10	47.94	25.75	6.42	44.94	24.91
140.00	275.70	47.94	25.75	6.74	44.94	24.90
143.50	285.00	47.89	25.75	6.27	44.94	24.86
147.00	294.00	47.87	25.74	6.98	44.94	24.85
150.00	300.10	47.91	25.75	6.29	44.94	24.89

Appendix E

Algorithm E.1 - MATLAB Script – DPU, DC-DC Converter, Subsea Power Inverter in Underwater Combo Power Grid System

Table E.2- DC Output from 6.4 kW-DPU-Power System (4-Hours Subsea Operations)

Table E.3 - DC BUS (4-Hours Subsea Operation)

Table E.4 - AC Output to Underwater Power Grid System (4-Hours Subsea Operation)

Algorithm E.1 - MATLAB Script – DPU, DC-DC Converter, Subsea Power Inverter in Underwater Combo Power Grid System

```
%%%%%%%%%%%%%%%%%%%%%%%%%%%%%%%%%%%%%%%%%%%%%%%%%%%%%%%%%%%%%%%%%%%%%%%%%%%%%%%%
%                                                                              %
%   Dept. of Naval Architecture, Ocean & Marine Engineering                    %
%   University of Strathclyde, Glasgow, Scotland, United Kingdom.              %
%                                                                              %
%   Project Name:  Deepwater Thermoelectricity                                 %
%                          in                                                  %
%                  Underwater Combo Power Grid                                 %
%                                                                              %
%                                                                              %
%                                                                              %
%   File Description: Underwater Combo Power Grid                              %
%                     6.4KW_DPU_Source                                         %
%                     SubseaPowerInverter,                                     %
%                     Switch Mode DC-DC Boost Converter                        %
%                     Design Parameters                                        %
%                                                                              %
%  Inputs:         DC Voltage Source, Inductor, Capacitor                      %
%                  IGBT, Diode,Underwater Power Grid Frequency                 %
%                                                                              %
%   Author:        Austin Asuquo                                               %
%   Date:          19th December, 2019                                         %
%                                                                              %
%%%%%%%%%%%%%%%%%%%%%%%%%%%%%%%%%%%%%%%%%%%%%%%%%%%%%%%%%%%%%%%%%%%%%%%%%%%%%%%%
%
%        Design of Subsea Power Inverter, switch mode DC-DC Converter
%        for DPU & Underwater Combo Power Grid
%
clc, clear, close all

Ts=10e-6;                          % Sampling Time
P=6e3;                             % DPU Rated Power
U=380;                             % Underwater Inverter Phase to Phase Voltage
f=50;                              % Underwater Power Grid Frequency
fsw=5e3;                           % Switching frequency of Subsea Inverter

Lf=((0.1*U^2)/(2*pi*f*(P/3)));

%Design of DC-DC Switch Mode Boost Converter
Vopp=174;                                   % Optimum Power Point Voltage for 6.4KW-DPU Source
V_bus_ref=570;                              % Bus Voltage (VBus) also known as DC-Link
Vin=Vopp;                                   % Input Voltage to DC-DC Switch Mode Boost Converter
Vo=V_bus_ref;                               % Output Voltage of DC-DC Switch Mode Boost Converter
fsw_boost=5e3;                              % Switching Frequency of DC-DC Switch Mode Boost Converter
D=1-(Vin/Vo);                               % Duty Circle Computation
L_bound=((1-D)^2)*D*(Vo^2)/(2*fsw_boost*P); % DC-DC Switch Mode Boost Converter Inductor Boundary
L_boost=10*L_bound;                         % DC-DC Switch Mode Boost Converter Inductor
C_boost_min=(D*P)/(0.01*Vo^2*fsw_boost);    % DC-DC Switch Mode Boost Converter Minimum Capacitor
C_boost=1000e-6;                            % DC-DC Switch Mode Boost Converter Capacitor
```

Table E.2- DC Output from 6.4 kW-DPU-Power System (4-Hours Subsea Operations)

DC Output from 6.4 kW-DPU-Power System (4-Hours Subsea Operations)				
Time (Hours)	Subsea Temp. Diff. (degC)	DC- Current (A)	6.4kW-DPU-Source Power (kW)	Tracked Power (kW)
0.0000	0.3707	0.1166	0.0000	0.0158
0.0166	0.3707	0.1164	0.0023	0.0158
0.0332	0.3707	0.1162	0.0046	0.0158
0.0498	0.3707	0.1160	0.0069	0.0158
0.0664	0.3707	0.1158	0.0091	0.0158
0.0830	0.3707	0.1151	0.0111	0.0158
0.0996	0.3707	0.1086	0.0125	0.0158
0.1162	0.3707	0.1022	0.0122	0.0158
0.1328	0.3707	0.1084	0.0125	0.0158
0.1494	0.3707	0.1068	0.0124	0.0158
0.1660	0.3707	0.1064	0.0124	0.0158
0.1826	0.3707	0.1093	0.0125	0.0158
0.1992	0.3707	0.1088	0.0125	0.0158
0.2158	0.3707	0.1088	0.0125	0.0158
0.2324	0.3707	0.1087	0.0125	0.0158
0.2490	0.3707	0.1081	0.0125	0.0158
0.2656	0.3707	0.1085	0.0125	0.0158
0.2822	0.4236	0.1086	0.0135	0.0181
0.2988	0.4236	0.1267	0.0143	0.0181
0.3154	0.4236	0.1177	0.0142	0.0181
0.3320	0.4237	0.1259	0.0143	0.0181
0.3486	0.4237	0.1206	0.0143	0.0181
0.3652	0.4237	0.1234	0.0144	0.0181
0.3818	0.3707	0.1120	0.0123	0.0158
0.3984	0.3707	0.1041	0.0123	0.0158
0.4150	0.3431	0.0985	0.0115	0.0146
0.4316	0.2101	0.0648	0.0064	0.0090
0.4482	0.0374	0.0117	0.0008	0.0016
0.4648	0.2237	0.0701	0.0038	0.0095
0.4814	0.5508	0.1723	0.0112	0.0235
0.4980	1.0772	0.3337	0.0355	0.0459
0.5146	1.7127	0.1194	0.0174	0.0730
0.5312	2.4909	0.5280	0.0748	0.1062
0.5478	3.3965	0.9897	0.1305	0.1448
0.5644	4.3899	1.2560	0.1702	0.1872
0.5810	5.4431	1.5808	0.2143	0.2321
0.5976	6.4842	1.8981	0.2580	0.2764
0.6142	7.8666	2.3112	0.3163	0.3354
0.6308	9.4158	2.7716	0.3821	0.4014
0.6474	10.9977	3.2368	0.4495	0.4689
0.6640	12.6265	3.6658	0.5184	0.5383
0.6806	13.7789	4.0696	0.5687	0.5874
0.6972	15.3734	4.5531	0.6379	0.6554
0.7138	16.6803	4.9666	0.6935	0.7111
0.7304	17.0844	5.0448	0.7118	0.7284
0.7470	16.1644	4.7494	0.6717	0.6891
0.7636	19.3025	5.7639	0.8067	0.8229

DC Output from 6.4 kW-DPU-Power System (4-Hours Subsea Operations)				
Time (Hours)	**Subsea Temp. Diff. (degC)**	**DC- Current (A)**	**6.4kW-DPU-Source Power (kW)**	**Tracked Power (kW)**
0.7802	20.4640	6.1051	0.8576	0.8724
0.7968	24.3243	7.2683	1.0255	1.0370
0.8134	26.4511	7.9216	1.1178	1.1277
0.8300	30.7679	9.1354	1.3080	1.3117
0.8466	33.1040	9.6256	1.4127	1.4113
0.8632	35.3291	10.6886	1.4997	1.5062
0.8798	38.3450	11.6709	1.6149	1.6348
0.8964	40.2868	11.6309	1.7194	1.7176
0.9130	40.5789	8.2870	1.3355	1.7300
0.9296	44.8487	13.7351	1.8736	1.9120
0.9462	47.3960	11.9640	1.8704	2.0206
0.9628	49.3118	15.0851	2.0700	2.1023
0.9794	51.5854	13.7128	2.1175	2.1993
0.9960	53.9429	16.5021	2.2681	2.2998
1.0126	56.1293	13.3385	2.1195	2.3930
1.0292	58.5452	17.7004	2.5049	2.4960
1.0458	60.7848	18.5862	2.5622	2.5915
1.0624	62.6015	16.9826	2.6125	2.6689
1.0790	64.8576	19.8058	2.7430	2.7651
1.0956	67.3290	16.4607	2.6099	2.8705
1.1122	69.6619	20.9452	2.9978	2.9699
1.1288	72.1134	21.1505	3.1268	3.0744
1.1454	74.0466	21.2193	3.1837	3.1569
1.1620	76.6581	23.2882	3.2691	3.2682
1.1786	78.3322	19.6332	3.1028	3.3396
1.1952	80.4698	24.2944	3.4526	3.4307
1.2118	82.7474	25.1905	3.5187	3.5278
1.2284	84.7428	23.5940	3.6067	3.6129
1.2450	86.6357	26.0389	3.7281	3.6936
1.2616	88.6525	26.8197	3.7955	3.7796
1.2782	91.1537	27.4712	3.9210	3.8862
1.2948	93.0376	27.0472	4.0141	3.9665
1.3114	95.1086	28.6629	4.0828	4.0548
1.3280	96.8233	25.1408	3.9340	4.1279
1.3446	99.3308	30.0609	4.2448	4.2348
1.3612	101.3805	30.6767	4.3319	4.3222
1.3778	103.5697	28.3797	4.3552	4.4155
1.3944	105.5181	31.3993	4.5468	4.4986
1.4110	106.7998	32.1324	4.5792	4.5532
1.4276	108.9543	32.8378	4.6640	4.6451
1.4442	110.7475	33.2368	4.7525	4.7215
1.4608	112.6488	33.6985	4.8399	4.8026
1.4774	114.1915	33.2409	4.9182	4.8684
1.4940	115.8685	34.8273	4.9615	4.9399
1.5106	117.4117	34.8848	5.0488	5.0057
1.5272	118.3820	35.2664	5.0868	5.0470
1.5438	120.1752	35.7890	5.1626	5.1235
1.5604	121.2620	36.3304	5.1952	5.1698
1.5770	122.7138	36.8455	5.2489	5.2317
1.5936	124.4243	36.0271	5.3356	5.3046

DC Output from 6.4 kW-DPU-Power System (4-Hours Subsea Operations)				
Time (Hours)	**Subsea Temp. Diff. (degC)**	**DC- Current (A)**	**6.4kW-DPU-Source Power (kW)**	**Tracked Power (kW)**
1.6102	125.7846	37.4519	5.3969	5.3626
1.6268	127.5082	37.9836	5.4659	5.4361
1.6434	129.2425	35.9019	5.4510	5.5100
1.6600	130.1042	35.9031	5.4674	5.5468
1.6766	131.9116	39.1409	5.6549	5.6238
1.6932	133.0543	39.4857	5.7005	5.6725
1.7098	134.1161	39.7878	5.7461	5.7178
1.7264	134.9889	37.2903	5.6696	5.7550
1.7430	136.3336	40.4781	5.8347	5.8124
1.7596	137.2071	40.6736	5.8725	5.8496
1.7762	137.6581	40.7303	5.8925	5.8688
1.7928	138.5334	41.1281	5.9252	5.9061
1.8094	139.6069	41.4989	5.9674	5.9519
1.8260	140.8709	41.8241	6.0208	6.0058
1.8426	142.0452	40.8404	6.0542	6.0559
1.8592	142.3384	42.1406	6.0839	6.0684
1.8758	143.1570	42.3799	6.1175	6.1033
1.8924	144.3905	42.1719	6.1684	6.1558
1.9090	145.1359	42.9625	6.1983	6.1876
1.9256	145.4706	42.9626	6.2136	6.2019
1.9422	145.3552	42.6717	6.2180	6.1970
1.9588	146.5066	42.1278	6.2401	6.2461
1.9754	146.6727	42.3921	6.2512	6.2531
1.9920	147.3240	43.5560	6.2882	6.2809
2.0086	147.3575	43.5820	6.2895	6.2823
2.0252	147.0214	42.0664	6.2513	6.2680
2.0418	147.0574	43.5849	6.2753	6.2695
2.0584	147.9928	43.8527	6.3150	6.3094
2.0750	148.6816	43.9124	6.3444	6.3388
2.0916	149.0979	44.0059	6.3633	6.3565
2.1082	148.8276	43.8795	6.3513	6.3450
2.1248	149.2130	44.0066	6.3684	6.3614
2.1414	149.4662	44.1538	6.3762	6.3722
2.1485	149.9083	44.4046	6.3813	6.3951
2.1746	149.5010	44.1576	6.3772	6.3737
2.1912	148.8400	44.0526	6.3497	6.3455
2.2078	148.4928	43.8712	6.3362	6.3307
2.2244	149.3693	44.1021	6.3731	6.3681
2.2410	148.5987	43.6808	6.3422	6.3353
2.2576	147.8076	43.7300	6.3081	6.3015
2.2742	147.6442	43.8145	6.2974	6.2946
2.2908	147.5415	43.7434	6.2940	6.2902
2.3074	148.1344	42.4366	6.2975	6.3155
2.3240	146.6793	43.4617	6.2606	6.2534
2.3406	145.6545	42.1037	6.2098	6.2097
2.3572	145.2312	43.1840	6.1969	6.1917
2.3738	144.4006	42.9456	6.1621	6.1563
2.3904	144.5336	42.9312	6.1701	6.1619
2.4070	143.7966	42.7384	6.1385	6.1305
2.4236	143.1886	42.2490	6.1280	6.1046

DC Output from 6.4 kW-DPU-Power System (4-Hours Subsea Operations)				
Time (Hours)	**Subsea Temp. Diff. (degC)**	**DC- Current (A)**	**6.4kW-DPU-Source Power (kW)**	**Tracked Power (kW)**
2.4402	141.6521	41.1819	6.0526	6.0391
2.4568	141.5910	41.5418	6.0569	6.0365
2.4734	141.5118	42.1349	6.0424	6.0331
2.4900	139.4433	41.1236	5.9682	5.9449
2.5066	139.0826	40.8907	5.9525	5.9296
2.5232	138.0069	41.2107	5.8946	5.8837
2.5398	137.5009	38.8908	5.8340	5.8621
2.5564	136.3421	40.6779	5.8287	5.8127
2.5730	135.1491	40.4628	5.7692	5.7619
2.5896	133.8782	39.4193	5.7376	5.7077
2.6062	133.2802	40.0666	5.6796	5.6822
2.6228	131.9555	39.7270	5.6196	5.6257
2.6394	129.4836	38.5336	5.5476	5.5203
2.6560	128.9851	38.6390	5.5140	5.4991
2.6726	126.2717	37.9264	5.3945	5.3834
2.6892	125.2826	37.6982	5.3476	5.3412
2.7058	125.2013	35.0143	5.3108	5.3378
2.7224	123.5071	33.0604	5.1073	5.2655
2.7390	121.9272	34.1416	5.1786	5.1982
2.7556	120.1513	32.9718	5.0422	5.1225
2.7722	118.4753	35.0602	5.0948	5.0510
2.7888	117.7548	34.3780	5.0639	5.0203
2.8054	115.2461	34.5908	4.9399	4.9133
2.8220	113.9795	34.5110	4.8532	4.8593
2.8386	112.8671	34.1422	4.8200	4.8119
2.8552	110.6290	28.1158	4.4230	4.7165
2.8718	107.9550	32.3378	4.6383	4.6025
2.8884	107.5282	28.8261	4.4663	4.5843
2.9050	105.4123	30.3821	4.5318	4.4941
2.9216	103.8684	30.9127	4.4880	4.4283
2.9382	102.6334	30.3819	4.4278	4.3756
2.9548	99.7747	29.5840	4.3174	4.2537
2.9714	97.4985	29.4071	4.1787	4.1567
2.9880	95.5812	22.8061	3.6436	4.0749
3.0046	93.2462	28.4608	3.9389	3.9754
3.0212	92.0100	23.8772	3.7363	3.9227
3.0378	90.0426	27.5503	3.7853	3.8388
3.0544	88.0655	23.2024	3.6140	3.7545
3.0710	85.8184	26.0283	3.6633	3.6587
3.0876	84.0335	20.3445	3.2400	3.5826
3.1042	81.7721	24.9706	3.4563	3.4862
3.1208	79.8726	19.0469	3.0417	3.4052
3.1374	77.6139	23.5603	3.3111	3.3089
3.1540	75.5976	16.8826	2.7247	3.2230
3.1706	72.9480	22.4053	3.0392	3.1100
3.1872	71.0034	17.7000	2.7952	3.0271
3.2038	69.2355	15.4217	2.4899	2.9517
3.2204	67.3085	20.1700	2.8990	2.8696
3.2370	65.0059	19.7035	2.7879	2.7714
3.2536	62.6131	17.1813	2.6308	2.6694

DC Output from 6.4 kW-DPU-Power System (4-Hours Subsea Operations)				
Time (Hours)	**Subsea Temp. Diff. (degC)**	**DC- Current (A)**	**6.4kW-DPU-Source Power (kW)**	**Tracked Power (kW)**
3.2702	60.5441	18.5671	2.5387	2.5812
3.2868	58.3271	16.6161	2.4954	2.4867
3.3034	56.4923	17.3749	2.3438	2.4085
3.3200	54.4103	15.9729	2.3444	2.3197
3.3366	52.1290	12.5521	1.9919	2.2224
3.3532	50.3371	15.5292	2.0522	2.1460
3.3698	48.3986	13.7537	2.0617	2.0634
3.3864	46.1332	8.8655	1.4421	1.9668
3.4030	43.7823	13.2915	1.8641	1.8666
3.4196	41.7296	12.8057	1.7302	1.7791
3.4362	39.6571	11.0993	1.6693	1.6907
3.4528	37.3163	6.9286	1.1224	1.5909
3.4694	35.2044	5.8004	0.9475	1.5009
3.4860	33.2166	6.8973	1.1039	1.4161
3.5026	31.1182	7.1537	1.1245	1.3267
3.5192	28.9592	8.8115	1.2099	1.2346
3.5358	26.8712	8.1498	1.1298	1.1456
3.5524	25.0099	5.6556	0.8848	1.0663
3.5690	23.1232	6.9373	0.9700	0.9858
3.5856	20.9530	6.3342	0.8749	0.8933
3.6022	19.1431	5.1681	0.7700	0.8161
3.6188	17.2300	5.2446	0.7076	0.7346
3.6354	15.6391	4.6303	0.6486	0.6667
3.6520	13.9771	4.1524	0.5771	0.5959
3.6686	12.2782	3.5696	0.5036	0.5235
3.6852	10.6899	3.1737	0.4362	0.4557
3.7018	9.1628	2.7085	0.3713	0.3906
3.7184	7.7021	2.2650	0.3094	0.3284
3.7350	6.3989	1.8943	0.2545	0.2728
3.7516	5.1761	1.5248	0.2036	0.2207
3.7682	4.0807	1.2009	0.1585	0.1740
3.7848	3.0915	0.9182	0.1181	0.1318
3.8014	2.2155	0.6638	0.0828	0.0945
3.8180	1.4587	0.4449	0.0522	0.0622
3.8346	0.7289	0.2276	0.0191	0.0311
3.8512	0.3716	0.1165	0.0052	0.0158
3.8678	0.0480	0.0151	0.0003	0.0020
3.8844	0.2049	0.0644	0.0007	0.0087
3.9010	0.3614	0.1136	0.0015	0.0154
3.9176	0.3760	0.1181	0.0019	0.0160
3.9342	0.4226	0.1328	0.0024	0.0180
3.9508	0.4233	0.1330	0.0026	0.0180
3.9974	0.4233	0.1330	0.0026	0.0180
3.9986	0.4234	0.1330	0.0027	0.0180

Table E.3 - DC BUS (4-Hours Subsea Operation)

DC BUS (4-Hours Subsea Operation)		
Time (Hours)	Subsea Temp. Diff. (degC)	BUS-Voltage (V)
0.0000	0.37	0.0003
0.0166	0.37	421.4952
0.0332	0.37	833.8416
0.0498	0.37	1042.5283
0.0664	0.37	1035.6732
0.0830	0.37	830.7507
0.0996	0.37	599.7381
0.1162	0.37	419.8177
0.1328	0.37	355.5696
0.1494	0.37	403.5135
0.1660	0.37	513.9689
0.1826	0.37	622.4790
0.1992	0.37	683.4886
0.2158	0.37	677.0273
0.2324	0.37	622.4360
0.2490	0.37	558.8020
0.2656	0.37	515.9031
0.2822	0.42	504.2692
0.2988	0.42	523.4905
0.3154	0.42	556.2139
0.3320	0.42	584.3612
0.3486	0.42	597.4484
0.3652	0.42	589.9297
0.3818	0.37	573.7726
0.3984	0.37	556.9513
0.4150	0.34	548.7612
0.4316	0.21	549.3665
0.4482	0.04	556.5298
0.4648	0.22	565.7558
0.4814	0.55	571.3187
0.4980	1.08	572.4098
0.5146	1.71	570.2683
0.5312	2.49	564.8257
0.5478	3.40	562.6458
0.5644	4.39	561.9922
0.5810	5.44	562.8084
0.5976	6.48	564.9473
0.6142	7.87	566.6370
0.6308	9.42	567.5119
0.6474	11.00	568.5125
0.6640	12.63	567.7272
0.6806	13.78	567.3948
0.6972	15.37	566.8040
0.7138	16.68	565.9727
0.7304	17.08	565.9774
0.7470	16.16	565.4963

DC BUS (4-Hours Subsea Operation)		
Time (Hours)	Subsea Temp. Diff. (degC)	BUS-Voltage (V)
0.7636	19.30	565.5689
0.7802	20.46	566.8796
0.7968	24.32	569.3983
0.8134	26.45	569.9035
0.8300	30.77	571.7176
0.8466	33.10	572.0525
0.8632	35.33	571.6023
0.8798	38.34	570.1611
0.8964	40.29	570.3585
0.9130	40.58	568.3662
0.9296	44.85	567.8418
0.9462	47.40	569.4118
0.9628	49.31	571.4646
0.9794	51.59	571.5388
0.9960	53.94	571.6253
1.0126	56.13	571.5329
1.0292	58.55	571.4448
1.0458	60.78	571.3035
1.0624	62.60	570.2838
1.0790	64.86	571.7466
1.0956	67.33	572.5014
1.1122	69.66	573.4433
1.1288	72.11	572.9694
1.1454	74.05	571.7795
1.1620	76.66	574.1654
1.1786	78.33	575.5222
1.1952	80.47	573.3522
1.2118	82.75	571.5781
1.2284	84.74	573.1272
1.2450	86.64	575.7751
1.2616	88.65	575.7621
1.2782	91.15	573.4429
1.2948	93.04	572.8489
1.3114	95.11	576.5555
1.3280	96.82	575.4281
1.3446	99.33	573.0615
1.3612	101.38	572.1616
1.3778	103.57	576.2707
1.3944	105.52	578.1653
1.4110	106.80	575.3060
1.4276	108.95	573.9432
1.4442	110.75	575.2850
1.4608	112.65	577.3321
1.4774	114.19	577.7081
1.4940	115.87	574.9229
1.5106	117.41	575.6588
1.5272	118.38	579.0136
1.5438	120.18	578.9854
1.5604	121.26	576.9886
1.5770	122.71	573.8224

DC BUS (4-Hours Subsea Operation)		
Time (Hours)	Subsea Temp. Diff. (degC)	BUS-Voltage (V)
1.5936	124.42	574.8099
1.6102	125.78	578.4066
1.6268	127.51	578.5948
1.6434	129.24	578.3532
1.6600	130.10	578.1787
1.6766	131.91	579.4689
1.6932	133.05	579.9472
1.7098	134.12	579.7615
1.7264	134.99	577.9976
1.7430	136.33	578.3334
1.7596	137.21	580.3255
1.7762	137.66	580.1257
1.7928	138.53	578.7018
1.8094	139.61	577.8895
1.8260	140.87	578.8995
1.8426	142.05	580.4932
1.8592	142.34	580.4296
1.8758	143.16	580.0369
1.8924	144.39	579.8534
1.9090	145.14	580.2356
1.9256	145.47	581.2084
1.9422	145.36	582.2529
1.9588	146.51	581.4043
1.9754	146.67	580.0937
1.9920	147.32	580.1727
2.0086	147.36	580.0750
2.0252	147.02	580.2526
2.0418	147.06	579.0529
2.0584	147.99	579.5573
2.0750	148.68	579.9529
2.0916	149.10	581.4962
2.1082	148.83	581.2205
2.1248	149.21	581.6140
2.1414	149.47	580.7499
2.1485	149.91	580.1585
2.1746	149.50	579.0833
2.1912	148.84	579.0738
2.2078	148.49	579.0291
2.2244	149.37	580.5369
2.2410	148.60	579.8518
2.2576	147.81	579.6496
2.2742	147.64	578.0478
2.2908	147.54	577.7745
2.3074	148.13	578.9013
2.3240	146.68	579.3492
2.3406	145.65	576.7308
2.3572	145.23	575.9323
2.3738	144.40	576.6371
2.3904	144.53	577.5001
2.4070	143.80	576.9855

DC BUS (4-Hours Subsea Operation)		
Time (Hours)	Subsea Temp. Diff. (degC)	BUS-Voltage (V)
2.4236	143.19	578.1576
2.4402	141.65	577.1634
2.4568	141.59	576.8251
2.4734	141.51	577.0310
2.4900	139.44	576.0654
2.5066	139.08	575.7946
2.5232	138.01	575.1065
2.5398	137.50	576.0816
2.5564	136.34	576.5139
2.5730	135.15	574.4277
2.5896	133.88	572.9755
2.6062	133.28	572.0414
2.6228	131.96	570.9721
2.6394	129.48	571.0178
2.6560	128.99	572.9889
2.6726	126.27	573.1332
2.6892	125.28	572.6251
2.7058	125.20	573.0245
2.7224	123.51	571.8070
2.7390	121.93	571.4079
2.7556	120.15	568.6589
2.7722	118.48	568.3492
2.7888	117.75	570.1058
2.8054	115.25	572.0530
2.8220	113.98	571.0613
2.8386	112.87	569.7235
2.8552	110.63	568.1231
2.8718	107.95	566.1362
2.8884	107.53	564.9222
2.9050	105.41	565.3291
2.9216	103.87	568.3882
2.9382	102.63	570.0556
2.9548	99.77	570.7694
2.9714	97.50	568.0542
2.9880	95.58	565.2915
3.0046	93.25	562.7026
3.0212	92.01	562.6907
3.0378	90.04	562.9333
3.0544	88.07	562.8511
3.0710	85.82	564.9102
3.0876	84.03	566.1157
3.1042	81.77	567.4812
3.1208	79.87	566.4242
3.1374	77.61	564.7629
3.1540	75.60	562.9622
3.1706	72.95	563.4899
3.1872	71.00	562.5192
3.2038	69.24	563.8093
3.2204	67.31	562.0408
3.2370	65.01	562.8676

DC BUS (4-Hours Subsea Operation)		
Time (Hours)	**Subsea Temp. Diff. (degC)**	**BUS-Voltage (V)**
3.2536	62.61	562.1457
3.2702	60.54	563.5782
3.2868	58.33	562.0145
3.3034	56.49	563.2810
3.3200	54.41	562.3191
3.3366	52.13	562.0256
3.3532	50.34	561.8505
3.3698	48.40	561.0464
3.3864	46.13	560.3679
3.4030	43.78	561.4286
3.4196	41.73	561.2274
3.4362	39.66	560.8825
3.4528	37.32	559.9855
3.4694	35.20	560.3406
3.4860	33.22	561.4363
3.5026	31.12	561.7260
3.5192	28.96	562.3560
3.5358	26.87	561.5460
3.5524	25.01	559.7548
3.5690	23.12	560.3526
3.5856	20.95	561.0104
3.6022	19.14	560.9074
3.6188	17.23	561.9964
3.6354	15.64	562.4137
3.6520	13.98	561.3184
3.6686	12.28	560.7382
3.6852	10.69	560.5128
3.7018	9.16	560.5048
3.7184	7.70	560.9727
3.7350	6.40	562.0686
3.7516	5.18	562.9781
3.7682	4.08	563.7495
3.7848	3.09	562.5648
3.8014	2.22	560.8003
3.8180	1.46	560.9017
3.8346	0.73	561.7889
3.8512	0.37	564.4336
3.8678	0.05	566.0186
3.8844	0.20	565.9346
3.9010	0.36	565.0813
3.9176	0.38	564.1280
3.9342	0.42	563.1570
3.9508	0.42	563.1648
3.9974	0.42	563.9855
3.9986	0.42	565.3379

Table E.4 - AC Output to Underwater Power Grid System (4-Hours Subsea Operation)

AC Output to Underwater Power Grid System (4-Hours Subsea Operation)					
Time (Hours)	**Subsea Temp. Diff. (degC)**	**Phase C-AC Current (A)**	**Active Power (kW)**	**Reactive Power (kW)**	**THD**
0.0000	0.3707	-0.0676	-0.0363	0.0000	0.0000
0.0166	0.3707	4.2774	1.0362	-2.1320	0.0000
0.0332	0.3707	2.5883	-17.2410	-0.4830	15.0000
0.0498	0.3707	-8.9651	-3.8731	17.1861	15.0000
0.0664	0.3707	2.1333	8.2015	13.5401	15.0000
0.0830	0.3707	20.5057	12.7652	8.2543	15.0000
0.0996	0.3707	17.3442	8.7960	-0.0946	15.0000
0.1162	0.3707	12.1066	3.1294	-5.1228	15.0000
0.1328	0.3707	16.0739	-0.0451	-7.5795	10.9945
0.1494	0.3707	8.4253	-2.1668	-5.7010	7.9695
0.1660	0.3707	2.8769	-3.7963	-2.2152	12.7036
0.1826	0.3707	1.8355	-3.3970	1.6742	15.0000
0.1992	0.3707	-1.0975	-1.4431	3.2694	15.0000
0.2158	0.3707	-3.2734	1.2439	3.3504	15.0000
0.2324	0.3707	-4.6040	2.0524	1.6186	15.0000
0.2490	0.3707	-3.4408	1.6620	-0.1171	15.0000
0.2656	0.3707	-3.5937	0.5469	-1.7373	15.0000
0.2822	0.4236	-4.0074	-0.3877	-1.8456	13.7394
0.2988	0.4236	-2.6804	-1.0510	-1.4220	12.1490
0.3154	0.4236	-1.0413	-1.0085	-0.1571	15.0000
0.3320	0.4237	-0.4777	-0.9393	0.6616	15.0000
0.3486	0.4237	0.0217	-0.1225	1.3379	15.0000
0.3652	0.4237	0.9570	0.4000	0.8005	15.0000
0.3818	0.3707	1.6353	0.5778	0.5567	15.0000
0.3984	0.3707	0.7585	0.3538	-0.0328	15.0000
0.4150	0.3431	0.7237	0.1732	-0.2889	15.0000
0.4316	0.2101	0.8211	-0.2330	-0.3057	15.0000
0.4482	0.0374	0.5353	-0.2554	-0.1451	15.0000
0.4648	0.2237	0.6725	-0.4061	0.1478	15.0000
0.4814	0.5508	0.0745	-0.0985	0.1107	15.0000
0.4980	1.0772	-0.0936	-0.0031	0.3874	15.0000
0.5146	1.7127	-0.3522	0.3021	0.3048	15.0000
0.5312	2.4909	-0.8216	0.2819	0.2645	15.0000
0.5478	3.3965	-0.8069	0.3744	-0.0382	15.0000
0.5644	4.3899	-0.1375	0.1009	-0.0326	15.0000
0.5810	5.4431	0.2856	0.3227	-0.1117	15.0000
0.5976	6.4842	0.6244	0.3349	0.1552	15.0000
0.6142	7.8666	-0.0069	0.3109	0.0902	15.0000
0.6308	9.4158	-0.9073	0.3190	0.2778	15.0000
0.6474	10.9977	-1.0191	0.4753	-0.0667	15.0000
0.6640	12.6265	0.3586	0.4742	0.2714	15.0000
0.6806	13.7789	1.0785	0.5506	0.1302	15.0000
0.6972	15.3734	0.9295	0.5760	0.3076	15.0000
0.7138	16.6803	0.2429	0.6412	-0.0196	15.0000
0.7304	17.0844	-1.2514	0.6163	0.1513	15.0000
0.7470	16.1644	-1.5552	0.6890	-0.2319	15.0000

AC Output to Underwater Power Grid System (4-Hours Subsea Operation)					
Time (Hours)	Subsea Temp. Diff. (degC)	Phase C-AC Current (A)	Active Power (kW)	Reactive Power (kW)	THD
0.7636	19.3025	0.1617	0.5412	0.1210	15.0000
0.7802	20.4640	1.1491	0.6803	-0.0575	15.0000
0.7968	24.3243	1.1911	0.7551	0.2478	15.0000
0.8134	26.4511	0.1522	0.9081	-0.0518	15.0000
0.8300	30.7679	-2.4981	1.0917	0.4345	15.0000
0.8466	33.1040	-1.9983	1.1284	0.0679	15.0000
0.8632	35.3291	0.7872	1.2627	0.3138	13.2782
0.8798	38.3450	2.6499	1.4323	-0.1116	13.4151
0.8964	40.2868	2.3785	1.4860	0.1984	12.2752
0.9130	40.5789	-0.2827	1.3569	-0.0103	10.9865
0.9296	44.8487	-3.2736	1.5396	0.2690	10.8275
0.9462	47.3960	-3.0413	1.6757	-0.1645	10.1759
0.9628	49.3118	1.0788	1.9324	0.1824	9.3436
0.9794	51.5854	3.6348	1.8028	-0.0330	8.9896
0.9960	53.9429	2.7172	1.9852	0.3149	8.2955
1.0126	56.1293	-0.9287	2.1140	-0.0519	8.6368
1.0292	58.5452	-4.9747	2.3620	0.1496	7.9315
1.0458	60.7848	-3.5088	2.2946	-0.0386	7.2411
1.0624	62.6015	2.2568	2.3706	0.3814	7.4308
1.0790	64.8576	5.1342	2.4476	-0.0224	7.6078
1.0956	67.3290	3.7828	2.7359	0.0358	7.1040
1.1122	69.6619	-1.7211	2.5598	-0.0974	5.9121
1.1288	72.1134	-5.7449	2.6505	0.3537	6.2697
1.1454	74.0466	-3.2504	2.7309	0.1737	6.7677
1.1620	76.6581	3.0420	3.1912	0.1289	6.1412
1.1786	78.3322	6.2806	2.9480	-0.1747	5.6967
1.1952	80.4698	2.9643	3.0205	0.3504	5.4395
1.2118	82.7474	-3.7303	3.0794	0.3492	5.0660
1.2284	84.7428	-8.0903	3.7600	0.2897	5.6895
1.2450	86.6357	-3.8197	3.4415	-0.0658	4.7429
1.2616	88.6525	3.9887	3.3271	0.1553	4.6615
1.2782	91.1537	7.2796	3.4063	0.3673	5.0116
1.2948	93.0376	3.1910	4.1373	0.3958	6.2947
1.3114	95.1086	-4.5893	3.9813	-0.1660	4.5933
1.3280	96.8233	-7.9817	3.7340	-0.0114	4.3342
1.3446	99.3308	-2.3478	3.7343	0.3845	4.9307
1.3612	101.3805	6.9788	4.3714	0.6797	4.1177
1.3778	103.5697	9.7457	4.6103	0.0605	3.8839
1.3944	105.5181	2.8481	4.2272	0.0685	3.8669
1.4110	106.7998	-6.5439	4.0914	0.4143	3.8919
1.4276	108.9543	-9.5768	4.7166	0.5907	4.2792
1.4442	110.7475	-2.3158	4.9714	0.2690	4.3257
1.4608	112.6488	7.0466	4.7786	-0.1924	3.5850
1.4774	114.1915	8.7488	4.2683	0.0496	3.7246
1.4940	115.8685	1.5027	4.6714	0.2779	4.2026
1.5106	117.4117	-9.0121	5.0740	0.5406	3.8004
1.5272	118.3820	-10.6846	5.2590	-0.1247	3.7363
1.5438	120.1752	-1.5051	4.8287	0.0050	3.5269
1.5604	121.2620	8.5442	4.8594	0.1750	3.3028
1.5770	122.7138	9.3299	5.0247	0.6101	3.3087

AC Output to Underwater Power Grid System (4-Hours Subsea Operation)					
Time (Hours)	Subsea Temp. Diff. (degC)	Phase C-AC Current (A)	Active Power (kW)	Reactive Power (kW)	THD
1.5936	124.4243	0.6245	5.5020	0.1704	3.4770
1.6102	125.7846	-9.6798	5.3627	0.0693	3.5507
1.6268	127.5082	-10.1410	5.2603	-0.1252	3.1898
1.6434	129.2425	0.5018	5.3004	0.3446	3.3042
1.6600	130.1042	10.8662	5.6763	0.2828	3.2637
1.6766	131.9116	10.5392	5.7714	0.0611	3.1894
1.6932	133.0543	0.1432	5.6940	-0.3054	3.2492
1.7098	134.1161	-10.2507	5.3573	-0.0627	3.0462
1.7264	134.9889	-9.7412	5.5420	0.0302	2.9697
1.7430	136.3336	1.8376	5.8052	0.2498	3.0869
1.7596	137.2071	11.0868	5.7471	-0.3566	3.3897
1.7762	137.6581	9.2840	5.5648	0.0648	3.2137
1.7928	138.5334	-1.3140	5.5395	-0.3167	3.1512
1.8094	139.6069	-12.0119	5.8211	0.2829	3.1399
1.8260	140.8709	-9.5488	5.9135	-0.0740	2.9852
1.8426	142.0452	3.1334	5.9387	0.1050	2.9456
1.8592	142.3384	11.8141	5.7862	-0.2779	3.0511
1.8758	143.1570	8.8586	5.8646	-0.0274	3.0541
1.8924	144.3905	-3.0844	5.8354	-0.2623	3.0796
1.9090	145.1359	-12.4808	5.8946	0.2060	3.0851
1.9256	145.4706	-8.6193	5.9478	-0.1652	2.9679
1.9422	145.3552	4.5628	5.8681	0.0833	2.9269
1.9588	146.5066	12.3537	5.8515	-0.2691	2.8985
1.9754	146.6727	7.7313	6.0992	0.1122	2.8709
1.9920	147.3240	-5.0657	6.0172	-0.0983	2.8297
2.0086	147.3575	-13.1906	6.1549	0.0673	2.8262
2.0252	147.0214	-7.3088	5.8723	-0.1823	2.8524
2.0418	147.0574	5.9698	5.8676	0.0676	2.8428
2.0584	147.9928	12.4886	5.8169	-0.1633	2.8062
2.0750	148.6816	6.3843	6.1027	0.0925	2.8511
2.0916	149.0979	-6.7917	6.0719	0.0181	2.8404
2.1082	148.8276	-13.5464	6.3131	0.0730	2.7801
2.1248	149.2130	-5.9796	5.9460	-0.1553	2.8847
2.1414	149.4662	12.6461	6.2997	0.1120	2.7484
2.1485	149.9083	13.7289	6.3890	0.0009	2.7173
2.1746	149.5010	12.5451	6.2177	0.3020	2.7225
2.1912	148.8400	-8.3169	6.1338	0.0775	2.7847
2.2078	148.4928	-13.3613	6.3171	0.0614	2.7712
2.2244	149.3693	-4.5144	6.0494	-0.1181	2.8423
2.2410	148.5987	8.8734	6.0968	0.0675	2.7765
2.2576	147.8076	12.3347	5.9089	0.0535	2.7589
2.2742	147.6442	3.0042	6.2488	0.2931	2.7447
2.2908	147.5415	-9.9254	6.2003	0.2707	2.8287
2.3074	148.1344	-12.8370	6.2849	0.1462	2.8468
2.3240	146.6793	-2.4170	6.0517	0.1363	2.7676
2.3406	145.6545	10.0099	6.1451	0.0105	2.8837
2.3572	145.2312	11.9991	5.9866	0.0767	2.9166
2.3738	144.4006	1.9692	6.1421	-0.0194	2.8555
2.3904	144.5336	-10.5345	6.0156	0.1839	2.9923
2.4070	143.7966	-12.2104	6.2596	0.0876	2.9370

AC Output to Underwater Power Grid System (4-Hours Subsea Operation)					
Time (Hours)	Subsea Temp. Diff. (degC)	Phase C-AC Current (A)	Active Power (kW)	Reactive Power (kW)	THD
2.4236	143.1886	-1.0601	6.0934	0.0166	3.0734
2.4402	141.6521	10.6790	6.0478	-0.1216	3.1154
2.4568	141.5910	11.1983	5.8865	0.0105	3.0765
2.4734	141.5118	0.7407	5.8485	-0.2223	2.9122
2.4900	139.4433	-11.3235	5.9314	0.2665	2.9556
2.5066	139.0826	-11.2242	6.0461	-0.1006	2.9714
2.5232	138.0069	0.6783	5.9436	0.0669	3.0402
2.5398	137.5009	10.7852	5.8196	-0.4346	3.2712
2.5564	136.3421	9.9918	5.5724	-0.1305	3.2487
2.5730	135.1491	-0.6115	5.4821	-0.2900	3.0881
2.5896	133.8782	-10.7195	5.3958	0.0380	3.1899
2.6062	133.2802	-9.4272	5.4244	-0.2196	3.7344
2.6228	131.9555	2.7470	5.5421	0.3592	3.5137
2.6394	129.4836	11.5620	5.6816	0.0470	3.1042
2.6560	128.9851	8.9903	5.6420	0.0130	3.4526
2.6726	126.2717	-1.3882	5.2177	-0.5602	3.4538
2.6892	125.2826	-9.9885	4.9109	-0.3024	3.5572
2.7058	125.2013	-7.8046	4.6984	-0.4828	3.2457
2.7224	123.5071	3.0712	4.6964	0.0751	3.3702
2.7390	121.9272	9.9023	4.7356	-0.1133	3.3538
2.7556	120.1513	6.4561	5.0242	0.3676	3.6349
2.7722	118.4753	-3.5581	5.1256	-0.1394	3.7081
2.7888	117.7548	-10.8433	5.1290	-0.1884	3.7297
2.8054	115.2461	-7.2697	4.5852	-0.7672	3.6054
2.8220	113.9795	2.7901	4.2547	-0.4729	3.7596
2.8386	112.8671	8.2694	3.8992	-0.4408	4.1491
2.8552	110.6290	4.3181	3.9938	0.2407	3.8172
2.8718	107.9550	-4.1463	3.9738	0.1000	3.8476
2.8884	107.5282	-9.5727	4.4476	0.4062	4.0761
2.9050	105.4123	-4.5576	4.4954	0.1462	4.3843
2.9216	103.8684	5.3185	4.6814	0.0587	4.5385
2.9382	102.6334	8.9637	4.1530	-0.5334	4.2003
2.9548	99.7747	4.6647	3.8390	-0.5180	4.1217
2.9714	97.4985	-3.1944	3.3340	-0.5067	4.7101
2.9880	95.5812	-7.1711	3.3518	-0.0387	4.3733
3.0046	93.2462	-2.5434	3.2645	0.0882	4.2691
3.0212	92.0100	5.3085	3.4920	0.3847	4.3615
3.0378	90.0426	7.5124	3.6237	0.4599	4.4760
3.0544	88.0655	1.9500	3.8530	0.3808	4.8774
3.0710	85.8184	-5.3822	3.7710	-0.0248	4.4023
3.0876	84.0335	-8.2221	3.8406	-0.3830	4.9096
3.1042	81.7721	-2.9129	3.4095	-0.4556	5.1074
3.1208	79.8726	4.3335	3.2170	-0.4025	5.0367
3.1374	77.6139	6.1103	2.9218	-0.1615	5.1406
3.1540	75.5976	1.4699	2.7259	-0.1199	6.0428
3.1706	72.9480	-4.6201	2.6759	0.1906	6.2757
3.1872	71.0034	-5.7207	2.8419	0.0035	6.5559
3.2038	69.2355	-0.5587	2.8440	0.1571	5.6852
3.2204	67.3085	4.8752	2.9225	-0.0975	5.4116
3.2370	65.0059	5.4751	2.7398	-0.1113	6.3286

AC Output to Underwater Power Grid System (4-Hours Subsea Operation)					
Time (Hours)	**Subsea Temp. Diff. (degC)**	**Phase C-AC Current (A)**	**Active Power (kW)**	**Reactive Power (kW)**	**THD**
3.2536	62.6131	1.5152	2.5726	-0.4917	6.6595
3.2702	60.5441	-3.9686	2.4268	-0.3151	7.2679
3.2868	58.3271	-4.7612	2.3099	-0.3644	7.1007
3.3034	56.4923	-0.4744	2.0806	-0.1773	8.1233
3.3200	54.4103	3.2912	1.9775	-0.3616	8.4637
3.3366	52.1290	3.4957	1.9135	0.0189	8.3277
3.3532	50.3371	0.4806	1.8049	-0.2995	9.1754
3.3698	48.3986	-3.3850	1.7522	0.0134	8.6508
3.3864	46.1332	-3.3470	1.6792	-0.3133	9.5224
3.4030	43.7823	0.2080	1.5531	-0.0659	10.8090
3.4196	41.7296	2.2885	1.3679	-0.5057	10.9948
3.4362	39.6571	2.4597	1.3302	-0.1647	12.6694
3.4528	37.3163	0.3139	1.2215	-0.3548	12.5736
3.4694	35.2044	-2.3706	1.1736	-0.0154	13.5462
3.4860	33.2166	-1.8424	1.0574	-0.1072	15.0000
3.5026	31.1182	0.8701	1.1087	0.1559	15.0000
3.5192	28.9592	1.6692	0.8978	-0.3266	15.0000
3.5358	26.8712	1.5094	0.9139	-0.0882	15.0000
3.5524	25.0099	0.4012	0.7198	-0.4124	15.0000
3.5690	23.1232	-1.2321	0.6105	-0.1142	15.0000
3.5856	20.9530	-1.1892	0.5589	-0.2487	15.0000
3.6022	19.1431	0.8385	0.5199	0.2230	15.0000
3.6188	17.2300	0.7918	0.3537	0.1275	15.0000
3.6354	15.6391	0.2569	0.4513	0.1925	15.0000
3.6520	13.9771	-0.1384	0.2202	-0.0276	15.0000
3.6686	12.2782	-0.7083	0.3376	-0.0813	15.0000
3.6852	10.6899	-0.6136	0.2084	-0.2044	15.0000
3.7018	9.1628	0.2755	0.2796	-0.0015	15.0000
3.7184	7.7021	0.0037	0.0026	-0.0392	15.0000
3.7350	6.3989	-0.3857	0.1024	0.2664	15.0000
3.7516	5.1761	-0.6169	0.0917	0.2801	15.0000
3.7682	4.0807	-0.2745	0.1298	0.0453	15.0000
3.7848	3.0915	0.2507	-0.1468	0.0574	15.0000
3.8014	2.2155	-0.0736	0.1155	-0.1220	15.0000
3.8180	1.4587	-0.1156	-0.0537	0.0037	15.0000
3.8346	0.7289	0.0342	0.1014	0.0253	15.0000
3.8512	0.3716	-0.3140	0.0022	0.1847	15.0000
3.8678	0.0480	-0.3654	0.1985	0.1537	15.0000
3.8844	0.2049	0.2171	-0.0482	0.0902	15.0000
3.9010	0.3614	0.1772	0.1602	-0.0332	15.0000
3.9176	0.3760	0.0704	0.0664	0.1397	15.0000
3.9342	0.4226	0.0649	0.1358	0.0066	15.0000
3.9508	0.4233	-0.4064	0.0685	0.2004	15.0000
3.9974	0.4233	-0.4798	0.1955	-0.1251	15.0000
3.9986	0.4234	-0.2686	0.0775	-0.1114	15.0000

Appendix F

Table F.1- DC Output from 6.4 kW-DPU-Power System (24-Hours Subsea Operations)

Table F.2 - DC BUS (24-Hours Subsea Operation)

Table F.3 - AC Output to Underwater Power Grid System (24-Hours Subsea Operation)

Table F.1- DC Output from 6.4 kW-DPU-Power System (24-Hours Subsea Operations)

DC Output from 6.4 kW-DPU-Power System (24-Hours Subsea Operation)				
Time (Hours)	**Subsea Temp. Diff. (degC)**	**DC-Current (A)**	**6.4kW-DPU-Source Power (kW)**	**Tracked Power (kW)**
0.00	0	-0.00157287	0.00000000	-0.0002132
0.10	0	0.12489284	0.00763586	0.0170107
0.20	1	0.14826027	0.01712183	0.0213167
0.30	0	0.09368832	0.00753094	0.0127900
0.40	0	0.12975241	0.00212891	0.0176076
0.50	2	0.58410314	0.07644464	0.0880378
0.60	70	21.74190479	2.87156085	3.0019409
0.70	113	33.62985499	4.87847813	4.8303567
0.80	137	40.24344292	5.84722126	5.8194500
0.90	146	43.03035605	6.22758932	6.2159400
1.00	147	43.30109852	6.27666735	6.2671000
1.10	147	43.45641228	6.25621724	6.2500467
1.20	146	43.26122747	6.24157112	6.2329933
1.30	146	43.13822989	6.23449492	6.2244667
1.40	145	42.95298159	6.21018373	6.1988867
1.50	143	41.45593272	6.10894389	6.0965667
1.60	126	37.81481163	5.37083237	5.3632733
1.70	80	20.99865455	3.28275668	3.4149300
1.80	47	11.77452769	1.84642696	2.0165567
1.90	39	11.99778281	1.57863760	1.6584367
2.00	37	7.90298995	1.25933134	1.5561167
2.10	37	9.52527380	1.46627885	1.5561167
2.20	37	10.89851287	1.59658899	1.5944867
2.30	37	11.38448015	1.51661851	1.5774333
2.40	36	10.98858621	1.46115560	1.5220100
2.50	37	11.22814128	1.49705404	1.5561167
2.60	58	17.34677949	2.48466524	2.4599433
2.70	65	18.33881200	2.76088200	2.7498500
2.80	71	21.67397614	2.99152375	3.0227033
2.90	89	26.61931252	3.83793326	3.7943667
3.00	129	38.95934239	5.48300010	5.4997000
3.10	131	39.38184818	5.58569072	5.5849667
3.20	128	36.23533922	5.44218047	5.4528033
3.30	124	35.63447124	5.29826212	5.2737433
3.40	122	36.26488179	5.23374406	5.1970033
3.50	126	37.10683039	5.38947238	5.3504833
3.60	125	36.71911629	5.38560921	5.3334300
3.70	124	37.45771270	5.30916130	5.3035867
3.80	123	37.04051177	5.23592707	5.2353733
3.90	116	34.32995927	4.99137925	4.9454667
4.00	96	28.36197254	4.14495467	4.0928000
4.10	58	13.49971362	2.16160278	2.4897867
4.20	30	7.07146363	1.10556495	1.2576833
4.30	10	3.03706484	0.40917109	0.4305967
4.40	1	0.15658969	0.00861635	0.0213167
4.50	1	0.14529991	0.01713984	0.0213167
4.60	0	0.03139423	0.00079478	0.0042633
4.70	0	0.09424674	0.00160075	0.0127900

DC Output from 6.4 kW-DPU-Power System (24-Hours Subsea Operation)				
Time (Hours)	**Subsea Temp. Diff. (degC)**	**DC-Current (A)**	**6.4kW-DPU-Source Power (kW)**	**Tracked Power (kW)**
4.80	1	0.15419260	0.01611250	0.0213167
4.90	0	0.12326229	0.01273908	0.0170533
5.00	0	-0.00000004	0.00000000	0.0000000
5.10	0	0.00000000	0.00000000	0.0000000
5.20	1	0.28163623	0.01819736	0.0383700
5.30	2	0.48779349	0.06163856	0.0711977
5.40	6	1.55709194	0.22226598	0.2532420
5.50	22	6.49651877	0.92571629	0.9379333
5.60	26	7.94614450	1.11631900	1.1255200
5.70	30	8.91048169	1.28952244	1.2875267
5.80	36	10.91630560	1.47590089	1.5177467
5.90	44	11.01971879	1.72176406	1.8716033
6.00	56	16.97688317	2.33534040	2.3661500
6.10	63	14.94806036	2.38635572	2.6901633
6.20	69	16.78292955	2.66571222	2.9246467
6.30	74	22.40816620	3.17340511	3.1548667
6.40	80	20.46433671	3.21655057	3.4064033
6.50	86	23.57204435	3.61924378	3.6451500
6.60	88	26.27522170	3.79039566	3.7474700
6.70	90	22.58881474	3.57045430	3.8497900
6.80	92	25.79338438	3.91957361	3.9265300
6.90	95	29.02026095	4.05426462	4.0672200
7.00	105	27.43932666	4.28466588	4.4765000
7.10	111	32.56790844	4.76648555	4.7152467
7.20	115	31.71224404	4.83930180	4.8900433
7.30	119	32.77463633	4.99554025	5.0520500
7.40	122	35.78774251	5.24813993	5.2055300
7.50	125	37.36079646	5.32465535	5.3078500
7.60	126	37.60061861	5.39019582	5.3590100
7.70	124	37.33169700	5.28526282	5.2822700
7.80	122	34.96232879	5.21090834	5.1884767
7.90	121	32.21815853	4.98268365	5.1458433
8.00	122	35.23122517	5.21509632	5.1799500
8.10	122	35.61517759	5.22298314	5.1799500
8.20	121	36.49235940	5.17737289	5.1671600
8.30	120	35.23658053	5.16065413	5.1160000
8.40	116	35.12338454	4.97008965	4.9625200
8.50	108	32.75840646	4.59583623	4.6044000
8.60	108	32.40891139	4.63655054	4.6044000
8.70	105	27.70087656	4.30358243	4.4551833
8.80	104	31.55237364	4.45497970	4.4466567
8.90	105	31.61956043	4.48546928	4.4679733
9.00	102	25.49108632	4.03030694	4.3486000
9.10	100	30.43467756	4.24258101	4.2633333
9.20	91	22.76349530	3.60155435	3.8966867
9.30	84	23.40761732	3.58483290	3.5982533
9.40	82	25.02085875	3.47263029	3.4959333
9.50	82	23.04086673	3.50697159	3.4959333
9.60	80	22.27432985	3.40540287	3.4106667

DC Output from 6.4 kW-DPU-Power System (24-Hours Subsea Operation)				
Time (Hours)	Subsea Temp. Diff. (degC)	DC-Current (A)	6.4kW-DPU-Source Power (kW)	Tracked Power (kW)
9.70	62	12.30495224	2.00979676	2.6347400
9.80	46	9.91612015	1.59310626	1.9440800
9.90	38	11.51088210	1.63119264	1.6328567
10.00	36	7.53468138	1.20255362	1.5134833
10.10	22	6.87160072	0.89439430	0.9507233
10.20	17	5.01967094	0.68465110	0.7077133
10.30	14	4.00898036	0.56105997	0.5798133
10.40	9	2.79563516	0.38513709	0.4045051
10.50	1	0.44800868	0.04561644	0.0613920
10.60	1	0.20853218	0.02369098	0.0293317
10.70	1	0.13881286	0.01687738	0.0213167
10.80	1	0.19944226	0.02438682	0.0298433
10.90	1	0.29316443	0.03580696	0.0426333
11.00	1	0.29207608	0.03580038	0.0426333
11.10	0	0.06268300	0.00287293	0.0085267
11.20	0	0.00000000	0.00000000	0.0000000
11.30	1	0.26727944	0.00921517	0.0363236
11.40	5	1.46752292	0.20229185	0.2218639
11.50	18	5.07027065	0.72767054	0.7460833
11.60	57	16.96637367	2.46422310	2.4343633
11.70	66	16.54608161	2.61716616	2.8308533
11.80	65	17.25208667	2.68083253	2.7882200
11.90	65	14.27536692	2.30190752	2.7498500
12.00	64	16.96691516	2.63832203	2.7498500
12.10	58	17.96268233	2.43581697	2.4940500
12.20	54	12.27360213	1.96729240	2.3022000
12.30	44	13.51752068	1.77696717	1.8673400
12.40	25	6.31358006	0.96986815	1.0743600
12.50	0	-0.00001040	-0.00000064	0.0000000
12.60	0	0.00000000	0.00000000	0.0000000
12.70	0	0.00000000	0.00000000	0.0000000
12.80	0	0.06289218	0.00031682	0.0085267
12.90	1	0.25781697	0.00566002	0.0350020
13.00	2	0.61202775	0.07868998	0.0897432
13.10	2	0.52611070	0.06622521	0.0761724
13.20	5	1.31908703	0.17839969	0.1953819
13.30	7	2.03410253	0.27559739	0.2941700
13.40	9	2.54197432	0.34736852	0.3666467
13.50	13	3.88272819	0.53447198	0.5542333
13.60	18	5.38949367	0.76007936	0.7759267
13.70	19	5.73994625	0.80110063	0.8185600
13.80	23	6.71716866	0.97405320	0.9890933
13.90	30	7.76761616	1.19208282	1.2832633
14.00	33	10.00233482	1.32722753	1.3855833
14.10	36	7.55939735	1.20703227	1.5220100
14.20	39	11.85617035	1.59564916	1.6456467
14.30	39	11.72338052	1.68241896	1.6712267
14.40	42	11.65067271	1.75625859	1.7778100
14.50	57	15.12720129	2.34171064	2.4087833
14.60	64	19.62360046	2.69537295	2.7327967

DC Output from 6.4 kW-DPU-Power System (24-Hours Subsea Operation)				
Time (Hours)	**Subsea Temp. Diff. (degC)**	**DC-Current (A)**	**6.4kW-DPU-Source Power (kW)**	**Tracked Power (kW)**
14.70	74	19.94131455	3.07748961	3.1463400
14.80	79	24.01556033	3.34982808	3.3595067
14.90	80	24.28819155	3.39446692	3.4021400
15.00	85	25.03328149	3.68572255	3.6238333
15.10	87	23.83827703	3.66038338	3.7091000
15.20	90	27.43372435	3.83535389	3.8455267
15.30	93	24.33877586	3.79641336	3.9563733
15.40	94	26.41232439	4.02129515	4.0160600
15.50	95	23.46712506	3.72158346	4.0501667
15.60	103	30.58909512	4.44123308	4.3912333
15.70	106	30.50490941	4.56001690	4.5276600
15.80	107	32.18730638	4.62189557	4.5788200
15.90	109	32.60400471	4.65381093	4.6257167
16.00	111	32.06112341	4.75403142	4.7109833
16.10	116	33.33423097	4.96458848	4.9326767
16.20	119	34.76514952	5.13223109	5.0776300
16.30	123	36.91062298	5.25602225	5.2396367
16.40	128	35.39408902	5.37738742	5.4357500
16.50	132	39.31661715	5.62305484	5.6062833
16.60	143	42.06209753	6.10155248	6.0837767
16.70	147	43.23913275	6.26420359	6.2543100
16.80	148	42.61274948	6.30255898	6.3139967
16.90	149	44.00753212	6.35608501	6.3523667
17.00	149	44.04470256	6.35654337	6.3523667
17.10	149	44.05514998	6.35649964	6.3523667
17.20	149	43.98750812	6.37029835	6.3651567
17.30	150	42.49966487	6.33793842	6.3736833
17.40	150	44.02277137	6.38999393	6.3736833
17.50	150	42.18807203	6.31904049	6.3736833
17.60	149	43.98281352	6.34736864	6.3395767
17.70	146	43.23627608	6.25164734	6.2415200
17.80	144	41.69481641	6.15703299	6.1562533
17.90	143	42.28874504	6.12047795	6.1050933
18.00	142	42.17502590	6.06624090	6.0539333
18.10	142	42.25071087	6.08414526	6.0709867
18.20	141	40.63208087	6.02534468	6.0240900
18.30	140	41.69985890	5.99592511	5.9814567
18.40	140	41.57672680	5.97973417	5.9644033
18.50	140	41.51088220	5.96137642	5.9473500
18.60	141	41.77425202	6.01384399	5.9985100
18.70	142	41.82966570	6.08072589	6.0624600
18.80	143	42.46965052	6.11732272	6.1050933
18.90	144	42.33647699	6.14567168	6.1221467
19.00	144	42.70044570	6.15012890	6.1392000
19.10	145	42.87613506	6.18431310	6.1733067
19.20	144	42.21914927	6.16940949	6.1562533
19.30	145	42.59785262	6.18679797	6.1647800
19.40	145	42.93118661	6.16786885	6.1605167
19.50	141	41.79924957	6.00261371	5.9899833
19.60	139	41.42559708	5.95380419	5.9388233

DC Output from 6.4 kW-DPU-Power System (24-Hours Subsea Operation)				
Time (Hours)	**Subsea Temp. Diff. (degC)**	**DC-Current (A)**	**6.4kW-DPU-Source Power (kW)**	**Tracked Power (kW)**
19.70	139	40.95081719	5.96169097	5.9388233
19.80	139	40.71041838	5.95999951	5.9388233
19.90	139	39.93865680	5.92971253	5.9260333
20.00	139	41.30426829	5.94307256	5.9260333
20.10	137	40.73149462	5.86029555	5.8407667
20.20	136	39.51859927	5.81633696	5.7938700
20.30	133	36.93323025	5.60146078	5.6659700
20.40	130	38.67052788	5.54273116	5.5210167
20.50	132	39.34040894	5.62170264	5.6062833
20.60	131	37.19891871	5.57799621	5.5892300
20.70	121	35.60825178	5.17998929	5.1373167
20.80	114	34.20055427	4.86886466	4.8474100
20.90	114	34.14585583	4.87932445	4.8516733
21.00	113	29.79672882	4.63513892	4.8175667
21.10	110	33.15592411	4.69268418	4.6811400
21.20	108	32.56771974	4.60703516	4.5958733
21.30	102	30.96702854	4.31955058	4.3400733
21.40	91	27.87279542	3.81593213	3.8796333
21.50	79	24.09235753	3.34719914	3.3680333
21.60	79	23.94367539	3.33910576	3.3509800
21.70	79	23.98259841	3.31595185	3.3467167
21.80	76	23.24538159	3.18910501	3.2358700
21.90	70	15.91965398	2.55719843	2.9672800
22.00	60	17.96331412	2.58272011	2.5580000
22.10	59	16.34920487	2.49626949	2.5068400
22.20	55	16.70352224	2.36722707	2.3533600
22.30	49	13.81588827	2.08024497	2.0719800
22.40	39	11.42336740	1.66818458	1.6627000
22.50	27	6.51836341	1.01143415	1.1511000
22.60	23	6.93444210	0.92077593	0.9635133
22.70	14	4.12577469	0.58884458	0.6096567
22.80	7	2.01777382	0.27543616	0.2941700
22.90	3	0.75685272	0.09838649	0.1108467
23.00	1	0.30336921	0.03522550	0.0426333
23.10	2	0.45669028	0.05756206	0.0667504
23.20	2	0.55221799	0.07000180	0.0802719
23.30	2	0.55362457	0.07000500	0.0802719
23.40	2	0.46047275	0.05758716	0.0667504
23.50	1	0.29698005	0.03575474	0.0426333
23.60	0	0.13437004	0.01359465	0.0185163
23.70	0	0.03671603	0.00171298	0.0049948
23.80	0	0.03683640	0.00024728	0.0049948
23.90	0	0.07359256	0.00147998	0.0099896
24.00	0	-0.00000001	0.00000000	0.0000000

Table F.2 - DC BUS (24-Hours Subsea Operation)

Power Stability (24-Hours Subsea Operating)		
Time (Hours)	**Subsea Temp. Diff. (degC)**	**BUS-Voltage (V)**
0.00	0	0.00033789
0.10	0	594.08081759
0.20	1	685.79490602
0.30	0	599.02427679
0.40	0	599.94411181
0.50	2	598.81338284
0.60	70	601.58117920
0.70	113	600.55296619
0.80	137	583.42651291
0.90	146	581.52306479
1.00	147	579.04167583
1.10	147	578.36130710
1.20	146	578.35164315
1.30	146	578.45150516
1.40	145	578.78016652
1.50	143	577.79790741
1.60	126	565.67695905
1.70	80	544.98582340
1.80	47	565.91239917
1.90	39	555.31137020
2.00	37	566.15086653
2.10	37	568.12642682
2.20	37	563.50298960
2.30	37	563.77230612
2.40	36	566.49367255
2.50	37	565.27807475
2.60	58	576.58348572
2.70	65	563.90132913
2.80	71	569.94120349
2.90	89	578.28798244
3.00	129	586.29016734
3.10	131	570.79832032
3.20	128	571.45928068
3.30	124	570.71229689
3.40	122	573.18171961
3.50	126	575.62195425
3.60	125	572.40459948
3.70	124	572.72016536
3.80	123	571.86929725
3.90	116	570.01106210
4.00	96	561.85072080
4.10	58	550.82768643
4.20	30	560.20417873
4.30	10	561.29801303
4.40	1	561.38052726
4.50	1	564.71484555

Power Stability (24-Hours Subsea Operating)		
Time (Hours)	**Subsea Temp. Diff. (degC)**	**BUS-Voltage (V)**
4.60	0	564.96611877
4.70	0	564.50352678
4.80	1	564.67157157
4.90	0	564.32024135
5.00	0	564.90567553
5.10	0	564.68660874
5.20	1	564.73913458
5.30	2	565.36640647
5.40	6	565.78714975
5.50	22	570.32370456
5.60	26	565.33486000
5.70	30	564.54236702
5.80	36	568.96384115
5.90	44	568.04893957
6.00	56	571.20923323
6.10	63	570.53129410
6.20	69	566.65898969
6.30	74	572.54017303
6.40	80	572.33388958
6.50	86	573.19967480
6.60	88	570.06684322
6.70	90	570.02453888
6.80	92	567.31221952
6.90	95	569.50752982
7.00	105	575.24264017
7.10	111	576.67145507
7.20	115	576.03928815
7.30	119	574.65832099
7.40	122	574.05527662
7.50	125	574.88252824
7.60	126	573.90355727
7.70	124	571.52613826
7.80	122	572.30772243
7.90	121	573.95452907
8.00	122	573.70516968
8.10	122	573.32388659
8.20	121	573.53692752
8.30	120	572.77783492
8.40	116	572.80636511
8.50	108	570.16732716
8.60	108	574.93681289
8.70	105	570.30307621
8.80	104	571.91888247
8.90	105	572.07536905
9.00	102	569.54568612
9.10	100	567.90897475
9.20	91	561.89981072
9.30	84	570.87919292
9.40	82	570.08645596
9.50	82	570.87296520

Power Stability (24-Hours Subsea Operating)		
Time (Hours)	**Subsea Temp. Diff. (degC)**	**BUS-Voltage (V)**
9.60	80	570.50759511
9.70	62	554.98476044
9.80	46	566.31957470
9.90	38	560.26556827
10.00	36	564.20824279
10.10	22	561.83330726
10.20	17	563.83699175
10.30	14	562.73795152
10.40	9	562.04423471
10.50	1	562.47871076
10.60	1	563.90727079
10.70	1	564.79882718
10.80	1	564.19027297
10.90	1	564.31292271
11.00	1	564.58051413
11.10	0	564.42929595
11.20	0	564.46682498
11.30	1	564.82463883
11.40	5	566.42391522
11.50	18	568.58986141
11.60	57	582.61706496
11.70	66	560.82768000
11.80	65	565.24660782
11.90	65	567.06192673
12.00	64	565.11034650
12.10	58	564.33904970
12.20	54	565.70374127
12.30	44	559.24080782
12.40	25	560.43380760
12.50	0	557.86898192
12.60	0	563.96350329
12.70	0	565.65064250
12.80	0	564.72020250
12.90	1	564.44228634
13.00	2	565.28589067
13.10	2	564.08686346
13.20	5	565.29179217
13.30	7	564.68035711
13.40	9	565.83576687
13.50	13	565.57358772
13.60	18	566.65963591
13.70	19	563.61933858
13.80	23	568.48284348
13.90	30	564.00944668
14.00	33	566.41198812
14.10	36	565.08262863
14.20	39	567.02823738
14.30	39	563.47371025
14.40	42	569.25740903
14.50	57	571.81443082

Power Stability (24-Hours Subsea Operating)		
Time (Hours)	**Subsea Temp. Diff. (degC)**	**BUS-Voltage (V)**
14.60	64	569.81309087
14.70	74	571.44771918
14.80	79	569.48364281
14.90	80	571.75265246
15.00	85	572.92716293
15.10	87	570.64542210
15.20	90	569.70638688
15.30	93	567.77290312
15.40	94	568.07389160
15.50	95	568.02604181
15.60	103	572.52110565
15.70	106	572.15270351
15.80	107	574.55218264
15.90	109	573.99648848
16.00	111	573.89290815
16.10	116	576.91379690
16.20	119	574.60569636
16.30	123	574.85858330
16.40	128	575.00274551
16.50	132	575.01159222
16.60	143	582.45886211
16.70	147	578.58983976
16.80	148	579.61103964
16.90	149	579.64618329
17.00	149	579.68289050
17.10	149	580.05001026
17.20	149	619.55987734
17.30	150	605.49959900
17.40	150	604.95381927
17.50	150	600.41569296
17.60	149	591.13317395
17.70	146	581.24490902
17.80	144	578.14331755
17.90	143	578.44965207
18.00	142	578.07613237
18.10	142	578.90212376
18.20	141	577.95046134
18.30	140	577.98169866
18.40	140	578.21791889
18.50	140	577.50776060
18.60	141	578.82547420
18.70	142	578.70571644
18.80	143	579.00013454
18.90	144	579.71787725
19.00	144	578.95824691
19.10	145	579.75303761
19.20	144	578.95060858
19.30	145	579.93293937
19.40	145	577.53439613
19.50	141	577.53206718

Power Stability (24-Hours Subsea Operating)		
Time (Hours)	**Subsea Temp. Diff. (degC)**	**BUS-Voltage (V)**
19.60	139	577.11284695
19.70	139	578.02387732
19.80	139	577.52806281
19.90	139	578.55058649
20.00	139	578.38528902
20.10	137	578.16960743
20.20	136	577.56810969
20.30	133	574.92713270
20.40	130	572.96052479
20.50	132	574.98016101
20.60	131	573.91601171
20.70	121	565.35964207
20.80	114	575.34524494
20.90	114	572.68156073
21.00	113	575.03605765
21.10	110	572.55816191
21.20	108	572.89707763
21.30	102	567.51253963
21.40	91	564.57709101
21.50	79	567.38069473
21.60	79	571.15864968
21.70	79	569.35514982
21.80	76	567.49137778
21.90	70	566.21506195
22.00	60	564.66077542
22.10	59	567.82056261
22.20	55	565.13749840
22.30	49	564.07261035
22.40	39	562.86023045
22.50	27	561.80763287
22.60	23	565.65517282
22.70	14	561.22420802
22.80	7	563.52135867
22.90	3	562.16004604
23.00	1	563.90536403
23.10	2	564.83191279
23.20	2	564.70810259
23.30	2	564.79973108
23.40	2	564.86848189
23.50	1	564.31960182
23.60	0	563.72749815
23.70	0	564.60600486
23.80	0	564.63086616
23.90	0	564.52449894
24.00	0	564.39913740

Table F.3 - AC Output to Underwater Power Grid System (24-Hours Subsea Operation)

AC Output to Underwater Power Grid System (24-Hours Subsea Operation)					
Time (Hours)	**Subsea Temp. Diff. (degC)**	**Phase C-AC Current (A)**	**Active Power (kW)**	**Reactive Power (kW)**	**THD**
0.00	0	-0.06757844	-0.03631390	-0.00000492	1.49012E-06
0.10	0	15.94208921	8.70048917	-0.23069537	15
0.20	1	1.57246251	-1.00061147	3.19676761	15
0.30	0	-3.74705739	-1.02901570	-1.70547641	13.98675171
0.40	0	0.43858912	0.44193171	-0.35720674	15
0.50	2	0.06646403	0.05952554	-0.04123613	15
0.60	70	6.26608449	2.86542420	0.86944939	7.85327205
0.70	113	8.39794146	4.69052559	-0.30737348	4.19874739
0.80	137	10.85310049	5.89402884	-0.10662524	3.78358220
0.90	146	11.60729843	6.23365530	0.00713650	2.85536769
1.00	147	11.42619088	6.21467314	-0.12856144	2.80738319
1.10	147	11.35346121	6.15027768	-0.08472244	3.00622994
1.20	146	11.55185669	6.24121414	-0.05756129	2.71536998
1.30	146	11.46514821	6.24169399	-0.13910120	2.73392523
1.40	145	11.39603419	6.20395065	-0.13805957	2.88577199
1.50	143	11.04029410	6.07988402	-0.25429491	3.12117823
1.60	126	10.26543999	5.58555196	-0.11932558	3.30093037
1.70	80	5.43922422	3.38731135	-0.80413225	5.02603279
1.80	47	2.40533438	1.47272954	-0.31194247	14.78193893
1.90	39	1.66613873	1.28034604	-0.66677228	11.68967537
2.00	37	2.59087395	1.59979393	-0.35932308	13.37034043
2.10	37	2.52571156	1.38585436	-0.04942243	13.92707742
2.20	37	2.05931679	1.27129193	-0.28511758	12.85366155
2.30	37	2.31243761	1.43011536	-0.32460143	13.20941236
2.40	36	1.94497482	1.20630439	-0.27898605	15
2.50	37	2.13328903	1.27706206	-0.22625792	13.14633397
2.60	58	4.09164781	2.24744917	-0.08416541	9.33480374
2.70	65	4.60181354	2.60615503	-0.23059680	6.78756020
2.80	71	5.44335266	2.95801931	-0.05673385	6.72635836
2.90	89	6.15689391	3.37091849	-0.10772767	5.06443580
3.00	129	10.02377908	5.17422498	0.36817418	3.62633731
3.10	131	10.83728304	5.72882976	0.16478498	3.00360263
3.20	128	10.54448188	5.58733292	0.13732359	3.13525942
3.30	124	9.52672725	5.07728755	0.07341586	3.23370231
3.40	122	8.39645180	4.65801282	-0.25244630	3.40704319
3.50	126	9.88545544	5.26383366	0.08421492	3.27074742
3.60	125	9.65692295	5.17757974	0.02089165	3.19912509
3.70	124	9.55678211	5.06324319	0.12571665	3.24940931
3.80	123	9.26005079	4.99435820	-0.03117037	3.60379318
3.90	116	8.30653878	4.61631300	-0.26391167	3.33591282
4.00	96	7.98196546	4.33855308	-0.08493220	5.17352608
4.10	58	3.86967717	2.44841463	-0.63885941	7.20173091
4.20	30	1.59411049	1.07878898	-0.38470955	14.57534411
4.30	10	-0.16054271	0.15332413	-0.41499931	15
4.40	1	-0.81364648	-0.18246093	-0.44131550	15

AC Output to Underwater Power Grid System (24-Hours Subsea Operation)					
Time (Hours)	**Subsea Temp. Diff. (degC)**	**Phase C-AC Current (A)**	**Active Power (kW)**	**Reactive Power (kW)**	**THD**
4.50	1	-0.42932698	0.00629325	-0.41052039	15
4.60	0	-0.37325447	0.02537865	-0.39138466	15
4.70	0	-0.42170789	0.01602140	-0.42027816	15
4.80	1	-0.59579519	-0.07057671	-0.43232734	15
4.90	0	-0.49957407	-0.03108117	-0.41117243	15
5.00	0	-0.47953063	-0.02801047	-0.39783448	15
5.10	0	-0.47947151	-0.02153785	-0.40899035	15
5.20	1	-0.47395453	0.00558554	-0.45083421	15
5.30	2	-0.44167802	-0.00351495	-0.40502853	15
5.40	6	-0.25127752	0.05520852	-0.32951462	15
5.50	22	1.48699504	0.85311223	-0.09352967	15
5.60	26	1.45971770	0.88897930	-0.18104317	15
5.70	30	2.01702910	1.20195938	-0.20439172	15
5.80	36	2.26989524	1.25308149	-0.05756846	14.50763932
5.90	44	2.82249412	1.67997764	-0.28261187	11.06032342
6.00	56	3.89414923	2.11858655	-0.04480167	8.48397109
6.10	63	4.57602998	2.50684525	-0.08258671	6.79800207
6.20	69	5.32497166	2.81082962	0.08801641	6.17724740
6.30	74	5.73191926	3.27093710	-0.33012382	6.20163978
6.40	80	5.92984720	3.39071452	-0.35335187	5.55086899
6.50	86	5.66683472	3.19807210	-0.26449903	4.76398431
6.60	88	5.97654777	3.25151886	-0.06878874	4.57899349
6.70	90	6.21657944	3.40112499	-0.10449121	4.91310994
6.80	92	6.87300601	3.61752859	0.13169263	4.54998345
6.90	95	7.04928405	3.69547650	0.16076356	4.88443958
7.00	105	8.93491911	4.87962377	-0.13507906	4.38145585
7.10	111	8.23103367	4.71473986	-0.50467261	4.11132703
7.20	115	8.05461929	4.54769975	-0.37955823	3.64925299
7.30	119	8.38587975	4.65132705	-0.25070672	3.51400390
7.40	122	8.77803602	4.82363294	-0.18412782	3.65439204
7.50	125	9.58018443	5.11826558	0.05219810	3.34272661
7.60	126	9.86869804	5.29463921	0.01526024	3.22392786
7.70	124	9.85869647	5.24120645	0.09849898	3.15746268
7.80	122	8.65973638	4.76137071	-0.18640052	3.42869338
7.90	121	8.46571020	4.68477587	-0.23433511	3.38552111
8.00	122	8.61999567	4.73586098	-0.17920726	3.37290034
8.10	122	8.66355214	4.76324326	-0.18609213	3.43051053
8.20	121	8.58306701	4.74661623	-0.23220933	3.41239361
8.30	120	8.39895409	4.67884891	-0.28620631	3.45119689
8.40	116	8.15811285	4.54612018	-0.28048990	3.60300252
8.50	108	7.79680358	4.66898685	-0.82961010	3.99646005
8.60	108	8.35242185	4.73640431	-0.42920769	4.15756351
8.70	105	8.64172466	4.86145674	-0.37652002	3.98305175
8.80	104	9.00116189	4.95147985	-0.19787826	4.08278168
8.90	105	8.50219024	4.79264621	-0.38721617	4.00461706
9.00	102	8.79472202	4.81726502	-0.15756685	4.12799574
9.10	100	8.92051422	4.70183833	0.15944619	4.25062059
9.20	91	6.96137927	3.71954920	0.03724611	4.36732195
9.30	84	5.19415824	3.00190158	-0.36469186	4.67418627
9.40	82	5.39163310	3.14815787	-0.43420439	4.90560075

AC Output to Underwater Power Grid System (24-Hours Subsea Operation)					
Time (Hours)	**Subsea Temp. Diff. (degC)**	**Phase C-AC Current (A)**	**Active Power (kW)**	**Reactive Power (kW)**	**THD**
9.50	82	5.30912174	3.07442671	-0.38330035	4.74951421
9.60	80	5.51431340	3.22004215	-0.44452005	5.03968359
9.70	62	4.28723649	2.59842342	-0.51001548	5.95285933
9.80	46	2.84450640	1.77506550	-0.42681972	10.86263227
9.90	38	1.86956518	1.25119011	-0.42692216	12.31686344
10.00	36	2.23677419	1.39247698	-0.32983781	12.85508485
10.10	22	0.98634061	0.71286410	-0.31662498	15
10.20	17	1.00402641	0.60987119	-0.12177398	15
10.30	14	0.68227896	0.45348211	-0.15038464	15
10.40	9	0.38469647	0.31468890	-0.18697934	15
10.50	1	-0.47859625	-0.00247625	-0.44119132	15
10.60	1	-0.36547314	0.02582660	-0.38491761	15
10.70	1	-0.50179695	-0.02169655	-0.42949612	15
10.80	1	-0.55350196	-0.04095667	-0.44426397	15
10.90	1	-0.54357240	-0.06715300	-0.38964810	15
11.00	1	-0.57425324	-0.07625190	-0.40244625	15
11.10	0	-0.53030795	-0.01736893	-0.46352999	15
11.20	0	-0.56295367	-0.04531955	-0.44550494	15
11.30	1	-0.52452165	-0.01299166	-0.46572573	15
11.40	5	-0.37489097	-0.02079890	-0.31292605	15
11.50	18	1.04952248	0.63593103	-0.12456292	15
11.60	57	4.73471248	2.38136743	0.28244990	7.534260116
11.70	66	4.61012689	2.69998522	-0.38537734	5.889960069
11.80	65	5.22119304	2.78199203	0.04136681	6.313007383
11.90	65	4.80148252	2.66552039	-0.14756750	6.620087947
12.00	64	4.89762467	2.66365668	-0.05484977	6.513880313
12.10	58	3.90557265	2.22016062	-0.21010014	7.816566634
12.20	54	3.42572398	1.92038296	-0.13751607	8.276862965
12.30	44	2.46605285	1.63772571	-0.54120709	9.924644549
12.40	25	1.16738134	0.84135848	-0.37066996	15
12.50	0	-0.92981185	-0.13937706	-0.62406639	15
12.60	0	-0.16954075	0.06419661	-0.26900135	15
12.70	0	-0.45470749	0.00977885	-0.44018196	15
12.80	0	-0.46933989	-0.02051780	-0.40132657	15
12.90	1	-0.54188110	-0.02313192	-0.46432057	15
13.00	2	-0.49083285	-0.02338995	-0.41635762	15
13.10	2	-0.48100024	-0.02207011	-0.40949140	15
13.20	5	0.06492633	0.17953047	-0.25052208	15
13.30	7	-0.00212002	0.19220966	-0.33489022	15
13.40	9	0.26729206	0.30130735	-0.27308256	15
13.50	13	0.73564744	0.41446767	-0.03313393	15
13.60	18	1.12781326	0.63701746	-0.05357114	15
13.70	19	1.02936179	0.60410235	-0.08819973	15
13.80	23	1.19207637	0.73441453	-0.16245132	15
13.90	30	1.95866276	1.19774277	-0.25141607	15
14.00	33	2.10376970	1.28344204	-0.26478515	15
14.10	36	2.05348249	1.25736139	-0.26641978	14.75179793
14.20	39	2.34726814	1.39802734	-0.23660287	13.00922873
14.30	39	2.47319250	1.57696346	-0.42931816	12.46557472
14.40	42	2.85461486	1.64315576	-0.18893632	12.67702606

AC Output to Underwater Power Grid System (24-Hours Subsea Operation)					
Time (Hours)	**Subsea Temp. Diff. (degC)**	**Phase C-AC Current (A)**	**Active Power (kW)**	**Reactive Power (kW)**	**THD**
14.50	57	4.10735788	2.19221551	0.02612515	8.52673812
14.60	64	4.62352592	2.54527409	-0.10493789	7.32035994
14.70	74	5.63528243	3.16428890	-0.23535387	6.49134582
14.80	79	5.54992044	3.20906549	-0.39236465	5.22363953
14.90	80	5.90611831	3.38615856	-0.36754770	5.79120977
15.00	85	5.65861827	3.20715521	-0.28787935	5.11826981
15.10	87	5.83724508	3.23059985	-0.16221973	4.80877432
15.20	90	6.23657533	3.37714069	-0.04433688	4.94111379
15.30	93	7.03316987	3.69684694	0.14339071	4.82384984
15.40	94	7.32582014	3.82106810	0.20063401	4.74134222
15.50	95	7.51639690	3.93572699	0.17942900	4.63557222
15.60	103	9.12061739	4.82455482	0.13315226	4.25749701
15.70	106	8.14355864	4.69984666	-0.56029912	4.36134808
15.80	107	8.30745163	4.75494537	-0.50318028	4.32216056
15.90	109	8.24024007	4.72579728	-0.51525526	4.09505760
16.00	111	8.10875491	4.66489717	-0.53216035	3.67370576
16.10	116	8.28934945	4.60200501	-0.25512944	3.48426386
16.20	119	8.40186605	4.64489743	-0.22469015	3.43823265
16.30	123	9.01984036	4.86377639	-0.02858538	3.19570476
16.40	128	10.35921615	5.42699496	0.24259060	3.29695233
16.50	132	11.00038932	5.77221128	0.24146631	3.05831518
16.60	143	11.09377956	6.03029492	-0.11861947	3.04267397
16.70	147	11.63130762	6.29705620	-0.08032916	2.86201397
16.80	148	11.48752063	6.22705843	-0.09292727	2.94792071
16.90	149	11.49425960	6.28488278	-0.18680931	2.75021383
17.00	149	11.46325275	6.26513659	-0.18146928	2.77257345
17.10	149	11.40837257	6.21861155	-0.15196835	2.82040919
17.20	149	11.39957207	6.22802662	-0.17646729	2.73903940
17.30	150	12.54997748	5.96351646	-1.81225861	10.25106252
17.40	150	13.08206055	6.34216273	-0.05884623	2.70982447
17.50	150	12.70031569	6.34164458	0.05389895	2.92811861
17.60	149	12.21048564	6.22381951	0.06600770	2.65527423
17.70	146	11.21297116	6.14231955	-0.20170756	3.18148517
17.80	144	11.05339219	6.03808346	-0.16970242	3.02162429
17.90	143	11.16645854	6.10935117	-0.18789887	3.09262029
18.00	142	10.90134284	5.98141358	-0.21307579	2.89243104
18.10	142	10.79619800	5.93726722	-0.23448149	3.15008516
18.20	141	10.89299225	5.99080313	-0.23711174	2.94715457
18.30	140	10.74147347	5.91450165	-0.24598831	2.96467242
18.40	140	10.59392658	5.84293679	-0.25937188	3.10783689
18.50	140	10.49291214	5.78789812	-0.25806696	3.01524477
18.60	141	10.57140472	5.83504800	-0.26667156	3.08529700
18.70	142	10.96354095	6.00722422	-0.19988674	2.90771976
18.80	143	11.03224762	6.01434886	-0.14827438	3.08002106
18.90	144	11.06486128	6.04768679	-0.17566039	3.02586197
19.00	144	11.21853324	6.05953684	-0.05314647	2.97396676
19.10	145	11.18974247	6.09038926	-0.13338306	2.88928942
19.20	144	11.16863783	6.11916583	-0.20286986	3.04452862
19.30	145	11.19201145	6.12665443	-0.19408419	3.00433897
19.40	145	11.31931408	6.13814309	-0.09548907	2.86318313

AC Output to Underwater Power Grid System (24-Hours Subsea Operation)					
Time (Hours)	**Subsea Temp. Diff. (degC)**	**Phase C-AC Current (A)**	**Active Power (kW)**	**Reactive Power (kW)**	**THD**
19.50	141	10.61419651	5.87452692	-0.29522020	2.97686365
19.60	139	10.63410109	5.87113272	-0.27081398	2.96319897
19.70	139	10.61059642	5.87338141	-0.29658712	2.98337907
19.80	139	10.68805858	5.88595879	-0.24626953	2.89651839
19.90	139	10.56486911	5.85858227	-0.31351750	3.07504609
20.00	139	10.48934455	5.82961650	-0.33364605	3.04900233
20.10	137	10.54964906	5.90959850	-0.41604712	3.14339420
20.20	136	10.64654060	5.89606589	-0.30242072	3.10829182
20.30	133	10.52674667	5.80806942	-0.26151128	3.16280816
20.40	130	10.36092234	5.50443856	0.11004248	3.25863337
20.50	132	10.99630787	5.77681349	0.22969599	3.05724203
20.60	131	10.97756437	5.79456131	0.18150932	3.09035828
20.70	121	9.18327624	5.00066635	-0.11355861	3.26058009
20.80	114	7.84018022	4.56636255	-0.61148434	3.63259666
20.90	114	7.89795571	4.46169899	-0.37642396	3.66580283
21.00	113	7.63819057	4.44467037	-0.58872050	3.90000922
21.10	110	7.96359900	4.64679941	-0.63592612	4.01854538
21.20	108	8.19213684	4.78483399	-0.66228461	4.24297096
21.30	102	8.22207461	4.69832940	-0.48458801	4.23785839
21.40	91	6.55761282	3.50615761	0.03102292	4.69502728
21.50	79	5.30377160	3.18166058	-0.57401480	5.10954253
21.60	79	5.95480297	3.36754468	-0.28999154	5.45764071
21.70	79	5.65346723	3.31716488	-0.48321631	5.93250263
21.80	76	5.64593155	3.34726096	-0.54235851	5.71841354
21.90	70	5.58544090	3.19840575	-0.34083879	5.94015234
22.00	60	3.91958620	2.26854251	-0.28085614	7.89414899
22.10	59	3.88405585	2.22519224	-0.23884313	7.71145698
22.20	55	3.43794277	2.06304707	-0.37324423	8.67452915
22.30	49	2.87988666	1.78490418	-0.41092865	8.81214599
22.40	39	2.60394419	1.60016599	-0.34780165	12.28093824
22.50	27	1.25178567	0.83852873	-0.28720461	15
22.60	23	1.01591908	0.76287543	-0.37571532	15
22.70	14	0.62782788	0.50160014	-0.28441089	15
22.80	7	-0.13241092	0.09815995	-0.29326690	15
22.90	3	-0.35618525	0.03204361	-0.38704056	15
23.00	1	-0.41779985	0.02137030	-0.42590509	15
23.10	2	-0.57797747	-0.08038601	-0.39875229	15
23.20	2	-0.41795841	0.01454507	-0.41423104	15
23.30	2	-0.32850685	0.05891981	-0.40782828	15
23.40	2	-0.46201684	0.01044536	-0.44813997	15
23.50	1	-0.55947037	-0.05204656	-0.43061115	15
23.60	0	-0.52540193	-0.04631596	-0.40882571	15
23.70	0	-0.47010973	-0.00933320	-0.42141541	15
23.80	0	-0.42204458	-0.00492755	-0.38430690	15
23.90	0	-0.41536343	0.00710473	-0.39892856	15
24.00	0	-0.39673940	0.03354223	-0.42738430	15